

Universiteit
Leiden
The Netherlands

Drug-target residence time : a case for the adenosine A1 and A2A receptors

Guo, D.

Citation
Guo, D. (2014, June 25). *Drug-target residence time : a case for the adenosine A1 and A2A receptors*. Retrieved from https://hdl.handle.net/1887/26833

Version:	Not Applicable (or Unknown)
License:	Leiden University Non-exclusive license
Downloaded from:	https://hdl.handle.net/1887/26833

Note: To cite this publication please use the final published version (if applicable).

Cover Page



Universiteit Leiden



The handle http://hdl.handle.net/1887/26833 holds various files of this Leiden University dissertation.

Author: Guo, Dong
Title: Drug-target residence time : a case for the adenosine A1 and A2A receptors
Issue Date: 2014-06-25

Drug-target residence time
A case for the adenosine A_1 and A_{2A} receptors

Cover description: a putative trajectory of ZM241385 binding to or unbinding from the human adenosine A_{2A} receptor. The figure is generated with ICM browser v3.7 (Molsoft) based on the first adenosine A_{2A} receptor crystal structure (PDB: 3EML).

Cover design: Dong Guo
Thesis layout: Dong Guo
Printed in the Netherlands



© Copyright, Dong Guo, 2014
All rights reserved. No part of this book may be reproduced in any form or by any means without permission of the author.

ISBN: 978-94-61086-97-6

Drug-target residence time
A case for the adenosine A_1 and A_{2A} receptors

PROEFSCHRIFT
ter verkrijging van
de graad van Doctor aan de Universiteit Leiden,
op gezag van Rector Magnificus prof. dr. C.J.J.M. Stolker,
volgens besluit van het College voor Promoties
te verdedigen op woensdag 25 juni 2014
klokke 16.15 uur

door

Dong Guo
geboren te Xuzhou, P. R. China
in 1984

Promotiecommissie

Promotor:	Prof. Dr. A. P. IJzerman
Copromotor:	Dr. L. H. Heitman
Overige leden:	Prof. Dr. P. H. van der Graaf
	Prof. Dr. B. van de Water
	Prof. Dr. M. Danhof
	Prof. Dr. G. Vauquelin (Vrije Universiteit Brussel, Belgium)

to my parents

谨以此书献给我的父亲母亲

Contents

Chapter 1	General introduction	9
Chapter 2	Drug-target residence time: A case for G protein-coupled receptors	25
Chapter 3	Dual-point competition association assay: A fast and high-throughput kinetic screening method for assessing ligand-receptor binding kinetics	81
Chapter 4	Binding kinetics of ZM241385 derivatives at the human adenosine A_{2A} receptor	109
Chapter 5	Functional efficacy of adenosine A_{2A} receptor agonists is positively correlated to their receptor residence time	145
Chapter 6	Molecular basis of allosteric modulation: Insight from a binding kinetics study at the human adenosine A_1 receptor	175
Chapter 7	Conclusions and perspectives	205
Summary		221
Samenvatting		223
Curriculum Vitae		227
List of publications		229
Acknowledgements		231

Chapter 1

General introduction

About this thesis

Drug design and discovery is a daunting task. To date, the pharmaceutical industry is continuously experiencing high attrition rates in research and development (R&D) of drug candidates. One of the major reasons for drug failure is lack of efficacy.[1] Apparently, the current evaluation strategies, often measurements based on examining a compound's affinity and selectivity, are not sufficient to predict *in vivo* drug efficacy. A more predictive experimental paradigm is, therefore, highly desired. Several recent reviews, in an *a posteriori* perspective, showed that many marketed drugs—in other words successful examples—favor certain kinetic aspects.[2-4] In particular, the residence time of a drug on its target may be more relevant for the *in vivo* efficacy of medicines than their typical *in vitro* equilibrium binding constants, e.g., K_i values. However, this hypothesis is merely supported from retrospective studies. Only a few kinetics-directed studies have been performed so far. As such, more insight into ligand-receptor binding kinetics, in an *a priori* manner, might be beneficial in the early phases of drug discovery.

1.1 Drug discovery and development pipeline

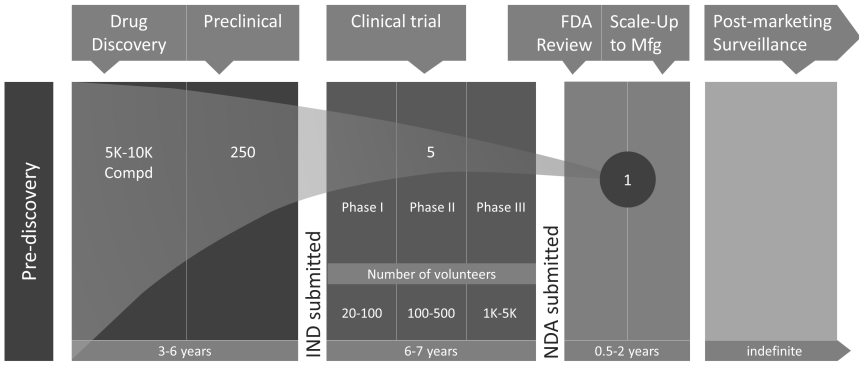


Figure 1.1 | Figure is adapted from Drug Discovery and Development: Understanding the R&D Process, www.innovation.org; CBO, Research and Development in the Pharmaceutical Industry, 2006.

Figure 1.1 represents a summary of the sequential steps that are essential for a drug to progress through the R&D pipeline. This process on average takes 10-15 years. It usually starts from a large number of hits (e.g. 5,000-10,000) which are selected from high-throughput screening, a step that enables running more than 50,000 compounds a day with complex work-stations.[5] In a typical scenario, approximately 250 candidates (leads) are selected for preclinical testing. Following a program with 3-6 years' duration, about 5 candidate drugs will progress into clinical trials of three consecutive phases (I-III) to examine their efficacy and safety among an increasing number of volunteers and patients. Finally, only one will receive approval, if at all. The average cost to research and develop a successful drug is estimated to be $800 million to $1 billion.

1.2 Lack of efficacy: the main reason of drug attrition

An investigation into the causes of drug attrition is very necessary and instructive in the identification of strategies and tactics to improve the

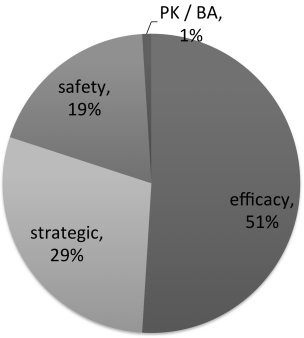


Figure 1.2 | Phase II failures: 2008-2010. The 108 failures are divided according to reasons for failure when reported (87 drugs). Figure is adapted from Arrowsmith, 2011.[1]

efficiency of drug development. In a recent survey of 108 reported phase II failures from 2008 to 2010 (Figure 1.2),[1] 44 drugs had failed due to insufficient efficacy, which accounted for 51% of 87 cases with reported reasons for failure. Following this, 29% (25 out of 87) were due to strategic reasons and 19% (17 out 87) were due to clinical or preclinical safety concerns. Pharmacokinetics (PK) or bioavailability (BA) issues are seldom reported.[1] Apparently, lack of efficacy is the main reason for drug attrition. This, in part, results from the insufficiently predictive efficacy in animal models for translation into clinical efficacy. The development of more predictive animal models—where possible—is therefore needed. Yet, what might be more important is to develop experimental paradigms that are more predictive of clinical outcomes in much earlier phases of drug design and discovery.

1.3 Drug-target residence time: the 'time' to fix the leaky drug candidate pipeline?

Drug-target residence time (RT) is the duration a drug stays in a complex with the target, which is defined as the reciprocal of the dissociation rate constant of the drug-target complex ($1 / k_{off}$).[6] Recently, awareness of the importance of residence time has started to increase since accumulating evidence suggested that the *in vivo* efficacy of a ligand may be attributed

to the time it resides at its receptor.[2,7-9] However, this parameter has so far been overlooked or neglected in the traditional drug discovery process. Currently, mostly steady-state metrics have been used in practice, e.g. affinity or potency, as predictor for *in vivo* drug efficacy. Yet, the aforementioned high attrition rate and the insufficient *in vivo* efficacy led to the realization that this equilibrium-based strategy might be too simplistic. Thus, introducing analysis of binding kinetics in the pipeline of drug research might provide a better predictor for *in vivo* efficacy in the earlier phases of drug design and discovery, and should be explored better. This added knowledge might foster a better strategy in the triage and advancement of drug candidates towards the clinic.

Clinical benefits of drugs with optimized residence time

Supposed that marketed drugs are the most successful clinical candidates, many of them have been shown, in retrospect, to favor certain kinetic aspects. In a survey of 50 drugs on 12 different drug targets by Swinney, about 70% of long residence time therapeutics displayed higher efficacy than comparable faster dissociating drugs.[10] One example is the well-known HIV-1 protease inhibitor, Darunavir, which is an extremely effective drug due to its RT of more than 14 days (over 340 h).[11] Examples in the field of G protein-coupled receptors (GPCRs) include tiotropium,[12] the muscarinic M_3 receptor antagonist for clinical indication of Chronic Obstructive Pulmonary Disease (COPD),[13] maraviroc, an allosteric inhibitor of the CCR5 receptor for HIV/AIDS,[14] and 'sartan' antagonists for the angiotensin II receptor to treat hypertension.[15] Notably, tiotropium is non-selective in its affinity for the five subtypes of muscarinic receptors. However, due to its very slow dissociation kinetics from the M_3 receptor compared to the other subtypes it is kinetically selective. On the other hand, there are cases where mechanism-based or 'on-target' toxicity outweighs the therapeutic advantages of long receptor occupancy. In this situation, a fast dissociating compound displaying short-lived receptor intervention is preferred. This is the case for some antipsychotic D_2 dopamine receptor antagonists, where long RT is undesirable due to on-target toxicity associated with strong extrapyrimidal motor effects. The clinical benefits of optimized RT will be further discussed in Chapter 2.

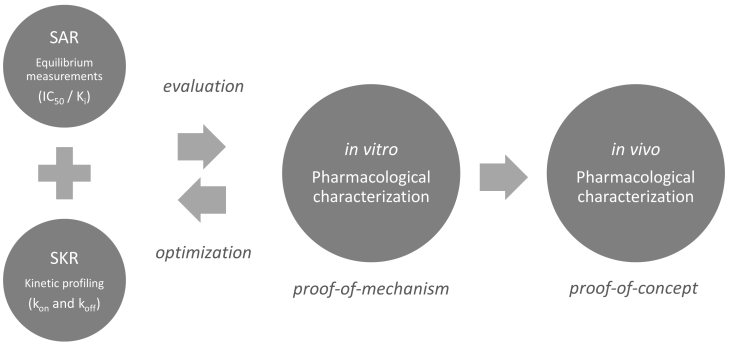


Figure 1.3 | Structure-kinetics relationships (SKR) and structure-affinity relationships (SAR)—an *a priori* approach for the design of chemical entities with desired kinetics.

Finding new chemical entities with optimized kinetics

The examples mentioned above are prospective drivers for design and development of new candidate compounds with appealing kinetic profiles for proof of concept. Figure 1.3 describes such a scheme of a kinetics-directed process in combination with the affinity-based evaluation. It includes the kinetic profiling (on-rate and off-rate) of compounds of interest (SKR, structure-kinetics relationships), complementary to the traditional equilibrium measurements (SAR, structure-affinity relationships), such as IC_{50} or K_i, and the characterization of pharmacological responses upon the formation of the ligand-receptor binary complex. The information obtained from the latter further stimulates a second round of optimization. This quick synthesis and evaluation loop can lead to more candidate compounds with desired kinetics profile to fuel further *in vivo* proof-of-concept experiments.

1.4 Adenosine receptors—the prototypic targets

Adenosine receptors (ARs) are used as prototypical targets for binding kinetics investigations in the present thesis. These receptors belong to the superfamily of G protein-coupled receptors (GPCRs) and have four subtypes: A_1, A_{2A},



Figure 1.4 | Schematic representation of the adenosine A_{2A} receptor in complex with the antagonist ZM241385 embedded in a lipid bilayer. The structure is based on the first crystallographic structure of the adenosine A_{2A} receptor (PDB: 3EML). The receptor contains heptahelical transmembrane motifs connected by three intracellular and three extracellular loops, with the amino terminus located at the extracellular side and the carboxyl terminus at the intracellular side.

A_{2B} and A_3. Figure 1.4 is a schematic representation of the adenosine A_{2A} receptor in complex with the antagonist ZM241385 which is based on the first crystallographic structure of this receptor (PDB: 3EML). Like all GPCRs, it contains heptahelical transmembrane motifs connected by three intracellular and three extracellular loops, with the amino terminus located at the extracellular side and the carboxyl terminus at the intracellular side. The adenosine A_1 and A_3 receptors are mainly coupled to the enzyme adenylate cyclase in an inhibitory fashion via a G_i protein, whereas the A_{2A} and A_{2B} receptors stimulate this enzyme via a G_s protein.[16] Adenosine receptors are promising therapeutic targets. They are involved in a wide range of conditions, including cerebral and cardiac ischemic diseases, sleep disorders, immune and inflammatory disorders and cancer.[17] As such, decades of medicinal chemistry research has resulted in a plethora of AR ligands, which are good starting points for binding kinetics investigations. In this thesis we will focus on the A_1R and $A_{2A}R$.

A_1 receptor

The A_1R is widely expressed throughout the body.[18] Its activation inhibits adenylyl cyclase activity, activates potassium channels (including K_{ATP} channels in neurons and the myocardium), blocks transient calcium channels and increases intracellular calcium and phospholipase C (PLC).[19] This receptor can exert many physiologically important effects in different organs and cells. For instance, A_1R activation in the cardiovascular system reduces heart rate and atrial contractility, and attenuates the stimulatory actions of catecholamines on the heart.[20] However, for long-term indications, selective A_1R agonists are required to avoid side effects related to other AR subtypes such as hypotension ($A_{2A}R$).[17,19,20] A_1R inhibition in the nervous system was reported to have potential therapeutic effects in divergent conditions, such as dementia, hyperactivity, anxiety, schizophrenia and sleep disorders.[16,21,22]

A_{2A} receptor

The $A_{2A}R$ is highly expressed in the brain striatum, leukocytes and blood platelets, and is also found in the heart, lung and blood vessels.[16] Its activation stimulates the cyclic AMP-protein kinase A (PKA) pathway by coupling to a G_s protein in peripheral tissues or G_{olf} in the brain.[23-25] In the central nervous system, $A_{2A}R$ plays significant roles in regulating motor activity, psychiatric behaviors, the sleep-wake cycle and neuronal cell death. In peripheral tissues, $A_{2A}R$ is involved in the modulation of inflammation, myocardial oxygen consumption, coronary blood flow, angiogenesis and the control of cancer pathogenesis.[19] Thus, activation of $A_{2A}R$ has clinical relevance in various pathological conditions such as respiratory disorders and inflammation,[26,27] while inhibition of this receptor may have potential therapeutic roles for syndromes such as insomnia, pain, depression, drug addiction and Parkinson's disease (PD).[28-30]

Status quo: translation of current knowledge towards clinical progress

The translation of the current knowledge of adenosine receptors to clinical progress has been disappointingly slow. After decades of research, only two adenosine receptor agonists have been approved by the US Food and Drug Administration (FDA). They are adenosine itself (Adenocard; Astellas Pharma) for restoring normal heart rhythm in patients with paroxysmal supraventricular tachycardia (PSVT) and an A_1R agonist regadenoson (Lexiscan; Astellas Pharma) for myocardial perfusion imaging in patients with suspected coronary artery disease.[17,31] Currently, several trials are in progress, which are summarized in Table 1.1.[19] Revisiting the database with a kinetic perspective may provide additional knowledge for future medicinal chemistry projects. The proof of mechanism in pre-clinical trials—for instance, preladenant's long duration-of-action (> 12 h in a rat model)[32]—could still direct us to find compounds bearing chemical resemblance for similar or better kinetic behavior, even though the starting compound has been discontinued in clinical trials. Such strategy is exemplified in Chapter 4. On the other hand, investigating the residence time of UK432,097, an $A_{2A}R$ agonist that in Phase II clinical trials was not efficacious for COPD, may provide clues for its failure.

Long or short receptor residence time for AR ligands?

The question whether to aim for long or short residence time A_1R and $A_{2A}R$ ligands needs careful consideration in the early phase of drug design and discovery. The same holds for all GPCRs and other drug targets as well. It is thus necessary to weigh both potential beneficial and detrimental outcomes upon longer or shorter AR occupancy. For example, myocardial A_1Rs have been shown to inhibit a number of myocardial pathologies associated with ischemia and reperfusion injury.[33,34] However, such desired A_1R-mediated protective and regenerative cardiovascular effects might be counteracted by unintended side-effects like bradycardia or atrioventricular block, due to the broad physiologic spectrum of cardiac responses upon myocardial

Table 1.1 | List of ongoing or recently completed phase IIb-III clinical trials targeting A_1 and A_{2A} receptors. The table summarizes the status found at the ClinicalTrials.gov website, accessed at December 6, 2013, and was adapted from Chen *et al*.[19]

Compound	*Name of the study*	*Status*
Adenosine	Salvage: postconditioning after STEMI	Phase II ongoing
	Prophylactic intra-coronary adenosine to prevent post coronary artery stenting myonecrosis	Phase III terminated
Caffeine	Clinical study of caffeine for apnea of prematurity	Phase III completed
	Magnetic resonance imaging (MRI) and neurodevelopmental outcomes in preterm infants following administration of high-dose caffeine	Phase IV Recruiting
	Caffeine for motor manifestations of Parkinson's disease	Phase II Completed
	Caffeine for excessive daytime somnolence in Parkinson's disease	Phase II Completed
GW493838	The study of GW493838, an adenosine A_1 agonist, in peripheral neuropathic pain	Phase II terminated
INO-8875	A dose-escalation study designed to evaluate the tolerability, safety, pharmacokinetics (PK), and efficacy of chronic topical ocular application of INO-8875 in adults with ocular hypertension or primary open-angle glaucoma	Phase II Completed
CV-3146 (regadenoson)	ADVANCE MPI 2: study of regadenoson versus Adenoscan® in patients undergoing myocardial perfusion imaging (MPI)	Phase III Completed
	Regadenoson blood flow in type I diabetes (RABIT1D)	Phase IV Completed
ALT-146e (apadenoson)	Study of the safety and efficacy of apadenoson for detection of myocardial perfusion defects using SPECT MPI (ASPECT)	Phase III terminated
UK432,097	Safety and efficacy of UK432,097 administration in patients with chronic obstructive pulmonary disease	Phase II terminated
BG9928 (tonapofylline)	Phase 2b study to assess the safety and tolerability of IV tonapofylline in subjects with acute decompensated heart failure (ADHF) and renal insufficiency (TRIDENT-1)	Phase II completed
KW-3902 (Rolofylline)	PROTECT-1: a study of the selective A_1 adenosine receptor antagonist KW-3902 for patients hospitalized with acute HF and volume overload to assess treatment effect on congestion and renal function	Phase III completed
	PROTECT-2: a study of the selective A_1 adenosine receptor antagonist KW-3902 for patients hospitalized with acute HF and volume overload to assess treatment effect on congestion and renal function	Phase III completed
KW-6002 (istradefylline)	Study of KW-6002 (istradefylline) for the treatment of Parkinson's disease in patients taking Levodopa (6002-009)	Phase III completed
	Long-term safety study of istradefylline in patients with Parkinson's disease	Phase III completed
Preladenant	A placebo- and active-controlled study of preladenant in early Parkinson's disease (P05664 AM5)	Phase III terminated
	A placebo- and active-controlled study of preladenant in subjects with moderate to severe Parkinson's disease (Study P04938 AM5)	Phase III terminated
SYN-115	Safety and efficacy study of SYN115 in Parkinson's patients using L-DOPA to treat end of dose wearing off	Phase III completed

A_1R activation.[20,35] Receptor desensitization is another potential issue when long residence time A_1 receptor agonists are considered. Therefore, a short intervention might be preferred to overcome the restrictions mentioned above. There are also cases where long residence time AR ligands might be beneficial. One example could be the $A_{2A}R$ antagonists for the treatment of Parkinson's disease (PD) in combination with levodopa (the gold-standard medicine to boost dopamine levels in the brain). However, many PD patients' symptoms return in between doses, when levodopa's effects wear off—the fluctuation known as 'off' time.[36] In light of this, a slowly dissociating $A_{2A}R$ antagonist may have the advantage of decreasing the 'off' time compared to a short residence time compound. Additionally, longer receptor residence time on one AR subtype can provide so-called kinetic selectivity over the others. This feature could be of great use for further optimizing those less-selective AR ligands in terms of affinity (i.e. the non-selective AR agonist NECA[17]). Such an advantage is well exemplified by tiotropium, the M_3R antagonist highly selective over other muscarinic subtypes in terms of binding kinetics while less so in terms of affinity. To better define the optimal range of a target's residence time, it is necessary to obtain a series of candidate molecules having a divergent frame of residence times—for instance, the $A_{2A}R$ antagonists described in Chapter 4 – for later proof-of-concept tests.

1.5 Objectives and overview of this thesis

Investigating ligand-receptor binding kinetics, in particular the residence time, is a leading theme in this thesis, which will be explored by several case studies on adenosine A_1 and A_{2A} receptors.

In Chapter 2, the state of the art in drug-GPCR residence time is reviewed. We summarized a series of ligands for four prototypic GPCRs that have reported kinetic data, and extensively discussed these data from a molecular mechanism of action to *in vivo* pharmacology. In this chapter we also reviewed and summarized the emerging (*in vitro*) methods for studying binding kinetics. Among other assays, a newly developed kinetic screening method is listed, the so-called dual-point competition association assay. This assay enables fast and high-throughput assessment of ligand-receptor binding kinetics and is further described in Chapter 3.

At the start of this project, few SKR studies had been reported in the

field of GPCRs, if any. Thus, we proposed a novel strategy for compound optimization that combines an extensive SKR study with the classical SAR study in Chapter 2. This strategy is exemplified in Chapter 4. We demonstrated that compounds within one chemical class (chemotype) may have divergent kinetic properties, whilst diverse compounds may have similar kinetic characteristics ('kinotype').

Following this, we also investigated the mechanism of important pharmacological concepts, i.e., functional efficacy and GPCR allosterism, from a kinetic perspective (Chapters 5 and 6). These additional kinetic insights advanced our current understanding of these concepts.

In short, several case studies of drug-target residence time at the A_1R and A_{2A}R are presented in this thesis. In Chapter 7, this work is concluded with general remarks and future perspectives for this field of research. Hopefully, this thesis will contribute to stipulating the importance of kinetics-based drug design and discovery in the future.

References:

1. Arrowsmith J. Trial watch: Phase II failures: 2008-2010. *Nat Rev Drug Discov* 2011;10(5):328-329.
2. Copeland RA, Pompliano DL, Meek TD. Drug-target residence time and its implications for lead optimization. *Nat Rev Drug Discov* 2006;5(9):730-739.
3. Swinney DC. Biochemical mechanisms of New Molecular Entities (NMEs) approved by United States FDA during 2001-2004: mechanisms leading to optimal efficacy and safety. *Curr Top Med Chem* 2006;6(5):461-478.
4. Zhang R, Monsma F. The importance of drug-target residence time. *Curr Opin Drug Discov Devel* 2009;12(4):488-496.
5. Martis E, Radhakrishnan R, Badve R. High-throughput screening: the hits and leads of drug discovery-an overview. *Journal of Applied Pharmaceutical Science* 2011;1(1):2-10.
6. Copeland, RA. *Evaluation of enzyme inhibitors in drug discovery: a guide for medicinal chemists and pharmacologists*. New York: John Wiley & Sons; 2005. 153 p.
7. Swinney DC. The role of binding kinetics in therapeutically useful drug action. *Curr Opin Drug Discov Devel* 2009;12(1):31-39.
8. Zhang R, Monsma F. Binding kinetics and mechanism of action: toward the discovery and development of better and best in class drugs. *Expert Opin Drug Discov* 2010;5(11):1023-1029.
9. Nunez S, Venhorst J, Kruse CG. Target-drug interactions: first principles and their application to drug discovery. *Drug Discov Today* 2012;17(1-2):10-22.
10. Swinney DC. Biochemical mechanisms of drug action: what does it take for success? *Nat Rev Drug Discov* 2004;3(9):801-808.
11. Dierynck I, De Wit M, Gustin E, Keuleers I, Vandersmissen J, Hallenberger S, Hertogs K. Binding kinetics of darunavir to human immunodeficiency virus type 1 protease explain the potent

antiviral activity and high genetic barrier. *J Virol* 2007;81(24):13845-13851.
12. Casarosa P, Kollak I, Kiechle T, Ostermann A, Schnapp A, Kiesling R, Pieper M, Sieger P, Gantner F. Functional and biochemical rationales for the 24-hour-long duration of action of olodaterol. *J Pharm Exp Ther* 2011;337(3):600-609.
13. Tee AK, Koh MS, Gibson PG, Lasserson TJ, Wilson AJ, Irving LB. Long-acting $beta_2$-agonists versus theophylline for maintenance treatment of asthma. *Cochrane Database Syst Rev* 2007(3):CD001281.
14. Watson C, Jenkinson S, Kazmierski W, Kenakin T. The CCR5 receptor-based mechanism of action of 873140, a potent allosteric noncompetitive HIV entry inhibitor. *Mol Pharmacol* 2005;67(4):1268-1282.
15. Van Liefde I, Vauquelin G. Sartan-AT_1 receptor interactions: in vitro evidence for insurmountable antagonism and inverse agonism. *Mol Cell Endocrinol* 2009;302(2):237-243.
16. Fredholm BB, IJzerman AP, Jacobson KA, Linden J, Müller CE. International Union of Basic and Clinical Pharmacology. LXXXI. Nomenclature and classification of adenosine receptors--an update. *Pharmacol Rev* 2011;63(1):1-34.
17. Jacobson KA, Gao ZG. Adenosine receptors as therapeutic targets. *Nat Rev Drug Discov* 2006;5(3):247-264.
18. Dixon AK, Gubitz AK, Sirinathsinghji DJ, Richardson PJ, Freeman TC. Tissue distribution of adenosine receptor mRNAs in the rat. *Br J Pharmacol* 1996;118(6):1461-1468.
19. Chen JF, Eltzschig HK, Fredholm BB. Adenosine receptors as drug targets - what are the challenges? *Nat Rev Drug Discov* 2013;12(4):265-286.
20. Albrecht-Kupper BE, Leineweber K, Nell PG. Partial adenosine A_1 receptor agonists for cardiovascular therapies. *Purinerg Signal* 2012;8:S91-S99.
21. Stenberg D, Litonius E, Halldner L, Johansson B, Fredholm BB, Porkka-Heiskanen T. Sleep and its homeostatic regulation in mice lacking the adenosine A_1 receptor. *J Sleep Res* 2003;12(4):283-290.
22. Maemoto T, Tada M, Mihara T, Ueyama N, Matsuoka H, Harada K, Yamaji T, Shirakawa K, Kuroda S, Akahane A, Iwashita A, Matsuoka N, Mutoh S. Pharmacological characterization of FR194921, a new potent, selective, and orally active antagonist for central adenosine A_1 receptors. *J Pharmacol Sci* 2004;96(1):42-52.
23. Fredholm BB, Arslan G, Halldner L, Kull B, Schulte G, Wasserman W. Structure and function of adenosine receptors and their genes. *N-S Arch Pharmacol* 2000;362(4-5):364-374.
24. Kull B, Svenningsson P, Fredholm BB. Adenosine A_{2A} receptors are colocalized with and activate G_{olf} in rat striatum. *Mol Pharmacol* 2000;58(4):771-777.
25. Corvol JC, Studler JM, Schonn JS, Girault JA, Herve D. G alpha(olf) is necessary for coupling D_1 and A_{2a} receptors to adenylyl cyclase in the striatum. *J Neurochem* 2001;76(5):1585-1588.
26. Ohta A, Sitkovsky M. Role of G protein-coupled adenosine receptors in downregulation of inflammation and protection from tissue damage. *Nature* 2001;414(6866):916-920.
27. Gao Z, Li Z, Baker SP, Lasley RD, Meyer S, Elzein E, Palle V, Zablocki JA, Blackburn B, Belardinelli L. Novel short-acting A_{2A} adenosine receptor agonists for coronary vasodilation: inverse relationship between affinity and duration of action of A_{2A} agonists. *J Pharmacol Exp Ther* 2001;298(1):209-218.
28. Morelli M, Di Paolo T, Wardas J, Calon F, Xiao D, Schwarzschild MA. Role of adenosine A_{2A} receptors in parkinsonian motor impairment and l-DOPA-induced motor complications. *Prog Neurobiol* 2007;83(5):293-309.
29. Hack SP, Christie MJ. Adaptations in adenosine signaling in drug dependence: therapeutic

implications. *Crit Rev Neurobiol* 2003;15(3-4):235-274.
30. Ferre S, Diamond I, Goldberg SR, Yao L, Hourani SM, Huang ZL, Urade Y, Kitchen I. Adenosine A_{2A} receptors in ventral striatum, hypothalamus and nociceptive circuitry implications for drug addiction, sleep and pain. *Prog Neurobiol* 2007;83(5):332-347.
31. Ghimire G, Hage FG, Heo J, Iskandrian AE. Regadenoson: a focused update. *J Nucl Cardiol* 2013;20(2):284-288.
32. Hodgson RA, Bertorelli R, Varty GB, Lachowicz JE, Forlani A, Fredduzzi S, Cohen-Williams ME, Higgins GA, Impagnatiello F, Nicolussi E, Parra LE, Foster C, Zhai Y, Neustadt BR, Stamford AW, Parker EM, Reggiani A, Hunter JC. Characterization of the potent and highly selective A_{2A} receptor antagonists preladenant and SCH412348 [7-[2-[4-2,4-difluorophenyl]-1-piperazinyl] ethyl]-2-(2-furanyl)-7H-pyrazol o[4,3-e][1,2,4]triazolo[1,5-c]pyrimidin-5-amine] in rodent models of movement disorders and depression. *J Pharmacol Exp Ther* 2009;330(1):294-303.
33. Headrick JP, Hack B, Ashton KJ. Acute adenosinergic cardioprotection in ischemic-reperfused hearts. *Am J Physiol Heart Circ Physiol* 2003;285(5):H1797-1818.
34. Reichelt ME, Willems L, Molina JG, Sun CX, Noble JC, Ashton KJ, Schnermann J, Blackburn MR, Headrick JP. Genetic deletion of the A_1 adenosine receptor limits myocardial ischemic tolerance. *Circ Res* 2005;96(3):363-367.
35. Mustafa SJ, Morrison RR, Teng B, Pelleg A. Adenosine receptors and the heart: role in regulation of coronary blood flow and cardiac electrophysiology. *Handb Exp Pharmacol* 2009(193):161-188.
36. Salamone JD. Preladenant, a novel adenosine A_{2A} receptor antagonist for the potential treatment of parkinsonism and other disorders. *IDrugs* 2010;13(10):723-731.

Chapter 2

Drug-target residence time
A case for G protein-coupled receptors

Guo D, Hillger JM, IJzerman AP, Heitman LH.
Adapted from: *Med Res Rev.* 2014, DOI: 10.1002/med.21307

About this chapter

A vast number of marketed drugs act on G protein-coupled receptors (GPCRs), the most successful category of drug targets to date. These drugs usually possess high target affinity and selectivity, and such combined features have been the driving force in the early phases of drug discovery. However, attrition has also been high. Many investigational new drugs eventually fail in clinical trials due to a demonstrated lack of efficacy. A retrospective assessment of successfully launched drugs revealed that their beneficial effects in patients may be attributed to their long drug-target residence times. Likewise, for some other GPCR drugs short residence time could be beneficial to reduce the potential for on-target side effects. Hence, the compounds' kinetics behavior might in fact be the guiding principle to obtain a desired and durable effect *in vivo*. We therefore propose that drug-target residence time should be taken into account as an additional parameter in the lead selection and optimization process. This should ultimately lead to an increased number of candidate drugs moving to the pre-clinical development phase and on to the market. This chapter contains examples of the kinetics behavior of GPCR ligands with improved *in vivo* efficacy and summarizes methods for assessing drug-target residence time.

2.1 Introduction

Drug-target residence time (RT) is an emerging concept in the drug research community. Its definition, coined by Copeland in 2006, stands for an experimental measure of the lifetime of a drug-target complex, reflected by its dissociation rate (k_{off}).[1] This is an important pharmacological feature as a drug is only effective when bound to, and influencing the activity of its physiological target.[1,2] Recently, several notable reviews including Swinney *et al.*,[2-5] Copeland *et al.*,[1,6,7], Vauquelin *et al.*,[8-11] and Zhang and Monsma,[12,13] to name a few, have emphasized the pivotal role of RT in the early phases of drug discovery. These discussions led to increasing recognition that drug-target residence time may even be of greater importance for a drug's effect in the patient than its affinity, since the body, unlike an *in vitro* setting, is an open system where the concentration of free drug fluctuates over time.[13,14] The dynamic flow *in vivo*—absorption, distribution, metabolism, and excretion (ADME)—often prevents the free drug from reaching equilibrium conditions that are otherwise readily obtained in a test tube.[13,14] In this sense, optimizing drug candidates based on equilibrium-derived parameters alone, such as affinity (K_i) / potency (IC_{50}), may not be ideal.[15] Drug-target residence time may be a useful additional parameter as it is thought to represent a surrogate marker of drug clinical efficacy: the longer the drug occupies the receptor, the more profound the drug may exert its effect.[1,12] Although this reasoning most certainly is too simplistic, there is substantial evidence, as witnessed in a survey of 50 drugs on 12 different drug targets, that about 70% of long residence time therapeutics displayed higher efficacy than comparable faster dissociating drugs.[5]

It needs to be pointed out that the criteria for 'long' or 'short' residence time may vary for different targets and for divergent clinical indications.[16] For therapies requiring prolonged target occupancy, a long RT drug offers advantages as it remains bound to the target and continuously exerts its pharmacological effect even when most of the free drug has already been eliminated from circulation.[17] Importantly, this simultaneously implies that a slowly dissociating drug will only offer a noticeably increased effect over a faster dissociating drug, when its dissociation half-life ($t_{1/2}$) outlasts its pharmacokinetic half-life, or when there are large fluctuations in the endogenous competitor (e.g., hormone or neurotransmitter) concentrations.[11] Further proof for the importance of RT comes from numerous examples

of drugs that are best-in-class due to slow dissociation from their target receptor. One example is the well-known muscarinic M_3 receptor antagonist, tiotropium, which is a long-acting, 24 hour, anticholinergic bronchodilator used in the management of chronic obstructive pulmonary disease.[29] On the other hand, there are cases where the mechanism-based toxicity outweighs the therapeutic advantages by long receptor occupancy. In this situation, a fast dissociating compound displaying short-lived intervention is preferred. This may be the case for the antipsychotic D_2 dopamine receptor antagonists, where long RT is not desired due to on-target toxicity associated with strong extrapyramidal motor effects. We will discuss this in a later part of this chapter.

2.2 Mathematical definitions of drug-target residence time

Drug-target residence time is equal to the reciprocal of the dissociation rate constant ($RT = 1 / k_{off}$).[1] Its value is interchangeable with the dissociation half-life ($t_{1/2} = \ln 2 / k_{off}$) with a factor of ln2, i.e., $RT = t_{1/2} / \ln 2$. Both can be used to represent the duration of the drug-target binary complex. For the convenience of discussion, we chose to use the dissociation half-life to describe the drug-target residence time in the following part of this chapter, since most of the kinetic values in literature were reported with $t_{1/2}$ values.

As mentioned above, it is necessary to determine the dissociation rate constant to calculate the RT or $t_{1/2}$. However, the definition of k_{off} depends on the specific mechanism of ligand-receptor interaction.[1,14] In general, three situations are well known. Equation 1 represents a simple one-step association and dissociation process, where the receptor (R) and ligand (L) encounter each other to form a binary complex (RL) with association rate k_1 (k_{on}) and dissociation rate k_2 (k_{off}), respectively.

$$R + L \underset{k_2}{\overset{k_1}{\rightleftharpoons}} RL \tag{1}$$

In contrast, Equation 2 represents a more complicated process. Upon the binding of the ligand to the receptor, the initial complex (RL) undergoes a conformation isomerization leading to a much higher-affinity final complex

(RL*). This is also known as the 'induced-fit' mechanism. In this case, k_{off} entails both forward (k_3) and reverse steps (k_4) in receptor isomerization as well as the on- and off-rate constants for the free ligand bound to and unbound from the free receptor, such that $k_{off} = k_2 \cdot k_4 / (k_2 + k_3 + k_4)$. This isomerization step enhances the interaction between the ligand and the target, hence resulting in an extended overall $t_{1/2}$.

$$R + L \underset{k_2}{\overset{k_1}{\rightleftharpoons}} RL \underset{k_4}{\overset{k_3}{\rightleftharpoons}} RL^* \tag{2}$$

A third mechanism is represented in Equation 3, where the receptor is in equilibrium between two conformational states (R and R*) in the absence of ligand. Of these conformational states, the ligand specifically binds to one, R*, rather than the other (R), to form the R*L complex. This is also known as the 'conformation-selection' mechanism. The interconversion between conformational states R and R* is slow relative to the binding of the ligand to the R* state, thus it represents the rate-limiting step for the formation of the binary complex. For the dissociation rate constant, its value is equal to k_4.

$$R \underset{k_2}{\overset{k_1}{\rightleftharpoons}} R^* \underset{k_4}{\overset{k_3 \cdot [L]}{\rightleftharpoons}} R^*L \tag{3}$$

Among these three mechanisms, the first situation is most commonly encountered in ligand-GPCR binding kinetics, while the second mechanism can be the case for high-affinity ligand-receptor interactions, especially for enzyme inhibitors and receptor antagonists;[1,6,14] the third situation is rarely observed in ligand-receptor interactions.[14]

2.3 Experimental strategies to assess drug-target residence time

Measurement of drug-target complex lifetime, reflected by k_{off} or $t_{1/2}$, is not a new phenomenon *per se*. To date, there are several strategies available to examine the binding kinetics of ligand-GPCR interactions. The advantages and disadvantages / limitations of these experimental strategies to access drug-target residence time are briefly outlined in Table 2.1. Of these

Table 2.1 | The advantages and disadvantages / limitations of experimental strategies to access drug-target residence time.

Assay	*Advantages*	*Disadvantages / limitations*	*Ref.*
Direct kinetic radioligand binding assay	Straightforward; Robust; Quantitative measurement	Ligand of interest needs to be radiolabeled; Low throughput assay format	19-21
Indirect kinetic radioligand binding assay	Only one labeled ligand necessary; Quantitative measurement; Adjustable for high throughput screening	Need for suitable radiolabeled ligand; Intermediate filtration and / or 'washout' steps are needed	23-26
Competition association assay	Only one labeled ligand necessary; Quantitative measurement	Need for suitable radiolabeled ligand; Low throughput assay format	27-34
Dual-point competition association assay	Only one labeled ligand necessary; High throughput assay format; Easy readout for longer or shorter residence time compounds	Need for suitable radiolabeled ligand; Qualitative measurement	18,33
Dual-point IC_{50} / K_i value determination	Only one labeled ligand necessary; Adjustable for high throughput screening	Need for suitable radiolabeled ligand; Only selects long residence time compounds	30,34
Functional reversibility assay	No need for labeled ligands; Adjustable for high throughput screening	Qualitative measurement; Not suitable for binding kinetics at low temperatures.	35-46
Label-free kinetic measurement	No need for labeled ligands; Quantitative measurement	Need for protein purification and immobilization; Low throughput assay format	47-55

approaches, the most common and straightforward method is to radiolabel a compound of interest with high affinity and directly measure its on- and off-rate in a kinetic set-up of a radioligand binding experiment. Two examples, in the context of drug-target residence time, are radiolabeled aprepitant at the Neurokinin 1 (NK_1) receptor and tiotropium at the muscarinic M_3 receptor (M_3R). Both compounds have been well characterized by using this method.[19,20] Alternatively, a ligand can be fluorescently labeled to calculate its drug-target residence time. For instance, Keppler and coworkers have developed a so-called Tag-lite® platform, a combination of a Homogeneous Time-Resolved Fluorescence (HTRF®) detection method with a covalent labeling technology called SNAP-tag®.[21] One application note from Cisbio describes fluorescently labeled spiperone binding at the Tag-lite dopamine D_2 receptor.[22] Nevertheless, the process of radio- or fluorescent labeling is costly and labor intensive, which, as a consequence, confines kinetics determinations to a limited scope. Therefore, alternative approaches are highly desired (See Figure 2.1-2.4 for experimental schemes and representative results).

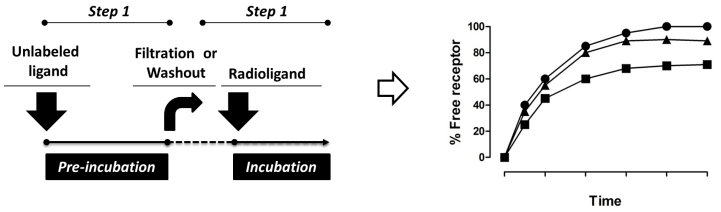


Figure 2.1 | Indirect kinetic radioligand binding assays: the receptor-bearing material is pre-incubated with a saturating concentration of unlabeled ligand, followed by an intermediate filtration and / or 'washout' step to initiate ligand dissociation. Subsequently, a fixed concentration of radioligand is added and incubated thereafter for a period before assay termination. This scheme is adapted from Vauquelin *et al*.[35] In this assay a slowly dissociating compound (squares) induces an apparent decrease in the amount of free receptor, compared to a fast dissociating compound (triangles), which allows the binding of a subsequently added radioligand; Control: no pre-incubation (spheres).

A. Indirect kinetic radioligand binding assays

Contrary to the abovementioned, one-step, direct measurement of radiolabeled ligands' dissociation rates, indirect approaches usually contain two consecutive parts (Figure 2.1). Firstly, the receptor-bearing material is pre-incubated with a saturating concentration of unlabeled ligand (to occupy the majority of receptors), followed by an intermediate filtration and/or 'washout' step—methods vary in different labs[23-26]—to initiate ligand dissociation. Secondly, a fixed concentration of radioligand is added and incubated thereafter for a short period before assay termination. Thus, the unlabeled competitor's dissociation rate could be inferred from the recovery of radioligand binding. Furthermore, this method can be adopted and modified for high-throughput screening; an example is at the dopamine D_2 receptor (D_2R).[26]

B. (Dual-point) competition association assay

The competition association assay has been shown to be highly accurate in determining the binding kinetics of unlabeled ligands at the beta-

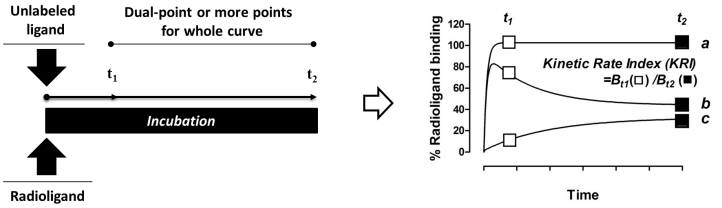


Figure 2.2 | (Dual-point) Competition association assay: an unlabeled competitor is co-incubated with a radioligand in a kinetic association experiment, and followed for two or more time points. ***a***: a radioligand association curve without co-incubation of an unlabeled competitor. ***b***: a co-incubated unlabeled competitor dissociates slower than the radioligand used. ***c***: a co-incubated unlabeled competitor dissociates faster than the radioligand used. B_{t1}: specific radioligand binding at the first time point (t_1); B_{t2}: specific radioligand binding at the second time point (t_2). Kinetic rate index (KRI) is defined as B_{t1} / B_{t2}. This scheme is adapted from Guo *et al.*[33]

adrenergic receptor,[27,28] and more recently, at the muscarinic M_3 receptor,[29] gonadotropin-releasing hormone (GnRH) receptor,[30] histamine H_1 receptor,[31] and adenosine receptors,[32,33] to name but a few. This method is based on a framework developed by Motulsky and Mahan,[34] where an unlabeled competitor is co-incubated with a radioligand during a kinetic association experiment (Figure 2.2). If the competitor dissociates faster from its target than the radioligand ($k_2 < k_4$), the specific binding of the radioligand will slowly and monotonically approach its equilibrium in time (Figure 2.2, ***c***). However, when the competitor dissociates slower ($k_2 > k_4$), the association curve of the radioligand will consist of two phases starting with a typical 'overshoot' followed by a decline until a new equilibrium is reached (Figure 2.2, ***b***).[34] In contrast, the association rates of either the competitor (k_3) or the radioligand (k_1) are usually less influential on the pattern of the curves.[34] Recently, the competition association assay has also been adopted and modified by Guo *et al.* for high-throughput kinetic screening studies at the adenosine A_1 receptor.[33] Briefly, in a so-called dual-point competition association assay, two time points are selected to measure radioligand binding: 1) at which the radiolabeled ligand just reaches equilibrium under control conditions in the absence of an unlabeled ligand (Figure 2.2, ***a*** and t_1), and 2) at which the incubation time is long enough for the labeled and unlabeled compound to equilibrate with the target (Figure 2.2, t_2). Next, the ratio of the binding at the first time point (B_{t1}) and that at the second time point (B_{t2}) is calculated, which Guo *et al.* defined as the 'kinetic rate index' (KRI).

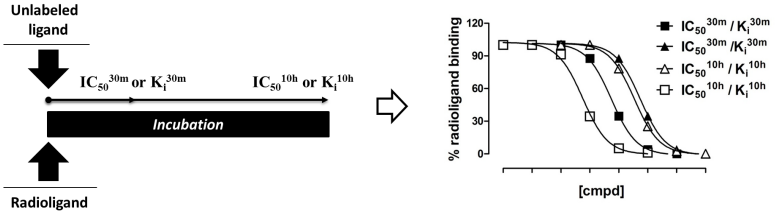


Figure 2.3 | Dual-point IC_{50} / K_i value determination: an unlabeled competitor is co-incubated with a radioligand for either a short time (in this case, e.g., 30 min) or a long time (in this case, e.g., 10 h) and their corresponding IC_{50} or K_i values are calculated. In the representative result, a slowly dissociation compound (squares) will have a more pronounced affinity shift than a fast dissociation compound (triangles).

In this manner, the compounds that quickly dissociate from their target will have a KRI below or equal to one (Figure 2.2, ***c***). Conversely, compounds that dissociate slowly from their target compared to the radioligand will have a KRI value larger than one, resulting from the typical 'overshoot' in the association curve (Figure 2.2, ***b***). Notably, the dual-point assay and KRI value can be applied to screen for candidate compounds with either long or short RT. This suggests the general applicability of this assay for other drug targets as well.

C. Dual-point IC_{50} / K_i value determination

Another method enabling kinetic screening was reported by Heise *et al.* They used a scintillation proximity assay (SPA) to measure an antagonist's affinity after 30 min or 10 h of incubation and examined their ratio ($K_i^{30\ min}$ / $K_i^{10\ h}$; Figure 2.3).[30] The theory behind this is based on the observation that displacement curves will shift leftward over time until a state of equilibrium is reached; the time to reach that state is determined by the dissociation rate of the slower unbinding process.[34] In other words, a slowly dissociating compound requires longer incubation times to reach equilibrium than a fast dissociating one, which is often neglected. This translates into markedly decreased experimental IC_{50} or K_i values over time. In this sense, the ratio of the dual-point IC_{50} or K_i values represents a surrogate of overall RT. However,

the principle of this approach also simultaneously implies its limited application, i.e. in screening long RT candidate compounds only, since for short RT compounds the state of equilibrium is quickly established and the K_i ratio derived thereof is hardly changed.

D. Fucntional reversibility assay

A ligand's binding kinetics profile could also be inferred from circumstantial evidence, which is commonly based on functional assays resembling the classical 'organ-bath' experiment. More specifically, it requires pre-incubating tissues / cells with antagonists (to allow them sufficient time to reach binding equilibrium conditions) before their challenge with an agonist (Figure 2.4).[35] As a result, fast dissociating antagonists can only cause a rightward shift of the agonist's concentration-dependent curve, since the receptor can quickly be liberated from the antagonist's blockade and thus readily respond to the subsequently administered agonist. These types of antagonists are categorized as 'surmountable' (Figure 2.4, pre-incubation experiment).[9,36,37] In contrast, slowly dissociating antagonists or, at the extreme, irreversible binders can induce not only a rightward shift but also a concomitant decline in maximal response of the agonist, due to sustained receptor blockade which, on a macroscopic scale, reduces the total receptor population available for an agonist's response.[38,39] Such antagonists are denoted as insurmountable (Figure 2.4, pre-incubation experiment).[9,36,37,40] Notably, such an insurmountable pattern can also be caused by a number of different mechanisms, such as allosteric interactions, receptor internalization or postreceptor functional response blockade.[41-44] None of these result from competitive antagonism. Nevertheless, these mechanisms can be distinguished in a co-incubation experiment, where a depressed maximal response can only be observed by a noncompetitive mechanism, but not for competitive antagonists, no matter how fast or slowly they dissociate from the target (Figure 2.4, co-incubation experiment). Thus, it is always necessary to perform a co-incubation experiment along with the pre-incubation experiment to clarify the mechanism of the insurmountable antagonism.[37,45,46] It is important to mention that the extent of the insurmountable effect, e.g. a decreased maximal response, is time dependent. During a short period of agonist exposure (following pre-incubation with a slowly dissociating antagonist), not all the

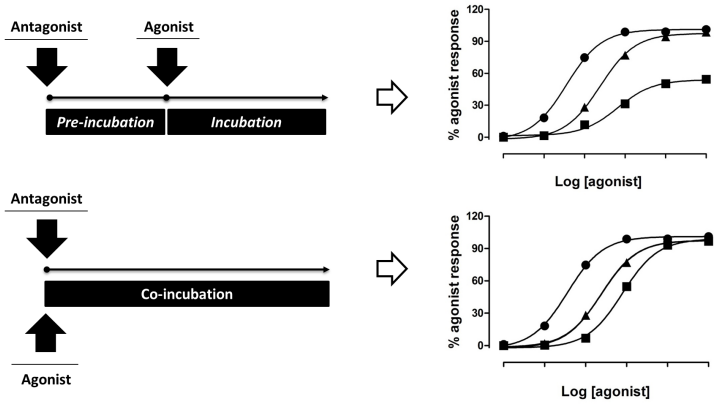


Figure 2.4 | Functional reversibility experiment: in the upper panel, tissues/cells are pre-incubated with an antagonist before challenge with an agonist. A slowly dissociating antagonist (squares) will cause a rightward shift of the concentration-response curve and a concomitant decline in maximal response of the agonist; a fast dissociating antagonist (triangles) will cause a rightward shift of the concentration-response curve without affecting the maximal response of the agonist. If as in the lower layer an antagonist is co-incubated with an agonist; both slowly and fast dissociating competitive antagonists will cause a rightward shift of the concentration-response curve without affecting the maximal response of the agonist. Otherwise they are non-competitive to the agonist; Control: agonist only (spheres). This scheme is adapted from Vauquelin *et al.*[35]

receptor sites are liberated before the response is measured, a state of so-called 'hemi-equilibrium'.[38,39,44] However, if the agonist exposure lasts longer, the occupancy of the receptors will readjust with time until, ultimately, both the agonist-receptor and the antagonist-receptor interactions reach equilibrium.[44] Evidently, the insurmountability of such slowly dissociating compounds will change if the response is measured at different time points.

E. Label-free kinetic measurements

One of the most well-established label-free measurements for kinetics is surface plasmon resonance measurement (SPR). In SPR, the protein is immobilized

on a coated gold chip, which is then exposed to the compound of interest under continuous flow. Ligand binding to the receptor immobilized on the chip's surface induces a real time change in the refractive index on the sensor surface. As such a change is linear to the number of molecules bound, it allows quantitative characterization of binding kinetics (for review, see[16,47,48]).

Another emerging label-free technology enabling kinetics measurement is by surface acoustic wave biosensor (SAW).[49] This methodology captures real-time mass changes on the surface, which result in a shifted phase and / or changed amplitude of the sound wave signal.[50] Besides these two biophysical assays, other equally valid technologies have also been reported elsewhere.[51]

However, these biophysical techniques have not been thoroughly tested on GPCRs. The difficulty is that these receptors are integral membrane proteins, and rapidly deteriorate when taken out of their natural environment, which is often a prerequisite for these newer biophysical approaches. Several strategies were developed to overcome this inherent difficulty. One of the successful examples is the application of a protein engineering method to generate a stabilized receptor (StaR), e.g. the adenosine A_{2A} receptor, minimally modified for thermostability.[52-54] The stabilized receptors can be purified in large quantities, whilst retaining correct folding, thus generating materials suitable for a broad range of structural and biophysical studies.[53] Another technique is to solubilize a given GPCR from whole cell pellets and capture it on antibody surfaces for analysis, exemplified by an SPR study on the CCR5 and CXCR4 chemokine receptors.[55] These solubilized receptor preparations could be useful materials for binding kinetics studies.

2.4 Revisit kinetics data on GPCRs

To date, nearly 800 genes encoding GPCRs have been identified, representing a substantial share of the human genome.[56] In general, all these receptors possess structurally conserved heptahelical transmembrane motifs (7TM) connected by alternating intracellular and extracellular loops, with the amino terminus located at the extracellular side and the carboxyl terminus at the intracellular side.[57] Despite these common features in their molecular structure, GPCRs are characterized by a relatively low overall sequence identity (less than 20%). According to phylogenetic classification, these receptors can be divided into five main families—*Rhodopsin* (Class A), *Secretin* (Class B), *Glutamate* (Class

Table 2.2 | Overview of GPCR ligand kinetics.

Cmpd	*Target*[a]	$t_{1/2}$[b]	*Clinical indications*	*Status*[c]	*Ref.*
Ritanserin	5-HT_2 receptor	160 min (37 °C)	Cocaine-related disorders	Phase II	160
Risperidone	5-HT_7 receptor	Irreversible (37 °C)	Schizophrenia; Alcohol abuse	Marketed	161
Clonidine	α_{2A}-autoreceptor	27.6 s (37 °C)	ADHD	Marketed	99
Bopindolol	β_1-adrenoceptor	> 4 h (rat)	Hypertension	Marketed	162
Olodaterol	β_2-adrenoceptor	17.8 h	COPD	Marketed	163
Lofentanil	μ receptor	260 min (37 °C)	Analgesia	Marketed	164
Candesartan	AT_1 receptor	120 min (37 °C)	Hypertension	Marketed	43
UK432,097	A_{2A} receptor	173 min (5 °C)	COPD	Terminated[d]	32
Taranabant	CB_1 receptor	122 min (37 °C)	Obesity	Terminated[e]	25
Maraviroc	CCR5	> 136 h (4 °C)	HIV	Marketed	165
SCH527123	CXCR2	22 h	Asthma; Psoriasis	Phase II	166
PF-4850890	CRF_1 receptor	6.79 h (rat)	Depression; Anxiety	Preclinical	153
Clozapine	D_2 receptor	14.5 s (37 °C)	Schizophrenia	Marketed	135
AM432	DP_2 receptor	90 min (37 °C)	COPD	Preclinical	167
Uracil 3	GnRH receptor	> 43 h	Reproductive-endocrine axis disorders	Preclinical	168
Desloratidine	H_1 receptor	> 6 h	Allergy	Marketed	169
JNJ7777120	H_4 receptor	62 min	Inflammation	Preclinical	170
Tiotropium	M_3 receptor	27 h	COPD	Marketed	80
Aprepitant	NK_1 receptor	154 min	Chemotherapy-induced emesis	Marketed	19
Ibodutant	NK_2 receptor	28 min	Irritable Bowel Syndrome	Phase II	171
Osanetant	NK_3 receptor	10 min	Schizophrenia	Phase II	172
Almorexant	OX_2 receptor	139 min	Chronic primary insomnia	Phase III	173
Clopidogrel	P_2Y_{12} receptor	Irreversible (37 °C)	Stroke; Heart attack; Severe chest pain	Marketed	62
Apafant	PAF receptor	50 min (guinea pig)	Arrhythmias; Breast cancer; Inflammation	Preclinical	174
GSK1562590	UT receptor	> 1 h (rat)	Hypertension	Preclinical	175
SCH500946	Y_5 receptor	71 min	Obesity	Preclinical	176

[a] Official IUPHAR receptor name. [b] Dissociation half-life at room temperature and on human receptors unless mentioned otherwise. [c] Clinical status obtained from ClinicalTrials.gov.[179] [d] Discontinued due to lack of efficacy. [e] Discontinued due to high level of central nervous system side effects.[177,178]

C), *Adhesion* and *Frizzled/Taste2*.[56,58] Receptors from Class A to C have been most addressed in drug discovery efforts. The natural ligands of GPCRs are highly variable ranging from small ions and photons to large glycoproteins, which indicates the important and versatile roles these proteins play in a vast number of biological processes. These are also the reasons why GPCRs have developed into a very 'druggable' class of targets for more than 30% of currently available drugs.[59] However, in the introduction we also mentioned the tremendous attrition along R&D pipelines, and suggested that detailed mechanism-based studies of drug-target interaction should be introduced in the early phases of drug discovery to prevent 'fail late, fail expensive' scenarios. For this we examined the gigantic 'pool' of GPCR ligands and retrospectively analyzed the 'kinotype' (kinetics features) of some cases. Without claiming to be exhaustive we have summarized a series of prototypic GPCR ligands that have known kinetics information (Table 2.2). We listed one representative (candidate) drug per target (26 targets in total) including their clinical indications. Several conclusions can be drawn from this table. Firstly, the existing kinetics data for GPCR ligands is nowhere near the number of affinity-based evaluations in the early phases of drug discovery. The sum of targets presented here is far behind the total population of 'druggable' GPCRs, estimated to be 300.[60,61] Clearly, ligand-receptor binding kinetics has been overlooked and less investigated in the past. Secondly, the range of drug-target residence times, reflected by $t_{1/2}$ in the table, varies from seconds to hours. Most of these are in line with the clinical applications of the related drug. For instance, patients with allergy can benefit from the long-lasting effect by desloratidine ($t_{1/2}$ > 6 h) in relieving nasal congestion, or patients with COPD from taking tiotropium ($t_{1/2}$ = 27 h) for a durable bronchodilatory effect. In both cases, their clinical indications favor sustained target occupancy. On the contrary, for some marketed drugs, serious adverse effects could go along with the desired effects due to unwanted kinetic rates. This is exemplified by clopidogrel, which is an antiplatelet agent used to inhibit the formation of blood clots. However, its irreversible inhibitory effect may prolong or exacerbate bleeding.[62] Another case is represented by lofentanil for analgesia. Although its longer duration of action has an advantage for certain types of analgesia,[63] it is still unsuitable for most practical applications.[64] Instead, short-acting derivatives such as sufentanil or remifentanil are preferred for medical use in human surgical procedures.[65,66] One can speculate that such clinical limitations could be avoided or at least foreseen if kinetics were to be incorporated in the early phase of candidate selection.

2.5 Structure-kinetics and structure-affinity relationships

Thus far the abovementioned analyses in retrospect are still largely based on 'hindsight' information; hardly any structure-kinetics relationship studies (SKR), in prospect, have been reported previously. Therefore, we should like to propose a strategy for compound optimization that combines an extensive structure-kinetics relationship study (SKR) with a classical structure-affinity relationship study (SAR). It is envisioned that this added metric, i.e., binding kinetics or the 'kinotype' of a given compound, offers several advantages over the traditional and simple SAR paradigm:

1) A better understanding of the molecular mechanism of action. This includes detailed characterization of not only the bound states under equilibrium conditions (SAR) but also the entire drug-target interaction that comprises metastable intermediate states and transition states (SKR).[14,67] Such gained knowledge offers rationales for efficient drug design.

2) A more steered drug design and development. Different targets may have distinct kinetics preferences. Aiming for long or short RT compounds is a crucial consideration in early phase discovery to triage and advance the best leads towards clinical applications.[16]

3) An efficient translation from *in vitro* to *in vivo* settings. This may decrease the prevalence of the 'fail late, fail expensive' scenario, especially considering that lack of efficacy is one of the major reasons for drug attrition.[68,69]

In addition, a detailed SKR study also describes the association rate of the ligand-receptor interaction, which has been less investigated and is often thought to be diffusion-limited.[14] As a consequence, this could lead to the assumption that optimizing for a long residence time is tantamount to optimizing the binding affinity, since $K_D = k_{off} / k_{on}$ and k_{on} reaches an (identical) limit. However, Vilums *et al.* have recently reported a thorough SKR study on the CCR2 receptor, in which it was shown that this general assumption is not necessarily valid.[18] They documented that the compounds' on-rates varied significantly from 0.01 $nM^{-1} \cdot min^{-1}$ to 0.0003 $nM^{-1} \cdot min^{-1}$ —more than three orders-of-magnitude from the diffusion-limited value (approximately 10^{10} $M^{-1} \cdot min^{-1}$)[1]. It is also notable that the affinity difference of two diastereomers in that paper with K_i values of 3.6 nM and 289 nM, was predominantly caused by their 18-fold difference in the on-rate, rather than their very similar RTs (135 min and 77 min). Such valuable information can

only be obtained by a detailed SKR study, which has not been reported for many GPCRs so far.

Evidently, a detailed SKR offers added value to the traditional metric of affinity. This new strategy of combining SAR and SKR can be expected to further enhance the success of drug discovery and development. To further illustrate the importance of incorporating SKR into the pipeline of early phases of drug research, in the following part of this chapter we will primarily address small molecules targeting class A and B GPCRs, which have been reported to have optimized binding kinetics, more specifically dissociation kinetics. Specific evidence will be given for three 'long RT' targets and one 'short RT' target; muscarinic M_3, tachykinin NK_1 and CRF_1 receptor, and dopamine D_2 receptors, respectively, since these targets have been (most) extensively studied in this area.

2.6 Drug-target residence time for class A GPCRs

Muscarinic receptors

Muscarinic receptors, or muscarinic acetylcholine receptors (mAchRs), are a group of class A GPCRs, which are endogenously activated by acetylcholine.[70] To date, five subtypes of muscarinic receptors are identified, namely M_1-M_5.[71,72] These receptors can be further categorized into two broad groups based on their primary coupling efficiency to G proteins; M_2 and M_4 muscarinic receptors couple to the pertussis toxin-sensitive $G_{i/o}$ proteins, while M_1, M_3 and M_5 muscarinic receptors to $G_{q/11}$ proteins.[70,73] Of all five muscarinic subtypes, M_3 receptor is located in the smooth muscles of blood vessels throughout the body as well as in the lung. Hyperactivation of the lung M_3 receptor can cause over constriction of smooth muscle, such as that observed during bronchoconstriction. Thus, antagonizing M_3 receptor can lead to relaxation of airway smooth muscles and result in symptom relief of chronic obstructive pulmonary disease (COPD).[74,75] Additionally, for the treatment of chronic illness, long duration of action (preferably 24 h) is an important feature of drugs that enables both prolonged efficacy and patient compliance.[76] Therefore, the treatment of COPD can benefit from a long-

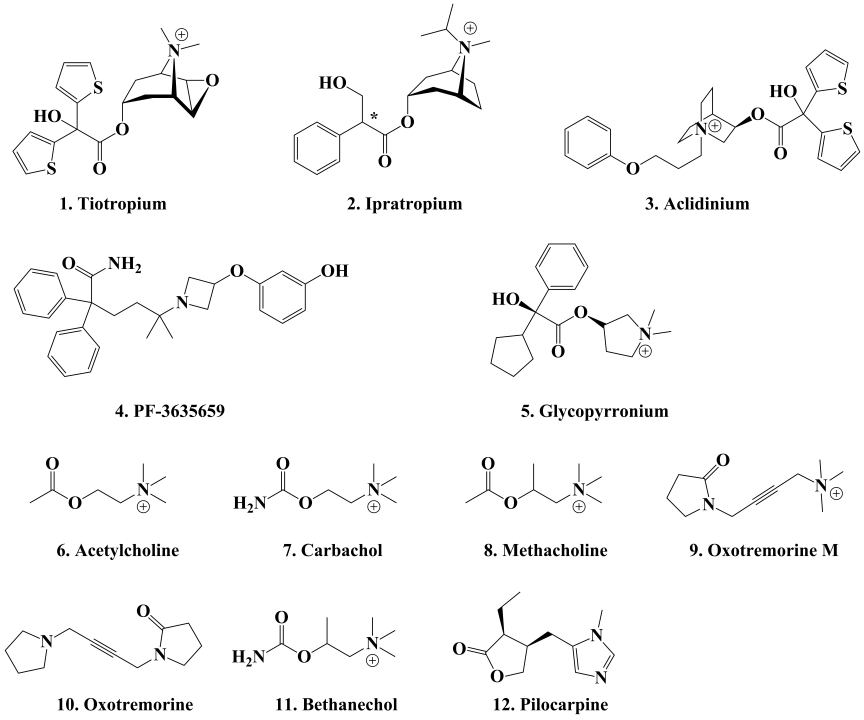


Figure 2.5 | Structures of small molecule M_3 muscarinic receptor ligands.

acting muscarinic antagonist (LAMA), as evidenced by tiotropium and other M_3 antagonists summarized below.

1. Tiotropium

Tiotropium is a long-acting anticholinergic bronchodilator, which is currently marketed under the trade name Spiriva™ (Figure 2.5, Compound 1).[77-79] Given its long *in vivo* duration of action, several groups, in retrospect, performed *in vitro* time-dependent IC_{50} value analysis to obtain the accurate affinity and binding kinetics of tiotropium.[29,80] It was found that equilibrium is reached only after 18-20 h in a radioligand binding assay. This phenomenon is consistent with the theory by Motulsky and Mahan that a long incubation time is needed for a radioligand to reach equilibrium in the presence of a slowly dissociating competitor.[34] Thus, it also explains that different affinities were published by different groups; after a period of 20 h incubation, the K_i value of tiotropium was 8 pM,[29,80] while after only 4 h incubation, its K_D value was 0.33 nM.[78] The $t_{1/2}$ of [^{3}H]-tiotropium was 34.6 h at room temperature, which was much longer than ipratropium (Figure 2.5, Compound 2; $t_{1/2}$ = 0.26 h, Table 2.3), a relatively short-acting agent requiring up to four doses per day.[74,78] Similarly, a kinetics study performed by Dowling and Charlton using a competition association assay has also demonstrated that tiotropium has a very long $t_{1/2}$ (7.7 h) at room temperature,[29] which, however, is shorter than the value (34.6 h) reported by Disse *et al.*[78] This may be due to the difference in their buffer for membrane preparation and / or the binding buffer for kinetic measurements, for instance, the presence of sodium ions. Likewise, tiotropium has an even shorter dissociation half-life (46.2 min) under mock physiological conditions at 37 °C, where the ionic strength (including Na^+, Ca^{2+}, K^+, Mg^{2+} and Cl^- ions) of the assay buffer was increased.[81] This example furthermore highlights the importance of careful choices in assay development for kinetic measurements. Another important pharmacological feature of tiotropium is its 'kinetic receptor subtype selectivity', namely a longer dissociation half-life at the M_3 receptor, 34.7 h, than at the M_1 and M_2 receptors (14.6 h and 3.6 h, respectively).[78] In contrast, tiotropium's affinities at these receptors were similar and in the subnanomolar concentration

Table 2.3 | Binding kinetics of M_3 muscarinic receptor ligands.

Nr	*Cmpd*[a]	*Affinity (K_i or pK_i)*[b]	*Dissociation half-life ($t_{1/2}$)*[c]	*Ref*
1.	Tiotropium	8 pM	34.6 h	29,78
2.	Ipratropium	0.69 nM	0.26 h	78
3.	Aclidinium	18 pM	10.7 h	80
4.	PF-335659	132 pM	> 24 h	96
5.	Glycopyrronium	10.04	6.3 h	80
6.	Acetylcholine	4.87	7.8 s	98
7.	Carbachol	4.09	6.3 s	98
8.	Methacholine	4.52	6.0 s	98
9.	Oxotremorine-M	4.61	7.2 s	98
10.	Oxotremorine	5.61	2.6 s	98
11.	Bethanechol	3.71	3.7 s	98
12.	Pilocarpine	4.78	3.0 s	98

[a] Compound names and synonyms used in original references. [b] Affinity, expressed as K_i values or pK_i as reported in original references; result on human receptor unless mentioned otherwise. [c] Dissociation half-life at room temperature.

range.[78] Taken together, these features make tiotropium the most widely used LAMA worldwide so far.[81,82]

To understand the molecular basis of the exceedingly long RT of tiotropium, Tautermann *et al.* performed a 'kinetic mapping' of its binding sites and the 'exit' channel from the M_3 receptor by testing the kinetics of tiotropium at mutant M_3 receptors.[83] They found that the slowly dissociating profile of tiotropium was attributed to interactions in the binding site particularly with $N508^{6.52}$ ($N507^{6.52}$ on the rat M_3 receptor, see Figure 2.6). Importantly, this residue appeared to 'anchor' tiotropium at the receptor via directly interacting with its hydroxyl-group and ester-group so as to restrict the movement of the ligand towards the exit channel. Consequently, tiotropium's RT was 45-fold longer on the wild type M_3 receptor than that of its analogue lacking the hydroxyl-group, while little difference was observed at the $N508^{6.52}$A mutant.

Furthermore, a recent structural biology study of the M_3 receptor (from rat) co-crystallized with tiotropium (PDB code: 4DAJ) provided a clear image for the molecular mechanism behind its long RT profile.[84] As presented in

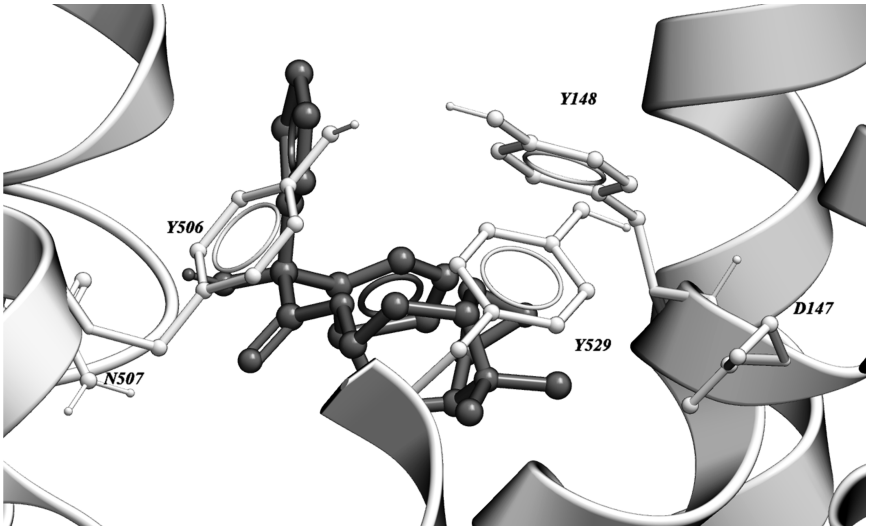


Figure 2.6 | The co-crystal structure of tiotropium in the rat M_3 receptor.[84] This figure was generated with ICM Browser v3.7 (Molsoft) from PDB code: 4DAJ. Tiotropium (black) binds within the pocket. Three tyrosine residues, Y148$^{3.33}$, Y506$^{6.51}$ and Y529$^{7.39}$, together prevent the ligand from moving out of the receptor. N507$^{6.52}$ interacts with the carbonyl and hydroxyl groups through H-bonds, while the ligand's typical quaternary ammonium group interacts with D147$^{3.32}$.

Figure 2.6, tiotropium binds deeply in the receptor core and is covered by an aromatic 'lid' comprised of three conserved tyrosines—Y148$^{3.33}$, Y506$^{6.51}$ and Y529$^{7.39}$. This aromatic 'lid' nearly occludes the ligand from the solvent thus preventing it from being 'wetted' by water molecules and then 'washed' off the binding pocket. In addition, the abovementioned N507$^{6.52}$ interacts with the carbonyl and hydroxyl groups of tiotropium through H-bonds, while the ligand's typical quaternary amine interacts with D147$^{3.32}$.

The elucidation of the co-crystal structure of tiotropium in the rat M_3 receptor also facilitated molecular dynamic simulations to characterize the pathway by which tiotropium binds to and dissociates from the rat M_3 receptor.[84] In contrast to a simple one-step dissociation process, the ligand appeared to firstly leave the orthosteric ligand binding pocket and then 'pause' at an extracellular 'vestibule', forming a loosely connected intermediate state, before tiotropium finally dissociated from the receptor. During this process,

the first step formed a large energy barrier that involved the aromatic 'lid' (Y148$^{3.33}$, Y506$^{6.51}$ and Y529$^{7.39}$) around the charged ligand head group opening up, while the second step posed a smaller energetic barrier. In this sense, the RT of tiotropium is greatly determined by the first step, which is rate-limiting for the ligand dissociation process.

As expected from the kinetic binding profile of tiotropium, an insurmountable antagonist behavior was observed in a functional reversibility experiment. This was detailed by Casarosa *et al.* during the preclinical evaluation of several long- and short-acting muscarinic antagonists, where tiotropium was pre-incubated for 15 min before the addition of the agonist muscarine in the inositol phosphate accumulation assay.[80] Fitting the dose ratios over a large range of tiotropium concentrations (10^{-10}-10^{-5} M) generated a Schild plot with a slope of 1.29, higher than unity. Such a value indicated the insurmountable M_3R antagonism of tiotropium, which was a result of a hemi-equilibrium due to its long M_3R residence time profile.[37]

Taken together, the *in vitro* results mentioned above combined with further evidence unveil the molecular basis of the long RT profile of tiotropium. These results correlate with this compound's long *in vivo* duration of bronchoprotection (> 24 h) as determined in a model of acetylcholine-induced bronchoconstriction in anesthetized dogs.[80] Moreover, despite the possible influence of drug metabolism and pharmacokinetic factors,[85] the clinical profile of tiotropium in COPD highlights an inextricable link between long receptor RT and long duration of action that enables a simple, once-daily dosage regime.[77,86,87]

2. Aclidinium

Aclidinium (Figure 2.5, Compound 3) is a long-acting, inhaled muscarinic antagonist recently approved by the FDA as a maintenance treatment for COPD.[88] The synthesis and biological evaluation of aclidinium and its analogues were elaborately reported by Prat *et al.* and Gavalda *et al.*[20,89] This antagonist was specifically designed for a maintained bronchodilatory efficacy with fewer unwanted systematic anticholinergic effects, such as dry mouth (reported in 11.6% of patients treated with tiotropium bromide versus 3.5%

of patients treated with placebo), glaucoma, constipation, increased heart rate, and urinary retention.[90] According to Prat *et al.*, aclidinium had a rapid hydrolysis in human plasma, hence minimizing the class-related systematic side effect. However, such a fast pharmacokinetics profile of aclidinium did not influence its long duration of action (over 24 h), as evaluated in an animal model.[20] This phenomenon was attributed to aclidinium's slowly dissociating profile from the M_3 receptor.

Compared to tiotropium, aclidinium had a similar affinity for the M_3 receptor (K_i = 18 pM), while its $t_{1/2}$ (10.7 h) was approximately two-fold shorter (Table 2.3).[80] In another study, Gavalda *et al.* used radiolabeled aclidinium and found a K_D value of 0.32 nM; combined with $t_{1/2}$ of 29.24 h, which was shorter than [^{3}H]-tiotropium (62.19 h).[20]

In vitro functional activity and *in vivo* duration of bronchoprotection of aclidinium was also examined by Gavalda *et al.*[20] More specifically, they used the isolated guinea pig trachea and treated it with carbachol to generate dose-dependent contraction. A 60 min pretreatment with aclidinium or tiotropium shifted the concentration-response curves of carbachol to the right. Along with the potency shift, tiotropium also suppressed the maximal agonist effect while aclidinium did not. Such a result is indicative of the relatively shorter RT of aclidinium than that of tiotropium at the M_3 receptor.

In addition to the characterization of aclidinium's functional activity, the onset of action of this compound was also studied in the carbachol-induced contraction assay. Notably, aclidinium displayed a faster onset of action ($t_{1/2}$ = 6.8 min, t_{max} = 35.9 min) than tiotropium ($t_{1/2}$ = 13.6 min, t_{max} = 61.2 min). For the *in vivo* duration of bronchoprotection, the effect half-life of aclidinium (defined as the time taken to reduce the maximal bronchoconstriction by 50%) was 29 h. This duration of action was considerably longer than that of ipratropium (8 h) yet shorter than tiotropium (64 h). Likewise, Casarosa *et al.* reported that aclidinium and tiotropium displayed different levels of bronchoprotection at 24 h after equi-effective dose administration (tiotropium = 35%, aclidinium = 21%).[80] Clearly, these *in vivo* results are in line with the *in vitro* binding kinetics.

Furthermore, compared to tiotropium's once-daily dose regime, aclidinium required a twice-daily dose regime for a 24 h bronchodilation effect in clinical trials.[91-95] Such a difference appears to be derived from their divergent RTs at the M_3 receptor. In addition, aclidinium's faster onset of action, mostly due to its fast association rate, can provide quicker symptom relief as compared to tiotropium.

3. PF-3635659

The synthesis and biological evaluation of PF-3635659 (Figure 2.5, Compound 4) and its analogues was reported by Glossop *et al.*[96] This study nicely exemplifies a systematic combination of both a structure-affinity and structure-kinetics relationship study for early-phase drug design and development. More specifically in this study, Glossop *et al.* demonstrated that a *gem*-dimethyl substitution adjacent to the basic amine moiety of PF-3635659 exerted a profound effect on the dissociation rate. As evidence, the $t_{1/2}$ of the initial *gem*-dimethyl-free compound (38 min) was extended to over 1440 min, indicating the importance of the *gem*-dimethyl substitution for attaining ligand receptor RT. Further chemical modifications on the heterocyclic ring and the right side of the phenyl ring induced corresponding changes in ligand affinity and kinetics, which eventually led to the discovery of the candidate compound, i.e., PF-3635659 (Compound 47 in the original paper). Following-up binding kinetics characterization of this compound in a competition association assay revealed that it had an on-rate of 1.05×10^7 $M^{-1}\cdot min^{-1}$, slower than tiotropium and ipratropium ($k_{on} = 2.12 \times 10^8$ $M^{-1}\cdot min^{-1}$ and 1.00×10^9 $M^{-1}\cdot min^{-1}$) and an off-rate of 1.39×10^{-4} min^{-1}, translating into a $t_{1/2}$ of more than 24 h (Table 2.3).

Importantly, the *in vivo* onset and duration of action data for PF-3635659 were in line with its *in vitro* binding kinetics. The profiling of PF-3635659 in a conscious dog model of bronchoconstriction illustrated a slower onset of action compared to ipratropium and tiotropium, with yet a longer duration of action (> 24 h) than ipratropium.[96] This compound has now progressed into a phase II clinical trial. Data from healthy volunteers demonstrated that PF-3635659 provided efficacious bronchodilation over 24 h from a single inhaled dose, thus confirming the suitability of PF-3635659 as a novel once-daily inhaled muscarinic M_3 receptor antagonist for the treatment of COPD.

4. Glycopyrronium

Glycopyrronium (Figure 2.5, compound 5) is the cation and active moiety of glycopyrronium bromide, of which the dry-powder formulation is also known as NVA237.[81] *In vitro* binding kinetics profiling of this compound

in a radioligand competition association assay revealed a dissociation rate of 0.11 ± 0.02 h^{-1} from the M_3 receptor, equal to a dissociation $t_{1/2}$ of 6.3 h (Table 2.3). This value was much longer than the short-acting M_3 antagonist ipratropium (0.22 h) but shorter than tiotropium (27 h).[80] However, glycopyrronium had a more rapid rate of onset of action (3- to 4.8-fold) than tiotropium, as determined in an *in vitro* calcium assay and rat tracheal strip assay.[81] This profile was similar to that obtained with ipratropium bromide in preparations of guinea-pig and human airways.[97]

Notably, glycopyrronium also displayed higher equilibrium binding and kinetic selectivity for M_3 versus M_2 receptors as compared to both tiotropium and ipratropium.[80,81,97] Its kinetic selectivity resulted from a 16.5-fold longer receptor RT at the M_3 receptor than at the M_2 receptor, which was higher than tiotropium (10.4-fold) and ipratropium (7.3-fold). Such a property may provide a better therapeutic window.

5. M_3 receptor agonists

The RTs of seven M_3 agonists (Figure 2.5, Compound 6-12) were recently reported by Sykes *et al.*[98] These agonists are acetylcholine, carbachol, methacholine, oxotremorine-M, oxotremorine, bethanechol and pilocarpine, and are not very selective. The data, however, were only collected on the M_3 receptor subtype. Among the seven agonists, oxotremorine displayed the shortest $t_{1/2}$ at the M_3 receptor (2.6 s), while acetylcholine had the longest receptor RT ($t_{1/2}$ = 7.8 s). In general, these agonists' off-rates were much faster than that of the abovementioned M_3 antagonists (Table 2.3). Further *in vitro* functional characterization of the M_3 agonists demonstrated that they had different relative agonist efficacies. Notably, Sykes *et al.* found that there was no relationship between agonist efficacy and the equilibrium binding affinity of each agonist. Interestingly, when efficacy was compared with the dissociation rate constant, the two were highly correlated. This result suggests a relationship between the duration of agonist binding at the receptor and the intrinsic efficacy, a finding also reported by Guo *et al.* and Hoeren *et al.* at the adenosine A_{2A} receptor and at the α_{2A}-adrenoceptor.[32,99] Importantly, such a finding again emphasizes that equilibrium models and assays alone are not sufficient to describe a dynamic signaling system; instead, a combination of kinetic models alongside the traditional affinity determination might be

preferred to better capture the nature of efficacy and to develop efficacious drugs for GPCRs.[98]

In summary, several case studies of long acting M_3 receptor antagonists suggest their sustained pharmacological effect lies in these compounds' long receptor occupancy time. The design and development of long residence time antagonists may provide further candidate drugs with once-daily application for COPD. We also included the kinetics data of several M_3 agonists, since they provide important information that agonist efficacy may be correlated to its drug-target residence time rather than the commonly tested equilibrium affinity. This further indicates the importance of combining both binding and kinetics information in the early phase of drug design and development.

Tachykinin receptors

Tachykinin receptors comprise three different subtypes, namely the NK_1R, NK_2R and NK_3R, which can be activated by tachykinin peptides, including Substance P (SP), neurokinin A (NKA) and neurokinin B (NKB).[100-102] The three members of the neurokinin receptor class are differentiated by their varying affinities for these three tachykinins, which are SP > NKA > NKB for the NK_1R, NKA > NKB > SP for NK_2R and NKB > NKA > SP for NK_3R (for reviews, see[100-102]). All three subtypes are functionally coupled to $G_{q/11}$, which leads to the activation of phospholipase C-IP_3/DAG signaling and results in elevation of intracellular Ca^{2+} levels.[102] The localization of the tachykinin receptors varies between subtypes in the human body: the NK_1R and NK_3R are prominent both in the central nervous system (CNS) and in peripheral tissues, while the NK_2R is widely expressed in the smooth muscle of the gastrointestinal, respiratory, and urinary tracts and to a much lesser extent in the CNS.[102-104] A large body of preclinical evidence has suggested that pharmacological or gene manipulation of the NK_1R has potential clinical utility in the treatment of chronic pain, migraine, neurogenic inflammation and emesis.[105-107] These diseases could benefit from therapeutics with a long duration of NK_1R antagonism.

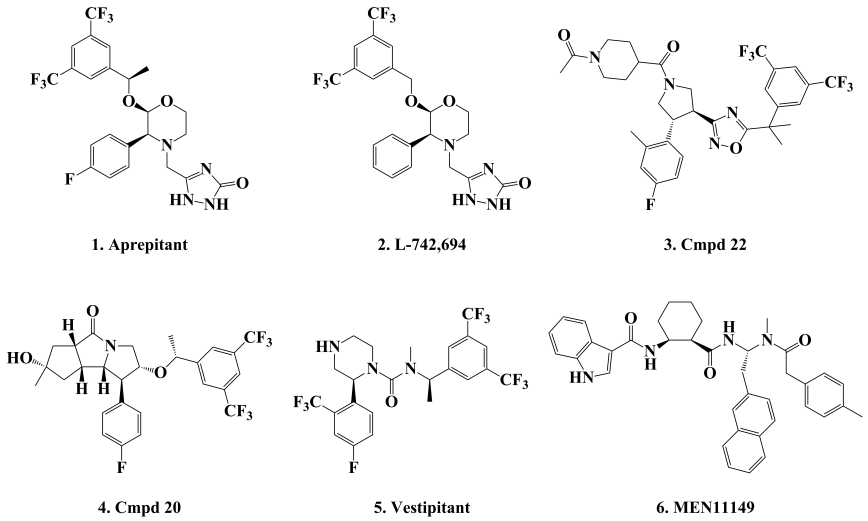


Figure 2.7 | Structures of small molecule NK_1 receptor antagonists.

1. Aprepitant

Aprepitant, also known as L-754,030, MK0869 or Emend (Figure 2.7, Compound 1),[19,108-110] is the only tachykinin receptor antagonist on the market to date. It is a selective, slowly dissociating NK_1 antagonist with a $t_{1/2}$ of 154 min at 22 °C (Table 2.4).[19] In comparison, it was found by Cascieri *et al*. that the dissociation rate of the radiolabeled NK_1's natural ligand SP (i.e., ^{125}I-[Tyr^8]-SP) was too rapid to be measured accurately at a comparable temperature.[111] At 15 °C, this peptide dissociates with $t_{1/2}$ = 46 min and 0.2 min for the G protein-coupled and -uncoupled receptor states, respectively.[112] Evidently, aprepitant had a much longer residence time on the NK_1 receptor than the natural ligand which has been speculated to be the reason for its high potency and *in vivo* efficacy.

As expected from a slowly dissociating ligand, aprepitant's activity was found to be insurmountable in functional assays compared to other, fast dissociating NK_1R antagonists. This functional effect was associated with its long-lasting *in vivo* efficacy, a finding shared by many authors.[19,108,110] One of the most elaborate studies reported on aprepitant was conducted by

Table 2.4 | Binding kinetics of NK_1 receptor antagonists.

Nr	*Cmpd*[a]	*Affinity (K_i, nM)*[b]	*Dissociation half-life ($t_{1/2}$)*[c]	*Ref.*
1	Aprepitant	0.019	154 min (22 °C)	19
2	L-742,694	0.037	27 min (22 °C)	111
5	Vestipitant	0.027	59.7 min (37 °C)	119

[a] Compound names and synonyms used in original references. [b] Affinity, expressed as K_i values that were reported in original references; results on human receptor unless mentioned otherwise. [c] Dissociation half-life at different temperatures indicated in brackets.

Lindström *et al.*[108] Several functional experiments (i.e., pre-incubation, co-incubation and washout experiments) were used to reaffirm that aprepitant was a competitive yet pseudo-irreversible antagonist with slow functional reversibility. Next to the measurement of its functional interactions *in vitro*, the authors also examined the pharmacokinetic/pharmacodynamics relationship of aprepitant *in vivo* by using the gerbil foot tap (GFT) assay, a model reflecting central NK_1R activation.[113] It was found that the duration of GFT inhibition by aprepitant outlasted the time course of its plasma or brain concentrations, indicating that its long duration of action was indeed more likely due to a sustained receptor blockade rather than a slow pharmacokinetic half-life. In contrast, two other structurally unrelated NK_1 antagonists, CP-99994 and ZD6021, demonstrated rapid functional reversibility that was in line with their pharmacokinetic profile.[108] Furthermore, these authors also examined *ex vivo* receptor occupancy by autoradiography, reaffirming that time-dependent inhibition of GFT by aprepitant correlated well with NK_1 occupancy in the gerbil brain, a finding that was shared by Duffy *et al.* in 2002.[109] Taken together, all *in vitro* and *in vivo* results provide strong evidence that aprepitant is a slowly dissociating NK_1R antagonist.

2. L-742,694

Aprepitant was originally developed from L-742,694 (Figure 2.7, Compound 2),[109,111,112] which was shown to be a pseudo-irreversible yet competitive antagonist by Cascieri *et al.* in 1997.[111] The $t_{1/2}$ of [^{3}H]-L-742,694 (27 min, Table 2.4) at 22 °C is considerably shorter than the half-life of aprepitant but longer than the natural ligand SP.[19,111,112] Its functional interaction was

further characterized by Cascieri *et al*. by using both human and rat NK_1 receptor.[111] Interestingly, its nature of NK_1 receptor antagonism was species related as L-742,694 was insurmountable on the hNK_1 receptor but not on the rNK_1 receptor. A follow-up mutational analysis revealed that mutating $H197^{5.39}$ in TM5 into Serine reduced L-742,694 affinity and simultaneously abolished its functional insurmountability at the hNK_1 receptor, making it a key amino acid for L-742,694 interaction and function. When testing several structural analogues of L-742,694, the authors found that the addition of the triazoline moiety (as in L-742,694) converted a surmountable antagonist into an insurmountable one, possibly by slowing the dissociation rate.[111]

3. Compound 22

Aprepitant has formed the basis for the discovery of more potentially long acting NK_1R antagonists. Young *et al*. developed a series of pyrrolidine-carboxamides and oxadiazoles based on aprepitant, aiming for feasible clinical candidates for a once-daily dosing regimen.[114] Their screening strategy was to find compounds with enduring functional activity *in vitro* and long duration of action *in vivo* at lower drug levels as to obtain an improved safety profile. Overall, Compound 22 (Figure 2.7, Compound 3) was found to be the best compound with efficacious functional activity in an IP-1 functional assay and long duration of action (over 24 h) in the GFT model. During the course of compound optimization, the authors were also able to establish a kinetically informed structure-activity relationship. They concluded that both receptor binding affinity and functional insurmountability are highly sensitive to both absolute and relative stereochemistry,[114] which was reaffirmed for another compound series by Morriello *et al*.[115]

4. Compound 20

Morriello *et al*. employed virtually the same screening technique as described by Young *et al*.[114,115] to develop both a series of long acting 5,5-fused pyrrolidines[115-117] and later a series of 5,5,5-fused tricyclic antagonists with even slower dissociation rates, with cyclopentane compound 20 (Figure 2.7,

Compound 4) being the most active.[118] The authors found that increasing the overall compound rigidity as well as modifying some other specific molecular components, such as by the addition of a substituent on the pyrrolidine nitrogen, increased functional insurmountability.

5. Vestipitant and its analogues

Vestipitant (Figure 2.7, Compound 5) has a $t_{1/2}$ of 59.7 min (Table 2.4, 37 °C) from the human NK_1R.[119] It is an insurmountable yet competitive antagonist with long duration of action (over 8 h) in the *in vivo* GFT model.[119] Compared to other structural analogues of vestipitant, it appeared that certain features such as the benzylic substitution patterns and its stereochemistry were important for vestipitant's mode of antagonism,[119] which was reaffirmed in another publication by Di Fabio *et al.*[120] Surprisingly, even a small, hydrophobic substituent, for instance a methyl substituent, played an important role in determining the magnitude of an antagonist's insurmountability and duration of action.[120]

6. MEN1149

This peptidomimetic compound (Figure 2.7, Compound 6) set the example that long acting small molecule antagonists can be developed from short acting peptide antagonists, in this case from FK888, by simple structural modifications. The main modification introduced, originally to increase metabolic stability, was the β-aminocycloalkyl carboxylic acid residue replacing FK888´s prolyl group.[121] Interestingly, these modifications turned the purely surmountable FK888 into the insurmountable MEN1149 with much slower reversibility during organ bath washout assays and a longer duration of action *in vivo* of over 3 h.[121] The authors speculated that introduction of the β-amino cycloalkyl carboxylic acid caused a slower rate of dissociation which was likely to be responsible for the change in type antagonism, but only provided circumstantial evidence and no direct kinetics measurements.[121]

Overall, the examples summarized above provide a strong indication that NK_1R are amongst the targets for which slowly dissociating antagonists could offer therapeutic advantages.

Dopamine receptors

Dopamine receptors are a group of class A GPCRs, which are named after their endogenous ligand dopamine.[122] To date, five subtypes of dopamine receptors have been identified, namely D_1 to D_5.[123] These receptors can be further categorized into D_1-like (D_1 and D_5) and D_2-like (D_2, D_3 and D_4) subfamilies, based on their similarities in sequence, pharmacology and ability to stimulate or inhibit adenylyl cyclase activity: the D_1-like subfamily couples to G_s and mediates excitatory neurotransmission, while the D_2-like (D_2, D_3 and D_4) subfamily couples to $G_{i/o}$ and mediates inhibitory neurotransmission.[124] Dopamine receptors, particularly D_1 and D_2 receptors, are prominent in the vertebrate CNS,[123,125] indicating their functional importance in neuronal signaling (for reviews, see[126-131]). To date, numerous drugs targeting the D_2 receptor are available on the market. Antagonizing the dopamine D_2 receptor has been reported as the molecular foundation of schizophrenia treatment.[132] Currently, all known marketed anti-schizophrenia drugs bind to the D_2 receptor and are supposed to modulate dopamine hyperfunction.[26,133] In general, these drugs can be categorized into two groups. The first generation or the so-called typical antipsychotics (e.g., haloperidol) can effectively treat positive schizophrenia symptoms (i.e., hallucination and delusions), yet they invoke concomitant on-target adverse effects, such as extrapyrimidal symptoms (EPS) and hyperprolactinaemia, through excessive blockade of the D_2 receptor. The second generation, also known as 'atypical' antipsychotics, are defined according to their 'clozapine-like' properties, i.e., low incidence of the on-target/mechanism-based side effects, which are mostly attributed to their short residence times at the D_2 receptor.[134] Other theories have also been proposed to explain 'atypicality'. One of these is the multi-receptor hypothesis or polypharmacology.[180] Many atypical antipsychotics were found to have high affinity at other neurotransmitter receptors in addition to D_2 receptors, in particular at serotonin 5-HT_{2A} receptors, while typical antipsychotics, like haloperidol, bind more specifically to D_2 receptors.[135] However, fully occupying serotonin 5-HT_{2A} receptors with different antipsychotics at

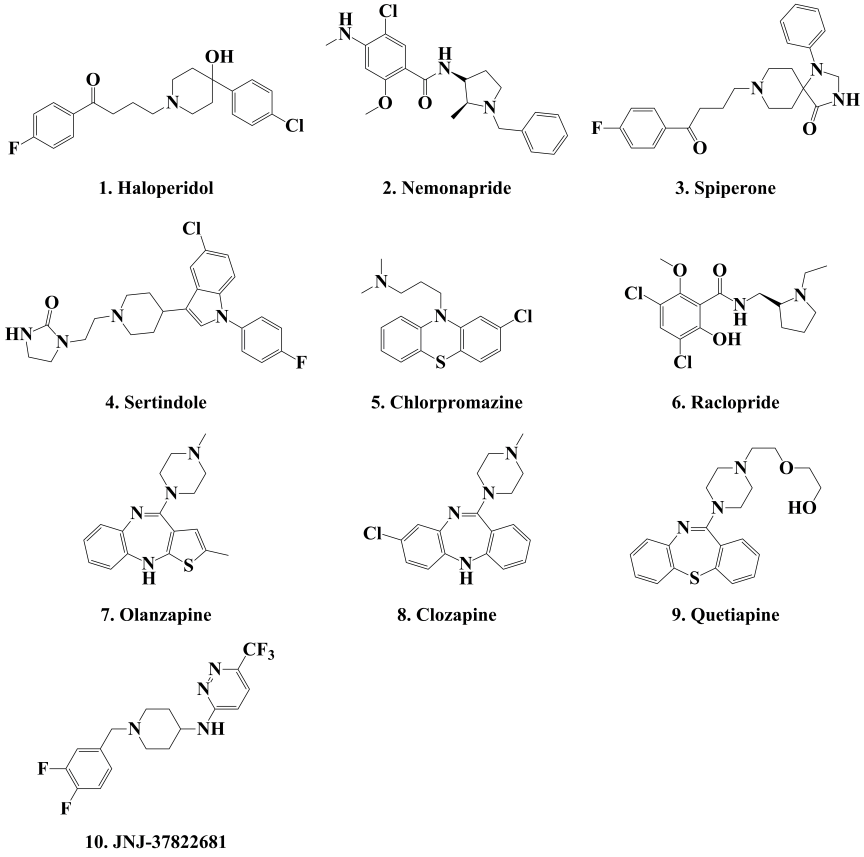


Figure 2.8 | Structures of small molecule D_2 receptor antagonists.

clinically relevant doses did not induce EPS to the same level.[134] Hence, the atypicality is more likely connected to the compounds' short residence times at the D_2 receptor than their antagonism at the 5-HT_{2A} receptors.

Additionally, it is worth mentioning that interaction of atypical antipsychotics with additional receptors may cause undesired off-target side-effects—distinct from its on-target side-effect (e.g., EPS and hyperprolactinaemia), such as $5HT_{2C}$ receptors (weight gain), α_1-adrenoceptors (orthostatic hypotension, reflex tachycardia, and hypnosedation), α_2-adrenoceptors (tachycardia), histamine H_1 receptors (sedation and weight gain), and muscarinic receptors (blurred vision, dry mouth, constipation, and cognitive impairment).[135] These side-effects can logically be minimized by decreasing the compound's affinity or residence time on the off-targets.

Contrary to aforementioned cases of other GPCRs, where long RT ligands are desired for optimal clinical outcomes, short residence time D_2 receptor antagonists are preferred, since they will supposedly induce less on-target 'mechanism-based toxicology'.[25,35] In the following part of this section we will focus on published binding kinetics data of dopamine D_2 antagonists and the related benefit from short RT in clinical applications.

1. Haloperidol and other slowly dissociating D_2 receptor antagonists

Haloperidol (Figure 2.8, Compound 1) was approved by the U.S. Food and Drug Administration (FDA) in 1967 and marketed as Haldol in U.S. and other countries. Haloperidol exhibited high-affinity antagonism for human dopamine D_2 receptor (1.8 nM) with a k_{off} of 0.01 s^{-1}, equal to a $t_{1/2}$ of 72.4 s (Table 2.5).[135] Notably, its $t_{1/2}$ was substantially changed when the kinetics were tested at rat striatal membranes (i.e., $t_{1/2}$ = 42 min), indicating significant species differences.[134] One might argue that the absolute value of haloperidol's $t_{1/2}$ is much smaller than other classical slowly dissociating GPCR antagonists, such as aforementioned NK_1R antagonist aprepitant ($t_{1/2}$ = 154 min). It should be realized that the time scale for endogenous dopamine concentration burst can be within a millisecond to second range, which is much shorter than the $t_{1/2}$ of haloperidol.[136] In this sense, the receptor blockade by haloperidol is already too lengthy to allow normal physiological responses to fast and small changes in the neurotransmitter concentration.

Table 2.5 | Binding kinetics of D_2 receptor antagonists.

Nr	*Cmpd*[a]	*Affinity (K_i, nM)*[b]	*Dissociation half-life ($t_{1/2}$)*[c]	*Ref*
1	Haloperidol	1.8	72.4 s	135
2	Nemonapride	0.025 (rat)	355 min (rat)	134
3	Spiperone	0.1 (rat)	200 min (rat)	134
4	Sertindole	1.2 (rat)	47 min (rat)	134
5	Chlorpromazine	1.3 (rat)	35 min (rat)	134
6	Raclopride	1.6 (rat)	28 min (rat)	134
7	Olanzapine	6.4 (rat)	18 min (rat)	134
8	Clozapine	137	14.5 s	135
9	Quetiapine	67.6 (rat)	23 s (rat)	139
10	JNJ-37822681	158	6.5 s	135

[a] Compound names and synonyms used in original references. [b] Affinity, expressed as K_i values that reported in original references; result on human receptor unless mentioned otherwise. [c] Dissociation half-life at room temperatures and on human receptors unless mentioned otherwise.

Next to the result from the direct kinetic binding assay at both human and rat D_2 receptor preparations, haloperidol was found to have long-lasting D_2 blockade by using an indirect kinetic measurement. Only 48% (lower than that of clozapine) of the total receptor population was recovered and able to bind to subsequently added [^{3}H]-spiperone after pre-incubating haloperidol for one hour with the receptor.[135]

The binding kinetics of other slowly dissociating D_2 receptor antagonists were elaborately studied by Kapur and Seeman.[134] The authors investigated the affinity and the kinetics of nine typical and atypical antipsychotics (main results are included in Table 2.5; compound structures in Figure 2.8). Among these compounds, nemonapride and spiperone had a $t_{1/2}$ of 355 min and 200 min, respectively, indicative of D_2 receptor blockade for more than 3 h; these two compounds were followed by sertindole (47 min), haloperidol (40 min), chlorpromazine (35 min), raclopride (28 min) and olanzapine (18 min) in terms of their $t_{1/2}$ values. In contrast, the two atypical antipsychotics clozapine and quetiapine displayed faster dissociation half-lives, i.e., less than 1 min. Furthermore, it is important to note that the k_{off} values varied a 1000-fold from 0.002 min^{-1} to 3.013 min^{-1}, yet less variation was found in k_{on}. Apparently, the rate at which antipsychotic agents come off the receptor (k_{off})

causes the variation in their affinity for the D_2 receptor, while differences in k_{on} do not account for that. Moreover, since atypical antipsychotics display relatively faster dissociation than typical ones, it can be inferred that the atypical antipsychotic effects are mostly attributed to their high k_{off} values for the D_2 receptor.

2. Clozapine

Clozapine was the first atypical antipsychotic drug on the market (Figure 2.8, Compound 8). Compared to haloperidol, clozapine had a relatively low affinity for the D_2 receptor (K_i = 137 nM) and a 5-fold shorter $t_{1/2}$ of approximately 14.5 s (Table 2.5).[135] This (partially) explained the observation by Kapus and Seeman, that clozapine reached equilibrium 100 times faster than haloperidol in the displacement assay.[134] Such a fast molecular interaction enabled clozapine to have a fast-on and then fast-off blockade of the D_2 receptor. Therefore, the receptor was readily responsive to the endogenous dopamine burst upon physical stimulation, hence lowering the risk of EPS or hyperprolactinaemia. This mechanism was further supported by the *in vivo* observation that clozapine caused a surmountable blockade of striatal dopamine receptors in contrast to cataleptogenic neuroleptics (the insurmountable control).[137] Moreover, clinical positron emission tomography (PET) analysis of a subject receiving clozapine (400 mg) revealed transiently high D_2 receptor occupancy (i.e., 80%) that rapidly declined to low levels (i.e., 15%) within 48 h. In comparison, D_2 receptor occupancy by haloperidol (5 mg) peaked at approximately 80%, but it declined more slowly over time, showing D_2 occupancy of over 10% even 3–5 days later.[138] This reaffirmed that fast kinetics may be favorable for a low incidence of mechanism-based, on-target, toxicology.

3. Quetiapine

Quetiapine (Figure 2.8, Compound 9), also known as Seroquel, Xeroquel or Ketipinor, is another marketed atypical antipsychotic approved for

schizophrenia treatment. Similar to the molecular properties of clozapine, Caboni *et al*. found that quetiapine displayed low D_2 receptor affinity (K_i = 67.6 nM) and a fast dissociation rate (1.8 min^{-1}), equal to a $t_{1/2}$ of 23 s, at a rat striatum homogenate (Table 2.5).[139] In the subsequent *in vivo* profiling, Caboni *et al*. performed time-dependent analysis of plasma prolactin levels, a surrogate of peripheral D_2 receptor blockade, after orally treating rats with vehicle or different dose of quetiapine or haloperidol. They found that compared to haloperidol treatment quetiapine displayed a short-lived increase of prolactin level, which was in line with its short RT profile at the D_2 receptor. Moreover, serial PET scans evaluating the D_2 receptor occupancy of quetiapine demonstrated that this compound dissociated very rapidly from the D_2 receptor.[140] Taken together, all *in vitro* and *in vivo* results provided strong evidence that quetiapine is a fast dissociating D_2 receptor antagonist.

4. JNJ-37822681

JNJ-37822681 (Figure 2.8, Compound 10) was developed by Janssen Pharmaceuticals. One of the most elaborate studies on JNJ-37822681 has been reported by Langois *et al.*.[135] The compound was initially selected from an indirect kinetic screening assay (for method, see[23,135]), where JNJ-37822681 was estimated to have a k_{off} similar to clozapine. Subsequently, a kinetic [^{3}H]-JNJ-37822681 binding experiment revealed that this compound had an extremely short $t_{1/2}$ (6.5 s, Figure 2.5) at the D_2 receptor, which was approximately 2-fold and 11-fold shorter than clozapine and haloperidol, respectively. In the follow-up *in vivo* profiling, JNJ-37822681 displayed a larger specific margin (compared with haloperidol) between the inhibition and blockade of apomorphine-induced behaviors, which represents a model for psychosis. This result was further reaffirmed in phase IIb clinical trials, where JNJ-37822681 displayed an efficacious antipsychotic effect but low propensity of EPS and prolactin liability.[141,142]

5. Overall structural determinants for binding kinetics at the dopamine D_2 receptor

Compared to the residence times of M_3R or NK_1R antagonists, D_2 receptor antagonists are preferred to have a short RT to circumvent on-target side effects. It is therefore highly desired to analyze the structural determinants that increase ligand dissociation from the receptor for future rational drug design. For this reason, Tresadern *et al.* performed a comprehensive statistical analysis of the binding kinetics of over 1800 D_2 receptor antagonists and examined their physicochemical properties that potentially discriminate fast dissociating compounds from slowly dissociating ones.[26] They discovered that faster dissociating antagonists were in general less lipophilic and had lower molecular weight. This seems to hold true for other fast dissociating GPCR ligands as well, a finding shared by Miller *et al.*[143] However, it is also important to note that other descriptors, for instance polar surface area, partial positive charge or the amount of hydrogen bond donor and acceptor groups, caused different effects on the ligand's dissociation, depending on the particular cluster of chemicals that was analyzed. This suggested that local effects of a specific chemical scaffold on the binding kinetics could be dominant over other physiochemical descriptors. Thus, instead of intuitively modifying a compound' lipophilicity, molecular weight or other molecular properties, a more specific structure-kinetics relationship study is needed to direct future drug design and discovery.

In summary, examples presented here demonstrate the benefit of fast dissociating D_2 receptor antagonists for lowering the risk of mechanism-based toxicology. Such an advantage over long RT antagonists is supported by evidence from preclinical and clinical aspects of the typical and atypical antipsychotics. This case study on the D_2 receptor further emphasizes the necessity of characterizing a ligand's binding kinetics profile in the early phases of candidate drug selection.

2.7 Drug-target residence time for class B GPCRs

Corticotrophin releasing factor type-1 receptor

Corticotrophin releasing factor (CRF) is a 41 amino-acid peptide that exerts its effects through activation of CRF receptors, which are members of the family B GPCRs.[144] The CRF receptor subfamily has two subtypes, namely CRF_1 and CRF_2. Both receptors are primarily coupled to G_s protein, resulting in the activation of adenylate cylase and increased cAMP levels.[145,146] Since CRF acts on the pituitary gland to regulate the hypothalamic-pituitary-adrenal axis and the CNS to modulate behavior responses to stress, it has caught considerable attention in drug discovery for psychiatric diseases.[144-147] In particular, antagonism of the CRF_1 receptor has been proposed for rebalancing a dysfunctional stress axis.[147-149] Although highly potent *in vitro* and efficacious in animal models, early reported compounds such as CP-154,526 and NBI-27914 are highly lipophilic, which leads to compound accumulation in tissues or long elimination half-life, and thus high risks of toxicity.[150] For this reason, efforts have been specifically directed towards discovering less lipophilic, fast clearance CRF_1 receptor antagonists to decrease the incidence of toxicity but with maintained drug efficacy. A long residence time CRF_1 receptor antagonist is therefore highly desired, which could provide the benefit of a long duration of action and at the same time less accumulation on the unwanted targets. Such compounds would exemplify new mechanisms for depression treatment beyond classical monoamine modulators.[148,151]

1. The binding kinetics of CRF_1R antagonists and their *in vivo* pharmacodynamics

One of the most elaborate binding kinetics studies at the CRF_1 receptor was performed by Fleck *et al.*[151] In this article, the authors investigated a series of CRF_1 receptor antagonists regarding their *in vitro* binding kinetics and *in vivo* pharmacodynamics. They found that the k_{off} and k_{on} values of 12 CRF_1

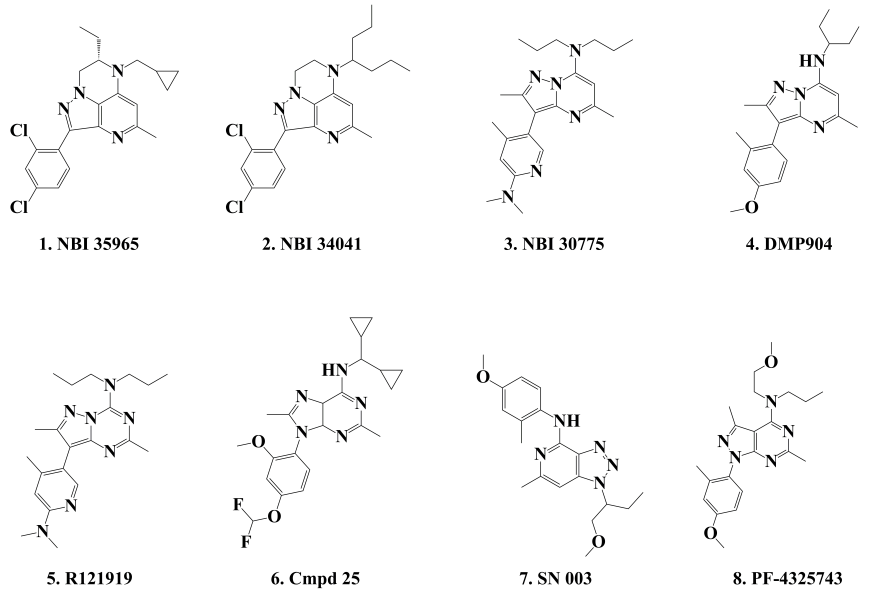


Figure 2.9 | Structures of small molecule CRF_1 receptor antagonists.

receptor compounds varied 170-fold and 13-fold, respectively, which resulted in a maximal change of around 510-fold in the kinetically derived affinity ($K_D = k_{off} / k_{on}$) at 37 °C. Notably, this finding was in stark contrast with the previous reported K_i values measured in radioligand displacement assays, where little difference was observed between compounds. This discrepancy was mostly attributed to insufficient incubation time to reach equilibrium for compounds with long residence time profile. For instance, less than 40% of NBI 30775 dissociated from the CRF_1 receptor after 2 h, far from equilibrium, hence the K_i values were underestimated. Furthermore, several lead compounds displayed divergent dissociation half-lives; NBI 35965 with 16 min, NBI 34041 with 53 min and NBI 30775 with 130 min (Figure 2.9, Compound 1-3; Table 2.6). This ranking of their binding kinetics, in fact, was consistent with the ranking of their *in vivo* pharmacodynamic profiles, at least in adrenalectomized rats, where NBI 34041 and NBI 30775 produced sustained suppression of adrenocorticotropin for 4 h and 6 h, respectively, while NBI 35965 induced a more transient effect (less than 2 h). In addition, all three compounds (NBI 35965, NBI 34041 and NBI 30775)

Table 2.6 | Binding kinetics of CRF_1 receptor antagonists.

Nr	*Cmpd*[a]	*Affinity (K_i, nM)*[b]	*Dissociation half-life ($t_{1/2}$)*[c]	*Ref*
1.	NBI 35965	2.3	16 min (37°C)	151
2.	NBI 34041	1.7	53 min (37°C)	151
3.	NBI 30775	0.36	130 min (37°C)	151
4.	DMP-904	1.5	5.5 h	152
5.	R121919	12	12.8 h	152
6.	Cmpd 25 (Pfizer)	11	10.7 h	152
7.	SN003	3.64 (rat)	0.35 h (rat)	153
8.	PF-4325743	8.22 (rat)	0.37 h (rat)	153

[a] Compound names and synonyms used in original references. [b] Affinity, expressed as K_i values that were reported in original references; result on human receptor unless mentioned otherwise. [c] Dissociation half-life at room temperature and on human receptor unless mentioned otherwise.

had similar pharmacokinetics. This confirmed that the unique sustained adrenocorticotropin suppression evoked by NBI 30775 was derived from its prolonged CRF_1 receptor occupancy rather than its pharmacokinetics.

Functional reversibility assays were also performed to kinetically profile CRF_1 receptor antagonists.[152,153] Briefly, cells expressing recombinant CRF_1 receptor were incubated with CRF in either the presence or absence of an antagonist to measure the suppression of the maximal cell response to CRF by the tested antagonist. Although CRF binds to a different site on the receptor than the non-peptide small molecule antagonists, the insurmountability of the non-competitive antagonists still correlated to their off-rates. In particular, Miller *et al*. plotted the antagonists' dissociation half-lives against their suppression of the maximal CRF_1 receptor response to its endogenous ligand. They found a good correlation between the two parameters, although the exact molecular mechanism of this link is yet to be discovered.[152] By using this assay, at least in a qualitative manner, Miller *et al*. investigated several other long RT compounds reported in literature. They found that DMP-904 and R121919 almost completely suppressed the maximal CRF response (Figure 2.9, Compound 4 and 5). Both compounds were found to have slow dissociation half-lives, i.e., 5.5 h and 12.8 h, respectively, which were calculated from k_{off} values determined in a competition association assay.[152] In comparison, shorter residence time CRF_1 receptor antagonists (Figure 2.9,

Compound 7 and 8) such as SN003 ($t_{1/2}$ = 0.35 h, Table 2.6) or PF-4325743 ($t_{1/2}$ = 0.37 h, Table 2.6) did not significantly decrease the maximal CRF response.[153]

2. Overall structural determinants for binding kinetics at the CRF_1 receptor

A detailed structure-kinetics relationship (SKR) study was performed by Fleck *et al.*, in which the authors performed a retrospective binding kinetics investigation on a set of CRF_1 receptor ligands including the initial, low-affinity chemical starting points up to the lead compounds. Key features of the high affinity or long residence time CRF_1 receptor ligand are represented in Figure 2.10A (adapted from the models developed by Gilligan *et al.*, Kehne and De Lombaert, and Fleck *et al.*[151,154,155]) and the SKRs are summarized as follows: 1) *ortho*-position substitution (R_1) on the low ring was necessary to enforce a twisted bioactive conformation to enhance ligand-receptor interactions. This can be illustrated by the conformation of CP-376395 in the recently elucidated CRF_1R crystal structure (PDB code: 4K5Y, Figure 2.10B). Apparently, the pose of the compound's trimethylphenoxy moiety is rotated to fit in a hydrophobic pocket formed by $F284^{5.51}$, $L287^{5.54}$, $T316^{6.42}$, $L319^{6.45}$ and $L320^{6.46}$ with the pyridine nitrogen at the core to form a hydrogen bond with $N283^{5.50}$.[156] In contrast, the association rate of an *ortho*-substitutent free analogue decreased 33-fold compared to its chloro-substituted analogue, suggesting a substantial barrier for the free rotating ligand to fit into the binding pocket. 2) Adding a methyl moiety at R_2 resulted in an increased k_{on} and decreased k_{off}, indicating a raised probability of successful collision between this group and a rigid binding pocket on the receptor, combined with a stabilized ligand-receptor conformation. This finding was in agreement with other published results which suggested that the methyl-group interacted with a hydrophobic pocket in the receptor.[154,155,157,158] 3) Chemical modifications on the upper aliphatic groups at R_3 demonstrated varying effects on the binding kinetics depending on their size, branching pattern and the stereochemical configuration, which may affect the compound's interaction with $F203^{3.44}$ and $Y327^{6.53}$, two aromatic residues gating the small access channel from the extracellular part (Figure 2.10B).[156]

In another SKR study, Miller *et al.* started from a bicyclic purine core and

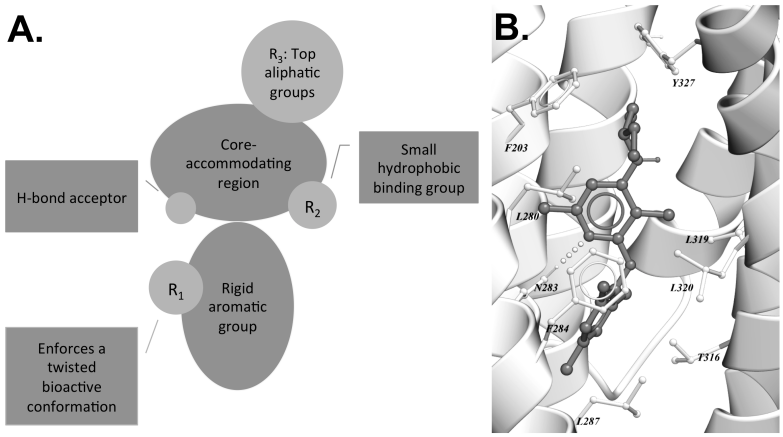


Figure 2.10 | (A) Diagram of the putative functional groups implicated in structure-kinetics relationships of non-peptide antagonists. This diagram was adapted from literature,[160,162,163] based on the comprehensive analysis of ligand SAR. (B) The co-crystal structure of CP-376395 in the human CRF_1 receptor. This figure was generated with ICM Browser v3.7 (Molsoft) from PDB code: 4K5Y. CP-376395 (black) binds deeply within the pocket. Two aromatic residues, F203$^{3.44}$ and Y327$^{6.53}$, together prevent the ligand from moving out of the receptor. The pose of the compound's trimethylphenoxy moiety is rotated to fit in a hydrophobic pocket formed by F284$^{5.51}$, L287$^{5.54}$, T316$^{6.42}$, L319$^{6.45}$ and L320$^{6.46}$ with its pyridine nitrogen at the core to form a hydrogen bond with N283$^{5.50}$.[156]

performed a series of chemical modifications on the substitution patterns at the low ring and the upper branched groups. Follow-up functional investigations *in vitro* led to the identification of compound 25 (Figure 2.9, Compound 6) which displayed 79% suppression of the maximal CRF response. Binding kinetics characterization of this compound revealed that it had a slow $t_{1/2}$ of 10.7 h, correlating well with its insurmountable antagonist behavior.[152]

2.8 Concluding remarks

We reviewed the existing kinetics data for a number of GPCRs. The examples presented make a strong case for the value of measuring drug-target residence time, or, more generally speaking, the kinetic profile of interaction for

compound optimization in the early phases of the drug discovery process. Thus, a strategy is warranted that comprises both a structure-kinetics relationship study (SKR) and a classical structure-affinity relationship study (SAR). This may offer added value to the traditional metric of affinity-based drug evaluation.

This chapter further summarized the factors influencing drug-target residence time, in particular, to find a universal molecular determinant or a certain 'hot spot' on GPCRs for designing kinetics-favorable ligands. Several kinetics-related statistical analyses indicated that manipulating physicochemical properties such as lipophilicity or molecular weight can lead to tuned drug-target residence times.[26,143] Alternatively, this could be achieved by modulating the rigidity / flexibility of a drug candidate.[117] However, these 'intuitive', 'one size-fits-all' approaches are very likely too simple and may increase the concern of binding to collateral targets, thereby resulting in unwanted side effects.[67,159] In this sense, fine-tuning drug-target residence time should probably be more specific. Despite this challenge, progress can still be made by gaining knowledge from both the ligand and target perspectives, such as by ligand modifications with subtle changes to probe relevant pharmacophores, mutation studies, co-crystallization and molecular dynamic studies to establish the corresponding 'anchoring' sites on the receptor.

We also summarized the kinetic methodologies in this chapter. Several screening schemes are available and new assays are emerging, which enable quick identification of compounds of interest. Quantitative characterization of a compound's binding kinetics can be obtained in a kinetic binding assay or competition association assay. Functional reversibility experiments prevail in drug discovery as well, which offer an alternative way to interpret a ligand's kinetics profile. In addition, *ex vivo* receptor occupancy experiments or *in vivo* duration of action experiments can translate the *in vitro* binding kinetics into the effect in an *in vivo* setting, which provides further evidence for a compound's drug-target residence time. Notably, it is also necessary to take into account the PK profile of the candidate compound, particular for one aiming at long drug-target residence time, since RT can only prolong the duration of action only when the RT outlasts the PK.[2,15]

The compounds summarized in the present chapter are predominantly GPCR antagonists. This reflects a lack of kinetic information on agonists in the literature. However, more kinetics studies focused on the latter are emerging. For instance the case studies at the M_3 and A_{2A} receptors

explored the molecular basis of the compounds' intrinsic efficacy from a kinetic perspective.[32,98] In addition to examining an agonist's mechanism of action, one can also specifically optimize an agonist's kinetic properties for therapeutic benefit. This can be exemplified by the administration of long-acting agonists at the GnRH receptor to intentionally desensitize the GnRH receptor and therefore antagonize gonadotropin secretion in hormone-dependent cancers.[181] Such a strategy could be a therapeutic substitute for targets where no antagonist is available. On the other hand, one needs to take into consideration that agonist-induced desensitization or internalization by prolonged or repeated administration can cause drug tolerance, for instance opiate drugs targeting μ-opioid receptors.[182] In such a case, it might be tempting to search for shorter residence time agonists to prevent their target's internalization. Thus, a study that compares agonist binding kinetics and GPCR desensitization / internalization kinetics would be of great interest.

Taken together, a rapid expansion of the field of GPCR binding kinetics may be anticipated in the near future, which hopefully will lead to the identification of novel and better-in-class drugs for clinical applications.

References:

1. Copeland RA, Pompliano DL, Meek TD. Drug-target residence time and its implications for lead optimization. *Nat Rev Drug Discov* 2006;5(9):730-739.
2. Swinney DC. Can binding kinetics translate to a clinically differentiated drug? From theory to practice. *Lett Drug Des Discov* 2006;3(8):569-574.
3. Swinney DC. Biochemical mechanisms of New Molecular Entities (NMEs) approved by United States FDA during 2001-2004: mechanisms leading to optimal efficacy and safety. *Curr Top Med Chem* 2006;6(5):461-478.
4. Swinney DC, Anthony J. How were new medicines discovered? *Nat Rev Drug Discov* 2011;10(7):507-519.
5. Swinney DC. Biochemical mechanisms of drug action: what does it take for success? *Nat Rev Drug Discov* 2004;3(9):801-808.
6. Copeland, RA. *Evaluation of enzyme inhibitors in drug discovery: a guide for medicinal chemists and pharmacologists*. New York: John Wiley & Sons; 2005. 153 p.
7. Copeland RA. Conformational adaptation in drug-target interactions and residence time. *Future Med Chem* 2011;3(12):1491-1501.
8. Vauquelin G, Charlton SJ. Long-lasting target binding and rebinding as mechanisms to prolong *in vivo* drug action. *Br J Pharmacol* 2010;161(3):488-508.
9. Vauquelin G, Fierens F, Verheijen I, Vanderheyden P. Insurmountable AT_1 receptor antagonism: the need for different antagonist binding states of the receptor. *Trends Pharmacol Sci*

2001;22(7):343-344.
10. Vauquelin G, Morsing P, Fierens FL, De Backer JP, Vanderheyden PM. A two-state receptor model for the interaction between angiotensin II type 1 receptors and non-peptide antagonists. *Biochem Pharmacol* 2001;61(3):277-284.
11. Vauquelin G, Van Liefde I. Slow antagonist dissociation and long-lasting *in vivo* receptor protection. *Trends Pharmacol Sci* 2006;27(7):356-359.
12. Zhang R, Monsma F. The importance of drug-target residence time. *Curr Opin Drug Discov Devel* 2009;12(4):488-496.
13. Zhang R, Monsma F. Binding kinetics and mechanism of action: toward the discovery and development of better and best in class drugs. *Expert Opin Drug Discov* 2010;5(11):1023-1029.
14. Tummino PJ, Copeland RA. Residence time of receptor-ligand complexes and its effect on biological function. *Biochemistry* 2008;47(20):5481-5492.
15. Dahl G, Akerud T. Pharmacokinetics and the drug-target residence time concept. *Drug Discov Today* 2013;18(15-16):697-707.
16. Nunez S, Venhorst J, Kruse CG. Target-drug interactions: first principles and their application to drug discovery. *Drug Discov Today* 2012;17(1-2):10-22.
17. Swinney DC. The role of binding kinetics in therapeutically useful drug action. *Curr Opin Drug Discov Devel* 2009;12(1):31-39.
18. Vilums M, Zweemer AJ, Yu Z, de Vries H, Hillger JM, Wapenaar H, Bollen IA, Barmare F, Gross R, Clemens J, Krenitsky P, Brussee J, Stamos D, Saunders J, Heitman LH, IJzerman AP. Structure-kinetic relationships-an overlooked parameter in hit-to-lead optimization: a case of cyclopentylamines as chemokine receptor 2 antagonists. *J Med Chem* 2013;56(19):7706-7714.
19. Hale JJ, Mills SG, MacCoss M, Finke PE, Cascieri MA, Sadowski S, Ber E, Chicchi GG, Kurtz M, Metzger J, Eiermann G, Tsou NN, Tattersall FD, Rupniak NM, Williams AR, Rycroft W, Hargreaves R, MacIntyre DE. Structural optimization affording 2-(R)-(1-(R)-3, 5-bis(trifluoromethyl) phenylethoxy)-3-(S)-(4-fluoro)phenyl-4- (3-oxo-1,2,4-triazol-5-yl)methylmorpholine, a potent, orally active, long-acting morpholine acetal human NK-1 receptor antagonist. *J Med Chem* 1998;41(23):4607-4614.
20. Gavalda A, Miralpeix M, Ramos I, Otal R, Carreno C, Vinals M, Domenech T, Carcasona C, Reyes B, Vilella D, Gras J, Cortijo J, Morcillo E, Llenas J, Ryder H, Beleta J. Characterization of aclidinium bromide, a novel inhaled muscarinic antagonist, with long duration of action and a favorable pharmacological profile. *J Pharmacol Exp Ther* 2009;331(2):740-751.
21. Keppler A, Gendreizig S, Gronemeyer T, Pick H, Vogel H, Johnsson K. A general method for the covalent labeling of fusion proteins with small molecules *in vivo*. *Nat Biotechnol* 2003;21(1):86-89.
22. Pierre N. Determination of association (k_{on}) and dissociation (k_{off}) rates of spiperone on the dopamine D_2 receptor using a platform for GPCR applications. Volume 2013. Bedford: *American Laboratory*; 2011.
23. Leysen JE, Gommeren W. The dissociation rate of unlabelled dopamine antagonists and agonists from the dopamine-D_2 receptor, application of an original filter method. *J Recept Res* 1984;4(7):817-845.
24. Malany S, Hernandez LM, Smith WF, Crowe PD, Hoare SR. Analytical method for simultaneously measuring *ex vivo* drug receptor occupancy and dissociation rate: application to (R)-dimethindene occupancy of central histamine H_1 receptors. *J Recept Signal* Transduct Res 2009;29(2):84-93.
25. Packeu A, Wennerberg M, Balendran A, Vauquelin G. Estimation of the dissociation rate of

unlabelled ligand-receptor complexes by a 'two-step' competition binding approach. *Br J Pharmacol* 2010;161(6):1311-1328.
26. Tresadern G, Bartolome JM, Macdonald GJ, Langlois X. Molecular properties affecting fast dissociation from the D_2 receptor. *Bioorg Med Chem* 2011;19(7):2231-2241.
27. Affolter H, Hertel C, Jaeggi K, Portenier M, Staehelin M. (-)-S-[^{3}H]CGP-12177 and its use to determine the rate constants of unlabeled beta-adrenergic antagonists. *Proc Natl Acad Sci U S A* 1985;82(3):925-929.
28. Contreras ML, Wolfe BB, Molinoff PB. Kinetic analysis of the interactions of agonists and antagonists with beta adrenergic receptors. *J Pharmacol Exp Ther* 1986;239(1):136-143.
29. Dowling MR, Charlton SJ. Quantifying the association and dissociation rates of unlabelled antagonists at the muscarinic M_3 receptor. *Br J Pharmacol* 2006;148(7):927-937.
30. Heise CE, Sullivan SK, Crowe PD. Scintillation proximity assay as a high-throughput method to identify slowly dissociating nonpeptide ligand binding to the GnRH receptor. *J Biomol Screen* 2007;12(2):235-239.
31. Slack RJ, Russell LJ, Hall DA, Luttmann MA, Ford AJ, Saunders KA, Hodgson ST, Connor HE, Browning C, Clark KL. Pharmacological characterization of GSK1004723, a novel, long-acting antagonist at histamine H_1 and H_3 receptors. *Br J Pharmacol* 2011;164(6):1627-1641.
32. Guo D, Mulder-Krieger T, IJzerman AP, Heitman LH. Functional efficacy of adenosine A_{2A} receptor agonists is positively correlated to their receptor residence time. *Br J Pharmacol* 2012;166(6):1846-1859.
33. Guo D, van Dorp EJ, Mulder-Krieger T, van Veldhoven JP, Brussee J, IJzerman AP, Heitman LH. Dual-point competition association assay: a fast and high-throughput kinetic screening method for assessing ligand-receptor binding kinetics. *J Biomol Screen* 2013;18(3):309-320.
34. Motulsky HJ, Mahan LC. The kinetics of competitive radioligand binding predicted by the law of mass action. *Mol Pharmacol* 1984;25(1):1-9.
35. Vauquelin G, Bostoen S, Vanderheyden P, Seeman P. Clozapine, atypical antipsychotics, and the benefits of fast-off D_2 dopamine receptor antagonism. *Naunyn Schmiedebergs Arch Pharmacol* 2012;385(4):337-372.
36. Gaddum JH, Hameed KA, Hathway DE, Stephens FF. Quantitative studies of antagonists for 5-hydroxytryptamine. *Q J Exp Physiol Cogn Med Sci* 1955;40(1):49-74.
37. Kenakin T, Jenkinson S, Watson C. Determining the potency and molecular mechanism of action of insurmountable antagonists. *J Pharmacol Exp Ther* 2006;319(2):710-723.
38. Paton WD, Waud DR. The margin of safety of neuromuscular transmission. *J Physiol* 1967;191(1):59-90.
39. Paton WDM, Rang HP. *A kinetic approach to the mechanism of drug action.* In: Harper NJ, Simmonds AB, editor. Adv. Drug Res. London & New York: Academic Press; 1998. p57-80.
40. Rang HP. The kinetics of action of acetylcholine antagonists in smooth muscle. *Proc R Soc Lond B Biol Sci* 1966;164(996):488-510.
41. Fierens FL, Vanderheyden PM, De Backer JP, Vauquelin G. Insurmountable angiotensin AT_1 receptor antagonists: the role of tight antagonist binding. *Eur J Pharmacol* 1999;372(2):199-206.
42. Morsing P, Vauquelin G. How can the differences among AT_1-receptor antagonists be explained? *Cell Biochem Biophys* 2001;35(1):89-102.
43. Vauquelin G, Fierens FL, Verheijen I, Vanderheyden PM. Distinctions between non-peptide angiotensin II AT_1-receptor antagonists. *J Renin-angio-aldo S* 2001;2(1 suppl):S24-S31.
44. Vauquelin G, Van Liefde I, Birzbier BB, Vanderheyden PM. New insights in insurmountable antagonism. *Fundam Clin Pharmacol* 2002;16(4):263-272.

45. Vauquelin G, Van Liefde I, Vanderheyden P. Models and methods for studying insurmountable antagonism. *Trends Pharmacol Sci* 2002;23(11):514-518.
46. Vauquelin G, Szczuka A. Kinetic versus allosteric mechanisms to explain insurmountable antagonism and delayed ligand dissociation. *Neurochem Int* 2007;51(5):254-260.
47. Shiau AK, Massari ME, Ozbal CC. Back to basics: Label-free technologies for small molecule screening. *Comb Chem High T Scr* 2008;11(3):231-237.
48. Rich RL, Myszka DG. Higher-throughput, label-free, real-time molecular interaction analysis. *Anal Biochem* 2007;361(1):1-6.
49. Gronewold TMA, Baumgartner A, Hierer J, Sierra S, Blind M, Schafer F, Blumer J, Tillmann T, Kiwitz A, Kaiser R, Zabe-Kuhn M, Quandt E, Famulok M. Kinetic binding analysis of aptamers targeting HIV-1 proteins by a combination of a microbalance array and mass spectrometry (MAMS). *J Proteome Res* 2009;8(7):3568-3577.
50. Gronewold TMA. Surface acoustic wave sensors in the bioanalytical field: Recent trends and challenges. *Analytica Chimica Acta* 2007;603(2):119-128.
51. Rich RL, Myszka DG. Grading the commercial optical biosensor literature—Class of 2008: 'The Mighty Binders'. *J Mol Recogn* 2010;23(1):1-64.
52. Zhukov A, Andrews SP, Errey JC, Robertson N, Tehan B, Mason JS, Marshall FH, Weir M, Congreve M. Biophysical mapping of the adenosine A_{2A} receptor. *J Med Chem* 2011;54(13):4312-4323.
53. Robertson N, Jazayeri A, Errey J, Baig A, Hurrell E, Zhukov A, Langmead CJ, Weir M, Marshall FH. The properties of thermostabilised G protein-coupled receptors (StaRs) and their use in drug discovery. *Neuropharmacol* 2011;60(1):36-44.
54. Congreve M, Andrews SP, Dore AS, Hollenstein K, Hurrell E, Langmead CJ, Mason JS, Ng IW, Tehan B, Zhukov A, Weir M, Marshall FH. Discovery of 1,2,4-triazine derivatives as adenosine A(2A) antagonists using structure based drug design. *J Med Chem* 2012;55(5):1898-1903.
55. Navratilova I, Dioszegi M, Myszka DG. Analyzing ligand and small molecule binding activity of solubilized GPCRs using biosensor technology. *Anal Biochem* 2006;355(1):132-139.
56. Bjarnadottir TK, Gloriam DE, Hellstrand SH, Kristiansson H, Fredriksson R, Schioth HB. Comprehensive repertoire and phylogenetic analysis of the G protein-coupled receptors in human and mouse. *Genomics* 2006;88(3):263-273.
57. Pierce KL, Premont RT, Lefkowitz RJ. Seven-transmembrane receptors. *Nat Rev Mol Cell Biol* 2002;3(9):639-650.
58. De Amici M, Dallanoce C, Holzgrabe U, Trankle C, Mohr K. Allosteric ligands for G protein-coupled receptors: a novel strategy with attractive therapeutic opportunities. *Med Res Rev* 2010;30(3):463-549.
59. Overington JP, Al-Lazikani B, Hopkins AL. Opinion - How many drug targets are there? *Nat Rev Drug Discov* 2006;5(12):993-996.
60. Russ AP, Lampel S. The druggable genome: an update. *Drug Discovery Today* 2005;10(23-24):1607-1610.
61. Chen L, Jin L, Zhou N. An update of novel screening methods for GPCR in drug discovery. *Expert Opin Drug Discov* 2012;7(9):791-806.
62. Post JM, Alexander S, Wang YX, Vincelette J, Vergona R, Kent L, Bryant J, Sullivan ME, Dole WP, Morser J, Subramanyam B. Novel P_2Y_{12} adenosine diphosphate receptor antagonists for inhibition of platelet aggregation (II): pharmacodynamic and pharmacokinetic characterization. *Thromb Res* 2008;122(4):533-540.
63. Foldes FF. Pain control with intrathecally and peridurally administered opioids and other drugs.

Anaesthesiol Reanim 1991;16(5):287-298.
64. Laduron PM, Janssen PFM. Axoplasmic-transport and possible recycling of opiate receptors labeled with H-3-labeled lofentanil. *Life Sci* 1982;31(5):457-462.
65. Savoia G, Loreto M, Gravino E. Sufentanil: an overview of its use for acute pain management. *Minerva Anestesiol* 2001;67(9 Suppl 1):206-216.
66. Patel S, Spencer C. Remifentanil. *Drugs* 1996;52(3):417-427.
67. Pan AC, Borhani DW, Dror RO, Shaw DE. Molecular determinants of drug-receptor binding kinetics. *Drug Discov Today* 2013;18(13-14):667-673.
68. Kola I, Landis J. Can the pharmaceutical industry reduce attrition rates? *Nature Reviews Drug Discovery* 2004;3(8):711-715.
69. Kola I. The state of innovation in drug development. *Clin Pharmacol Ther* 2008;83(2):227-230.
70. Caulfield MP, Birdsall NJ. International Union of Pharmacology. XVII. Classification of muscarinic acetylcholine receptors. *Pharmacol Rev* 1998;50(2):279-290.
71. Bonner TI, Buckley NJ, Young AC, Brann MR. Identification of a family of muscarinic acetylcholine receptor genes. *Science* 1987;237(4814):527-532.
72. Bonner TI. The molecular basis of muscarinic receptor diversity. *Trends Neurosci* 1989;12(4):148-151.
73. Wess J. Molecular biology of muscarinic acetylcholine receptors. *Crit Rev Neurobiol* 1996;10(1):69-99.
74. Barnes PJ. The role of anticholinergics in chronic obstructive pulmonary disease. *Am J Med* 2004;117 Suppl 12A:24S-32S.
75. Rabe KF, Hurd S, Anzueto A, Barnes PJ, Buist SA, Calverley P, Fukuchi Y, Jenkins C, Rodriguez-Roisin R, van Weel C, Zielinski J. Global strategy for the diagnosis, management, and prevention of chronic obstructive pulmonary disease: GOLD executive summary. *Am J Respir Crit Care Med* 2007;176(6):532-555.
76. Tashkin DP. Is a long-acting inhaled bronchodilator the first agent to use in stable chronic obstructive pulmonary disease? *Curr Opin Pulm Med* 2005;11(2):121-128.
77. Disse B, Speck GA, Rominger KL, Witek TJ, Jr., Hammer R. Tiotropium (Spiriva): mechanistical considerations and clinical profile in obstructive lung disease. *Life Sci* 1999;64(6-7):457-464.
78. Disse B, Reichl R, Speck G, Traunecker W, Rominger KL, Hammer R. Ba 679 Br, a Novel Long-Acting Anticholinergic Bronchodilator. *Life Sci* 1993;52(5-6):537-544.
79. Haddad EB, Mak JC, Barnes PJ. Characterization of [^{3}H]Ba 679 BR, a slowly dissociating muscarinic antagonist, in human lung: radioligand binding and autoradiographic mapping. *Mol Pharmacol* 1994;45(5):899-907.
80. Casarosa P, Bouyssou T, Germeyer S, Schnapp A, Gantner F, Pieper M. Preclinical evaluation of long-acting muscarinic antagonists: comparison of tiotropium and investigational drugs. *J Pharmacol Exp Ther* 2009;330(2):660-668.
81. Sykes DA, Dowling MR, Leighton-Davies J, Kent TC, Renard E, Trifilieff A, Charlton SJ. The influence of receptor kinetics on the onset and duration of action, and the therapeutic index of NVA237 and tiotropium. *J Pharmacol Exp Ther* 2012;343(2):520-528.
82. D'Urzo A, Ferguson GT, van Noord JA, Hirata K, Martin C, Horton R, Lu YM, Banerji D, Overend T. Efficacy and safety of once-daily NVA237 in patients with moderate-to-severe COPD: the GLOW1 trial. *Resp Res* 2011;12: 156
83. Tautermann CS, Kiechle T, Seeliger D, Diehl S, Wex E, Banholzer R, Gantner F, Pieper MP, Casarosa P. Molecular basis for the long duration of action and kinetic selectivity of Tiotropium for the muscarinic M_3 receptor. *J Med Chem* 2013; 56 (21): 8746-8756.

84. Kruse AC, Hu J, Pan AC, Arlow DH, Rosenbaum DM, Rosemond E, Green HF, Liu T, Chae PS, Dror RO, Shaw DE, Weis WI, Wess J, Kobilka BK. Structure and dynamics of the M_3 muscarinic acetylcholine receptor. *Nature* 2012;482(7386):552-556.
85. Smith DA, Jones BC, Walker DK. Design of drugs involving the concepts and theories of drug metabolism and pharmacokinetics. *Med Res Rev* 1996;16(3):243-266.
86. Tashkin DP, Celli B, Senn S, Burkhart D, Kesten S, Menjoge S, Decramer M. A 4-year trial of tiotropium in chronic obstructive pulmonary disease. *N Engl J Med* 2008;359(15):1543-1554.
87. van Noord JA, Smeets JJ, Custers FL, Korducki L, Cornelissen PJ. Pharmacodynamic steady state of tiotropium in patients with chronic obstructive pulmonary disease. *Eur Respir J* 2002;19(4):639-644.
88. Traynor K. Aclidinium bromide oral inhalation powder approved for COPD. *Am J Health Syst Pharm* 2012;69(17):1446.
89. Prat M, Fernandez D, Buil MA, Crespo MI, Casals G, Ferrer M, Tort L, Castro J, Monleon JM, Gavalda A, Miralpeix M, Ramos I, Domenech T, Vilella D, Anton F, Huerta JM, Espinosa S, Lopez M, Sentellas S, Gonzalez M, Alberti J, Segarra V, Cardenas A, Beleta J, Ryder H. Discovery of novel quaternary ammonium derivatives of (3R)-quinuclidinol esters as potent and long-acting muscarinic antagonists with potential for minimal systemic exposure after inhaled administration: identification of (3R)-3-{[hydroxy(di-2-thienyl)acetyl]oxy}-1-(3-phenoxypropyl)-1-azoniabicyclo[2.2.2]octane bromide (aclidinium bromide). *J Med Chem* 2009;52(16):5076-5092.
90. Kesten S, Jara M, Wentworth C, Lanes S. Pooled clinical trial analysis of tiotropium safety. *Chest* 2006;130(6):1695-1703.
91. Suppli Ulrik C. Aclidinium Bromide: Clinical benefit in patients with moderate to severe COPD. *Open Respir Med J* 2012;6:150-154.
92. Singh D, Magnussen H, Kirsten A, Mindt S, Caracta C, Seoane B, Jarreta D, Garcia Gil E. A randomised, placebo- and active-controlled dose-finding study of aclidinium bromide administered twice a day in COPD patients. *Pulm Pharmacol Ther* 2012;25(3):248-253.
93. Maltais F, Milot J. The potential for aclidinium bromide, a new anticholinergic, in the management of chronic obstructive pulmonary disease. *Ther Adv Respir Dis* 2012;6(6):345-361.
94. Gupta V, Singh D. Aclidinium bromide for the treatment of chronic obstructive pulmonary disease. *Expert Rev Respir Med* 2012;6(6):581-588.
95. Jones PW, Singh D, Bateman ED, Agusti A, Lamarca R, de Miquel G, Segarra R, Caracta C, Garcia Gil E. Efficacy and safety of twice-daily aclidinium bromide in COPD patients: the ATTAIN study. *Eur Respir J* 2012;40(4):830-836.
96. Glossop PA, Watson CA, Price DA, Bunnage ME, Middleton DS, Wood A, James K, Roberts D, Strang RS, Yeadon M, Perros-Huguet C, Clarke NP, Trevethick MA, Machin I, Stuart EF, Evans SM, Harrison AC, Fairman DA, Agoram B, Burrows JL, Feeder N, Fulton CK, Dillon BR, Entwistle DA, Spence FJ. Inhalation by design: novel tertiary amine muscarinic M_3 receptor antagonists with slow off-rate binding kinetics for inhaled once-daily treatment of chronic obstructive pulmonary disease. *J Med Chem* 2011;54(19):6888-6904.
97. Haddad EB, Patel H, Keeling JE, Yacoub MH, Barnes PJ, Belvisi MG. Pharmacological characterization of the muscarinic receptor antagonist, glycopyrrolate, in human and guinea-pig airways. *Br J Pharmacol* 1999;127(2):413-420.
98. Sykes DA, Dowling MR, Charlton SJ. Exploring the mechanism of agonist efficacy: a relationship between efficacy and agonist dissociation rate at the muscarinic M_3 receptor. *Mol Pharmacol* 2009;76(3):543-551.

99. Hoeren M, Brawek B, Mantovani M, Loffler M, Steffens M, van Velthoven V, Feuerstein TJ. Partial agonism at the human alpha$_{2A}$-autoreceptor: role of binding duration. *Naunyn Schmiedebergs Arch Pharmacol* 2008;378(1):17-26.
100. Pantaleo N, Chadwick W, Park SS, Wang L, Zhou Y, Martin B, Maudsley S. The mammalian tachykinin ligand-receptor system: an emerging target for central neurological disorders. *CNS Neurol Disord Drug Targets* 2010;9(5):627-635.
101. Pennefather JN, Lecci A, Candenas ML, Patak E, Pinto FM, Maggi CA. Tachykinins and tachykinin receptors: a growing family. *Life Sci* 2004;74(12):1445-1463.
102. Almeida TA, Rojo J, Nieto PM, Pinto FM, Hernandez M, Martin JD, Candenas ML. Tachykinins and tachykinin receptors: structure and activity relationships. *Curr Med Chem* 2004;11(15):2045-2081.
103. Simonsen KB, Juhl K, Steiniger-Brach B, Nielsen SM. Novel NK$_3$ receptor antagonists for the treatment of schizophrenia and other CNS indications. *Curr Opin Drug Discov Devel* 2010;13(4):379-388.
104. Stout SC, Owens MJ, Nemeroff CB. Neurokinin(1) receptor antagonists as potential antidepressants. *Annu Rev Pharmacol* 2001;41:877-906.
105. Albert JS. Neurokinin antagonists and their potential role in treating depression and other stress disorders. *Exp Opin Inv Drug* 2004;14(10):1421-1433.
106. Lecci A, Maggi CA. Peripheral tachykinin receptors as potential therapeutic targets in visceral diseases. *Exp Opin Ther Targets* 2003;7(3):343-362.
107. Quartara L, Altamura M, Evangelista S, Maggi CA. Tachykinin receptor antagonists in clinical trials. *Exp Opin Inv Drug* 2009;18(12):1843-1864.
108. Lindstrom E, von Mentzer B, Pahlman I, Ahlstedt I, Uvebrant A, Kristensson E, Martinsson R, Noven A, de Verdier J, Vauquelin G. Neurokinin 1 receptor antagonists: correlation between *in vitro* receptor interaction and *in vivo* efficacy. *J Pharmacol Exp Ther* 2007;322(3):1286-1293.
109. Duffy RA, Varty GB, Morgan CA, Lachowicz JE. Correlation of neurokinin (NK) 1 receptor occupancy in gerbil striatum with behavioral effects of NK$_1$ antagonists. *J Pharmacol Exp Ther* 2002;301(2):536-542.
110. Malherbe P, Knoflach F, Hernandez MC, Hoffmann T, Schnider P, Porter RH, Wettstein JG, Ballard TM, Spooren W, Steward L. Characterization of RO4583298 as a novel potent, dual antagonist with *in vivo* activity at tachykinin NK$_1$ and NK$_3$ receptors. *Br J Pharmacol* 2011;162(4):929-946.
111. Cascieri MA, Ber E, Fong TM, Hale JJ, Tang F, Shiao LL, Mills SG, MacCoss M, Sadowski S, Tota MR, Strader CD. Characterization of the binding and activity of a high affinity, pseudoirreversible morpholino tachykinin NK$_1$ receptor antagonist. *Eur J Pharmacol* 1997;325(2-3):253-261.
112. Cascieri MA, Ber E, Fong TM, Sadowski S, Bansal A, Swain C, Seward E, Frances B, Burns D, Strader CD. Characterization of the binding of a potent, selective, radioiodinated antagonist to the human neurokinin-1 receptor. *Mol Pharmacol* 1992;42(3):458-463.
113. Bristow LJ, Young L. Chromodacryorrhea and repetitive hind paw tapping: models of peripheral and central tachykinin NK$_1$ receptor activation in gerbils. Eur J Pharmacol 1994;253(3):245-252.
114. Young JR, Eid R, Turner C, DeVita RJ, Kurtz MM, Tsao KL, Chicchi GG, Wheeldon A, Carlson E, Mills SG. Pyrrolidine-carboxamides and oxadiazoles as potent hNK$_1$ antagonists. *Bioorg Med Chem Lett* 2007;17(19):5310-5315.
115. Morriello GJ, Chicchi G, Johnson T, Mills SG, Demartino J, Kurtz M, Tsao KL, Zheng S, Tong X, Carlson E, Townson K, Wheeldon A, Boyce S, Collinson N, Rupniak N, Devita RJ. Fused tricyclic pyrrolizinones that exhibit pseudo-irreversible blockade of the NK$_1$ receptor. *Bioorg Med Chem Lett* 2010;20(19):5925-5932.

116. Morriello GJ, DeVita RJ, Mills SG, Young JR, Lin P, Doss G, Chicchi GG, DeMartino J, Kurtz MM, Tsao K-LC, Carlson E, Townson K, Wheeldon A, Boyce S, Collinson N, Rupniak N, Moore S. Fused bicyclic pyrrolizinones as new scaffolds for human NK_1 antagonists. *Bioorg Med Chem* 2008;16(5):2156-2170.
117. Morriello GJ, Mills SG, Johnson T, Reibarkh M, Chicchi G, DeMartino J, Kurtz M, Davies P, Tsao KLC, Zheng S, Tong X, Carlson E, Townson K, Tattersall FD, Wheeldon A, Boyce S, Collinson N, Rupniak N, Moore S, DeVita RJ. Substituted fused bicyclic pyrrolizinones as potent, orally bioavailable hNK_1 antagonists. *Bioorg Med Chem Lett* 2010;20(6):2007-2012.
118. Morriello GJ, Chicchi G, Johnson T, Mills SG, Demartino J, Kurtz M, Tsao KL, Zheng S, Tong X, Carlson E, Townson K, Wheeldon A, Boyce S, Collinson N, Rupniak N, Devita RJ. Fused tricyclic pyrrolizinones that exhibit pseudo-irreversible blockade of the NK_1 receptor. *Bioorg Med Chem Lett* 2010;20(19):5925-5932.
119. Di Fabio R, Griffante C, Alvaro G, Pentassuglia G, Pizzi DA, Donati D, Rossi T, Guercio G, Mattioli M, Cimarosti Z, Marchioro C, Provera S, Zonzini L, Montanari D, Melotto S, Gerrard PA, Trist DG, Ratti E, Corsi M. Discovery process and pharmacological characterization of 2-(S)-(4-fluoro-2-methylphenyl)piperazine-1-carboxylic acid [1-(*R*)-(3,5-bis-trifluoromethylphenyl) ethyl]methylamide (vestipitant) as a potent, selective, and orally active NK_1 receptor antagonist. *J Med Chem* 2009;52(10):3238-3247.
120. Di Fabio R, Alvaro G, Griffante C, Pizzi DA, Donati D, Mattioli M, Cimarosti Z, Guercio G, Marchioro C, Provera S, Zonzini L, Montanari D, Melotto S, Gerrard PA, Trist DG, Ratti E, Corsi M. Discovery and biological characterization of (*2R*,*4S*)-1'-acetyl-*N*-{(*1R*)-1-[3,5-bis(trifluoromethyl)phenyl]ethyl}-2-(4-fluoro-2-methylphenyl)-*N*-methyl-4,4'-bipiperidine-1-carboxamide as a new potent and selective neurokinin 1 (NK_1) receptor antagonist clinical candidate. *J Med Chem* 2011;54(4):1071-1079.
121. Cirillo R, Astolfi M, Conte B, Lopez G, Parlani M, Terracciano R, Fincham CI, Manzini S. Pharmacology of the peptidomimetic, MEN 11149, a new potent, selective and orally effective tachykinin NK_1 receptor antagonist. *Eur J Pharmacol* 1998;341(2-3):201-209.
122. Carlsson A, Lindqvist M, Magnusson T. 3,4-Dihydroxyphenylalanine and 5-Hydroxytryptophan as Reserpine Antagonists. *Nature* 1957;180(4596):1200-1200.
123. Le Crom S, Kapsimali M, Barome PO, Vernier P. Dopamine receptors for every species: gene duplications and functional diversification in Craniates. *J Struct Funct Genomics* 2003;3(1-4):161-176.
124. Carlsson A, Civelli O, Kebabian J, Langer S, Scatton B, Schwartz JC, Sedvall G, Seeman P, Sokoloff P, Spano P, Van Tol H. Dopamine receptors. Last modified on 27/05/2013. Accessed on 29/08/2013. *IUPHAR database (IUPHAR-DB)*, http://www.iuphar-db.org/DATABASE/FamilyMenuForward?familyId=20.
125. Hurley MJ, Jenner P. What has been learnt from study of dopamine receptors in Parkinson's disease? *Pharmacol Therapeut* 2006;111(3):715-728.
126. Schneier FR, Liebowitz MR, Abi-Dargham A, Zea-Ponce Y, Lin SH, Laruelle M. Low dopamine D_2 receptor binding potential in social phobia. *Am J Psychiatry* 2000;157(3):457-459.
127. Kienast T, Heinz A. Dopamine and the diseased brain. CNS *Neurol Disord Drug Targets* 2006;5(1):109-131.
128. Fuxe K, Manger P, Genedani S, Agnati L. in: Riederer P, Reichmann H, Youdim MBH, Gerlach M. (Eds) *Parkinson's Diseases and Related Disorders*. Vienna: Springer; 2006. p 71-83.
129. Mihara K, Kondo T, Suzuki A, Yasui-Furukori N, Ono S, Sano A, Koshiro K, Otani K, Kaneko S. Relationship between functional dopamine D_2 and D_3 receptors gene polymorphisms and

neuroleptic malignant syndrome. *Am J Med Genet B* 2003;117B(1):57-60.
130. Faraone SV, Khan SA. Candidate gene studies of attention-deficit/hyperactivity disorder. *J Clin Psychiat* 2006;67:13-20.
131. Hummel M, Unterwald EM. D_1 dopamine receptor: a putative neurochemical and behavioral link to cocaine action. *J Cell Physiol* 2002;191(1):17-27.
132. Seeman P, Weinshenker D, Quirion R, Srivastava LK, Bhardwaj SK, Grandy DK, Premont RT, Sotnikova TD, Boksa P, El-Ghundi M, O'Dowd B F, George SR, Perreault ML, Mannisto PT, Robinson S, Palmiter RD, Tallerico T. Dopamine supersensitivity correlates with D_2High states, implying many paths to psychosis. *Proc Natl Acad Sci U S A* 2005;102(9):3513-3518.
133. Miyamoto S, Duncan GE, Marx CE, Lieberman JA. Treatments for schizophrenia: a critical review of pharmacology and mechanisms of action of antipsychotic drugs. *Mol Psychiatry* 2005;10(1):79-104.
134. Kapur S, Seeman P. Antipsychotic agents differ in how fast they come off the dopamine D_2 receptors. Implications for atypical antipsychotic action. *J Psychiatr Neurosci* 2000;25(2):161-166.
135. Langlois X, Megens A, Lavreysen H, Atack J, Cik M, te Riele P, Peeters L, Wouters R, Vermeire J, Hendrickx H, Macdonald G, De Bruyn M. Pharmacology of JNJ-37822681, a specific and fast-dissociating D2 antagonist for the treatment of schizophrenia. *J Pharmacol Exp Ther* 2012;342(1):91-105.
136. Schultz W. Multiple dopamine functions at different time courses. *Annu Rev Neurosci* 2007;30:259-288.
137. Bartholi.G, Haefely W, Jalfre M, Keller HH, Pletsche.A. Effects of Clozapine on Cerebral Catecholaminergic Neuron Systems. *Br J Pharmacol* 1972;46(4):736-740.
138. Jones C, Kapur S, Remington G, Zipursky RB. Transient D_2 dopamine receptor occupancy in low EPS-incidence drugs: PET evidence. *Biol Psychiat* 2000;47(8):112s-112s.
139. Carboni L, Negri M, Michielin F, Bertani S, Fratte SD, Oliosi B, Cavanni P. Slow dissociation of partial agonists from the D_2 receptor is linked to reduced prolactin release. *Int J Neuropsychopharmacol* 2012;15(5):645-656.
140. Kapur S, Seeman P. Does fast dissociation from the dopamine D_2 receptor explain the action of atypical antipsychotics?: A new hypothesis. *Am J Psychiat* 2001;158(3):360-369.
141. Schmidt ME, de Boer P, Andrews R, Neyens M, Rossenu S, William Falteos D, Mannaert E. D_2 receptor occupancy measurement of JNJ-37822681, a novel fast off-rate D_2 receptor antagonist, in healthy subjects using positron emission tomography: single dose versus steady state and dose selection. *Psychopharmacology (Berl)*. 2012;224(4):549-557.
142. Schmidt ME, Kent JM, Daly E, Janssens L, Van Osselaer N, Husken G, Anghelescu IG, Van Nueten L. A double-blind, randomized, placebo-controlled study with JNJ-37822681, a novel, highly selective, fast dissociating D_2 receptor antagonist in the treatment of acute exacerbation of schizophrenia. E*ur Neuropsychopharmacol* 2012;22(10):721-733.
143. Miller DC, Lunn G, Jones P, Sabnis Y, Davies NL, Driscoll P. Investigation of the effect of molecular properties on the binding kinetics of a ligand to its biological target. *MedChemComm* 2012;3(4):449-452.
144. Vale W, Spiess J, Rivier C, Rivier J. Characterization of a 41-residue ovine hypothalamic peptide that stimulates secretion of corticotropin and beta-endorphin. *Science* 1981;213(4514):1394-1397.
145. Dautzenberg FM, Hauger RL. The CRF peptide family and their receptors: yet more partners discovered. *Trends Pharmacol Sci* 2002;23(2):71-77.
146. Bale TL, Vale WW. CRF and CRF receptors: Role in stress responsivity and other behaviors.

Annu Rev Pharmacol 2004;44:525-557.
147. Schulz DW, Mansbach RS, Sprouse J, Braselton JP, Collins J, Corman M, Dunaiskis A, Faraci S, Schmidt AW, Seeger T, Seymour P, Tingley FD, Winston EN, Chen YL, Heym J. CP-154,526: A potent and selective nonpeptide antagonist of corticotropin releasing factor receptors. *Proc Natl Acad Sci U S A* 1996;93(19):10477-10482.
148. Grigoriadis DE. The corticotropin-releasing factor receptor: a novel target for the treatment of depression and anxiety-related disorders. *Expert Opin Ther Tar* 2005;9(4):651-684.
149. Holsboer F. The corticosteroid receptor hypothesis of depression. *Neuropsychopharmacol* 2000;23(5):477-501.
150. Chen C. Recent advances in small molecule antagonists of the corticotropin-releasing factor type-1 receptor-focus on pharmacology and pharmacokinetics. *Curr Med Chem* 2006;13(11):1261-1282.
151. Fleck BA, Hoare SR, Pick RR, Bradbury MJ, Grigoriadis DE. Binding kinetics redefine the antagonist pharmacology of the corticotropin-releasing factor type 1 receptor. *J Pharmacol Exp Ther* 2012;341(2):518-531.
152. Miller DC, Klute W, Brown AD. Discovery of potent, metabolically stable purine CRF-1 antagonists with differentiated binding kinetic profiles. *Bioorg Med Chem Lett* 2011;21(20):6108-6111.
153. Ramsey SJ, Attkins NJ, Fish R, van der Graaf PH. Quantitative pharmacological analysis of antagonist binding kinetics at CRF_1 receptors *in vitro* and *in vivo*. *Br J Pharmacol* 2011;164(3):992-1007.
154. Gilligan PJ, Robertson DW, Zaczek R. Corticotropin releasing factor (CRF) receptor modulators: Progress and opportunities for new therapeutic agents. *J Med Chem* 2000;43(9):1641-1660.
155. Kehne J, De Lombaert S. Non-peptidic CRF_1 receptor antagonists for the treatment of anxiety, depression and stress disorders. Curr Drug Targets *CNS Neurol Disord* 2002;1(5):467-493.
156. Hollenstein K, Kean J, Bortolato A, Cheng RKY, Dore AS, Jazayeri A, Cooke RM, Weir M, Marshall FH. Structure of class B GPCR corticotropin-releasing factor receptor 1. *Nature* 2013;499(7459):438-443.
157. Arvanitis AG, Gilligan PJ, Chorvat RJ, Cheeseman RS, Christos TE, Bakthavatchalam R, Beck JP, Cocuzza AJ, Hobbs FW, Wilde RG, Arnold C, Chidester D, Curry M, He L, Hollis A, Klaczkiewicz J, Krenitsky PJ, Rescinito JP, Scholfield E, Culp S, De Souza EB, Fitzgerald L, Grigoriadis D, Tam SW, Wong YN, Huang S, Shen HL. Non-peptide corticotropin-releasing hormone antagonists: syntheses and structure-activity relationships of 2-anilinopyrimidines and -triazines. *J Med Chem* 1999;42(5):805-818.
158. Hodge CN, Aldrich PE, Wasserman ZR, Fernandez CH, Nemeth GA, Arvanitis A, Cheeseman RS, Chorvat RJ, Ciganek E, Christos TE, Gilligan PJ, Krenitsky P, Scholfield E, Strucely P. Corticotropin-releasing hormone receptor antagonists: framework design and synthesis guided by ligand conformational studies. *J Med Chem* 1999;42(5):819-832.
159. Hann MM. Molecular obesity, potency and other addictions in drug discovery. *MedChemComm* 2011;2(5):349-355.
160. Decourcelles DC, Leysen JE, Roevens P, Vanbelle H. The Serotonin-S2 receptor: a receptor-transducer coupling model to explain insurmountable antagonist effects. *Drug Develop Res* 1986;8(1-4):173-178.
161. Smith C, Rahman T, Toohey N, Mazurkiewicz J, Herrick-Davis K, Teitler M. Risperidone irreversibly binds to and inactivates the h5-HT_7 serotonin receptor. *Mol Pharmacol* 2006;70(4):1264-1270.

162. Hosohata Y, Sasaki K, Shen Y, Hattori K, Suzuki J, Nagatomo T. Bopindolol is a slowly dissociating beta$_1$-adrenoceptor antagonist when compared to other beta-blockers. *Biol Pharm Bull* 1995;18(8):1066-1071.
163. Casarosa P, Kollak I, Kiechle T, Ostermann A, Schnapp A, Kiesling R, Pieper M, Sieger P, Gantner F. Functional and biochemical rationales for the 24-hour long duration of action of olodaterol. *J Pharmacol Exp Ther* 2011;337(3):600-609.
164. Leysen JE, Gommeren W. Drug-receptor dissociation time, new tool for drug research: receptor binding affinity and drug-receptor dissociation profiles of Serotonin-S_2, Dopamine-D_2, Histamine-H_1 Antagonists, and Opiates. *Drug Develop Res* 1986;8(1-4):119-131.
165. Watson C, Jenkinson S, Kazmierski W, Kenakin T. The CCR5 receptor-based mechanism of action of 873140, a potent allosteric noncompetitive HIV entry inhibitor. *Mol Pharmacol* 2005;67(4):1268-1282.
166. Gonsiorek W, Fan X, Hesk D, Fossetta J, Qiu H, Jakway J, Billah M, Dwyer M, Chao J, Deno G, Taveras A, Lundell DJ, Hipkin RW. Pharmacological characterization of Sch527123, a potent allosteric CXCR1/CXCR2 antagonist. *J Pharmacol Exp Ther* 2007;322(2):477-485.
167. Stock N, Volkots D, Stebbins K, Broadhead A, Stearns B, Roppe J, Parr T, Baccei C, Bain G, Chapman C, Correa L, Darlington J, King C, Lee C, Lorrain DS, Prodanovich P, Santini A, Evans JF, Hutchinson JH, Prasit P. Sodium [2'-[(cyclopropanecarbonyl-ethyl-amino)-methyl]-4'-(6-ethoxy-pyridin-3-yl)-6-methoxy-biphenyl-3-yl]-acetate (AM432): a potent, selective prostaglandin D_2 receptor antagonist. *Bioorg Med Chem Lett* 2011;21(3):1036-1040.
168. Sullivan SK, Hoare SRJ, Fleck BA, Zhu YF, Heise CE, Struthers RS, Crowe PD. Kinetics of nonpeptide antagonist binding to the human gonadotropin-releasing hormone receptor: Implications for structure-activity relationships and insurmountable antagonism. *Biochem Pharmacol* 2006;72(7):838-849.
169. Anthes JC, Gilchrest H, Richard C, Eckel S, Hesk D, West RE, Jr., Williams SM, Greenfeder S, Billah M, Kreutner W, Egan RE. Biochemical characterization of desloratadine, a potent antagonist of the human histamine H_1 receptor. *Eur J Pharmacol* 2002;449(3):229-237.
170. Smits RA, Lim HD, van der Meer T, Kuhne S, Bessembinder K, Zuiderveld OP, Wijtmans M, de Esch IJ, Leurs R. Ligand based design of novel histamine H_4 receptor antagonists; fragment optimization and analysis of binding kinetics. *Bioorg Med Chem Lett* 2012;22(1):461-467.
171. Meini S, Bellucci F, Catalani C, Cucchi P, Giolitti A, Santicioli P, Giuliani S. Multifaceted approach to determine the antagonist molecular mechanism and interaction of ibodutant ([1-(2-phenyl-1*R*-[[1-(tetrahydropyran-4-ylmethyl)-piperidin-4-ylmethyl]-carbamoyl]-ethylcarbamoyl)-cyclopentyl]-amide) at the human tachykinin NK_2 receptor. *J Pharmacol Exp* Ther 2009;329(2):486-495.
172. Malherbe P, Kratzeisen C, Marcuz A, Zenner MT, Nettekoven MH, Ratni H, Wettstein JG, Bissantz C. Identification of a critical residue in the transmembrane domain 2 of tachykinin neurokinin 3 receptor affecting the dissociation kinetics and antagonism mode of osanetant (SR 142801) and piperidine-based structures. *J Med Chem* 2009;52(22):7103-7112.
173. Mould R, Brown J, Marshall FH, Langmead CJ. Binding kinetics differentiates functional antagonism of orexin-2 receptor ligands. *Br J Pharmacol* 2014;171(2):351-363.
174. Ring PC, Seldon PM, Barnes PJ, Giembycz MA. Pharmacological characterization of a receptor for platelet-activating factor on guinea pig peritoneal macrophages using [^{3}H]apafant, a selective and competitive platelet-activating factor antagonist: evidence that the noncompetitive behavior of apafant in functional studies relates to slow kinetics of dissociation. *Mol Pharmacol* 1993;43(2):302-312.

175. Behm DJ, Aiyar NV, Olzinski AR, McAtee JJ, Hilfiker MA, Dodson JW, Dowdell SE, Wang GZ, Goodman KB, Sehon CA, Harpel MR, Willette RN, Neeb MJ, Leach CA, Douglas SA. GSK1562590, a slowly dissociating urotensin-II receptor antagonist, exhibits prolonged pharmacodynamic activity *ex vivo*. *Br J Pharmacol* 2010;161(1):207-228.
176. Mullins D, Adham N, Hesk D, Wu Y, Kelly J, Huang Y, Guzzi M, Zhang X, McCombie S, Stamford A, Parker E. Identification and characterization of pseudoirreversible nonpeptide antagonists of the neuropeptide Y Y_5 receptor and development of a novel Y_5-selective radioligand. *Eur J Pharmacol* 2008;601(1-3):1-7.
177. Aronne LJ, Tonstad S, Moreno M, Gantz I, Erondu N, Suryawanshi S, Molony C, Sieberts S, Nayee J, Meehan AG, Shapiro D, Heymsfield SB, Kaufman KD, Amatruda JM. A clinical trial assessing the safety and efficacy of taranabant, a CB_1R inverse agonist, in obese and overweight patients: a high-dose study. *Int J Obes (Lond)* 2010;34(5):919-935.
178. Kipnes MS, Hollander P, Fujioka K, Gantz I, Seck T, Erondu N, Shentu Y, Lu K, Suryawanshi S, Chou M, Johnson-Levonas AO, Heymsfield SB, Shapiro D, Kaufman KD, Amatruda JM. A one-year study to assess the safety and efficacy of the CB_1R inverse agonist taranabant in overweight and obese patients with type 2 diabetes. *Diabetes Obes Metab* 2010;12(6):517-531.
179. http://clinicaltrials.gov/
180. Meltzer HY. Multireceptor atypical antipsychotic drugs. In: Ellenbroek BA, Cools AR, editors. *Atypical Antipsychotics*. Basel: Birkhauser Verlag; 2000. p191–213.
181. Huirne JA, Lambalk CB. Gonadotropin-releasing-hormone-receptor antagonists. *Lancet* 2001;358(9295):1793-1803.
182. Keith DE, Anton B, Murray SR, Zaki PA, Chu PC, Lissin DV, Monteillet-Agius G, Stewart PL, Evans CJ, von Zastrow M. mu-opioid receptor internalization: Opiate drugs have differential effects on a conserved endocytic mechanism *in vitro* and in the mammalian brain. *Mol Pharmacol* 1998;53(3):377-384.

Chapter 3

Dual-point competition association assay A fast and high-throughput kinetic screening method for assessing ligand-receptor binding kinetics

Guo D, Van Dorp EJ, Mulder-Krieger T, Van Veldhoven JPD, Brussee J, IJzerman AP, Heitman LH.
Adapted from: *J Biomol Screen* 2013;18(3):309-320.

About this chapter

This chapter introduces a method that enables fast and large format kinetics screening—the dual-point competition association assay. It measures radioligand binding at two different time points in the absence or presence of unlabeled competitors. This assay yields the kinetic rate index (KRI), which is a measure for the binding kinetics of the unlabeled ligands screened. As a prototypical drug target the adenosine A_1 receptor (A_1R) was chosen for assay validation and optimization. A screen with 35 high affinity A_1R antagonists yielded seven compounds with a KRI-value above 1.0, which indicated a relatively slow dissociation from the target. All other compounds had a KRI-value below or equal to 1.0, predicting a relatively fast dissociation rate. Several compounds were selected for follow-up kinetic quantifications in classical kinetic assays and were shown to have kinetic rates that corresponded to their KRI-values. The dual-point assay and KRI-value may have general applicability at other GPCRs, and at drug targets from other protein families.

3.1 Introduction

The traditional paradigm of drug discovery places an emphasis on dose-dependent assessments (i.e., affinity or potency) to identify lead compounds, which are usually performed under equilibrium conditions.[1,2] With this approach ligand-receptor binding kinetics are usually overlooked. However, the importance of this latter aspect is increasingly recognized, since several lines of research have retrospectively suggested that the binding kinetics, especially the lifetime of the ligand-receptor interaction, is a critical differentiator and predictor for drug efficacy and safety.[1-5] This emerging paradigm shift from a classical affinity-based approach emphasizes ligand-receptor residence time (RT, the reciprocal of the dissociation rate constant k_{off}),[6] which is a measure for the duration that a ligand stays in complex with its target.

In this chapter we introduce an assay to perform kinetic binding screens, namely the dual-point competition association assay. This method is based on the theory developed by Motulsky and Mahan, where an unlabeled competitor is co-incubated with a radioligand during a kinetic association experiment.[11] If the competitor dissociates faster from its target than the radioligand, the specific binding of the radioligand will slowly and monotonically approach its equilibrium in time (Figure 3.1, Curve C). However, when the competitor dissociates slower, the association curve of the radioligand will consist of two phases starting with a typical 'overshoot' and then a decline until a new equilibrium is reached (Figure 3.1, Curve B). In the dual-point competition association assay, we select two time points to measure radioligand binding: 1) at which the radiolabeled ligand just reaches equilibrium under control conditions in the absence of an unlabeled ligand (Figure 3.1, Curve A and t_1), and 2) at which the incubation time is long enough for the labeled and unlabeled compound to equilibrate with the target (Figure 3.1, Curve B and C, t_2). Next, we calculate the ratio of the binding at the first time point (B_{t1}) and that at the second time point (B_{t2}), which we define as the 'kinetic rate index' (KRI) value for a certain unlabeled compound. In this manner, the compounds that quickly dissociate from their target will have a ratio below or equal to one (Figure 3.1, Curve C). Conversely, compounds that dissociate slowly from their target, compared to the radioligand used, will have a KRI value larger than one, resulting from the typical 'overshoot' in the association curve (Figure 3.1, Curve B).

In the present chapter, we have used the adenosine A_1 receptor (A_1R)

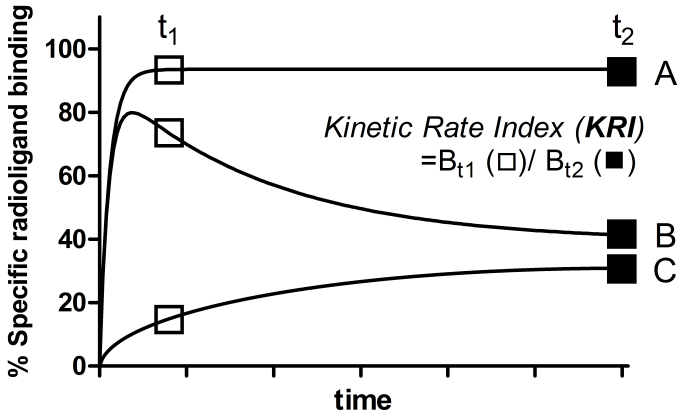


Figure 3.1 | Schematic presentation of the background for the dual-point competition association assay. Curve A: a radioligand association curve without a co-incubation of unlabeled competitor. Curve B: a co-incubated unlabeled competitor dissociates slower than the radioligand used ($k_2 > k_4$). Curve C: a co-incubated unlabeled competitor dissociates faster than the radioligand used ($k_2 < k_4$). B_{t1}: specific radioligand binding at the first time point (t_1); B_{t2}: specific radioligand binding at the second time point (t_2). Kinetic rate index (KRI) is defined as B_{t1} / B_{t2}.

as a prototypic target to illustrate the utility of the dual-point competition association screening method and the resulting KRI-values. The adenosine A_1R is one of four adenosine receptors subtypes (i.e., A_1, A_{2A}, A_{2B} and A_3 receptors), which belong to the superfamily of G protein-coupled receptors (GPCRs).[12,13] The A_1R is a promising therapeutic target, since it has clinical relevance in neurological disorders, such as cognition deficits, and is involved in cardiovascular preconditioning.[14,15] A tool compound, namely FSCPX (Figure 3.5), was used to set up the dual-point screening assay, since it is a known irreversibly binding antagonist for the A_1R.[16] In total 35 in-house synthesized A_1R antagonists were screened using the dual-point competition association assay.[17,18] Eight compounds with divergent KRI values were selected for extensive kinetic assessments. Moreover, we decided to radiolabel one of the slowly dissociating antagonists, namely LUF5962 (compound **31**, Figure 3.5),[17] tested its binding kinetics in traditional kinetic association and dissociation assays to validate the results from our dual-point screening assay, and used it subsequently to profile the same panel of 35 compounds.

3.2 Materials and methods

Chemicals and reagents

[^{3}H]-1,3-dipropyl-8-cyclopentyl-xanthine ([^{3}H]-DPCPX, specific activity 116.7 Ci/mmol) was purchased from ARC Inc. (St. Louis, USA). Adenosine deaminase (ADA) was purchased from Boehringer Mannheim (Mannheim, Germany). CHAPS [3-((3-cholamidopropyl)-dimethylammonio)-1-propanesulfonate)] were obtained from Carl Roth GmbH (Karlsruhe, Germany). DPCPX (selective A_1R antagonist[31]), PEI (Polyethyleneimine) and bovine serum albumin (BSA) were from Sigma (St. Louis, MO, U.S.A). Bicinchoninic acid (BCA) and BCA protein assay reagent were obtained from Pierce Chemical Company (Rockford, IL, U.S.A.). All 35 A_1R antagonists were synthesized in our laboratory as described previously.[17,18] Chinese hamster ovary cells stably expressing the hA_1R were obtained from Prof. Steve Hill (University of Nottingham, UK). All other chemicals were of analytical grade and obtained from standard commercial sources.

Preparation of [^{3}H]-LUF5962

[^{3}H]-8-cyclopentyl-2,6-diphenyl-9H-purine ([^{3}H]-LUF5962, specific activity 51.7 Ci/mmol) was customly labeled by RC Tritec (Teufen, Switzerland). Unlabeled LUF5962 was provided as a dehydrogenenated precursor compound, namely 8-cyclopent-3-en-1-yl-2,6-diphenyl-9H-purine. This compound was dissolved in ethanol, 10% Pd/C was added to the solution, and the reaction mixture was tritiated with tritium gas. After removal of labile tritium and purification by HPLC, the one-stage synthesis yielded [^{3}H]-LUF5962 with a specific activity of 54.0 Ci/mmol (2.0 TBq/mmol). The radiochemical purity was > 97%, as determined by HPLC.

[^{3}H]-LUF5962 binding assay optimization

The assay conditions for [^{3}H]-LUF5962 binding to CHOhA$_1$R membranes were optimized according to a general radioligand binding protocol in our laboratory.[21] Initial experiments were performed with 1.0 nM (approximately 12,000 DPM) [^{3}H]-LUF5962 and 5 µg of CHOhA$_1$R membranes in a simple buffer of low ionic strength (25 mM Tris-HCl, pH 7.4) to which 5 mM $MgCl_2$ was added. Next, we studied further buffer components, filters, filter pretreatment and different radioligand and membrane concentrations to improve the window of specific binding. Firstly, a relatively low concentration (1.0 nM) of [^{3}H]-LUF5962 was enough for an appreciable window of specific binding, which was improved by the addition of 0.1% CHAPS due to a decrease in non-specific binding, while the addition of 0.1% BSA had no effect. Secondly, coating GF/B or GF/C glass fiber filters with PEI to separate free from membrane-bound radioligand did not significantly reduce the non-specific binding (data not shown). Taken together, it was decided to add 0.1% CHAPS in the assay buffer, use uncoated GF/B filters and 5 µg of membranes to yield a desired window of approximately 2000 DPM. Total binding of the radioligand was around 35% of the amount added and thus resulted in radioligand depletion that was unavoidable due to relatively high non-specific binding of [^{3}H]-LUF5962 even under optimized conditions. Finally, initial kinetic association experiments taught us that the optimal incubation time to reach equilibrium was 30 min at 25 °C.

Cell culture and membrane preparation

Chinese hamster ovary cells stably expressing the human adenosine A_1 receptor (CHOhA$_1$R) were grown in Ham's F12 medium containing 10% (v/v) normal adult bovine serum, streptomycin (100 µg/mL), penicillin (100 IU/mL), and G418 (0.4 mg/mL) at 37 ˚C in 5% CO_2. Cells were subcultured twice weekly at a ratio of 1:20 on 10 cm ø culture plates. For membrane preparation, cells were subcultured 1:10 and then transferred to 15 cm ø plates. Cells grew to 80%-90% confluency were detached from plates by scraping them into 5 mL PBS, collected and centrifuged at 700 × g (3000 r.p.m.) for 5 min. Cell pellets derived from 30 plates were pooled and resuspended in 20 mL of ice-cold 25 mM Tris-HCl buffer, pH 7.4. An UltraThurrax (Heidolph Instruments, Schwabach, Germany) was used to homogenize the cell suspension. Membranes and the cytosolic fraction were

separated by centrifugation at 100,000 × g (31,000 r.p.m.) in a Beckman Optima LE-80K ultracentrifuge (Beckman Coulter, Fullerton, CA) at 4 ˚C for 20 min. The pellet was resuspended in 15 mL of the Tris-HCl buffer and the homogenization and centrifugation step was repeated. Tris-HCl buffer (10 mL) was used to resuspend the pellet and ADA was added (0.8 IU/mL) to break down endogenous adenosine. Membranes were stored in 250 µL aliquots at -80 ˚C. Concentrations of the membrane protein were measured using the BCA method.[19]

Radioligand saturation and displacement assays

Membrane aliquots containing 5 µg of protein were incubated in a total volume of 100 µL of assay buffer [25 mM Tris-HCl, pH 7.4, supplemented with 5 mM $MgCl_2$ and 0.1% (w/v) CHAPS] at 25 ˚C for one hour ([^{3}H]-DPCPX) or three hours ([^{3}H]-LUF5962). Notably, optimal incubation times were determined with Equation 5 under *Data analysis*, which ensured that binding of the radioligand at the lowest concentration also reached equilibrium. For saturation experiments, a range of concentrations of [^{3}H]-DPCPX (~0.2-20 nM) or [^{3}H]-LUF5962 (~0.1-13 nM) was used, respectively. In an initial experiment, nonspecific binding was determined at twelve concentrations of radioligand (i.e., [^{3}H]-DPCPX ~0.2-20 nM and [^{3}H]-LUF5962 ~0.1-13 nM) in the presence of 100 µM N^6-cyclopentyladenosine (CPA, selective A_1R agonist[32]). Since the nonspecific binding of both radioligands proved to be linear for these concentrations ($r^2 > 0.95$, $P < 0.0001$, data not shown), it was decided to use only three, evenly spaced, concentrations of radioligand to determine nonspecific binding in following saturation experiments. Displacement experiments were performed using eleven concentrations of competing ligands in the presence of 2.5 nM [^{3}H]-DPCPX. At this concentration, total radioligand binding did not exceed 10% of that added to prevent ligand depletion. Nonspecific binding was determined in the presence of 100 µM CPA. Incubations were terminated by rapid vacuum filtration to separate the bound and free radioligand through 96-well GF/B filter plates using a Perkin Elmer Filtermate-harvester (Perkin Elmer, Groningen, Netherlands) or through Whatman GF/B filters (Whatman International, Maidstone, UK) using a Millipore manifold (Millipore, Billerica, MA, USA). Filters were subsequently washed three times with ice-cold wash buffer (25

mM Tris-HCl, pH 7.4, supplemented with 5 mM $MgCl_2$). The filter-bound radioactivity was determined by scintillation spectrometry using the P-E 1450 Microbeta Wallac Trilux scintillation counter (Perkin Elmer, Groningen, Netherlands) for 96-well GF/B filter plates or by a liquid scintillation counter (Tri-Carb 2900 TR, Perkin-Elmer) for Whatman GF/B filters.

Radioligand association and dissociation assays

Association experiments were performed by incubating membrane aliquots containing 5 μg of protein in a total volume of 100 μL of assay buffer at 25 °C with 2.5 nM [^{3}H]-DPCPX or 1.0 nM [^{3}H]-LUF5962. The amount of radioligand bound to the receptor was measured at different time intervals during a total incubation of 20 min for [^{3}H]-DPCPX or one hour for [^{3}H]-LUF5962. Dissociation experiments were performed by pre-incubating membrane aliquots containing 5 μg of protein in a total volume of 100 μL of assay buffer either for 20 min for [^{3}H]-DPCPX or for one hour for [^{3}H]-LUF5962. After the pre-incubation, radioligand dissociation was initiated by the addition of 10 μM unlabeled CPA. The amount of radioligand still bound to the receptor was measured at various time intervals for a total of one hour for [^{3}H]-DPCPX or two hours for [^{3}H]-LUF5962 to ensure that they were fully dissociated from hA_1R. Incubations were terminated and samples were obtained as described under *Radioligand saturation and displacement assays.*

Competition association assay

The binding kinetics of unlabeled ligands was quantified using the competition association assay based on the theoretical framework by Motulsky and Mahan.[11] In the standard assay, three different concentrations of unlabeled DPCPX were tested, namely at 0.3-, 1- and 3-fold its K_i. For unlabeled LUF5962, 1-, 3- and 10-fold its K_i were used, while for FSCPX, 3-, 10- and 30-fold its K_i were used. In the simplified one-concentration competition association assay, only a concentration of 10-fold of the K_i value was used to determine the binding kinetics of unlabeled ligands. The competition association assay was initiated by adding membrane aliquots (5

μg/well) at different time points for a total of 90 min to a total volume of 100 μL of assay buffer at 25 °C with 2.5 nM [^{3}H]-DPCPX in the absence or presence of competing ligand (10-fold K_i). Only for FSCPX the assay time was increased to 180 min. Incubations were terminated and samples were obtained as described under *Radioligand saturation and displacement assays*.

Dual-point competition association assay

The dual-point competition association experiments were performed by incubating membrane aliquots containing 5 μg of protein for 15 min or 120 min in a total volume of 100 μL of assay buffer with 2.5 nM [^{3}H]-DPCPX and for 30 min or 120 min with 1.0 nM [^{3}H]-LUF5962 in the absence or presence of unlabeled ligands. The amount of radioligand bound to the receptor was measured after co-incubation of the unlabeled A_1R antagonists at 10-fold their respective K_i values. Incubations were terminated after either 15 min or 120 min for [^{3}H]-DPCPX and 30 min or 120 min incubation for [^{3}H]-LUF5962 and samples were obtained as described under *Radioligand saturation and displacement assays*. Kinetic rate index (KRI) values of unlabeled ligands were calculated by using Equation 6 as mentioned below in *Data analysis*.

Data analysis

All experimental data was analyzed by using GraphPad Prism 5.0 (GraphPad Software Inc., San Diego, CA). All values obtained are means of at least three independent experiments performed in duplicate. K_D and B_{max} values of [^{3}H]-DPCPX or [^{3}H]-LUF5962 at hA_1R membranes were obtained by computational analysis of saturation curves. IC_{50} values obtained from competition displacement binding data were converted into K_i values using the Cheng-Prusoff equation.[20] Association data was fitted using *one phase exponential association* as follows:

$$Y = Y_{\max} \cdot (1 - e^{-k_{obs} \cdot t}) \quad (1)$$

Where t is a given time, Y is the amount of specific radioligand binding, Y_{max} the specific radioligand binding at equilibrium, k_{obs} the observed rate constant to approach equilibrium. The time for a radioligand to reach half of the Y_{max} ($t_{1/2,\ association}$, the association half-life) is

$$t_{1/2,association} = \frac{\ln 2}{k_{obs}} \tag{2}$$

Values for k_{on} were obtained by converting k_{obs} values as follows:

$$k_{on} = \frac{k_{obs} - k_{off}}{[radioligand]} \tag{3}$$

where k_{off} was determined in independent dissociation experiments. Dissociation data was fitted using *one phase exponential decay*.

In the dual-point competition association assay, t_1 was set at the time that radioligand binding just reached equilibrium. Specifically, we have defined the time to reach equilibrium, when 99.5% of total binding was reached, i.e., at 8-fold the association half-life. Thus,

$$t_1 = 8 \cdot t_{1/2,association} \tag{4}$$

Taken together, t_1 was determined by combining Equations 2, 3 and 4 as follows:

$$t_{1/2,association} = \frac{\ln 2}{k_{on} \cdot [radioligand] + k_{off}} \tag{5}$$

The second time point (t_2) was arbitrarily set at a time long enough for the binding of the unlabeled ligand to reach a plateau. KRI (kinetic rate index) values were calculated by dividing the specific radioligand binding measured at t_1 (B_{t1}) by its binding at t_2 (B_{t2}) in the presence of unlabeled competing ligands as follows:

$$KRI = \frac{B_{t_1}}{B_{t_2}} \tag{6}$$

Association and dissociation rates for unlabeled ligands were calculated by fitting the data in the competition association model using '*kinetics of competitive binding*' in Prism 5 as follows:[11]

$$
\begin{aligned}
K_A &= k_1 \cdot [L] \cdot 10^{-9} + k_2 \\
K_B &= k_3 \cdot [I] \cdot 10^{-9} + k_4 \\
S &= \sqrt{(K_A - K_B)^2 + 4 \cdot k_1 \cdot k_3 \cdot L \cdot I \cdot 10^{-18}} \\
K_F &= 0.5 \cdot (K_A + K_B + S) \\
K_S &= 0.5 \cdot (K_A + K_B - S) \\
Q &= \frac{B_{\max} \cdot k_1 \cdot L \cdot 10^{-9}}{K_F - K_S} \\
Y &= Q \cdot \left(\frac{k_4 \cdot (K_F - K_S)}{K_F \cdot K_S} + \frac{k_4 - K_F}{K_F}(-K_F \cdot X) - \frac{k_4 - K_S}{K_S} e^{(-K_S \cdot X)}\right)
\end{aligned}
\tag{7}
$$

where X is the time (min), Y is the specific binding (DPM), k_1 the k_{on} ($M^{-1} \cdot min^{-1}$) of [^{3}H]-DPCPX predetermined in association experiments, k_2 the k_{off} (min^{-1}) of [^{3}H]-DPCPX predetermined in dissociation experiments, L the concentration of [^{3}H]-DPCPX used (nM), B_{max} the total binding (DPM) and I the concentration of unlabeled ligand (nM). Fixing these parameters into Equation 7 allows the following parameters to be calculated: k_3 is the k_{on} ($M^{-1} \cdot min^{-1}$) of the unlabeled ligand and k_4 is the k_{off} (min^{-1}) of the unlabeled ligand. The association and dissociation rates were used to calculate the 'kinetic K_D' as follows:

$$K_D = \frac{k_{off}}{k_{on}} \tag{8}$$

3.3 Results and discussion

Quantification of the K_D and B_{max} of [^{3}H]-DPCPX and [^{3}H]-LUF5962 in saturation binding experiments

Saturation binding experiments were performed with [^{3}H]-DPCPX and [^{3}H]-LUF5962 at 25°C. Both [^{3}H]-DPCPX and [^{3}H]-LUF5962 bound saturably and specifically to a single class of binding sites at CHOhA_1R membranes. The K_D value of [^{3}H]-DPCPX obtained from the saturation experiments was

2.5 ± 0.1 nM and the B_{max} value was 14.0 ± 1.0 pmol/mg protein, while the K_D value of [^{3}H]-LUF5962 was 0.83 ± 0.08 nM and the B_{max} was 17.1 ± 0.9 pmol/mg protein (Table 3.1). It should be kept in mind that ligand depletion was an issue when using [^{3}H]-LUF5962, and thus it represents a less than ideal radioligand. However, in the paragraphs below we discuss that it can still be effectively used in the kinetic characterization of unlabeled ligands. The K_D value for [^{3}H]-DPCPX obtained in this experiment was in line with the K_D value reported previously.[21] This K_D was used to derive K_i values from IC_{50} values for unlabeled ligands (see below).

Quantification of the association [k_{on} (k_1)] and dissociation rates [k_{off} (k_2)] of [^{3}H]-DPCPX and [^{3}H]-LUF5962 at CHOhA$_1$R membranes

Receptor association [k_{on} (k_1)] and dissociation rates [k_{off} (k_2)] of [^{3}H]-DPCPX and [^{3}H]-LUF5962 were determined in standard radioligand association and dissociation experiments. Association and dissociation assays were conducted at 25 ˚C for both radioligands. The observed association rates (k_{obs}) were converted to k_{on} values by using Equation 3 described in *Methods*. The binding of [^{3}H]-DPCPX and [^{3}H]-LUF5962 approached equilibrium after approximately 15 and 30 min, respectively (Figure 3.2). Both [^{3}H]-DPCPX and [^{3}H]-LUF5962 had relatively fast association rates of 0.20 ± 0.01 $nM^{-1}\cdot min^{-1}$ and 0.13 ± 0.01 $nM^{-1}\cdot min^{-1}$, respectively. Binding of both radioligands was reversible after the addition of 10 μM CPA and complete dissociation was reached after approximately 25 min for [^{3}H]-DPCPX and 120 min for [^{3}H]-LUF5962 (Figure 3.2). The dissociation rate of [^{3}H]-LUF5962 was eight-fold lower than that of [^{3}H]-DPCPX from the hA$_1$R (Figure 3.2 and Table 3.1). The dissociation binding constants (kinetic K_D) of the radioligands were derived from the dissociation and association rates. [^{3}H]-LUF5962 had an approximately five-fold higher affinity than [^{3}H]-DPCPX, 0.20 ± 0.02 nM compared to 1.1 ± 0.1 nM, respectively.

Quantification of the affinity (K_i) of A$_1$R ligands in displacement experiments

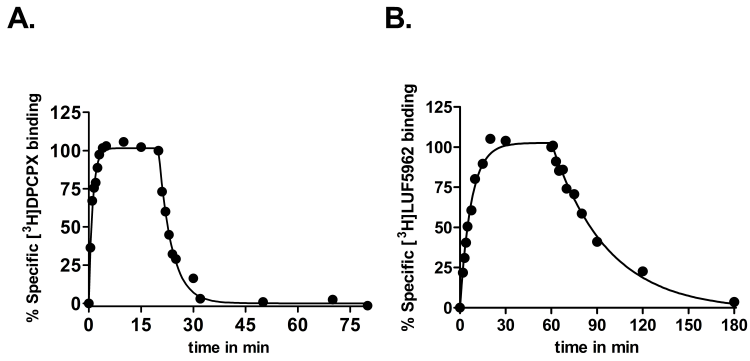


Figure 3.2 | Association and dissociation kinetics of [^{3}H]-DPCPX (Panel A) and [^{3}H]-LUF5962 (Panel B) at 25 ˚C to and from human adenosine A_1 receptors stably expressed on CHO membranes. Association data was fitted in Prism 5.0 using *one-phase exponential association*. Values for k_{on} were obtained by using Equation 3. Dissociation data was fitted using *one-phase exponential decay*. Representative graphs from one experiment performed in duplicate.

Displacement experiments with several A_1R ligands were performed at 25 ˚C to determine their affinities for the hA_1R. The tested hA_1R antagonists showed concentration-dependent inhibition of specific [^{3}H]-DPCPX binding and the data was best fitted to a one-site competition model. Unlabeled DPCPX and LUF5962 had affinities of 2.3 ± 0.3 nM and 0.24 ± 0.03 nM, respectively (Table 3.1). Affinities of other antagonists shown in Table 3.2 were taken from previously published in-house experiments.[17,18]

Validation and optimization of the competition association assay at the hA_1R

With the pre-characterized k_{on} (k_1) and k_{off} (k_2) values of [^{3}H]-DPCPX binding from direct association and dissociation experiments, k_{on} (k_3) and k_{off} (k_4) values of unlabeled DPCPX and LUF5962 were determined by fitting the values into Equation 7 described in *Methods*. Three different concentrations of the unlabeled reference compounds (DPCPX and LUF5962) were tested

Table 3.1 | Comparison of the affinity and kinetic rates of DPCPX and LUF5962 obtained in different radioligand binding assays.

Cmpd	*K_D (nM)*[a]	*K_i (nM)*[b]	*k_{on} ($nM^{-1}\cdot min^{-1}$)*[c]	*k_{off} (min^{-1})*[d]	*Kinetic K_D (nM)*[e]
DPCPX	2.5 ± 0.1	2.3 ± 0.3	0.20 ± 0.01	0.21 ± 0.01	1.1 ± 0.1
LUF5962	0.83 ± 0.08	0.24 ± 0.03	0.13 ± 0.01	0.025 ± 0.002	0.20 ± 0.02

Values are means ± s.e.m of at least three independent experiments performed in duplicate. [a] [^{3}H]-DPCPX (~0.2-20 nM) or [^{3}H]-LUF5962 (~0.1-13 nM) saturation binding to $CHOhA_1$ membranes at 25 ˚C. [b] from displacement of specific [^{3}H]-DPCPX binding from $CHOhA_1$ membranes at 25 ˚C. [c] Association [k_{on} (k_1)] of [^{3}H]-DPCPX or [^{3}H]-LUF5962 to $CHOhA_1R$ membrane at 25 ˚C. [d] Dissociation [k_{off} (k_2)] of [^{3}H]-DPCPX or [^{3}H]-LUF5962 from $CHOhA_1R$ membrane at 25 ˚C. [e] Kinetic $K_D = k_{off} / k_{on}$. k_{on} (k_1) values were generated from [^{3}H]-DPCPX (2.5 nM) or [^{3}H]-LUF5962 (1.0 nM) association assays; k_{off} (k_2) values were generated from [^{3}H]-DPCPX (2.5 nM) or [^{3}H]-LUF5962 (1.0 nM) dissociation assays at 25 ˚C.

(Figure 3.3). Their k_{on} (k_3) and k_{off} (k_4) values determined by the competition association method were 0.14 ± 0.02 $nM^{-1}\cdot min^{-1}$ and 0.25 ± 0.01 min^{-1} for unlabeled DPCPX (Figure 3.3A, Table 3.2), and 0.060 ± 0.010 $nM^{-1}\cdot min^{-1}$ and 0.021 ± 0.005 min^{-1} for LUF5962 (Figure 3.3B, Table 3.2), which were in accordance with the k_1 and k_2 values determined in 'traditional' association and dissociation experiments (Figure 3.2 and Table 3.1). Comparison of the dissociation constants and affinities obtained from the different equilibrium and kinetic experiments (Table 3.1) further verified that the competition association assay could be accurately used to determine the binding kinetics of unlabeled A_1R ligands.

Optimization of the dual-point competition association assay at the hA_1R

For the dual-point competition association assay it was necessary to decide on the optimal compound concentration and the two time points (t_1 and t_2) to obtain a robust kinetic screening assay. Therefore, we decided to optimize the assay using the reference antagonist FSCPX as a positive control, which is known to bind irreversibly to the hA_1R.[16]

Firstly, we used concentrations that represented 3-, 10- and 30-fold K_i values of unlabeled FSCPX to study the influence of different concentrations on the kinetic assay. It follows from Figure 3.4A that a long incubation time

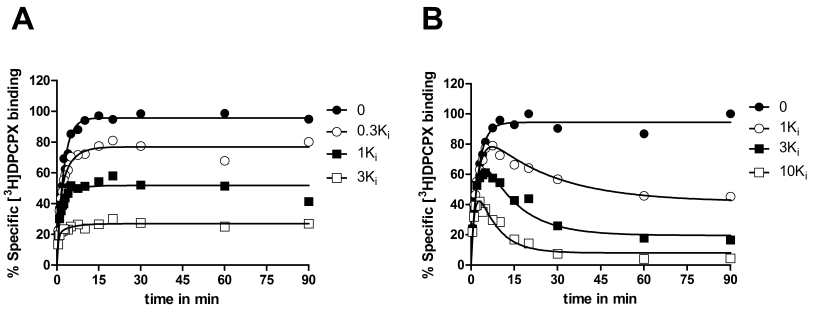


Figure 3.3 | Validation and optimization of the competition association assay at the hA_1R. Competition association assay with [^{3}H]-DPCPX at 25 ˚C from human adenosine A_1 receptors stably expressed on CHO membranes in the absence or presence of 0.3-fold, one-fold and three-fold K_i value of unlabeled DPCPX (Panel A) or one-fold, three-fold and ten-fold K_i value of LUF5962 (Panel B). Association and dissociation rates for unlabeled ligands were calculated by fitting the data in the competition association model as in Equation 7.[11] Representative graph from one experiment performed in duplicate.

(i.e., 180 min) is needed for FSCPX to abrogate all [^{3}H]-DPCPX binding at a low concentration, i.e., 3-fold its K_i value. The co-application of 30-fold its K_i value resulted in a faster knockdown of [^{3}H]-DPCPX binding sites, i.e., after approximately 60 min. Such a significant decrease of [^{3}H]-DPCPX binding reduced the KRI window. Incubation of the membranes with an FSCPX concentration equaling 10 times its K_i value led to an intermediate situation (Figure 3.4A). Notably, the set of three FSCPX concentrations are higher than the concentrations used in experiments with LUF5962 and DPCPX (Figure 3.3). In order to achieve radioligand equilibrium binding as much as possible with slowly dissociating competitors (or irreversibly binding competitors like FSCPX) in the same experimental incubation time, higher concentrations need to be used than for competitors with relatively faster or equal dissociation rates. The latter has also been described for the muscarinic M_3 and histamine H_3 receptor.[9,28] In the present chapter, we observed that 10-fold K_i of the competitor gave reasonably large assay windows for all three ligands displaying divergent off-rates (i.e., DPCPX, LUF5962 and FSCPX). Hence, for screening purposes it was decided to use concentrations equal to 10-fold the K_i values of the respective unlabeled ligands. It is important to note that 10-fold K_i is optimal for A_1R in the current protocol, yet this

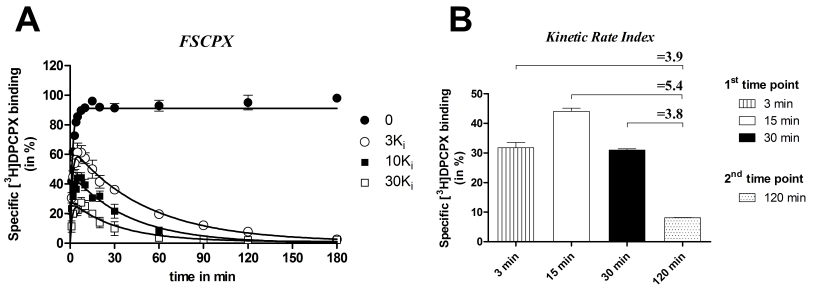


Figure 3.4 | Optimization of the dual-point competition association assay at hA_1R. Competition association assay with [^{3}H]-DPCPX at 25 ˚C from human adenosine A_1 receptors stably expressed on CHO membranes in the absence or presence of 3-fold, 10-fold and 30-fold K_i value of FSCPX (Panel A). Association and dissociation rates for unlabeled FSCPX were calculated by fitting the data in the competition association model using '*kinetics of competitive binding*' in Prism 5 in Equation 7.[11] Kinetic rate indexes of FSCPX calculated from the ratio of specific [^{3}H]-DPCPX binding at 3 min, 15 min or 30 min and its binding at 120 min (Panel B). KRI values were calculated by using Equation 6. Data are shown as mean ± s.e.m from three separate experiments each performed in duplicate.

concentration may not be suitable on other drug targets, especially when divergent concentrations of radioligand are used in the competition association assay. For instance, Dowling and Charlton used approximately 25-fold K_D of the radioligand in their competition association assay on the muscarinic M_3 receptor. This requires higher concentrations of unlabeled ligands (from 10-fold to 1000-fold their respective K_i values) to achieve full resolution of radioligand equilibrium binding within the frame of incubation time.[9] Similarly, Slack *et al.* used higher concentrations of unlabeled ligands (from less than 15-fold to over 200-fold K_i) in their competition association assays on histamine H_1 and H_3 receptors.[28] Therefore, for a general optimization of the dual-point assay on other drug targets, it is suggested that one should take into account the radioligand's concentration, assay incubation time and expected kinetic profiles of the competitors for optimization of the competitors concentration, since all these parameters influence the resolution of the assay.

Secondly, we optimized the two time points (t_1 and t_2). As for t_2 the incubation time was set at 120 min, which was based on the observation in Figure 3.4A that in the presence of an FSCPX concentration of 10-fold its

K_i value [^{3}H]-DPCPX binding was negligible after 120 min incubation. As mentioned above, we assumed that within this time frame most compounds would equilibrate with the target, even if they were kinetically different, as further corroborated by Figure 3.3. As for t_1 the incubation time was set at 15 min, since under control conditions (i.e., absence of unlabeled ligand) [^{3}H]-DPCPX binding reached equilibrium after 15 minutes at 25˚C according to Equation 5 and Figure 3.2A. It was also tried to set t_1 at a much longer (i.e., 30 min) or shorter incubation time (i.e., 3 min). From Figure 3.4B it follows that the selection of t_1 and t_2 clearly affects the KRI values obtained. In other words, a shorter or longer incubation time than 15 min for t_1 reduced its margin over the control (KRI = 1.0), i.e., KRI values = 3.9 or 3.8, respectively, while t_1 = 15 min provided a more significant KRI value of 5.4 for FSCPX. Therefore, incubation times of 15 min (t_1) and 120 min (t_2) were used for the dual-point competition association assay with [^{3}H]-DPCPX at the hA_1R. Notably, it is impossible to define an absolute value or cut-criterion of t_1 and t_2, since the two time point set-up is dependent on several factors (i.e., radioligand concentration, temperature). For a general application on other targets, we suggest that one can start with setting t_1 at a time when the radioligand just reaches equilibrium by using Equation 5, while for t_2 a later time point is chosen long enough for the binding of the unlabeled ligand to reach a plateau. A late t_2 of course compromises the convenience of this screening method, as the total assay time increases. Therefore, it may be necessary to perform similar 'tailored' optimizations of time points and concentrations, and even the choice of the radioligand, to obtain robust results on other drug targets.

Kinetic screening of hA_1R antagonists using dual-point competition association assay

In the present chapter, 35 hA_1R antagonists synthesized in-house[17,18] were screened in the newly developed dual-point competition association assay (Figure 3.5). The specific binding of [^{3}H]-DPCPX was measured after 15 min and 120 min and for [^{3}H]-LUF5962 after 30 min and 120 min in the absence and presence of a single concentration of unlabeled competitive ligand (10-fold K_i, in both [^{3}H]-DPCPX and [^{3}H]-LUF5962 assays). This allowed us to calculate the kinetic rate index (KRI) values for each compound by using

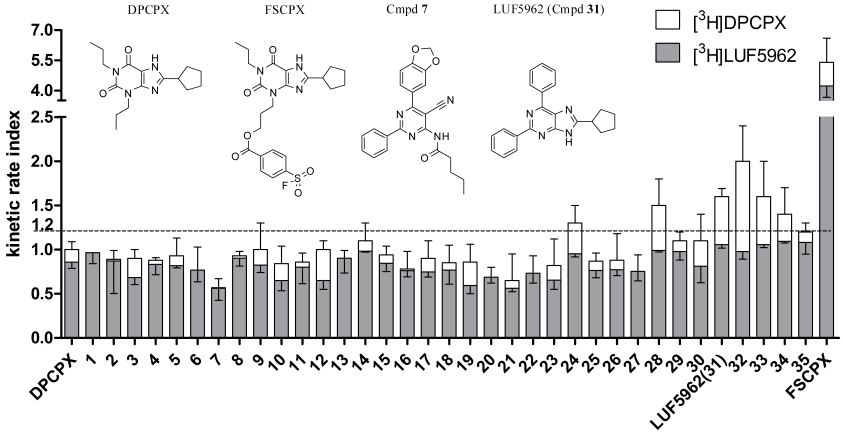


Figure 3.5 | Kinetic rate indexes (KRI) of 35 in-house hA_1R antagonists, DPCPX and FSCPX.[16-18] The KRI values of the same panel of unlabeled ligands against [^{3}H]-LUF5962 (gray bars) are integrated with the results obtained with [^{3}H]-DPCPX (white bars). Values were obtained from the dual-point assays and calculated by using Equation 6. The KRI of the reference compounds, unlabeled DPCPX or LUF5962 (compound **31**), were determined approximately 1.0 in the respective screen. FSCPX was the 'tool compound' and known to bind irreversibly to hA_1R. Seven compounds with a kinetic rate index ≥ 1.2 (the stippled line) were found using [^{3}H]-DPCPX and no compounds with a kinetic rate index ≥ 1.2 were found using [^{3}H]-LUF5962 (excluding FSCPX in both cases). Data are shown as mean ± s.e.m from three separate experiments each performed in duplicate. Chemical structures of DPCPX, FSCPX, compound **7** and LUF5962 (compound **31**) are also presented.

Equation 6. The KRI cut-off value for kinetically interesting compounds was arbitrarily set at 1.2 (Figure 3.5, the stippled line) rather than 1.0 to avoid false positives. It is worth mentioning that the cut-off value for the KRI can be flexible based on a different screening purpose. In other words, one can specifically set it higher to select only longer residence time compounds or lower to obtain more hits for future chemical modifications. In the present chapter, most compounds were found to have KRI values equal to or less than one (Figure 3.5) with both radioligands, which were thus considered to have similar or faster off-rates from the hA_1R compared to the radioligands used, i.e., [^{3}H]-DPCPX or [^{3}H]-LUF5962. Seven compounds, excluding FSCPX, had KRI values ≥ 1.2 with [^{3}H]-DPCPX as the radioligand, which indicated that these compounds dissociated more slowly from the receptor than [^{3}H]-DPCPX (Figure 3.5, white bars). KRI values for the same panel

of unlabeled ligands against [^{3}H]-LUF5962 were also determined (Figure 3.5, gray bars). In the latter situation all compounds displayed a KRI < 1.2, except FSCPX, since the radioligand used ([^{3}H]-LUF5962) has a relatively slow off-rate (0.021 min^{-1}). Interestingly, most of the compounds adopted a concerted trend with a decreased KRI value compared to that obtained with [^{3}H]-DPCPX. This is in accordance with the observation that indeed most compounds have faster dissociation rates than LUF5962 as determined by full kinetic experiments with [^{3}H]-DPCPX (Table 3.2). For validation of the dual-point assay, four compounds with lower or similar KRI values (compared to DPCPX, KRI ≤ 1) and four compounds with higher KRI values (≥1.2) were further characterized in follow-up kinetic assays (Table 3.2).

Subsequently, competition association assays in the presence of [^{3}H]-DPCPX were performed to determine the binding kinetics of the eight compounds that had divergent KRI values (Table 3.2). In the present chapter, we used FSCPX as a tool compound, which had a KRI value of 5.4 ± 1.2 at the hA_1R, indicative of negligible dissociation (Table 3.2 and Figure 3.4A). Similarly to FSCPX, the specific binding of [^{3}H]-DPCPX in the presence of unlabeled LUF5962 (compound **31**) became biphasic, which was represented by a decline towards equilibrium after a typical 'overshoot' (Figure 3.6A). Its dissociation rate was 0.021 ± 0.005 min^{-1}, which was approximately ten times slower than DPCPX's dissociation rate (Table 3.2). Next to that, we also decided to radiolabel this slow off-rate compound, which enabled us to directly determine its off-rate in a classic kinetic dissociation experiment. This assay yielded a dissociation rate of 0.025 ± 0.002 min^{-1}, which was in good agreement with the off-rate determined from the competition association assay (Table 3.1). In addition, this matched with its KRI value of 1.6 ± 0.4 determined in the dual-point screening method against [^{3}H]-DPCPX. Subsequent KRI screening with [^{3}H]-LUF5962 of the same set of compounds also supported our hypothesis that a KRI-value above 1.2 indicates a relatively slow dissociation from the target, while a lower KRI-value predicts a relatively fast dissociation rate. Moreover, additional kinetic experiments of other A_1R antagonists proved that the obtained KRI values were a good predictor for their off-rates (Table 3.2). The three other selected compounds with KRI values bigger than 1.2 (**32**: 2.0 ± 0.4, **33**: 1.6 ± 0.4 and **35**: 1.2 ± 0.3) had dissociation rates of 0.027 ± 0.004 min^{-1}, 0.038 ± 0.010 min^{-1} and 0.088 ± 0.003 min^{-1}, respectively. Next, four compounds (**7**, **13**, **19** and **22**) with KRI values ranging from 0.57 to 1.0 were selected for further characterization of the methodology. As expected, all four compounds had faster or similar off-

Table 3.2 | Kinetics rate indexes (KRI) and binding kinetics obtained from the dual-point or standard competition association assay of DPCPX, FSCPX and representative hA_1R antagonists.

Cmpd	*KRI*[a]	k_{on} *(nM^{-1}·min^{-1})*[b]	k_{off} *(min^{-1})*[b]	*RT (min)*[c]	*Kinetic K_D (nM)*[d]	K_i *(nM)*[e]
DPCPX	1.0 ± 0.1	0.14 ± 0.02	0.25 ± 0.01	4.0 ± 1.0	1.8 ± 0.3	2.3 ± 0.3
FSCPX	5.4 ± 1.2	0.0037 ± 0.0010	0.0010 ± 0.0002	1000 ± 33	0.27 ± 0.09	5.7 ± 1.0
LUF5962 (**31**)	1.6 ± 0.1	0.060 ± 0.010	0.021 ± 0.005	48 ± 12	0.35 ± 0.08	0.24 ± 0.03
32	2.0 ± 0.4	0.042 ± 0.006	0.027 ± 0.004	37 ± 6	0.64 ± 0.10	0.73 ± 0.07
33	1.6 ± 0.4	0.0012 ± 0.0004	0.038 ± 0.010	26 ± 11	32 ± 14	25 ± 5
35	1.2 ± 0.3	0.0043 ± 0.0007	0.088 ± 0.003	11 ± 2	20 ± 3	36 ± 4
7	0.57 ± 0.10	0.48 ± 0.10	3.0 ± 0.9	0.33 ± 0.10	6.3 ± 2.3	9.4 ± 3.0
13	1.0 ± 0.1	0.13 ± 0.07	0.57 ± 0.20	2.0 ± 0.7	4.4 ± 3.0	8.3 ± 0.2
19	0.89 ± 0.10	0.62 ± 0.05	0.68 ± 0.10	1.0 ± 0.2	1.1 ± 0.2	1.1 ± 0.2
22	0.73 ± 0.20	0.10 ± 0.01	0.29 ± 0.01	3.0 ± 0.2	2.9 ± 0.2	4.9 ± 2.0

Values are means ± s.e.m of at least three independent experiments performed in duplicate. [a] Kinetic rate indexes (KRI) were determined in the dual-point competition association assay. [b] k_{on} (k_3), k_{off} (k_4) of unlabeled antagonists values were determined in [^{3}H]-DPCPX (2.5 nM) competition association assay at 25 ˚C. [c] RT (residence time) = 1 / k_{off}. [d] Kinetic K_D = k_{off} / k_{on}. k_{on} (k_3) and k_{off} (k_4) values of unlabeled antagonists were generated from [^{3}H]-DPCPX (2.5 nM) competition association assay association assays at 25˚C. [e] K_i values were from displacement assays at 25 ˚C or obtained from Chang *et al.* and Van Veldhoven *et al.*[17,18]

rates compared to DPCPX (Table 3.2). Typically, [^{3}H]-DPCPX association in the presence of a 'fast' compound such as **7** (Figure 3.5, for its structure) resulted in a slow monophasic ascent of radioligand binding, indicative of a faster dissociation from the receptor than [^{3}H]-DPCPX (Figure 3.6A). Its dissociation rate was determined as 3.0 ± 0.9 min^{-1}, which was more than ten times faster than that of the radioligand. Notably, a good correlation (Figure 3.6B, r^2 = 0.8511, P < 0.0005) was observed between the negative logarithm of the ligands' dissociation rates (pk$_{off}$), excluding that of FSCPX (considering its unique irreversible binding character), and their KRI values derived from our new kinetic screening method. No significant correlation was observed between the negative logarithm of the ligands' association rates (pk$_{on}$) and their KRI values (r^2 = 0.2551, P = 0.1655). This further proved that the KRI value is a good predictor for a ligand's dissociation rate in the dual-point assay.

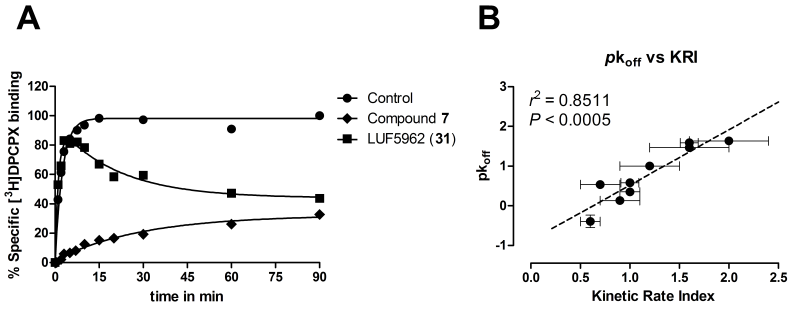


Figure 3.6 | Panel A: Competition association assay of [^{3}H]-DPCPX in the absence or presence of two unlabeled representative hA$_1$R antagonists. LUF5962 (**31**) and compound **7** were found in a dual-point screening assay to have kinetic rate indexes of 1.6 ± 0.1 and 0.57 ± 0.10, respectively. Association and dissociation rates for unlabeled ligands were calculated by fitting the data in the competition association model as in Equation 7.[11] Representative graph from one experiment performed in duplicate. Panel B: Correlation between the negative logarithm of the ligands' dissociation rates (*p*k$_{off}$) and their kinetic rate index (KRI) values derived from dual-point competition association assay (r^2 = 0.8511, P < 0.0005). Data used in this plot are detailed in Table 3.2 (excluding FSCPX, see text). Data are expressed as mean ± s.e.m from three independent experiments.

Advantages of the dual-point competition association assay and its future application in kinetic binding screening

Currently, there are several assays available developed for kinetics screening. For instance, Heise *et al.* developed a scintillation proximity assay (SPA) to measure K$_i$ values for gonadotropin-releasing hormone receptor (GnRH receptor) antagonists after 30 min and 10 h incubation.[22] This assay is based on the observation that a slowly dissociating compound will display a decrease of apparent K$_i$ value over time, since it requires a longer incubation time to reach equilibrium.[11,22] Another methodology is a functional assay described by Morriello *et al.*, where hNK$_1$R overexpressing CHO cells were pretreated with neurokinin 1 receptor (NK$_1$R) antagonists before a measurement of the remaining activity induced by subsequently added substance P (endogenous agonist of hNK$_1$R). A complete reversal of the hNK$_1$R antagonism indicated a short receptor residence time of the compound under evaluation, while

an insurmountable effect of the tested ligand suggested longer receptor occupancy. In such a way, the recovery of the response to substance P gave an indication of an antagonist's receptor off-rate.[23] Similarly, the dual-point assay and its resulting KRI values described in the present chapter allow for a fast selection of long receptor residence time compounds, e.g., compound **31** in the present chapter. Importantly, our new methodology has advantages over other assays. Firstly, as it only needs two assay points for testing one compound, the efficiency of kinetic screening is increased. Secondly, the KRI value derived from this assay yields direct information of a ligand's binding kinetics, thus it allows for discrimination between fast, slowly and very slowly dissociating compounds. Moreover, this assay also provides the ability to identify ligands with short receptor residence times (i.e., compounds with KRI values lower than 1). In terms of therapies that need enduring target occupancy and a long-acting biological efficiency, a slowly dissociating compound might be an appropriate strategy for a clinical application. An example of a marketed long-residence-time drug is candesartan, which is an angiotensin II type 1 (AT_1) receptor antagonist. Its enhanced long-lasting blood pressure lowering effects have been attributed to a slow receptor off-rate; they even persist after the candesartan plasma concentration has become undetectable.[24,25] In contrast, when an endogenous ligand has ubiquitous physiological functions, a rapidly dissociating exogenous ligand might be preferred to prevent the concomitant mechanism-based, on-target toxicity. An example is the short-lived intervention of dopamine-2 receptor (D_2 receptor) activity by clozapine. Its 'atypical', short receptor residence time is thought to prevent adverse effects caused by lasting occupation of striatal D_2 receptors, which respond to fast fluctuations in the local dopamine concentration.[26,27] Importantly, the dual-point assay and the KRI value could be employed to select both slowly and rapidly dissociating compounds (i.e., compound **31** and **7**). This versatility underscores its usability in future early phase drug discovery.

As represented in Figure 3.5, the same set of unlabeled A_1 receptor ligands have different KRI values if tested against two kinetically different radioligands. Indeed, since the dual-point approach and its derived KRI are mainly based on whether an unlabeled competitor dissociates faster or slower from its target than a particular radioligand, the choice of radioligand becomes the key for a reliable kinetic screening. Here we propose that the choice for an 'ideal' radioligand (if one has the luxury of a number of radioligands) should take into account the drug target and the particular screening purpose. More

specifically, if one searches for slowly dissociating compounds, a relatively long residence time radioligand would be preferred, while for short residence time compounds, a relatively fast dissociating radioligand may be needed. By following this principle the load of follow-up kinetic determinations for selected compounds can be reduced. However, it is also necessary to take the assay practicability into consideration. In the present chapter, for instance, LUF5962 has a slow off-rate. According to Equation 5 regarding the t_1 time point set-up, it would require nearly two hours for [^{3}H]-LUF5962 to reach equilibrium when a concentration of one-fold its K_i value (0.24 nM) is used. Logically, this results in an even later t_2 time point. Thus, we applied 1.0 nM [^{3}H]-LUF5962 (approximately four time its K_i) in our additional KRI experiments, enabling a relatively quick t_1 at approximately 30 min and the same t_2 as for [^{3}H]-DPCPX (120 min). The robustness of the dual-point competition assay is underscored by the fact that even a less than ideal radioligand, such as [^{3}H]-LUF5962, can still be used for screening purposes.

In the present chapter, we have merely described the application of the dual-point assay for a prototypical GPCR target, namely the adenosine A_1R. We believe that this assay can have a more general application for other drug targets as well. This consideration is supported by an increasing amount of studies that characterized receptor binding kinetics, such as for the histamine H_1 receptor, the corticotropin-releasing factor type-1 receptor (CRF_1R) and more recently the adenosine A_{2A} receptor, where Motulsky and Mahan's theory and their competition association assay were used.[28-30] Similar patterns of competition association curves were observed in these studies, i.e., in the presence of a fast dissociating competitor the specific radioligand binding approached equilibrium slowly; while in the presence of a slowly dissociating compound, it showed firstly the typical 'overshoot' followed by a constant decline to a plateau as in Figure 3.3B. This, as a proof-of-concept, implies the feasibility of a dual-point kinetic screening and the use of KRI for searching desired leads on other drug targets as well.

In summary, the dual-point competition association assay is a valid tool to perform fast and high-throughput screening for compounds having either long or short residence times. The KRI value, which we coined in the present chapter, is an effective predictor of a compound's dissociation rate from its target. We believe that this approach can be of general use at other drug targets, e.g., other GPCRs, after assay optimization for individual receptors.

References:

1. Zhang, R.; Monsma, F. The importance of drug-target residence time. *Curr Opin Drug Discov Devel* 2009, 12, 488-496.
2. Zhang, R.; Monsma, F. Binding kinetics and mechanism of action: toward the discovery and development of better and best in class drugs. *Expert Opin Drug Discov* 2010, 5, 1023-1029.
3. Swinney, D. C. Biochemical mechanisms of drug action: what does it take for success? *Nat Rev Drug Discov* 2004, 3, 801-808.
4. Copeland, R. A.; Pompliano, D. L.; Meek, T. D. Drug-target residence time and its implications for lead optimization. *Nat Rev Drug Discov* 2006, 5, 730-739.
5. Anthes, J. C.; Gilchrest, H.; Richard, C.; Eckel, S.; Hesk, D.; West, R. E.; Williams, S. M.; Greenfeder, S.; Billah, M.; Kreutner, W.; Egan, R. E. Biochemical characterization of desloratadine, a potent antagonist of the human histamine H_1 receptor. *Eur J Pharmacol* 2002, 449, 229-237.
6. Copeland, R. A. Evaluation of enzyme inhibitors in drug discovery: a guide for medicinal chemists and pharmacologists. *Methods Biochem Anal* 2005, 46, 1-265.
7. Ojima, M.; Inada, Y.; Shibouta, Y.; Wada, T.; Sanada, T.; Kubo, K.; Nishikawa, K. Candesartan (CV-11974) dissociates slowly from the angiotensin AT_1 receptor. *Eur J Pharmacol* 1997, 319, 137-146.
8. Casarosa, P.; Kollak, I.; Kiechle, T.; Ostermann, A.; Schnapp, A.; Kiesling, R.; Pieper, M.; Sieger, P.; Gantner, F. Functional and biochemical rationales for the 24-Hour long duration of action of olodaterol. *J Pharmacol Exp Ther* 2011, 337, 600-609.
9. Dowling, M. R.; Charlton, S. J. Quantifying the association and dissociation rates of unlabelled antagonists at the muscarinic M_3 receptor. *Br J Pharmacol* 2006, 148, 927-937.
10. Packeu, A.; Wennerberg, M.; Balendran, A.; Vauquelin, G. Estimation of the dissociation rate of unlabelled ligand-receptor complexes by a 'two-Step' competition binding approach. *Br J Pharmacol* 2010, 161, 1311-1328.
11. Motulsky, H. J.; Mahan, L. C. The kinetics of competitive radioligand binding predicted by the law of mass action. *Mol Pharmacol* 1984, 25, 1-9.
12. Fredholm, B. B.; IJzerman, A. P.; Jacobson, K. A.; Klotz, K. N.; Linden, J. International Union of Pharmacology. XXV. Nomenclature and Classification of Adenosine Receptors. *Pharmacol Rev* 2001, 53, 527-552.
13. Fredholm, B. B.; IJzerman, A. P.; Jacobson, K. A.; Linden, J.; Müller, C. E. International Union of Basic and Clinical Pharmacology. LXXXI. Nomenclature and Classification of Adenosine Receptors--an Update. *Pharmacol Rev* 2011, 63, 1-34.
14. Jacobson, K. A.; Gao, Z. G. Adenosine receptors as therapeutic targets. *Nat Rev Drug Discov* 2006, 5, 247-264.
15. Gao, Z. G.; Jacobson, K. A. Emerging adenosine receptor agonists. *Expert Opin Emerg Drugs* 2007, 12, 479-492.
16. Van Muijlwijk-Koezen, J. E.; Timmerman, H.; Van der Sluis, R. P.; Van de Stolpe, A. C.; Menge, W. M.; Beukers, M. W.; Van der Graaf, P. H.; De Groote, M.; IJzerman, A. P. Synthesis and use of FSCPX, an irreversible adenosine A_1 antagonist, as a 'receptor knock-down' tool. *Bioorg Med Chem Lett* 2001, 11, 815-818.
17. Chang, L. C.; Spanjersberg, R. F.; Von Frijtag Drabbe Kunzel, J. K.; Mulder-Krieger, T.; Brussee, J.; IJzerman, A. P. 2,6-disubstituted and 2,6,8-trisubstituted purines as adenosine receptor

antagonists. *J Med Chem* 2006, 49, 2861-2867.

18. Van Veldhoven, J. P.; Chang, L. C.; von Frijtag Drabbe Kunzel, J. K.; Mulder-Krieger, T.; Struensee-Link, R.; Beukers, M. W.; Brussee, J.; IJzerman, A. P. A new generation of adenosine receptor antagonists: from di- to trisubstituted aminopyrimidines. *Bioorg Med Chem* 2008, 16, 2741-2752.
19. Smith, P. K.; Krohn, R. I.; Hermanson, G. T.; Mallia, A. K.; Gartner, F. H.; Provenzano, M. D.; Fujimoto, E. K.; Goeke, N. M.; Olson, B. J.; Klenk, D. C. Measurement of protein using bicinchoninic acid. *Anal Biochem* 1985, 150, 76-85.
20. Cheng, Y., Prusoff, W. H. Relationship between the inhibition constant (K_I) and the concentration of inhibitor which causes 50 percent inhibition (I_{50}) of an enzymatic reaction. *Biochem Pharmacol* 1973, 22, 3099-3108.
21. Heitman, L. H.; Mulder-Krieger, T.; Spanjersberg, R. F.; von Frijtag Drabbe Kunzel, J. K.; Dalpiaz, A.; IJzerman, A. P. Allosteric modulation, thermodynamics and binding to wild-Type and mutant (T277A) adenosine A_1 receptors of LUF5831, a novel nonadenosine-Like agonist. *Br J Pharmacol 2006,* 147, 533-541.
22. Heise, C. E.; Sullivan, S. K.; Crowe, P. D. Scintillation proximity assay as a high-throughput method to identify slowly dissociating nonpeptide ligand binding to the GnRH receptor. *J Biomol Screen* 2007, 12, 235-239.
23. Morriello, G. J.; Chicchi, G.; Johnson, T.; Mills, S. G.; Demartino, J.; Kurtz, M.; Tsao, K. L.; Zheng, S.; Tong, X.; Carlson, E.; Townson, K.; Wheeldon, A.; Boyce, S.; Collinson, N.; Rupniak, N.; Devita, R. J. Fused tricyclic pyrrolizinones that exhibit pseudo-irreversible blockade of the NK_1 receptor. *Bioorg Med Chem Lett* 2010, 20, 5925-5932.
24. Fuchs, B.; Breithaupt-Grogler, K.; Belz, G. G.; Roll, S.; Malerczyk, C.; Herrmann, V.; Spahn-Langguth, H.; Mutschler, E. Comparative pharmacodynamics and pharmacokinetics of candesartan and losartan in man. *J Pharm Pharmacol* 2000, 52, 1075-1083.
25. Nunez, S.; Venhorst, J.; Kruse, C. G. Target-drug interactions: first principles and their application to drug discovery. *Drug Discov Today* 2012, 17, 10-22
26. Kapur, S.; Seeman, P. Ketamine has equal affinity for NMDA receptors and the high-affinity state of the dopamine D_2 receptor. *Biol Psychiatry* 2001, 49, 954-957
27. Schneider, L. S.; Dagerman, K.; Insel, P. S. Efficacy and adverse effects of atypical antipsychotics for dementia: meta-analysis of randomized, placebo-controlled trials. *Am J Geriatr Psychiatry* 2006, 14, 191-210.
28. Slack, R. J.; Russell, L. J.; Hall, D. A.; Luttmann, M. A.; Ford, A. J.; Saunders, K. A.; Hodgson, S. T.; Connor, H. E.; Browning, C.; Clark, K. L. Pharmacological characterization of GSK1004723, a novel, long-acting antagonist at histamine H_1 and H_3 receptors. *Br J Pharmacol* 2011, 164, 1627-1641.
29. Ramsey, S. J.; Attkins, N. J.; Fish, R.; van der Graaf, P. H. Quantitative pharmacological analysis of antagonist binding kinetics at CRF_1 receptors *In vitro* and *In vivo*. *Br J Pharmacol* 2011, 164, 992-1007
30. Guo, D.; Mulder-Krieger, T.; IJzerman, A. P.; Heitman, L. H. Functional efficacy of adenosine A_{2A} receptor agonists is positively correlated to their receptor residence time. *Br J Pharmacol* 2012, 166, 1846-1859
31. Martinson, E. A.; Johnson, R. A.; Wells, J. N. Potent adenosine receptor antagonists that are selective for the A_1 receptor subtype. *Mol Pharmacol* 1987, 31, 247–52
32. Williams, M.; Braunwalder, A.; Erickson, T. J. Evaluation of the binding of the A_1 selective adenosine radioligand, cyclopentyladenosine (CPA), to rat brain tissue. *N-S Arch Pharmacol* 1986, 332, 179–83.

Chapter 4

Binding kinetics of ZM241385 derivatives at the human adenosine A_{2A} receptor

Guo D, Xia L, Van Veldhoven JPD, Hazeu M, Mocking T, Brussee J,
IJzerman AP, Heitman LH.
Adapted from: *ChemMedChem,* 2014; 9(4): 752-761

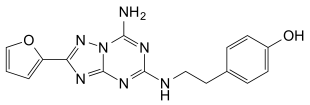
About this chapter

Classical drug design and development rely mostly on affinity- or potency-driven structure-activity relationships (SAR). So far a compound's binding kinetics has been largely ignored, which importance, however, is now increasingly recognized. In this chapter we performed an extensive structure-kinetics relationship (SKR) study in addition to a traditional SAR analysis at the adenosine A_{2A} receptor ($A_{2A}R$). The ensemble of 24 $A_{2A}R$ compounds, all triazolotriazine derivatives resembling the prototypic antagonist ZM241385 (4-(2-((7-amino-2-(furan-2-yl)-[1,2,4]triazolo[1,5-*a*][1,3,5]triazin-5-yl) amino)ethyl)phenol), displayed only minor differences in affinity, while they varied substantially in their dissociation rates from the receptor. We believe that such a combination of SKR and SAR analysis as on the $A_{2A}R$ will have general importance for the superfamily of G protein-coupled receptors, since it can serve as a new strategy to tailor the interaction between ligand and receptor.

4.1 Introduction

G protein-coupled receptors (GPCRs) are among the largest and most heavily investigated drug targets in the drug research community. Traditional early phase drug design and discovery campaigns of GPCRs largely depend on equilibrium affinity- or potency-based structure-activity relationships (SAR). This approach of lead optimization allows a quick synthesis-evaluation feedback loop to pool abundant candidate compound assemblies for further drug evaluation. Nevertheless, this classical SAR approach does not seem to predict clinical efficacy very well, which is witnessed by the high levels of attrition during the translation of a lead's *in vitro* activity into its *in vivo* and clinical evaluation. To address this issue, several recent reviews have emphasized the importance of binding kinetics, and in particular the life time of a drug-target binary complex, i.e., drug-target residence time (RT), as a critical differentiator and predictor for drug efficacy and safety.[1-5] Next to the RT, the association rate of a ligand-receptor interaction, which reflects the 'target-engagement time' (ET), should also be taken into consideration in the early phases of drug research. This is especially important for designing drugs that require a fast on-set of action and potentially for drugs that act on temporarily existing targets, such as protein-protein interactions.[6-11] Therefore, an extensive structure-kinetics relationship (SKR) investigation, in addition to the traditional SAR analysis, can be of great use in the early phases of candidate drug optimization.

The human adenosine A_{2A} receptor ($A_{2A}R$) is a subtype of adenosine receptors (others are A_1, A_{2B} and A_3), belonging to the superfamily of GPCRs.[12] Antagonists for this receptor have been reported as potential treatment for Parkinson's disease.[13] As such, many compounds with high $A_{2A}R$ affinities have been developed,[14-16] including the reference antagonist ZM241385 (4-(2-((7-amino-2-(furan-2-yl)-[1,2,4]triazolo[1,5-*a*][1,3,5]triazin-5-yl) amino)ethyl)phenol)—a triazolotriazine derivative (Figure 4.1).[17,18] These compounds were well characterized and optimized in terms of their binding affinity and thus benchmarked for later medicinal chemistry attempts at the $A_{2A}R$. For example, Vu and colleagues synthesized ZM241385 derivatives with increased bioavailability.[19-21] However, the success rate of the developed $A_{2A}R$ antagonist in clinical trials is disappointingly low. This indicates the results of currently used pre-clinical animal models don't translate well into clinical studies. Moreover, little is known about their binding kinetics so far.



ZM241385

Figure 4.1 | Chemical structure of ZM241385.

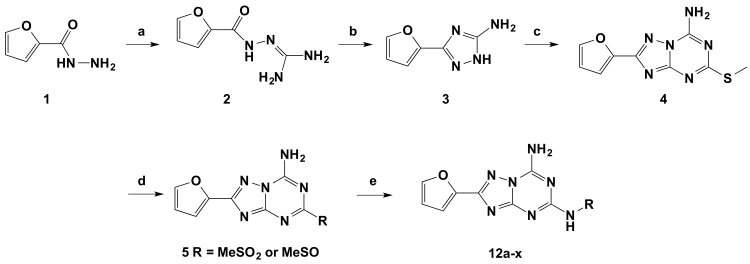
Thus, we decided to further extend this series of compounds by progressively modifying them at the C_2 position, which would generate an insight into both SKR and SAR. We believe that the present study adds knowledge to our current understanding of drug design and development for $A_{2A}R$ antagonists. Hopefully, this methodology of combining both SKR and SAR can be generally applied at other drug targets as well in the future.

4.2 Results and discussion

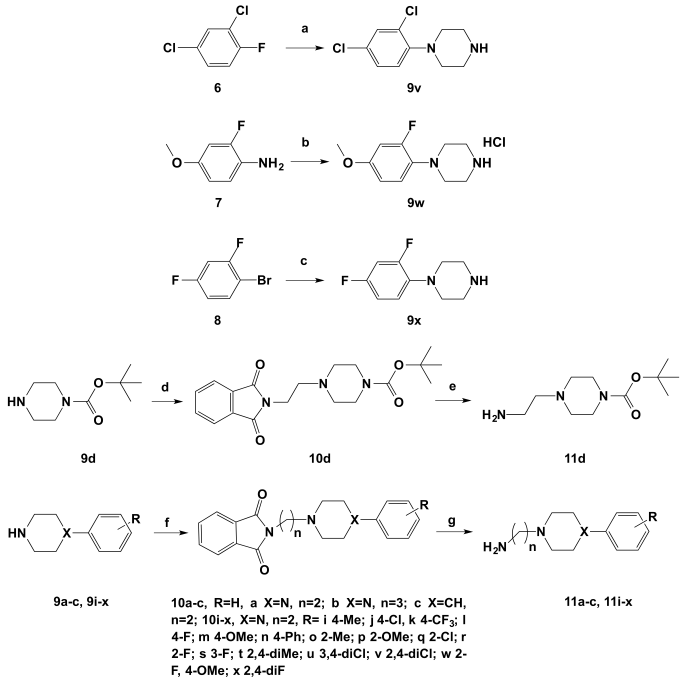
Chemical synthesis

Synthesis routes are depicted in Scheme 4.1 and Scheme 4.2. In total, an ensemble of 24 triazolotriazine derivatives (**12a-x**) was obtained. Notably, compounds **12a**, **12b** and **12x** were previously reported by Vu *et al.*,[21] and resynthesized in the present chapter, although in a different synthetic approach. All compounds (**12a-x**) started from furan-2-carbohydrazide (**1**) to generate 7-amino-2-(furyl)-5-methylthio[1,2,4]triazolo[1,5-*a*][1,3,5] triazine (**4**), following the synthetic approach reported by Dolzhenko *et al.* and Jörg *et al.*[22-25] Subsequently, **4** was oxidized with 3-chloroperbenzoic acid (MCPBA) to afford the corresponding sulfoxide/sulfone mixture **5**,[26] which was substituted with a variety of commercially available amines (**11f-h**) to generate **12f-h** or with in-house prepared amines (**11a-d** and **11i-x**) to generate **12a-d** and **12i-x**. **12e** was obtained by the *N*-Boc deprotection of **12d**.

For the preparation of intermediate amines **11a-d** and **11i-x**, synthetic routes are depicted in Scheme 4.2. In brief, reactions were carried out via *N*-alkylation of the commercially available piperazine derivatives (**9a-d** and **9i-u**) or the in-house synthesized phenylpiperazines (**9v-x**), which were



Scheme 4.1 | General synthesis route to 24 triazolotriazine derivatives. *Reagents and conditions*: (a) S-methylisothiourea sulfate (2:1), 4 % $NaOH_{(aq)}$ RT; (b) H_2O, RT; (c) (1) $(MeS)_2C{=}NCN$, heat, 180 ˚C, (2) CH_2Cl_2-CH_3OH (2:1), reflux; (d) *m*CPBA (70 % strength), CH_2Cl_2, 0 ˚C-> RT; (e) $(Et)_3N$, CH_3CN.



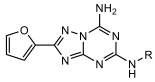
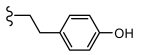
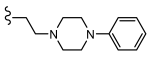
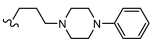
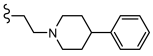
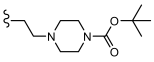
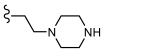
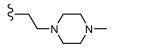
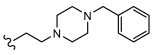
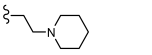
Scheme 4.2 | Preparation of key intermediates. *Reagents and conditions*: (a) piperazine, *N,N*-dimethylacetamide, 165 ˚C; (b) bis(2-chloroethyl)amine hydrochloride, Na_2CO_3, 130 ˚C, butanol; (c) *t*-BuONa, BINAP, $Pd_2(dba)_3$, toluene, N_2, 110 ˚C; (d) K_2CO_3, NaI, butanone, reflux; (e) H_2NNH_2-H_2O, EtOH; (f) 3-bromo-alkylphthamide, K_2CO_3, DMF, 70 ˚C; (g) H_2NNH_2-H_2O, EtOH, 70 ˚C.

derived from **6-8**, **27-30** to obtain the appropriate *N*-phthalimide-protected alkyl piperazines (**10a-d** and **10i-x**). This was followed by deprotection of the phthalimide to afford the free amines (**11a-d** and **11i-x**).

SAR and SKR of triazolotriazine derivatives

The SAR and SKR analyses were initiated by testing two compounds, **12a** and **12b**, and then chemical modifications were gradually introduced to these two compounds (Table 4.1). Several observations were made; (1) the molecule with a two-carbon spacer was superior to the compound with a three-carbon spacer. The former (**12a,** K_i = 0.30 ± 0.08 nM; RT = 164 ± 32 min) displayed a four-fold higher affinity and 41-fold longer RT than the latter (**12b**, K_i = 1.3 ± 0.1 nM; RT = 4 ± 1 min). Such a variation of the linker length also resulted in different association rates (**12a**, k_{on} = 0.051 ± 0.005 $nM^{-1}{\cdot}min^{-1}$; **12b**, k_{on} = 0.16 ± 0.06 $nM^{-1}{\cdot}min^{-1}$). (2) Upon different degrees of C_2-phenylpiperazine modification the ligands' affinities were moderately to largely affected, while their receptor RTs were drastically shortened (**12d-h**), except for the Boc-protected intermediate **12d**. This compound, in fact, had a 30-fold and 20-fold improved affinity and RT, respectively, in comparison to its truncated analogue (**12e**). Moreover, their ETs were also significantly influenced by the chemical modifications on the phenylpiperazine moiety. Specifically, **12g** displayed the fastest association rate of 0.046 ± 0.020 $nM^{-1}{\cdot}min^{-1}$. (3) Receptor RTs of **12a** or **12d** highlight the preference of an electron-withdrawing effect at the piperazine amine moiety. The insertion of an additional carbon into **12a** (between the piperazine and the phenyl group; **12g**) reversed the electron-withdrawing effect into a donating effect, which resulted in a reduced $A_{2A}R$ affinity (8.1 ± 0.5 nM) and RT (4 ± 1 min). Replacement of the nitrogen by a carbon atom on the 'right side' of the piperazine (compare **12a** and **12c**) resulted in strongly decreased RT values that further confirmed the nitrogen's importance in maintaining $A_{2A}R$ affinity and RT (Table 4.1, Figure 4.2 for **12c**). Notably, ET and RT of **12c** were the shortest of this series of compounds (except for the nearly 20-fold lower affinity compound **12h**) without a large compromise on its affinity. Taken together, these results highlight the importance of the C_2-phenylpiperazine-ethyl group, and more specifically show that the electron-deficient nitrogen (on the right side of the piperazine) has a role in preserving a tight and enduring ligand-receptor interaction.

Table 4.1 | Binding affinities and kinetics of ZM241385 and 12a-12h.

		$hA_{2A}R$				hA_1R
Compd	Structure, R=	K_i (nM)[a]	k_{on} ($nM^{-1}\cdot min^{-1}$)[b]	k_{off} (min^{-1})[b]	RT (min)[c]	K_i (nM) or %[d]
ZM241385		0.40 ± 0.03	0.13 ± 0.06	0.014 ± 0.003	71 ± 21	255[23]
12a		0.30 ± 0.08	0.051 ± 0.005	0.0061 ± 0.0020	164 ± 32	8%
12b		1.3 ± 0.1	0.16 ± 0.06	0.25 ± 0.01	4 ± 1	30%
12c		3.8 ± 0.8	0.20 ± 0.1	0.35 ± 0.03	3 ± 1	22%
12d		1.5 ± 0.1	0.030 ± 0.003	0.012 ± 0.004	83 ± 17	2%
12e		45 ± 0.1	0.0063 ± 0.0030	0.24 ± 0.10	4 ± 1	10%
12f		31 ± 6	0.0057 ± 0.0020	0.25 ± 0.10	4 ± 1	11%
12g		8.1 ± 0.5	0.046 ± 0.020	0.24 ± 0.10	4 ± 1	21%
12h		64 ± 1	0.020 ± 0.002	0.62 ± 0.08	2 ± 0	32%

[a] Displacement of specific [^{3}H]-ZM241385 binding from the $hA_{2A}R$ at 4 ˚C. [b] k_{on} and k_{off} were determined in competition association assay at 4 ˚C. [c] RT (Residence Time) = 1 / k_{off}. [d] % displacement of specific [^{3}H]-DPCPX binding at 1 μM from the hA_1R at 25 ˚C. Data are shown as mean ± s.e.m of three separate experiments each performed in duplicate.

SAR and SKR were further analyzed with 16 phenyl-substituted **12a** analogues (Table 4.2, **12i-x**). Upon *para*-substitution at the phenyl ring (**12i-n**), no significant change of the ligands' affinity (K_i values < 1 nM) was observed, except for **12n** which had a 4.7-fold decrease in affinity (1.4 ± 0.2 nM). The latter was probably caused by steric hindrance induced by the bulky phenyl substituent, which presumably also limited its RT to 29 ± 2 min and decreased the association rate to 0.018 ± 0.002 $nM^{-1}\cdot min^{-1}$. In contrast, the other *para*-substituted compounds **12i-m** displayed a similar duration of *in vitro* receptor occupancy as ZM241385 (RT = 71 ± 21 min). In comparison to the convergent results upon *para*-position modifications,

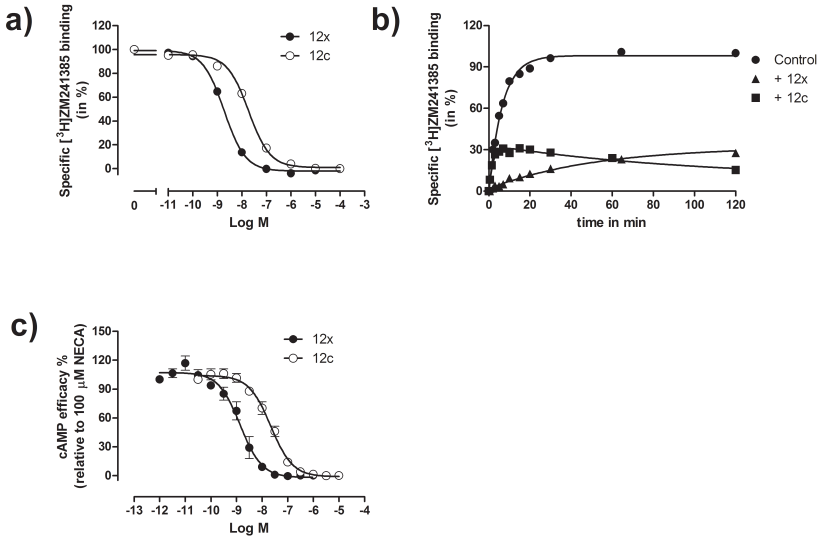
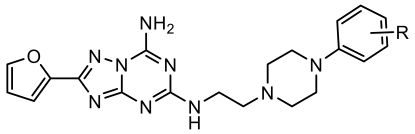


Figure 4.2 | (a) Displacement of specific [^{3}H]-ZM241385 binding from the hA_{2A} receptor by two representative compounds, namely **12x** and **12c**; (b) [^{3}H]-ZM241385 competition association binding in the absence of ligand (control) and in the presence of 10 × K_i of unlabeled **12x** or **12c**. Data was fitted to the equation described in the experimental section to calculate k_{on} and k_{off} of unlabeled ligands. Representative graphs from one experiment performed in duplicate (See Table 4.1 and 4.2 for affinity and kinetic values); (c) Concentration-effect curves for **12x** and **12c** in a cAMP assay. Data were obtained by adding HEK293hA_{2A}R cells to the mixture of the antagonist (**12x** or **12c**) and 100 nM NECA for an incubation of 30 min. Data are expressed as mean ± s.e.m from at least three independent experiments. (See Table 4.3 for potency values).

ortho-substituted analogues (**12o**-**12r**) displayed divergent affinities and binding kinetics. Specifically, an *ortho*-methoxy substituent (**12p**) decreased A_{2A}R affinity and RT compared to its *para*-substituted analogue (**12m**), while the methyl- (**12o**) or halogen-substituted (**12q**, **12r**) analogues displayed increased A_{2A}R affinities and RTs. For most compounds disubstitution of the phenylpiperazine did not dramatically change their affinities or binding kinetics (**12t-w**). Interestingly for **12x**, bearing an *ortho*- and *para*-fluoro substituent, an exceptionally long receptor RT of 323 ± 25 min was found (Table 4.2) that was much longer than the simple 'sum RT' of mono-fluorinated analogues (**12l**, **12r** and **12s**) and almost five-fold longer than

Table 4.2 | Binding affinities and kinetics of 12i-12x.



Compd	R=	$hA_{2A}R$				hA_1R
		K_i (nM) [a]	k_{on} ($nM^{-1}\cdot min^{-1}$) [b]	k_{off} (min^{-1}) [b]	RT (min) [c]	K_i (nM) or % [d]
12i	4-CH_3	0.79 ± 0.06	0.062 ± 0.020	0.016 ± 0.006	63 ± 18	14 %
12j	4-Cl	0.29 ± 0.10	0.090 ± 0.010	0.018 ± 0.006	56 ± 11	35 ± 13
12k	4-CF_3	0.38 ± 0.10	0.072 ± 0.009	0.020 ± 0.005	50 ± 37	64 %
12l	4-F	0.54 ± 0.05	0.10 ± 0.02	0.020 ± 0.005	50 ± 8	57 %
12m	4-OCH_3	0.51 ± 0.10	0.064 ± 0.005	0.0079 ± 0.0020	127 ± 19	11 %
12n	4-Ph	1.4 ± 0.2	0.018 ± 0.002	0.034 ± 0.010	29 ± 2	32 %
12o	2-CH_3	0.13 ± 0.04	0.062 ± 0.002	0.0075 ± 0.0020	133 ± 21	29 %
12p	2-OCH_3	3.5 ± 0.7	0.032 ± 0.003	0.070 ± 0.070	14 ± 11	19 %
12q	2-Cl	0.13 ± 0.03	0.068 ± 0.016	0.0065 ± 0.0010	154 ± 25	30 %
12r	2-F	0.12 ± 0.05	0.052 ± 0.012	0.011 ± 0.002	91 ± 15	28 %
12s	3-F	0.29 ± 0.03	0.055 ± 0.009	0.012 ± 0.003	83 ± 14	62 %
12t	2, 4-diCH_3	0.16 ± 0.01	0.11 ± 0.02	0.012 ± 0.001	78 ± 9	29 %
12u	3, 4-diCl	0.31 ± 0.10	0.10 ± 0.01	0.015 ± 0.004	67 ± 11	21 ± 4
12v	2, 4-diCl	0.15 ± 0.02	0.11 ± 0.01	0.014 ± 0.001	70 ± 5	80 ± 24
12w	2-F, 4-OCH_3	0.24 ± 0.05	0.054 ± 0.005	0.0083 ± 0.0010	120 ± 65	27%
12x	2, 4-diF	0.33 ± 0.04	0.034 ± 0.004	0.0031 ± 0.0002	323 ± 25	22%

[a] Displacement of specific [^{3}H]-ZM241385 binding from the $hA_{2A}R$ at 4 ˚C. [b] k_{on} and k_{off} were determined in competition association assay at 4 ˚C. [c] RT (Residence Time) = 1 / k_{off}. [d] % displacement of specific [^{3}H]-DPCPX binding at 1 μM from the hA_1R at 25 ˚C. Data are shown as mean ± s.e.m of three separate experiments each performed in duplicate.

ZM241385's RT. From Figure 4.2B it also follows that **12x** had a much longer RT than ZM241385 (the radioligand), since a typical 'overshoot' in specific radioligand binding was observed.[30] On the contrary, if a competitor dissociates faster from its target than the radioligand, the specific binding of the radioligand will slowly and monotonically approach its equilibrium over time, as observed for **12c** (Figure 4.2B).[30]

Almost all prepared ZM241385 derivatives displayed high selectivity over the human adenosine A_1 receptor (A_1R), i.e., < 50 % of [^{3}H]-DPCPX displacement at 1 μM (Table 4.1 and 4.2). Notably, the longest RT compound on the $A_{2A}R$, **12x**, had a very good $A_{2A}R$ selectivity over the A_1R (Table 4.2). In contrast, **12j**, **12u** and **12v**, with mono- or di-chloro substitution, lost some selectivity over the A_1R (K_i values at the A_1R ranged from 20 nM to 80 nM, Table 4.2). Interestingly, all these compounds contain a chloro-substituent in the *para*-position, yet the substituent in other positions (e.g., **12q**, *ortho*-substituent) didn't exhibit lower selectivity for the $A_{2A}R$ over the A_1R.

Functional characterization of **12x** and **12c** in a cAMP assay

Subsequently, the longest and shortest RT compounds with high affinity (i.e., **12x** and **12c**) were functionally characterized in an $A_{2A}R$ agonist-induced cAMP assay, which revealed their antagonistic behavior. Firstly, it follows from Figure 4.2C that both **12x** and **12c** induced a concentration-dependent decrease of intracellular cAMP levels with 16-fold difference in their IC_{50} values, which are 1.4 ± 0.1 nM and 21.8 ± 0.5 nM, respectively (Table 4.3). Secondly, pre-treatment of HEK293h$A_{2A}R$ cells with different concentrations of **12x** before stimulation with an AR agonist (i.e., 5'-*N*-ethylcarboxamidoadenosine, NECA) induced insurmountable antagonism. In other words, the NECA concentration-effect curve was shifted to the right with a concomitant decrease in the maximal response (Figure 4.3A). Conversely, **12c** displayed surmountable $A_{2A}R$ antagonism, shifting NECA's curves to the right yet without affecting its maximal response (Figure 4.3B). In addition, the pA_2 value for **12c** generated from a Schild-plot was 8.62 ± 0.29, which was similar to its pK_i value (8.40 ± 0.10), and the Schild-slope was close to unity (0.93 ± 0.11) suggesting that **12c** competed with NECA for the same receptor binding site. To further examine whether **12x** and **12c** both bound to the same site as the agonist, we also

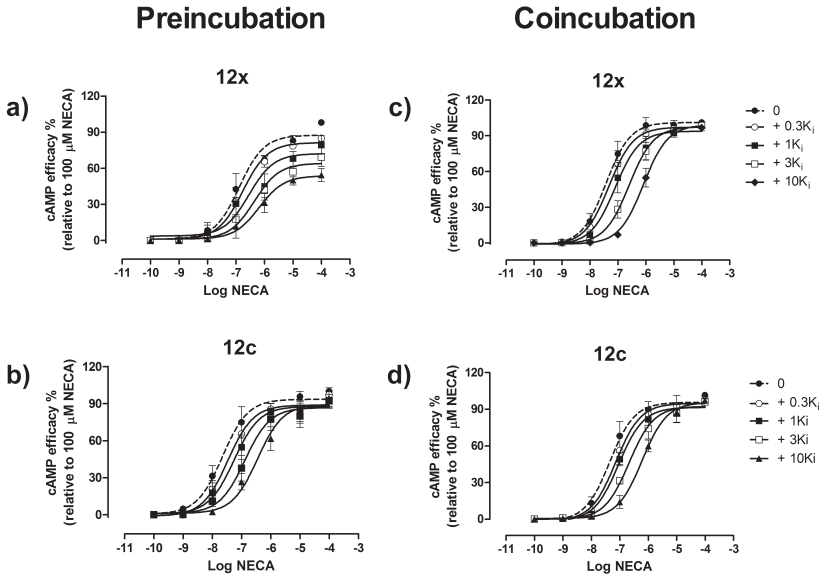


Figure 4.3 | cAMP experiments were performed on human embryonic kidney 293 cells stably expressing the $hA_{2A}R$ at ambient room temperature (22–25 °C). 12x (a) or **12c** (b) were incubated for 30 min prior to the challenge of the adenosine receptor agonist NECA at a concentration ranging from 100 µM to 0.1 nM for another 30 min. **12x** (c) or **12c** (d) were co-incubated with NECA, at a concentration ranging from 100 µM to 0.1 nM, for 30 min. The agonist curves were generated in the presence of increasing concentrations of antagonist, namely 0.3-, 1-, 3- and 10-fold their respective K_i values. Data were normalized according to the maximal response produced by 100 µM NECA. The shift in agonist EC_{50} was determined to perform Schild analyses. Data are expressed as mean ± s.e.m from at least three independent experiments performed in duplicate.

performed a co-incubation experiment with **12x** or **12c** in the presence of NECA. It follows from Figure 4.3C and 4.3D that in this experimental set-up both compounds produced a rightward shift in the NECA dose-response curve without a suppression of the maximal response, i.e., indicative of a competitive interaction. Hence, these findings oppose that insurmountable antagonism resulted from an allosteric mode of inhibition, which would be proven by a suppression of the maximal response in the co-incubation experiment.[31-33] Notably, the generated pA_2 values of **12x** and **12c** in this experimental set-up were similar to their pK_i values and the derived Schild

Table 4.3 | Functional characterization of 12x and 12c in a cAMP assay.

	Potency [a]	Pre-incubation [b]		Co-incubation [b]	
Compd	IC_{50} (nM)	pA_2	Schild slope	pA_2	Schild slope
12c	1.4 ± 0.1	8.62 ± 0.29	0.93 ± 0.11	8.57 ± 0.06	0.93 ± 0.02
12x	21.8 ± 0.5	*N.A*	*N.A*	9.69 ± 0.03	1.13 ± 0.01

[a] Antagonists' potency (IC_{50}) values were determined from concentration-response curves for **12x** and **12c** in the presence of 100 nM NECA for a co-incubation of 30 min. Antagonists were pre-incubated for 30 min [b] or co-incubated [c] with NECA at a concentration ranging from 100 μM to 0.1 nM. *N.A.*, not applicable. Data are shown as mean ± s.e.m of three separate experiments each performed in duplicate at room temperature (22–25 °C).

slopes were close to unity (Table 4.3). Together, this confirmed that **12x** or **12c** bound fully competitively with NECA and the insurmountable $A_{2A}R$ antagonism of **12x** was a result caused by so-called hemi-equilibrium during the functional assay due to its long $A_{2A}R$ residence time profile.[32]

It needs to point out that the results for functional characterization and binding kinetics determination are not obtained at a physiologically more relevant temperature (37 ˚C) and thus cannot be representative for residence times observed *in vivo*. However, it is reasonable to expect that the ranking of these compounds' RTs at 4 ˚C should agree with the result at the room temperature or at the physiologically more relevant 37 ˚C. Such a discussion has been documented in our previous publication at the $A_{2A}R$, where UK432,097 has a RT five-fold the length of CGS21680.[34,35] This difference at 4 ˚C well translates into distinct duration of action in an *in vivo* setting reported by Mantell *et al.*, that is, 8 h for UK432,097 and less than one hour for CGS21680.[36]

Generation of a 'kinetics map' and physicochemical correlation plots from $A_{2A}R$ antagonist SKR data

Next, we plotted an on-/off-rate graph or so-called 'kinetics map', including the data of all $A_{2A}R$ ligands obtained in this chapter (Figure 4.4).[37] Evidently, this kinetics map depicted the ligand-receptor binding affinity (K_D, represented by the parallel diagonal lines) into detailed kinetic rates that reflect the process of 'target-engagement time' (k_{on}, Y axis) and the target-residence time (k_{off}, X

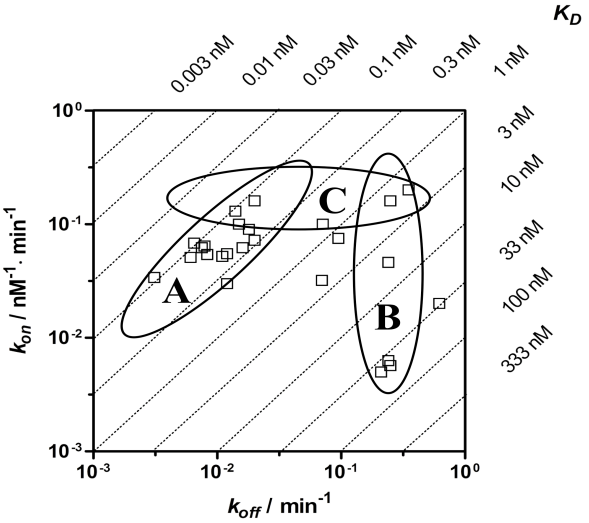


Figure 4.4 | The kinetics map (Y axis: k_{on}, $nM^{-1}{\cdot}min^{-1}$; X axis: k_{off}, min^{-1}) of all $A_{2A}R$ ligands that were tested in this chapter. The kinetically derived affinity ($K_D = k_{off} / k_{on}$) is represented by the parallel diagonal lines. Group A: compounds that have varied k_{on} and k_{off} values, while the K_D remained within a similar range (0.1-0.3 nM). Group B: compounds that have the same k_{off} values, but divergent K_D values. Group C: compounds that have the same k_{on} values, but divergent K_D values.

axis), respectively. We observed that the compounds can be divided into three groups; firstly, both k_{on} and k_{off} values can vary across one order of magnitude (Figure 4.4, Group A), while the K_D remained within a narrow range (0.1-0.3 nM), as mentioned above. This indicated that compounds with the same affinity may have many different combinations of on- and off-rates even within the same scaffold and target system. Such information, often ignored or unavailable in traditional SAR studies, in fact can be highly decisive in translating a lead's *in vitro* profile into *in vivo* pharmacokinetics (PK) and/or pharmacodynamics (PD) behavior.[38] Secondly, compounds sharing the same off-rate may bear divergent K_D values, due to different on-rates (Group B). It has been shown in several cases that a compound's slow dissociation rate was pivotal for a high *in vivo* efficacy.[34,35] Thus, in retrospect one could imagine that many compounds with promising k_{off} values were overlooked simply due to their 'low scores' in classical affinity- or potency-dominated evaluations.

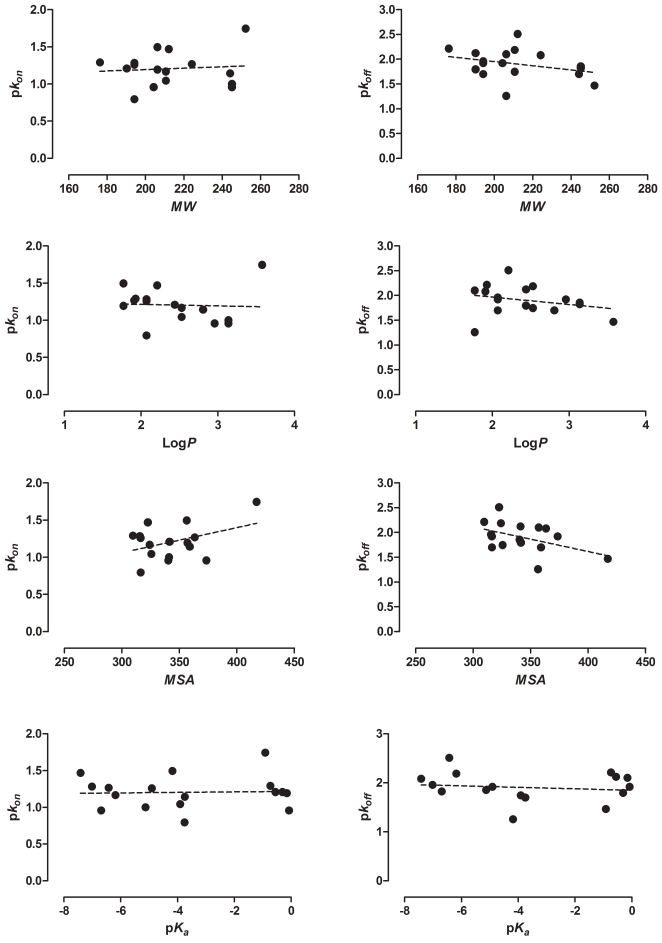


Figure 4.5 | Molecular descriptors of size (MW), lipophilicity (logP), molecular surface area (MSA, 3D), and charge (pK_a) of the substituted C_2-phenylpiperazine fragments and their correlation with the –log values of on- and off-rates. No obvious linear correlation was observed between the association-/dissociation-rates and MW (for association: r^2 = 0.0089, P = 0.7180; for dissociation: r^2 = 0.1059, P = 0.2024), logP (for association: r^2 = 0.0023, P = 0.8563; for dissociation: r^2 = 0.0731, P = 0.2938), MSA (for association: r^2 = 0.1629, P = 0.1082; for dissociation: r^2 = 0.2107, P = 0.0638) or pK_a (for association: r^2 = 0.0018, P = 0.8727; for dissociation: r^2 = 0.0187, P = 0.6010).

Thirdly, the same holds for a compound's on-rate (Group C), i.e., merely focusing on a ligand's K_D can result in compounds without the desired on-rate, as exemplified by candidate drugs aiming at acute diseases where a rapid on-set of action is desired (e.g., acute respiratory distress syndrome).[6,11] Taken together, the kinetics map provides a detailed interpretation of a ligand-receptor binding process with a full inventory of k_{on}, k_{off} and K_D values of a series of compounds.

Furthermore, molecular and physicochemical properties of the synthesized phenylpiperazine analogues (**12i-x** and **12a**) and their putative relationship with the on- and off-rates were examined in efforts to identify key factor(s) affecting their binding kinetics (Figure 4.5). Since the main scaffold of these series of compounds is the same, we specifically focused on the properties of C_2-phenylpiperazine fragments. Several descriptors were selected to be further examined in correlation plots. They were the size (molecular weight, MW), surface of the fragment (molecular surface area, MSA), lipophilicity (logP), and charge (ionization constant, pK_a). There was no obvious linear correlation between the association-/dissociation-rates and MW, logP, MSA or pK_a. We also performed a multiple linear regression analysis to check whether the compound's binding kinetics is directed by a combination of two or more of the physicochemical descriptors. However, no significant correlation was found either (significance $F > 0.05$ in all cases). Altogether, this indicated that the binding kinetics was compound specific and that there is no general trend in the correlation to their molecular and physicochemical properties.

Importance of the phenylpiperazine-fragment at the C_2 position and its location in the $A_{2A}R$'s 'vestibule'

In this chapter we observed that upon minor chemical modifications of the phenylpiperazine side chain on the triazolotriazine scaffold (Table 4.1 and 4.2), binding affinity of the derivatives underwent subtle changes only, while their binding kinetics were very sensitive to such structural variations. For instance, upon substitution of **12a**, **12k** (*para*-trifluoromethyl substituted) displayed a similar K_i value as **12a**, while its off-rate was 3.4-fold increased. In another case, the on- and off-rates of **12u** (*meta*-, *para*-chloro disubstituted) were increased and decreased, respectively, in a similar magnitude (approximately

2-fold), hence leading to an unchanged affinity value compared to **12a**. Table 4.2 as a whole exemplifies the difficulty of selecting a 'next-stage' candidate based on SAR alone. Most compounds have subnanomolar affinity, and compound **12x** does not stand out in any particular way.

The lack of large changes in binding affinities might be expected given the absence of direct interactions between the phenylhydroxyl group and the receptor in a recently determined high-resolution crystal structure of ZM241385-bound $A_{2A}R$.[39] In this structure, the phenylhydroxyl group points away from the binding pocket toward the extracellular space. Likewise, in another crystal structure of UK432,097-bound $A_{2A}R$, the bulky tail of the agonist UK432,097 at the adenine C_2 position extends outward of the ligand-binding cavity.[40] Notably, it was recently published that this agonist also has a slow association rate and long RT at the $A_{2A}R$.[34] Based on these findings, we postulated that the C_2-phenylpiperazine group protrudes outward without forming direct interactions with residues in the binding pocket of the triazolotriazine core. Instead, it may interact with residues that are located at the extracellular loops or the adjacent regions topping the binding cavity, on its trajectory of associating to or dissociating from the receptor. Such reasoning is supported by a recent molecular dynamics simulation study of the β_1- and β_2-adrenergic receptors by Dror *et al.*[41] They found that several beta blockers and one beta agonist all traverse the same well-defined, dominant pathway as they bind to the β_1- and β_2-adrenergic receptors, initially making contact with a so-called 'vestibule' on the receptor's extracellular surface. Interestingly, this holds true for the ligand binding dynamics of the M_3 muscarinic acetylcholine receptor too. Simulation results indicated that as tiotropium binds to or dissociates from the receptor, it 'pauses' at an alternative binding site in the extracellular 'vestibule'.[42] Taken together, such an extracellular 'vestibule' appears to play an important role in the on- or off-trajectory to and from the binding pocket of a GPCR.[41] These molecular dynamics calculations therefore support that an extracellular 'vestibule' appears to play an important role in the on- or off trajectory to and from the binding pocket of a GPCR, which is in accordance with our observation that a change in the C_2-phenylpiperazine group significantly affected the ligand's association and dissociation rates at the $A_{2A}R$, while their K_i values were minimally changed.

4.3 Conclusion

We have exemplified an extensive structure-kinetics relationship (SKR) in addition to a traditional SAR analysis at the adenosine A_{2A} receptor ($A_{2A}R$). Compound **12x**, the high-affinity $A_{2A}R$ ligand previously reported by Vu *et al.*,[21] was revealed to have an exceptional long RT (323 min). Compared to the traditional SAR analysis, such a kinetic insight provided a further rationale to support the selection of **12x** from otherwise chemically and biologically similar compounds for further testing. Kinetics mapping all tested $A_{2A}R$ ligands also provided a detailed interpretation of the ligand-receptor binding process. Next, a functional comparison between a short RT antagonist **12c** and **12x** in the pre-incubation experiment further revealed **12x**'s insurmountable antagonism at the $hA_{2A}R$—a phenomenon distinct from **12c**. In addition, investigation of the molecular properties indicated that the ligand-receptor binding kinetics were most likely driven by specific interactions between the ligand and the receptor. It could also be of great interest to subject the compounds having similar affinity yet different binding kinetics into (pre) clinical tests, especially to examine how relevant the variation in RT and on/off-rate is in terms of *in vivo* efficacy and duration of action. We believe that SKR, in combination with traditional SAR, can serve as an important tool for more directed medicinal chemistry efforts in the future.

4.4 Experimental section

Chemical synthesis

General: All solvents and reagents were purchased from commercial sources and were of analytical grade. Demineralised water is simply referred to as H_2O, as it was used in all cases unless stated otherwise (i.e., brine). ^{1}H and ^{13}C NMR spectra were recorded on a Bruker AV 400 liquid spectrometer (^{1}H NMR, 400 MHz; ^{13}C NMR, 101 MHz) at ambient temperature. Chemical shifts are reported in parts per million (ppm), are designated by δ and are downfield to the internal standard tetramethylsilane (TMS). Coupling-constants are reported in Hz and are designated as *J*. High resolution mass

spectrometry was performed by the Leiden Institute of Chemistry and recorded by direct injection (2 µL of a 2 µM solution in water/MeCN; 50/50; v/v and 0.1 % formic acid) on a mass spectrometer (Thermo Finnigan LTQ Orbitrap) equipped with an electrospray ion source in positive mode (source voltage 3.5 kV, sheath gas flow 10, capillary temperature 275 °C) with resolution R = 60000 at *m/z* 400 (mass range *m/z* = 150-2000) and calibrated for dioctylphthalate (*m/z* = 391.28428). Analytical purity of the final compounds was determined by high performance liquid chromatography (HPLC) with a Phenominex Gemini 3u C18 110A column (50 x 4.6 mm, 3 µm), measuring UV absorbance at 254 nm. Sample preparation and HPLC method were as follows, unless stated otherwise: 0.3-0.8 mg of compound was dissolved in 1 mL of a 1:1:1 mixture of $CH_3CN/H_2O/t$-BuOH and eluted from the column within 15 minutes, with a three component system of H_2O/CH_3CN/1 % TFA in H_2O, decreasing polarity of the solvent mixture in time from 80/10/10 to 90/0/10. All compounds showed a single peak at the designated retention time and are at least 95 % pure. Thin-layer chromatography (TLC) was routinely consulted to monitor the progress of reactions, using aluminum-coated Merck silica gel F254 plates. Purification by column chromatography was achieved by use of Grace Davison Davisil silica column material (LC60A 30-200 micron). Solutions were concentrated using a Heidolph laborota W8 2000 evaporation apparatus and by a high vacuum on a Binder APT line Vacuum Drying Oven. The procedure for a series of similar compounds is given as a general procedure for all within that series, annotated by the numbers of the compounds.

2-(Furan-2-carboxamido) guanidine (2). The mixture of the hydrazide (**1**) (0.1 mol, 12.6 g) and *S*-methylisothiourea sulfate (0.05 mol, 13.9 g) in an 1% aqueous sodium hydroxide solution (400 mL) was stirred at room temperature for 72 hrs. The precipitated solid (**2**), was filtered, washed with ice water, and used in next step without further purification. ^{1}H NMR (400 MHz, DMSO-d_6): δ 10.77 (br s, 1H, NH), 7.56 (s, 1H), 6.88 and 6.76 (2 x s due to dimer formation, 2H, NH_2), 6.64 (d, J = 2.8 Hz, 1H), 6.45 (dd, J = 2.0, 0.8 Hz, 1H).

5-(Furan-2-yl)-2H-1,2,4-triazol-3-amine (3). The guanidine (**2**) (53.6 mmol, 9.0 g) was stirred in a mixture of ethyl acetate and H_2O with a ratio of 1:1 (400 mL) for 3 hrs. After extraction by 150 mL of ethyl acetate twice, the organic layer was washed with H_2O and brine (2 × 100 mL), and dried over anhydrous Na_2SO_4. After removing the solvent, 6.51 g white solid (**4**) was obtained (two-step yield: 54 %). ^{1}H NMR (400 MHz, DMSO-d_6): δ 12.08 (br s, 1H, NH), 7.68 (s, 1H), 6.67 (s, 1H), 6.54 (s, 1H), 6.08 (s, 2H).

2-(Furan-2-yl)-5-(methylthio)-[1,2,4]triazolo[1,5-*a*][1,3,5]triazin-7-amine (4). A mixture of the amine (**3**) (43.4 mmol, 6.5 g) and dimethyl *N*-cyanodithio(imino)carbonate (47.8 mmol, 7.0 g) was heated at 180 ˚C in a stream of nitrogen for 4 hrs and cooled down to room temperature to add 30 mL of a solution of CH_2Cl_2 and CH_3OH with the ratio of 1:1. The mixture was refluxed for another 1.5 hrs and followed by a filtration. The solids were washed by the solution and the solvent was removed under reduced pressure. The residue was purified by column chromatography by eluting with CH_2Cl_2 containing increasing amounts of ethyl acetate (0% - 50%). This gave compound **4** as a pale yellow solid (3.2 g, yield: 30 %). ^{1}H NMR (400 MHz, CD_3OD): δ 7.91 (dd, J = 1.7, 0.7 Hz, 1H), 7.12 (dd, J = 3.4, 0.7 Hz, 1H), 6.70 (dd, J = 3.4, 1.7 Hz, 1H), 2.55 (s, 3H).

2-(Furan-2-yl)-5-(methylsulfonyl)-[1,2,4]triazolo[1,5-*a*][1,3,5]triazin-7-amine (5). A solution of MCPBA (70% strength, 32.5 mmol, 8.0 g) in CH_2Cl_2 (20 mL) was added to a stirred, ice-cooled suspension of the sulfide (R = MeSO) (13.0 mmol, 3.2 g) in CH_2Cl_2 (50 mL). The resulting solution was stirred overnight at room temperature. The solvent was removed and ethanol (70 mL) was added to the residue. The solid was collected by filtration, washed with ethanol, and dried in the vacuum oven to give white solid (R = MeSO2) (3.2 g, yield 88%). 1H NMR (400 MHz, DMSO-d_6): δ 9.81 and 9.48 (2 x s due to dimer formation, 2H, NH_2), 7.98 (dd, J = 1.2, 0.8 Hz, 1H), 7.34 (dd, J = 2.4, 0.8 Hz, 1H), 6.73 (dd, J = 2.4, 1.2 Hz, 1H), 3.35 (s, 3H).

1-(2,4-Dichlophenyl)piperazine (9v). A mixture of **6** (16.7 mmol, 2.0 mL) and piperazine (83.6 mmol, 7.2 g) in 10 mL of *N,N*-dimethylacetamide was heated in the microwave at 165 ˚C for 6.5 hrs after which 6 was consumed, shown by TLC. Water and CH_2Cl_2 was added and the pH value was adjusted to 1 with 1 mol/L HCl (aq.). The aqueous layer was washed three times with CH_2Cl_2 and subsequently basified to pH 12 with 5 mol/L $NaOH_{(aq)}$. After extraction of the basified aqueous layer with CH_2Cl_2 the combined organics were backwashed four times with water, dried over $MgSO_4$ and concentrated *in vacuo* to yield **9v** as yellow oil (2.4 g, yield 61%). ^{1}H NMR (400 MHz, $CDCl_3$): δ 7.36 (d, J = 2.4 Hz, 1H), 7.19 (dd, J = 8.8, 2.4 Hz, 1H), 6.95 (d, J = 8.4 Hz, 1H), 3.06-3.02 (m, 5H, 2 × CH_2 and NH), 2.99-2.96 (m, 4H).

1-(2-Fluoro-4-methoxyphenyl)piperazine hydrochloride (9w). A mixture of bis(2-chloroethyl) amine hydrochloride (9.59 mmol, 1.7 g) (**7**) and 1-butanol (20 mL) was treated slowly with 2-fluoro-4-methoxybenzenamine (9.14 mmol, 1.3 g) at room temperature. After the addition, the mixture was refluxed for 48 hrs and then cooled. The solid was filtered and rinsed with MeOH and Et_2O to give a white solid **9w** (660 mg, yield 29%). ^{1}H NMR (400 MHz, $CDCl_3$): δ 9.21 (br s, 2H, NH and HCl), 7.07-7.02 (m, 1H), 6.86-6.83 (m, 1H), 6.74-6.71 (m, 1H), 3.72 (s, 3H), 3.28-3.20 (m, 4H), 3.14-3.10 (m, 4H).

1-(2,4-Difluorophenyl)piperazine (9x). A mixture of piperazine (24.9 mmol, 2.14 g) and 1-bromo-2,4-difluorobenzene (**8**) (4.1 mmol, 0.8 g), *t*-BuONa (5.8 mmol, 0.56 g), BINAP (0.25 mmol, 0.16 g), and $Pd_2(dba)_3$ (0.083 mmol, 0.048 g) in dry toluene was heated at 110 ˚C under a nitrogen atmosphere for 24 hrs. The mixture was filtered over Celite and rinsed with dichloromethane. The solution was washed

with H_2O and brine (2 × 10 mL), dried over Na_2SO4 and the solvent evaporated *in vacuo*. The residue was purified by silica gel via CH_2Cl_2/CH_3OH, 10:1 to give compound **9x** as pale yellow oil (337 mg, yield 42%). ^{1}H NMR (400 MHz, $CDCl_3$): δ 6.91-6.87 (m, 1H), 6.83-6.78 (m, 2H), 3.06 (t, J = 3.6 Hz, 4H), 3.00-2.97 (m, 4H), 1.80 (s, 1H, NH)

General procedure for preparation of compounds **10a-d**, **10i-x**. The mixture of the appropriate phthalimide-protected alkyl bromide (7.5 mmol), piperazine derivative (5 mmol) and K_2CO_3 (10 mmol) in DMF (5 mL) was stirred at 70 ˚C overnight. The reaction mixture was cooled, washed with H_2O (5 mL) and then extracted with ethyl acetate (3 × 10 mL). The organic phase was then combined, dried over Na_2SO_4 and evaporated *in vacuo* to give the crude product, which was recrystallized from EtOH and/or CH_3OH, or purified by chromatography (petrol ether/ EtOAc).

2-(2-(4-Phenylpiperazin-1-yl)ethyl)isoindoline-1,3-dione (10a). Pale yellow solid was obtained by column chromatography with petrol ether/ EtOAc, 5:1~1:1 (1.5 g, yield 43 %). ^{1}H NMR (400 MHz, $CDCl_3$): δ 7.86-7.80 (m, 4H), 7.25-7.24 (m, 2H), 6.91-6.88 (m, 2H), 6.80 (t, J = 8.1 Hz, 1H), 3.87 (t, J = 6.3 Hz, 2H), 3.15-3.12 (m, 4H), 2.72-2.68 (m, 6H).

2-(3-(4-Phenylpiperazin-1-yl)propyl)isoindoline-1,3-dion (10b). Pale white solid was obtained by recrystallization from EtOH (1.4 g, yield 79 %). ^{1}H NMR (400 MHz, $CDCl_3$): δ 7.89-7.85 (m, 2H), 7.74-7.71 (m, 2H), 7.30-7.24 (m, 2H), 6.90-6.84 (m, 3H), 3.85-3.80 (m, 2H), 3.07 (br s, 4H), 2.57 (br s, 4H), 2.53-2.49 (m, 2H), 1.95-1.92 (m, 2H).

2-(2-(4-Phenylpiperidin-1-yl)ethyl)isoindoline-1,3-dione (10c). Pale white solid was obtained by recrystallization from EtOH (1.3 g, yield 37 %). ^{1}H NMR (400 MHz, $CDCl_3$): δ 7.88-7.85 (m, 2H), 7.76-7.71 (m, 2H), 7.30-7.28 (m, 2H), 7.21-7.18 (m, 3H), 3.87 (t, J = 6.8 Hz, 2H), 3.13 (d, J = 9.6 Hz, 2H), 2.71-2.65 (m, 2H), 2.51-2.44 (m, 1H), 2.19-2.13 (m, 2H), 1.83-1.66 (m, 4H).

***tert*-Butyl-4-(2-(1,3-dioxoisoindolin-2-yl)ethyl)piperazine-1-carboxylate (10d)**. White solid was obtained by silica gel with CH_2Cl_2/EtOAc (10:1~8:1) (558 mg, yield 57 %). ^{1}H NMR (400 MHz, $CDCl_3$): δ 7.79 (dd, J = 5.6, 3.2 Hz, 2H), 7.71 (dd, J = 5.6, 3.2 Hz, 2H), 3.77 (t, J = 6.4 Hz, 2H), 3.30 (t, J = 4.8 Hz, 4H), 2.59 (t, J = 6.4 Hz, 2H), 2.41 (t, J = 4.8 Hz, 4H), 1.39 (s, 9H).

2-(2-(4-(4-Methylphenyl)piperazin-1-yl)ethyl)isoindoline-1,3-dione (10i). Pale white solid was obtained by recrystallization from EtOH (1.5 g, yield 44 %). ^{1}H NMR (400 MHz, $CDCl_3$): δ 7.88-7.82 (m, 2H), 7.75-7.69 (m, 2H), 7.09-7.03 (m, 2H), 6.82 (t, J = 8.8 Hz, 2H), 3.87-3.84 (m, 2H), 3.08-3.06 (m, 4H), 2.70-2.66 (m, 6H), 2.26 (d, J =10 Hz, 3H).

2-(2-(4-(4-Chlorophenyl)piperazin-1-yl)ethyl)isoindoline-1,3-dione (10j). Pale white solid was obtained by recrystallization from EtOH (1.7 g, yield 58 %). ^{1}H NMR (400 MHz, CDCl3): δ 7.84 (dd, J

= 5.2, 2.8 Hz, 2H), 7.7.1 (dd, *J* = 5.2, 2.8 Hz, 2H), 7.17 (dd, *J* = 6.8, 2.4 Hz, 2H), 6.79 (dd, *J* = 6.8, 2.4 Hz, 2H), 3.85 (t, *J* = 6.4 Hz, 2H), 3.08 (t, *J* = 4.8 Hz, 4H), 2.69-2.66 (m, 6H).

2-(2-(4-(4-(Trifluoromethyl)phenyl)piperazin-1-yl)ethyl)isoindoline-1,3-dione (10k). White solid was obtained by recrystallization from EtOH/CH_3OH, 1:1 (985 mg, yield 49 %). ^{1}H NMR (400 MHz, $CDCl_3$): δ 7.83 (dd, *J* = 5.2, 2.8 Hz, 2H), 7.71 (dd, *J* = 5.2, 2.8 Hz, 2H), 7.45 (d, *J* = 8.8 Hz, 2H), 6.88 (d, *J* = 8.8 Hz, 2H), 3.86 (t, *J* = 6.4 Hz, 2H), 3.21 (t, *J* = 4.8 Hz, 4H), 2.71-2.66 (m, 6H).

2-(2-(4-(4-Fluorophenyl)piperazin-1-yl)ethyl)isoindoline-1,3-dione (10l). White solid was obtained by silica gel with Petrol Ether/ EtOAc, 5:1 (1.7 g, yield 49 %). ^{1}H NMR (400 MHz, $CDCl_3$): δ 7.87-7.85 (m, 2H), 7.84-7.82 (m, 2H), 6.98-6.81 (m, 4H), 3.05-3.02 (m, 2H), 3.19-3.07 (m, 4H), 2.70-2.66 (m, 6H).

2-(2-(4-(4-Methoxyphenyl)piperazin-1-yl)ethyl)isoindoline-1,3-dione (10m). Pale white solid was obtained by recrystallization from EtOH (813 mg, yield 45 %). ^{1}H NMR (400 MHz, $CDCl_3$): δ 7.84 (dd, *J* = 5.2, 2.8 Hz, 2H), 7.71 (dd, *J* = 5.2, 2.8 Hz, 2H), 6.88-6.86 (m, 2H), 6.82-6.80 (m, 2H), 3.88 (t, *J* = 6.4 Hz, 2H), 3.75 (s, 3H), 3.04-3.02 (m, 4H), 2.70-2.69 (m, 6H).

2-(2-(4-([1,1'-Biphenyl]-4-yl)piperazin-1-yl)ethyl)isoindoline-1,3-dione (10n). Pale white solid was obtained by recrystallization from EtOH (1.0 g, yield 55 %). ^{1}H NMR (400 MHz, $CDCl_3$): δ 7.84 (dd, *J* = 5.2, 2.8 Hz, 2H), 7.72 (dd, *J* = 5.2, 2.8 Hz, 2H), 7.54 (d, *J* = 7.6 Hz, 2H), 7.49 (d, *J* = 8.8 Hz, 2H), 7.39 (t, *J* = 7.6 Hz, 2H), 7.25 (s, 1H), 6.95 (d, *J* = 8.8 Hz, 2H), 3.87 (t, *J* = 6.8 Hz, 2H), 3.19-3.17 (m, 4H), 2.72-2.70 (m, 6H).

2-(2-(4-(2-Methylphenyl)piperazin-1-yl)ethyl)isoindoline-1,3-dione (10o). Pale white solid was obtained by column chromatography (CH_2Cl_2 - 2% MeOH/CH_2Cl_2) (1.9 g, yield 57 %). ^{1}H NMR (400 MHz, $CDCl_3$): δ 7.86-7.83 (m, 2H), 7.75-7.68 (m, 2H), 7.17-7.11 (m, 2H), 6.99-6.92 (m, 2H), 3.87 (d, *J* = 6.4 Hz, 2H), 2.90-2.84 (m, 4H), 2.76-2.68 (m, 6H), 2.29 (s, 3H).

2-(2-(4-(2-Methoxyphenyl)piperazin-1-yl)ethyl)isoindoline-1,3-dione (10p). Pale white solid was obtained by column chromatography (CH_2Cl_2 - 2% MeOH/CH_2Cl_2) (2.49 g, yield 60 %). ^{1}H NMR (400 MHz, $CDCl_3$): δ 7.86-7.83 (m, 2H), 7.73-7.70 (m, 2H), 7.00-6.96 (m, 1H), 6.92- 6.87 (m, 2H), 6.84 (d, *J* = 7.6 Hz, 1H), 3.87-3.84 (m, 5H), 3.10-2.93 (m, 4H), 2.74-2.67 (m, 6H).

2-(2-(4-(2-Chlorophenyl)piperazin-1-yl)ethyl)isoindoline-1,3-dione (10q). Pale white solid was obtained by column chromatography (CH_2Cl_2 – 2% MeOH/CH_2Cl_2) (2.11 g, yield 64%). ^{1}H NMR (400 MHz, $CDCl_3$): δ 7.88-7.83 (m, 2H), 7.74-7.70 (m, 2H), 7.33 (dd, *J* = 8.0, 1.6 Hz, 1H), 7.19 (td, *J* = 8.0, 1.6 Hz, 1H), 7.01 (dd, *J* = 8.0, 1.2 Hz, 1H), 6.94 (td, *J* = 7.6, 1.2 Hz, 1H), 3.87 (d, *J* = 6.8 Hz, 2H), 3.10-2.94 (m, 4H), 2.81-2.63 (m, 6H).

2-(2-(4-(2-Fluorophenyl)piperazin-1-yl)ethyl)isoindoline-1,3-dione (10r). Pale white solid was obtained by recrystallization from EtOH (1.97 g, yield 74%). ^{1}H NMR (400 MHz, $CDCl_3$): δ 7.87-7.83 (m, 2H), 7.74-7.70 (m, 2H), 7.21-7.17 (m, 2H), 6.97-6.93 (m, 2H), 3.90-3.84 (m, 2H), 3.10-3.00 (m, 4H), 2.65-2.52 (m, 6H).

2-(2-(4-(3-Fluorophenyl)piperazin-1-yl)ethyl)isoindoline-1,3-dione (10s). Pale white solid was obtained by recrystallization from EtOH (1.97 g, yield 74%). ^{1}H NMR (400 MHz, $CDCl_3$): δ 7.83-7.82 (m, 2H), 7.71-7.67 (m, 2H), 7.18-7.12 (m, 1H), 6.64-6.63 (m, 1H), 6.55-6.47 (m, 2H), 3.86-3.83 (m, 2H), 3.15-3.10 (m, 4H), 2.75-2.60 (m, 6H).

2-(2-(4-(2,4-Dimethylphenyl)piperazin-1-yl)ethyl)isoindoline-1,3-dione (10t). Pale white solid (852 mg, yield 45%) was obtained by column purification (2% MeOH/CH_2Cl_2). ^{1}H NMR (400 MHz, $CDCl_3$): δ 7.88-7.83 (m, 2H), 7.75-7.69 (m, 2H), 6.98 (s, 1H), 6.94 (d, J = 8.0 Hz, 1H), 6.89 (d, J = 8.4 Hz, 1H), 3.86 (t, J = 6.8 Hz, 2H), 2.90-2.81 (m, 4H), 2.73-2.68 (m, 6H).

2-(2-(4-(3,4-Dichlorophenyl)piperazin-1-yl)ethyl)isoindoline-1,3-dione (10u). Pale white solid was obtained by recrystallization from EtOH.(1.78 g, yield 88 %). ^{1}H NMR (400 MHz, $CDCl_3$): δ 7.85-7.83 (m, 2H), 7.72-7.70 (m, 2H), 7.23 (s, 1H), 6.92 (d, J = 2.8 Hz, 1H), 6.71 (dd, J = 8.8, 2.8 Hz, 1H), 3.87-3.84 (m, 2H), 3.11-3.08(m, 4H), 2.71-2.65 (m, 6H).

2-(2-(4-(2,4-dichlorophenyl)piperazin-1-yl)ethyl)isoindoline-1,3-dione (10v). Pale white solid (509 mg, yield 29%) was obtained by column purification (1% MeOH/CH_2Cl_2). ^{1}H NMR (400 MHz, $CDCl_3$): δ 7.88-7.83 (m, 2H), 7.74-7.70 (m, 2H), 7.33 (d, J = 2.4 Hz, 1H), 7.15 (dd, J = 8.4, 2.4 Hz, 1H), 6.91 (d, J = 8.4 Hz, 1H), 3.86 (t, J = 6.8 Hz, 2H), 3.06-2.95 (m, 4H), 2.78-2.68 (m, 6H).

2-(2-(4-(2-Fluoro-4-methoxyphenyl)piperazin-1-yl)ethyl)isoindoline-1,3-dione (10w). Pale white solid (859 mg, yield 54%) was obtained by column chromatography (CH_2Cl_2-2% MeOH/CH_2Cl_2). ^{1}H NMR (400 MHz, $CDCl_3$): δ 7.87-7.83 (m, 2H), 7.74-7.70 (m, 2H), 6.87 (t, J = 9.2 Hz, 1H), 6.65-6.58 (m, 2H), 3.86 (t, J = 6.8 Hz, 2H), 3.74 (s, 3H), 3.07-2.95 (m, 4H), 2.72-2.69 (m, 6H).

2-(2-(4-(2,4-Difluorophenyl)piperazin-1-yl)ethyl)isoindoline-1,3-dione (10x). White solid was obtained by silica gel with petrol ether/EtOAc, 20:1~5:1, (389 mg, yield 65 %). ^{1}H NMR (400 MHz, $CDCl_3$): δ 7.81-7.79 (m, 2H), 7.67-7.65 (m, 2H), 6.84-6.78 (m, 1H), 6.75-6.69 (m, 2H), 3.97 (m, 2H), 2.93 (m, 4H), 2.66 (m, 6H).

General Procedure for Preparation of Compounds **11a-d**, **11i-x**. Hydrazine hydrate was added in excess (1 ~ 5 mL) to a solution of isoindoline-1,3-dione (3 mmol) in EtOH (25 mL) and the mixture was stirred at 70 ˚C overnight. The solvent was removed *in vacuo* and EtOAc was added to the residue. The solids were

filtered, dried over Na_2SO_4 and evaporated *in vacuo* to give the crude product as a pale yellow oil or solid. The crude product is used in the next step without further purification.

General Procedure for Preparation of Compounds **12a-x**. The mixture of the related amine (0.75 mmol), the sulfone / sulfoxide mixture (**5**) (0.50 mmol) and Et_3N (1.0 mmol) was dissolved in CH_3CN and refluxed overnight. After removing the solvent *in vacuo*, EtOAc was added and the organic phase was washed with H_2O and brine (2 × 10 mL), dried over Na_2SO_4 and evaporated. The residue was purified by column chromatography using silica gel and EtOAc or EtOAc/MeOH to afford a white to off-white solid.

2-(Furan-2-yl)-*N*^{5}-(2-(4-phenylpiperazin-1-yl)ethyl)-[1,2,4]triazolo[1,5-*a*][1,3,5]triazine-5,7-diamine (12a). Eluted with EtOAc/MeOH, 10:1 to afford the title compound as white powder (55 mg, yield: 14%). ^{1}H NMR (400 MHz, MeOD): δ 7.68 (s, 1H), 7.22 (t, J = 8.4 Hz, 2H), 7.12 (d, J = 3.2 Hz, 1H), 6.96 (d, J = 8.4 Hz, 2H), 6.84-6.81 (m, 1H), 6.60 (d, J = 1.6 Hz, 1H), 3.61-3.60 (m, 2H), 3.20 (t, J = 4.8 Hz, 4H), 2.72 (t, J = 4.8 Hz, 4H), 2.68-2.67 (m, 2H). ^{13}C NMR (101 MHz, DMSO-d_6): 161.6, 159.7, 156.3, 151.5, 150.5, 146.7, 145.1, 129.4, 119.2, 115.8, 112.4, 112.1, 57.1, 53.2, 48.7, 38.5. HRMS (ESI) *m/z* [*M*+H]$^+$ calcd for $C_{20}H_{24}N_9O^+$: 406.2026, found: 406.2092; HPLC: ret. time =11.96 min., purity = 96.7%.

2-(Furan-2-yl)-*N*^{5}-(3-(4-phenylpiperazin-1-yl)propyl)-[1,2,4]triazolo[1,5-*a*][1,3,5]triazine-5,7-diamine (12b). Eluted with EtOAc/MeOH, 10:1 to afford the title compound as white powder (87 mg, yield: 41%). ^{1}H NMR (400 MHz, DMSO-d_6): δ 8.42 and 8.13 (2 x s due to dimer formation, 2H, NH_2), 7.86 (s, 1H), 7.55 and 7.44 (2 x t due to dimer formation, J = 5.2 Hz, 1H, NH), 7.19 (t, J = 8.0 Hz, 2H), 7.04-7.03 (m, 1H), 6.91 (d, J = 8.0 Hz, 2H), 6.75 (t, J = 6.8 Hz, 1H), 6.66 (s, 1H), 3.30-3.29 (m, 4H), 3.12-3.10 (m, 6H), 2.40-2.36 (m, 2H), 1.74-1.71 (m, 2H). ^{13}C NMR (101 MHz, DMSO-d_6): δ 162.0, 161.6, 159.7, 156.3, 151.5, 151.1, 150.4, 146.7, 145.1, 129.4, 122.9, 119.1, 115.7, 112.4, 112.1, 108.7, 56.1, 56.0, 53.3, 48.6, 26.5. HRMS (ESI) *m/z* [*M*+H]$^+$ calcd for $C_{21}H_{26}N_9O^+$: 420.2182, found 420.2253; HPLC: ret. time = 11.98 min., purity = 97.8 %.

2-(Furan-2-yl)-*N*^{5}-(2-(4-phenylpiperidin-1-yl)ethyl)-[1,2,4]triazolo[1,5-*a*][1,3,5]triazine-5,7-diamine (12c). Eluted with EtOAc/MeOH, 3:2 to afford the title compound as white powder (29 mg, yield: 14%). ^{1}H NMR (400 MHz, DMSO-d_6): 8.46 and 8.21 (2 x s due to dimer formation, 2H, NH_2), 7.88 (s, 1H), 7.35 and 7.33 (2 x t due to dimer formation, J = 7.2 Hz, 1H, NH), 7.31-7.22 (m, 4H), 7.20-7.17 (m, 1H), 7.07 (d, J = 3.6 Hz, 1H), 6.69-6.68 (m, 1H), 3.45-3.42 (m, 2H), 3.05-3.02 (m, 2H), 2.52-2.51 (m, 2H), 2.49-2.44 (m, 1H), 2.12-2.07(m, 2H), 1.76-1.63 (m, 4H). ^{13}C NMR (101 MHz, DMSO-d_6): 161.6, 159.7, 156.3, 150.5, 146.7, 146.6, 145.1, 128.8, 127.2, 126.4, 112.4, 112.1, 57.4, 54.3, 42.3, 38.6, 33.5. HRMS (ESI) *m/z* [*M*+H]$^+$ calcd for $C_{21}H_{25}N_8O^+$: 405.2073, found: 405.2142; HPLC: ret. time = 12.20 min., purity = 99.5%.

***tert*-Butyl-4-(2-(7-amino-2-(furan-2-yl)-[1,2,4]triazolo[1,5-*a*][1,3,5]triazin-5-ylamino)ethyl)**

piperazine-1-carboxylate (12d). Eluted with petrol ether/EtOAc from 1:1 to 1:9 to afford the title compound as white powder (20 mg, yield: 31%). ^{1}H NMR (400 MHz, MeOD): δ 7.69 (d, J = 0.8 Hz, 1H), 7.12 (d, J = 3.2 Hz, 1H), 6.61 (dd, J = 3.2 Hz, 0.8 Hz, 1H), 3.60-3.57 (m, 2H), 3.46-3.45 (m, 4H), 2.63-2.62 (m, 2H), 2.52-2.50 (m, 4H), 1.46 (s, 9H). HRMS (ESI) *m/z* [*M*+H]$^+$ calcd for $C_{19}H_{28}N_9O_3^+$: 430.2237, found: 430.2308; HPLC: ret. time = 11.86 min., purity = 96.3%.

2-(Furan-2-yl)-*N*^{5}-(2-(piperazin-1-yl)ethyl)-[1,2,4]triazolo[1,5-*a*][1,3,5]triazine-5,7-diamine di-trifluoroacetate (12e). The Boc-protected compound (**12d**) (20 mg) was dissolved in a CH_2Cl_2/TFA mixture, 1:1 (5 mL). The mixture was stirred at room temperature for 24 hrs. A brown solid was obtained (13 mg, yield: 82%). ^{1}H NMR (400 MHz, DMSO-d_6): 8.41 and 8.16 (2 x s due to dimer formation, 2H, NH_2), 7.86 (s, 1H), 7.30 (br s, 1H, NH), 7.04 (s, 1H), 6.67 (s, 1H), 3.50 (br s, 2H), 3.04 (br s, 4H), 2.60 (br s, 4H), 2.50 (br s, 2H). ^{13}C NMR (101 MHz, DMSO-d_6): 161.7, 159.6, 150.6, 146.7, 145.4, 112.4, 112.1, 108.6, 56.9, 50.3, 43.7, 38.2. HRMS (ESI) *m/z* [*M*+H]+ calcd for $C_{18}H_{22}F_6N_9O_5^+$: 557.1570, found: 330.1786 ([*M*+H$^+$]-2TFA); HPLC: ret. time = 11.92 min., purity = 98.9 %.

2-(Furan-2-yl)-*N*^{5}-(2-(4-methylpiperazin-1-yl)ethyl)-[1,2,4]triazolo[1,5-*a*][1,3,5]triazine-5,7-diamine (12f). Eluted with EtOAc/MeOH, 3:2 to afford the title compound as white powder (61 mg, yield: 35%). ^{1}H NMR (400 MHz, DMSO-d_6): 8.16 (2 x s due to dimer formation, 2H, NH_2), 7.81 (s, 1H), 7.24 and 7.16 (2 x t due to dimer formation, J = 5.6 Hz, 1H, NH), 7.00-6.99 (m, 1H), 6.62-6.61 (m, 1H), 3.33-3.32 (m, 2H), 2.46-2.45 (m, 2H), 2.42-2.36 (m, 4H), 2.27-2.24 (m, 4H), 2.07(s, 3H). ^{13}C NMR (101 MHz, DMSO-d_6): 161.6, 159.7, 156.3, 150.5, 146.6, 145.1, 129.6, 112.4, 112.1, 57.1, 55.2, 53.2, 46.2, 38.5. HRMS (ESI) *m/z* [*M*+H]$^+$ calcd for $C_{24}H_{34}N_9O^+$: 344.1869, found: 344.1942; HPLC: ret. time = 11.70 min., purity = 99.2%.

***N*^{5}-(2-(4-benzylpiperazin-1-yl)ethyl)-2-(furan-2-yl)-[1,2,4]triazolo[1,5-*a*][1,3,5]triazine-5,7-diamine (12g).** Eluted with EtOAc/MeOH, 3:2 to afford the title compound as white powder (34 mg, yield: 16%). ^{1}H NMR (400 MHz, DMSO-d_6): 8.39 and 8.13 (2 x s for due to dimer formation, 2H, NH_2), 7.82 (s, 1H), 7.28-7.17 (m, 6H), 7.01-7.00 (m, 1H), 6.63-6.62 (m, 1H), 3.39 (s, 2H), 3.34-3.33 (m,2H), 2.47-2.46 (m, 2H), 2.44-2.41 (m, 4H), 2.33-2.31 (m, 4H). ^{13}C NMR (101 MHz, DMSO-d_6): 161.6, 159.7, 156.3, 150.5, 146.6, 145.1, 138.7, 129.3, 128.6, 127.3, 112.4, 112.1, 62.6, 57.6, 57.1, 53.3, 53.1, 46.2, 38.5. HRMS (ESI) *m/z* [*M*+H]$^+$ calcd for $C_{21}H_{25}N_8O^+$: 420.2181, found: 420.2254; HPLC: ret. time = 12.14 min., purity = 99.6%.

2-(Furan-2-yl)-*N*^{5}-(2-(piperidin-1-yl)ethyl)-[1,2,4]triazolo[1,5-*a*][1,3,5]triazine-5,7-diamine (12h). Washed with CH_3CN and CH_2Cl_2 to afford the title compound as white powder (63 mg, yield: 43%). ^{1}H NMR (400 MHz, MeOD): δ 7.69 (s, 1H), 7.12 (d, J = 8.4 Hz, 1H), 6.61-6.60 (m, 1H), 3.57 (t, J = 6.8 Hz, 2H), 2.59-2.58 (m, 2H), 2.52-2.51 (m, 4H), 1.64-1.60 (m, 4H), 1.49-1.48 (m, 2H). ^{13}C NMR (101 MHz, DMSO-d_6): 161.6, 159.7, 156.3, 150.5, 146.7, 145.1, 112.4, 112.1, 57.8, 54.6, 38.6, 26.1, 24.5. HRMS (ESI) *m/z* [*M*+H]$^+$ calcd for $C_{15}H_{21}N_8O^+$: 329.1760, found: 329.1832; HPLC: ret.

time =11.31 min., purity = 96.3%.

2-(Furan-2-yl)-N^5-(2-(4-(4-methylphenyl)piperazin-1-yl)ethyl)-[1,2,4]triazolo[1,5-*a*][1,3,5]triazine-5,7-di-amine (12i). Eluted with EtOAc/MeOH, 5:1, to afford the title compound as white powder (65 mg, yield: 31%). ^{1}H NMR (400 MHz, DMSO-d_6): 8.42 and 8.19 (2 x s due to dimer formation, 2H, NH_2), 7.86 (s, 1H), 7.35 and 7.28 (2 x s due to dimer formation, 1H, NH), 7.05 (s, 1H), 7.01-7.00 (m, 2H), 6.84-6.82 (m,2H), 6.67 (s, 1H), 3.42 (br s, 2H), 3.06 (br s, 4H), 2.56 (br s, 2H), 2.50 (br s, 4H), 2.18 (s, 3H). ^{13}C NMR (101 MHz, DMSO-d_6): 161.6, 160.0, 156.3, 150.5, 149.4, 146.6, 145.1, 129.8, 128.0, 116.0, 112.4, 112.1, 57.1, 53.3, 49.1, 38.5, 20.5. HRMS (ESI) *m/z* [*M*+H]$^+$ calcd for $C_{21}H_{26}N_9O^+$: 420.2182, found: 420.2253; HPLC: ret. time = 12.16 min., purity = 96.0%.

***N*^{5}-(2-(4-(4-chlorophenyl)piperazin-1-yl)ethyl)-2-(furan-2-yl)-[1,2,4]triazolo[1,5-*a*][1,3,5]triazine-5,7-diamine (12j).** Eluted with EtOAc/MeOH, 10:1, to afford the title compound as white powder (30 mg, yield: 14%). ^{1}H NMR (400 MHz, DMSO-d_6): 8.41 and 8.19 (2 x s due to dimer formation, 2H, NH_2), 7.86 (s, 1H), 7.35 and 7.28 (2 x s due to dimer formation, 1H, NH), 7.22-7.20 (m, 2H), 7.05 (s, 1H), 6.93 (br s, 2H), 6.67 (s, 1H), 3.42 (br s. 2H), 3.12 (br s, 4H), 2.56 (br s, 2H), 2.50 (br s, 4H). ^{13}C NMR (101 MHz, DMSO-d_6): 161.9, 159.8, 156.4, 150.3, 146.8, 145.1, 129.0, 122.7, 117.2, 112.4, 112.1, 57.1, 53.0, 48.5, 38.5. HRMS (ESI) *m/z* [*M*+H]$^+$ calcd for $C_{20}H_{23}ClN_9O^+$: 440.1636, found: 440.1707; HPLC: ret. time = 12.41 min., purity = 95.0%.

***N*^{5}-(2-(4-(4-(trifluoromethyl)phenyl)piperazin-1-yl)ethyl)-2-(furan-2-yl)-[1,2,4]triazolo[1,5-*a*][1,3,5]triazine-5,7-diamine (12k).** Eluted with EtOAc/MeOH, 5:1, to afford the title compound as white powder (50 mg, yield: 21%). ^{1}H NMR (400 MHz, DMSO-d_6): 8.43 and 8.19 (2 x s due to dimer formation, 2H, NH_2), 7.86 (s, 1H), 7.49 (d, J = 8.8 Hz, 2H) 7.37 and 7.30 (2 x s due to dimer formation, 1H, NH), 7.06-7.05 (m, 1H), 7.05-7.04 (m, 2H), 6.67 (s, 1H), 3.43-3.42 (m, 2H), 3.27-3.25 (m, 4H), 2.57-2.53 (m, 6H). ^{13}C NMR (101 MHz, DMSO-d_6): 161.6, 159.7, 156.3, 153.7, 150.5, 146.7, 145.1, 126.6, 126.5, 118.4, 118.0, 114.6, 112.4, 112.1, 57.0, 53.0, 47.4, 38.5. HRMS (ESI) *m/z* [*M*+H]$^+$ calcd for $C_{21}H_{23}F_3N_9O^+$: 474.1899, found: 474.1969; HPLC: ret. time = 12.52 min., purity = 95.0%.

***N*^{5}-(2-(4-(4-fluorophenyl)piperazin-1-yl)ethyl)-2-(furan-2-yl)-[1,2,4]triazolo[1,5-*a*][1,3,5]triazine-5,7-diamine (12l).** Eluted with EtOAc/MeOH, 10:1, to afford the title compound as white powder (45 mg, yield: 21%). ^{1}H NMR (400 MHz, DMSO-d_6): 8.19 and 8.12 (2 x s for due to dimer formation, 2H, NH_2), 7.86 (s, 1H), 7.35 and 7.28 (2 x s due to dimer formation, 1H, NH), 7.05-7.01 (m, 2H), 7.00 (s, 1H), 6.94-6.91 (m, 2H), 6.67 (s,1H), 3.43-3.41 (m. 2H), 3.06 (br s, 4H), 2.57-2.53 (m, 6H). ^{13}C NMR (101 MHz, DMSO-d_6): 161.6, 161.1, 159.2, 156.7, 156.1, 155.8, 155.1, 150.7, 150.0, 147.9, 146.2, 144.6, 117.0, 116.9, 115.3, 115.1, 111.9, 111.6, 57.0, 56.6, 52.7, 49.0, 38.4, 38.0. HRMS (ESI) *m/z* [*M*+H]$^+$ calcd for $C_{20}H_{23}FN_9O^+$: 424.1931, found: 424.2002; HPLC: ret. time = 12.08 min., purity = 97.2%.

2-(Furan-2-yl)-*N*^{5}-(2-(4-(4-methoxyphenyl)piperazin-1-yl)ethyl)-[1,2,4]triazolo[1,5-*a*][1,3,5] triazine-5,7-diamine (12m). Eluted with EtOAc/MeOH, 5:1, to afford the title compound as white powder (64 mg, yield: 29%). ^{1}H NMR (400 MHz, DMSO-d_6): 8.44 and 8.20 (2 x s for due to dimer formation, 2H, NH_2), 7.86 (s, 1H), 7.34 and 7.27 (2 x s due to dimer formation, 1H, NH), 7.05 (d, J = 2.4 Hz, 1H), 6.87 (d, J = 8.8 Hz, 2H), 6.79 (d, J = 8.8 Hz, 2H), 6.67 (s, 1H), 3.66 (s, 3H), 3.42-3.39 (m, 2H), 3.00 (br s, 4H), 2.56-2.52 (m, 6H). ^{13}C NMR (101 MHz, DMSO-d_6): 161.6, 159.7, 156.3, 153.3, 150.5, 146.6, 145.9, 145.1, 117.7, 114.7, 112.4, 112.1, 57.1, 55.6, 53.3, 50.0, 38.5. HRMS (ESI) *m/z* [*M*+H]$^+$ calcd for $C_{21}H_{26}N_9O_2^+$: 436.2131, found: 436.2202; HPLC: ret. time = 11.75 min., purity = 95.6%.

***N*^{5}-(2-(4-([1,1'-biphenyl]-4-yl)piperazin-1-yl)ethyl)-2-(furan-2-yl)[1,2,4]triazolo[1,5-*a*][1,3,5] trizaine-5,7-diamine (12n).** Eluted with EtOAc/MeOH, 10:1, to afford the title compound as white powder (55 mg, yield: 23%). ^{1}H NMR (400 MHz, DMSO-d_6): 8.53 (s, 1H), 8.21 (br s, 2H, NH_2), 7.87 (s, 1H), 7.60-7.52 (m, 3H), 7.40-7.39 (m, 2H), 7.30-7.27 (m, 1H), 7.06-7.01 (m, 3H), 6.68 (s, 1H), 4.31 (m, 2H), 3.49-3.43 (m, 2H), 3.20-3.19 (m, 4H), 2.60-2.58 (m, 4H). ^{13}C NMR (101 MHz, DMSO-d_6): 161.6, 159.7, 156.3, 150.8, 150.5, 146.6, 146.5, 145.1, 140.5, 130.7, 129.3, 127.6, 126.8, 126.3, 115.9, 112.4, 112.1, 57.1, 53.2, 48.4, 38.5. HRMS (ESI) *m/z* [*M*+H]$^+$ calcd for $C_{26}H_{28}N_9O^+$: 482.2339, found: 482.2408; HPLC: ret. time = 11.98 min., purity = 97.8 %.

2-(furan-2-yl)-*N*^{5}-(2-(4-(2-methyphenyl)piperazin-1-yl)ethyl)-[1,2,4]triazolo[1,5-*a*][1,3,5]triazine-5,7-diamine (12o). Eluted with EtOAc/MeOH, 3:2 to afford the title compound as white powder (116 mg, yield: 55%). ^{1}H NMR (400 MHz, DMSO-d_6): 8.44 and 8.19 (2 x s due to dimer formation, 2H, NH_2), 7.88 (s, 1H), 7.35 and 7.27 (2 x s due to dimer formation, 1H, NH), 7.16-7.11 (m, 2H), 7.06 (s, 1H), 7.02 (d, J = 7.6 Hz, 1H), 6.95 (t, J = 7.2 Hz, 1H), 6.68 (s, 1H), 3.46-3.43 (m, 2H), 2.90-2.78 (m, 4H), 2.61-2.55 (m, 6H), 2.24 (s, 3H). ^{13}C NMR (101 MHz, DMSO-d_6): 161.6, 161.2, 159.2, 155.9, 151.3, 150.1, 146.2, 144.7, 131.7, 130.8, 126.5, 122.8, 118.7, 111.9, 111.7, 56.7, 53.3, 51.3, 38.0, 17.6. HRMS (ESI) *m/z* [*M*+H]$^+$ calcd for $C_{21}H_{26}N_9O^+$: 420.2182, found: 420.2252 ; HPLC: ret. time = 12.37 min., purity = 99.6%.

2-(furan-2-yl)-*N*^{5}-(2-(4-(2-methoxyphenyl)piperazin-1-yl)ethyl)-[1,2,4]triazolo[1,5-*a*][1,3,5] triazine-5,7-diamine (12p). Eluted with EtOAc/MeOH, 3:2 to afford the title compound as white powder (130 mg, yield: 60%). ^{1}H NMR (400 MHz, DMSO-d_6): 8.44 and 8.20 (2 x s due to dimer formation, 2H, NH_2), 7.86 (s, 1H), 7.40 and 7.27 (2 x s due to dimer formation, 1H, NH), 7.06 (s, 1H), 6.91-6.90 (m, 2H), 6.85-6.84 (m, 2H), 6.67 (s, 1H), 3.79 (s, 3H), 3.43-3.42 (m, 2H), 2.95-2.94 (m, 4H), 2.57-2.50 (m, 6H). ^{13}C NMR (101 MHz, DMSO-d_6): 161.2, 159.2, 155.9, 152.0, 150.0, 146.2, 144.7, 141.3, 122.3, 120.8, 117.9, 111.9, 111.8, 111.6, 56.7, 55.3, 53.1, 50.1, 38.3. HRMS (ESI) *m/z* [*M*+H]$^+$ calcd for $C_{21}H_{26}N_9O_2^+$: 436.2131, found: 436.2007; HPLC: ret. time = 12.08 min., purity = 99.9%.

***N*^{5}-(2-(4-(2-chlorophenyl)piperazin-1-yl)ethyl)-2-(furan-2-yl)-[1,2,4]triazolo[1,5-*a*][1,3,5] triazine-5,7-diamine (12q).** Eluted with EtOAc/MeOH, 3:2 to afford the title compound as white powder (113 mg, yield: 51%). ^{1}H NMR (400 MHz, DMSO-d_6): 8.42 and 8.18 (2 x s due to dimer formation, 2H, NH_2), 7.87 (s, 1H), 7.47-7.38 (dd, J = 7.6, 1.2 Hz, 1H), 7.35-7.25 (m, 2H), 7.15 (d, J = 8.0 Hz, 1H), 7.05-7.01 (m, 2H), 6.68-6.67 (m, 1H), 3.45-3.40 (m, 2H), 2.98-2.97 (m, 4H), 2.61-2.49 (m, 6H). ^{13}C NMR (101 MHz, DMSO-d_6): 161.2, 159.2, 155.9, 150.0, 149.1, 146.2, 144.7, 130.3, 128.1, 127.6, 123.8, 120.8, 118.7, 111.9, 111.7, 56.6, 52.9, 50.9, 38.0. HRMS (ESI) *m/z* [*M*+H]$^+$ calcd for $C_{20}H_{23}ClN_9O^+$: 440.1636, found: 440.1706 ; HPLC: ret. time = 12.27 min., purity = 99.5%.

***N*^{5}-(2-(4-(2-fluorophenyl)piperazin-1-yl)ethyl)-2-(furan-2-yl)-[1,2,4]triazolo[1,5-*a*][1,3,5]triazine-5,7-diamine (12r).** Eluted with EtOAc/MeOH, 10:1 to afford the title compound as white powder (66 mg, yield: 31%). ^{1}H NMR (400 MHz, DMSO-d_6): 8.46 and 8.21 (2 x s due to dimer formation, 2H, NH_2), 7.86 (s, 1H), 7.35 and 7.14 (2 x t due to dimer formation, J = 5.6 Hz, 1H, NH), 7.14-6.92 (m, 5H), 6.68-6.67 (m, 1H), 3.44-3.43 (m, 2H), 3.02-3.01 (m, 4H), 2.60-2.59 (m, 4H), 2.57-2.53 (m, 2H). ^{13}C NMR (101 MHz, DMSO-d_6): 161.6, 159.7, 156.6, 154.2, 150.5, 146.6, 145.1, 140.3, 125.3, 125.2, 122.7, 122.6, 119.6, 116.5, 116.3, 112.4, 112.1, 57.0, 53.3, 50.6, 50.5, 38.4. HRMS (ESI) *m/z* [*M*+H]$^+$ calcd for $C_{20}H_{23}FN_9O^+$: 424.1931, found: 424.2002; HPLC: ret. time = 12.00 min., purity = 95.6%.

***N*^{5}-(2-(4-(3-fluorophenyl)piperazin-1-yl)ethyl)-2-(furan-2-yl)-[1,2,4]triazolo[1,5-*a*][1,3,5]triazine-5,7-diamine (12s).** Eluted with EtOAc/MeOH, 3:2 to afford the title compound as white powder (96 mg, yield: 45%). ^{1}H NMR (400 MHz, DMSO-d_6): 8.44 and 8.19 (2 x s due to dimer formation, 2H, NH_2), 7.86 (s, 1H), 7.37 and 7.27 (2 x t due to dimer formation, J = 5.2 Hz, 1H, NH), 7.22-7.16 (m, 1H), 7.05-7.04 (d, J = 3.2 Hz, 1H), 6.75-6.66 (m, 3H), 6.54-6.49 (m, 1H), 3.44-3.39 (m, 2H), 3.15 (br s, 4H), 2.55-2.52 (m, 6H). ^{13}C NMR (101 MHz, DMSO-d_6): 164.9, 162.5, 162.0, 161.6, 159.7, 156.6, 156.3, 153.3, 153.2, 151.1, 150.5, 146.6, 145.1, 130.8, 130.7, 112.4, 112.1, 111.2, 105.1, 104.9, 102.2, 102.0, 57.5, 57.0, 53.0, 48.1, 38.9, 38.4. HRMS (ESI) *m/z* [*M*+H]$^+$ calcd for $C_{20}H_{23}FN_9O^+$: 424.1931, found 424.2002; HPLC: ret. time = 12.06 min., purity = 98.5%.

***N*^{5}-(2-(4-(2,4-dimethylphenyl)piperazin-1-yl)ethyl)-2-(furan-2-yl)-[1,2,4]triazolo[1,5-*a*][1,3,5] triazine-5,7-diamine (12t).** Eluted with EtOAc/MeOH, 5:1 to afford the title compound as white powder (128 mg, yield: 59%). ^{1}H NMR (400 MHz, DMSO-d_6): 8.40 and 8.17 (2 x s due to dimer formation, 2H, NH_2), 7.88 (s, 1H), 7.33 and 7.26 (2 x t, J = 5.2 Hz, 1H, NH), 7.06-7.05 (m, 1H), 6.99-6.90 (m, 4H), 6.68 (s, 1H), 3.43 (t, J = 6.0 Hz, 2H), 2.80 (br s, 4H), 2.59-2.51 (m, 6H), 2.20 (s, 6H). ^{13}C NMR (101 MHz, DMSO-d_6): 161.2, 159.2, 155.9, 150.0, 148.9, 146.2, 144.6, 131.5, 131.4, 126.9, 118.6, 111.9, 111.6, 56.7, 53.3, 51.5, 38.0, 20.3, 17.4. HRMS (ESI) *m/z* [*M*+H]$^+$ calcd for $C_{22}H_{28}N_9O^+$: 434.24113, found: 434.24088; HPLC: ret. time = 7.98 min., purity = 99.3%.

***N*^{5}-(2-(4-(3,4-dichlorophenyl)piperazin-1-yl)ethyl)-2-(furan-2-yl)-[1,2,4]triazolo[1,5-*a*] [1,3,5]-triazine-5,7-diamine (12u).** Eluted with EtOAc/MeOH, 10:1, to afford the title compound as

white powder (128 mg, yield: 59%). ^{1}H NMR (400 MHz, DMSO-d_6): 8.44 and 8.20 (2 x s due to dimer formation, 2H, NH_2), 7.87 (s, 1H), 7.38 (d, J = 8.8 Hz, 1H), 7.29 (t, J = 5.2 Hz, 1H, NH), 7.12 (d, J = 2.8 Hz, 1H), 7.05 (d, J = 3.2 Hz, 1H), 6.94 (dd, J = 9.2, 2.8 Hz, 1H), 6.68 (dd, J = 3.2, 1.6 Hz, 1H), 3.45-3.43 (m, 2H), 3.18 (br s, 4H), 2.55-2.51 (m, 6H). ^{13}C NMR (101 MHz, DMSO-d_6): 161.6, 159.7, 156.3, 151.2, 150.5, 146.7, 145.1, 131.9, 130.9, 120.0, 116.6, 115.7, 112.4, 112.1, 57.0, 52.9, 48.0, 38.4. HRMS (ESI) *m/z* [*M*+H]$^+$ calcd for $C_{20}H_{22}Cl_2N_9O^+$: 474.1246, found: 474.1317; HPLC: ret. time = 12.12 min., purity = 95.3%.

***N*^{5}-(2-(4-(2,4-dichlorophenyl)piperazin-1-yl)ethyl)-2-(furan-2-yl)-[1,2,4]triazolo[1,5-*a*][1,3,5] triazine-5,7-diamine (12v).** Eluted with EtOAc/MeOH, 5:1 to afford the title compound as white powder (94 mg, yield: 69%). ^{1}H NMR (400 MHz, DMSO-d_6): 8.40 and 8.16 (2 x s due to dimer formation, 2H, NH_2), 7.86 (s, 1H), 7.52 (d, J = 2.0 Hz, 1H), 7.34 (dd, J = 8.4, 2.0 Hz, 1H), 7.25 (t, J = 5.2 Hz, 1H, NH), 7.15 (d, J = 8.4 Hz, 1H), 7.05 (s, 1H), 6.67 (s, 1H), 3.41 (t, J = 5.2 Hz, 2H), 3.10-2.90 (m, 4H), 2.65-2.51 (m, 6H). ^{13}C NMR (101 MHz, DMSO-d_6): 161.2, 159.2, 155.8, 150.0, 148.1, 146.2, 144.6, 129.6, 128.4, 128.0, 126.9, 122.1, 111.9, 111.6, 56.6, 52.8, 50.8, 38.0. HRMS (ESI) *m/z* [*M*+H]$^+$ calcd for $C_{20}H_{22}Cl_2N_9O^+$: 474.13189, found: 474.13182; HPLC: ret. time = 7.98 min., purity = 97.8%.

***N*^{5}-(2-(4-(2-fluoro-4-methoxyphenyl)piperazin-1-yl)ethyl)-2-(furan-2-yl)-[1,2,4]triazolo[1,5-*a*] [1,3,5]triazine-5,7-diamine (12w).** Eluted with EtOAc/MeOH, 5:1 to afford the title compound as white powder (113 mg, yield: 51%). ^{1}H NMR (400 MHz, DMSO-d_6): 8.43 and 8.19 (2 x s due to dimer formation, 2H, NH_2), 7.87 (s, 1H), 7.34 and 7.25 (2 x t due to dimer formation, J = 5.2 Hz, 1H, NH), 7.05-7.04 (m, 1H), 6.97 (t, J = 9.6 Hz, 1H), 6.80 (dd, J = 14.0, 7.6 Hz, 1H), 6.69-6.67 (m, 2H), 3.70 (s, 3H), 3.44-3.41 (m, 2H), 2.91 (br s, 4H), 2.58-2.50 (m, 6H). ^{13}C NMR (101 MHz, DMSO-d_6): 161.6, 161.2,159.2, 156.8, 156.2, 155.9, 155.1, 155.0, 154.4, 150.7, 150.1, 146.2, 144.7, 133.5, 133.4, 119.9, 111.9, 111.7, 109.4, 103.0, 102.8, 57.1, 56.6, 55.5, 52.9, 50.8, 38.4, 38.0. HRMS (ESI) *m/z* [*M*+H]$^+$ calcd for $C_{21}H_{25}FN_9O_2^+$: 454.2037, found: 454.2105; HPLC: ret. time = 11.98 min., purity = 99.4%.

***N*^{5}-(2-(4-(3,4-difluorophenyl)piperazin-1-yl)ethyl)-2-(furan-2-yl)-[1,2,4]triazolo[1,5-*a*][1,3,5] triazine-5,7-diamine (12x).** Eluted with EtOAc to afford the title compound as white powder (14 mg, yield: 25%). ^{1}H NMR (400 MHz, MeOD): δ 7.69 (dd, J = 1.6, 0.8 Hz, 1H), 7.12 (d, J = 3.2 Hz, 1H), 7.06-7.04 (m, 1H), 6.94-6.84 (m, 2H), 6.61 (dd, J = 3.2, 1.6 Hz, 1H), 3.62-3.60 (m, 2H), 3.08-3.07 (m, 4H), 2.75-2.69 (m, 6H). HRMS (ESI) *m/z* [*M*+H]$^+$ calcd for $C_{20}H_{22}F_2N_9O^+$: 442.1837 found: 442.1907; HPLC: ret. time =12.18 min., purity = 95.9%.

Pharmacological characterization

Materials: [^{3}H]-ZM241385 (specific activity 50 Ci mmol^{-1}) was purchased from ARC Inc. (St. Louis, USA). [^{3}H]-1,3-dipropyl-8-cyclopentyl-xanthine ([^{3}H]-DPCPX, specific activity 116.7 Ci/mmol) was purchased from ARC Inc. (St. Louis, USA). Unlabeled ZM241385 was a gift from Dr. S. M. Poucher (Astra-Zeneca, Macclesfield, UK). CGS21680 was a gift from Dr. R. A. Lovell (Ciba-Geigy, Summit, NJ). NECA (5'-*N*-Ethylcarboxamidoadenosine) and DPCPX were purchased from Sigma-Aldrich (Steinheim, Germany). Adenosine deaminase (ADA) was purchased from Boehringer Mannheim (Mannheim, Germany). Bicinchoninic acid (BCA) and BCA protein assay reagent were obtained from Pierce Chemical Company (Rockford, IL, U.S.A.). Human embryonic kidney 293 cells stably expressing the $hA_{2A}R$ (HEK293$hA_{2A}R$) were kindly provided by Dr. J Wang (Biogen/IDEC, Cambridge, MA). Chinese hamster ovary cells stably expressing the hA_1R (CHOhA_1R) were kindly provided by Prof. Steve Hill (University of Nottingham, UK). All other chemicals were of analytical grade and obtained from standard commercial sources.

Cell culture and membrane preparation: Cell culture and membrane preparation were performed as reported previously.[34,43]

Radioligand displacement assay: The radioligand displacement from the hA_1R and $hA_{2A}R$ was determined using the displacement assay as described previously.[34,43]

Radioligand competition association assay: The binding kinetics of unlabeled $A_{2A}R$ ligands were determined at 4 °C using the competition association assay as described previously.[34,43]

cAMP assay: HEK293$hA_{2A}R$ cells were cultured as a monolayer on 10 cm ø culture plates to 80 %-90 % confluency. Cells were harvested and centrifuged two times at 200 × g for 5 min. The amount of cAMP produced was determined with the LANCE® ultra cAMP 384 kit (Perkin-Elmer, Groningen, Netherlands). In general, 1000 cells/well were seeded on 384-well plates and incubated at ambient room temperature (22–25 °C). cAMP generation was performed in the stimulation buffer [*N*-2-hydroxyethylpiperazine-*N*'-

ethanesulphonic acid (HEPES), 5 mM; 0.1 % (w·v^{-1}) BSA; cilostamide, 50 μM; rolipram, 50 μM; adenosine deaminase (ADA), 0.8 IU/mL] Concentration-effect curves for **12x** and **12c** were obtained by adding HEK293hA_{2A}R cells to the mixture of antagonist (**12x** or **12c**) and 100 nM NECA (prepared in the stimulation buffer) for a co-incubation of 30 min. For assessment of either surmountable or insurmountable behavior, the antagonists (**12x** and **12c**) were pre-incubated for 30 min or co-incubated with the agonist NECA at a concentration ranging from 100 μM to 0.1 nM for a duration of 30 min, where the antagonists' concentrations were 0.3-, 1-, 3- and 10-fold their respective K_i values. The incubation was stopped by adding detection mix and antibody solution, according to the instructions of the manufacturer. The generated fluorescence intensity was quantified on the EnVision® Multilabel Reader (PerkinElmer, Groningen, Netherlands). The data obtained were normalized according to the maximal response produced by 100 μM NECA. The shift in agonist EC_{50} was determined to perform Schild analyses.

Data analysis. All experimental data was analyzed by using GraphPad Prism 5.0 (GraphPad Software Inc., San Diego, CA). K_D and B_{max} values of [^{3}H]-ZM241385 at hA_{2A}R membranes were obtained from Guo *et al.*[34] IC_{50} values obtained from competition displacement binding data were converted into K_i values using the Cheng-Prusoff equation.[44] Association and dissociation rates for unlabeled ligands were calculated by fitting the data in the competition association model using '*kinetics of competitive binding*'[30], as described in Chapter 3.

Molecular property descriptors (MW, LogP, MSA, *p*K_a) of the substituted C_2-phenylpiperazine were calculated using MarinSketch 5.11 (ChemAxon, Huagary). (Multiple) Linear regression analysis was done by using Microsoft Excel 2003.

References:

1. Swinney DC. Biochemical mechanisms of drug action: what does it take for success? *Nat Rev Drug Discov* 2004;3(9):801-808.
2. Swinney DC. Can binding kinetics translate to a clinically differentiated drug? From theory to practice. *Lett Drug Des Discov* 2006;3(8):569-574.
3. Nunez S, Venhorst J, Kruse CG. Target-drug interactions: first principles and their application to

drug discovery. *Drug Discov Today* 2012;17(1-2):10-22.
4. Zhang R, Monsma F. Binding kinetics and mechanism of action: toward the discovery and development of better and best in class drugs. Expert Opin Drug Discov 2010;5(11):1023-1029.
5. Copeland RA, Pompliano DL, Meek TD. Drug-target residence time and its implications for lead optimization. *Nat Rev Drug Discov* 2006;5(9):730-739.
6. Rosethorne EM, Turner RJ, Fairhurst RA, Charlton SJ. Efficacy is a contributing factor to the clinical onset of bronchodilation of inhaled beta(2)-adrenoceptor agonists. *Naunyn Schmiedebergs Arch Pharmacol* 2010;382(3):255-263.
7. Govern CC, Paczosa MK, Chakraborty AK, Huseby ES. Fast on-rates allow short dwell time ligands to activate T cells. *Proc Natl Acad Sci U S A* 2010;107(19):8724-8729.
8. Foote J, Eisen HN. Kinetic and affinity limits on antibodies produced during immune responses. *Proc Natl Acad Sci U S A* 1995;92(5):1254-1256.
9. Schreiber G. Kinetic studies of protein-protein interactions. *Curr Opin Struct Biol* 2002;12(1):41-47.
10. Selzer T, Albeck S, Schreiber G. Rational design of faster associating and tighter binding protein complexes. *Nat Struct Biol* 2000;7(7):537-541.
11. Sykes DA, Dowling MR, Leighton-Davies J, Kent TC, Renard E, Trifilieff A, Charlton SJ. The Influence of Receptor Kinetics on the Onset and Duration of Action, and the Therapeutic Index of NVA237 and Tiotropium. *J Pharmacol Exp Ther* 2012;343(2):520-528.
12. Fredholm BB, IJzerman AP, Jacobson KA, Linden J, Müller CE. International Union of Basic and Clinical Pharmacology. LXXXI. Nomenclature and classification of adenosine receptors--an update. *Pharmacol Rev* 2011;63(1):1-34.
13. Jacobson KA, Gao ZG. Adenosine receptors as therapeutic targets. *Nat Rev Drug Discov* 2006;5(3):247-264.
14. Shook BC, Jackson PF. Adenosine A_{2A} Receptor Antagonists and Parkinson's Disease. *ACS Chem Neurosci* 2011;2(10):555-567.
15. Muller CE, Jacobson KA. Recent developments in adenosine receptor ligands and their potential as novel drugs. *Bba-Biomembranes* 2011;1808(5):1290-1308.
16. Shah U, Hodgson R. Recent progress in the discovery of adenosine A_{2A} receptor antagonists for the treatment of Parkinson's disease. *Curr Opin Drug Discov Devel* 2010;13(4):466-480.
17. Poucher SM, Keddie JR, Singh P, Stoggall SM, Caulkett PW, Jones G, Coll MG. The *in vitro* pharmacology of ZM 241385, a potent, non-xanthine A_{2a} selective adenosine receptor antagonist. *Br J Pharmacol* 1995;115(6):1096-1102.
18. Caulkett PWR, Jones G, Collis MG, Poucher SM; Imperial Chemical Indusry PLC, London, assignee. UK. 1991.
19. Vu CB, Pan D, Peng B, Kumaravel G, Smits G, Jin X, Phadke D, Engber T, Huang C, Reilly J, Tam S, Grant D, Hetu G, Petter RC. Novel diamino derivatives of [1,2,4]triazolo[1,5-*a*][1,3,5]triazine as potent and selective adenosine A_{2a} receptor antagonists. *J Med Chem* 2005;48(6):2009-2018.
20. Vu CB, Peng B, Kumaravel G, Smits G, Jin X, Phadke D, Engber T, Huang C, Reilly J, Tam S, Grant D, Hetu G, Chen L, Zhang J, Petter RC. Piperazine derivatives of [1,2,4]triazolo[1,5-*a*][1,3,5]triazine as potent and selective adenosine A_{2a} receptor antagonists. *J Med Chem* 2004;47(17):4291-4299.
21. Vu CB, Shields P, Peng B, Kumaravel G, Jin X, Phadke D, Wang J, Engber T, Ayyub E, Petter RC. Triamino derivatives of triazolotriazine and triazolopyrimidine as adenosine A_{2a} receptor antagonists. *Bioorg Med Chem Lett* 2004;14(19):4835-4838.
22. Dolzhenko AV, Dolzhenko AV, Chui WK. Practical synthesis of regioisomeric 5(7)-amino-

6,7(4,5)-dihydro[1,2,4]triazolo[1,5-*a*][1,3,5]triazines. *Tetrahedron* 2007;63(52):12888-12895.
23. Dolzhenko AV, Pastorin G, Dolzhenko AV, Chui WK. An aqueous medium synthesis and tautomerism study of 3(5)-amino-1,2,4-triazoles. *Tetrahedron Lett* 2009;50(18):2124-2128.
24. Jorg M, Agostino M, Yuriev E, Mak FS, Miller ND, White JM, Scammells PJ, Capuano B. Synthesis, molecular structure, NMR spectroscopic and computational analysis of a selective adenosine A(2A) antagonist, ZM 241385. *Struct Chem* 2013;24(4):1241-1251.
25. Jorg M, Shonberg J, Mak FS, Miller ND, Yuriev E, Scammells PJ, Capuano B. Novel adenosine A(2A) receptor ligands: A synthetic, functional and computational investigation of selected literature adenosine A(2A) receptor antagonists for extending into extracellular space. *Bioorg Med Chem Lett* 2013;23(11):3427-3433.
26. Caulkett PWR, Jones G, McPartlin M, Renshaw ND, Stewart SK, Wright B. Adenine isosteres with bridgehead nitrogen. Part 1. Two independent syntheses of the [1,2,4]triazolo[1,5-*a*][1,3,5] triazine ring system leading to a range of substituents in the 2, 5 and 7 positions. *J Chem Soc, Perkin Trans* 1 1995(7):801-808.
27. Tenbrink RE. Pharmacia & Upjohn Company, MI, assignee. USA. 1999.
28. Martin GE, Elgin RJ, Jr., Mathiasen JR, Davis CB, Kesslick JM, Baldy WJ, Shank RP, DiStefano DL, Fedde CL, Scott MK. Activity of aromatic substituted phenylpiperazines lacking affinity for dopamine binding sites in a preclinical test of antipsychotic efficacy. *J Med Chem* 1989;32(5):1052-1056.
29. Morita S, Kitano K, Matsubara J, Ohtani T, Kawano Y, Otsubo K, Uchida M. Practical application of the palladium-catalyzed amination in phenylpiperazine synthesis: An efficient synthesis of a metabolite of the antipsychotic agent aripiprazole. *Tetrahedron* 1998;54(19):4811-4818.
30. Motulsky HJ, Mahan LC. The kinetics of competitive radioligand binding predicted by the law of mass action. *Mol Pharmacol* 1984;25(1):1-9.
31. Vauquelin G, Van Liefde I, Vanderheyden P. Models and methods for studying insurmountable antagonism. *Trends Pharmacol Sci* 2002;23(11):514-518.
32. Kenakin T, Jenkinson S, Watson C. Determining the Potency and Molecular Mechanism of Action of Insurmountable Antagonists. *J Pharmacol Exp Ther* 2006;319(2):710-723.
33. Vauquelin G, Szczuka A. Kinetic versus allosteric mechanisms to explain insurmountable antagonism and delayed ligand dissociation. *Neurochem Int* 2007;51(5):254-260.
34. Guo D, Mulder-Krieger T, IJzerman AP, Heitman LH. Functional efficacy of adenosine A_{2A} receptor agonists is positively correlated to their receptor residence time. *Br J Pharmacol* 2012;166(6):1846-1859.
35. Sykes DA, Dowling MR, Charlton SJ. Exploring the mechanism of agonist efficacy: a relationship between efficacy and agonist dissociation rate at the muscarinic M_3 receptor. *Mol Pharmacol* 2009;76(3):543-551.
36. Mantell SJ, Stephenson PT, Monaghan SM, Maw GN, Trevethick MA, Yeadon M, Keir RF, Walker DK, Jones RM, Selby MD, Batchelor DV, Rozze S, Chavaroche H, Hobson TJ, Dodd PG, Lemaitre A, Wright KN, Stuart EF. Inhaled adenosine A(2A) receptor agonists for the treatment of chronic obstructive pulmonary disease. *Bioorg Med Chem Lett* 2008;18(4):1284-1287.
37. Andersson K, Karlsson R, Lofas S, Franklin G, Hamalainen MD. Label-free kinetic binding data as a decisive element in drug discovery. *Expert Opin Drug Dis* 2006;1(5):439-446.
38. Gabrielsson J, Dolgos H, Gillberg PG, Bredberg U, Benthem B, Duker G. Early integration of pharmacokinetic and dynamic reasoning is essential for optimal development of lead compounds: strategic considerations. *Drug Discov Today* 2009;14(7-8):358-372.
39. Liu W, Chun E, Thompson AA, Chubukov P, Xu F, Katritch V, Han GW, Roth CB, Heitman LH,

IJzerman AP, Cherezov V, Stevens RC. Structural basis for allosteric regulation of GPCRs by sodium ions. *Science* 2012;337(6091):232-236.

40. Xu F, Wu H, Katritch V, Han GW, Jacobson KA, Gao ZG, Cherezov V, Stevens RC. Structure of an agonist-bound human A_{2A} adenosine receptor. *Science* 2011;332(6027):322-327.
41. Dror RO, Pan AC, Arlow DH, Borhani DW, Maragakis P, Shan Y, Xu H, Shaw DE. Pathway and mechanism of drug binding to G-protein-coupled receptors. *Proc Natl Acad Sci U S A* 2011;108(32):13118-13123.
42. Kruse AC, Hu J, Pan AC, Arlow DH, Rosenbaum DM, Rosemond E, Green HF, Liu T, Chae PS, Dror RO, Shaw DE, Weis WI, Wess J, Kobilka BK. Structure and dynamics of the M3 muscarinic acetylcholine receptor. *Nature* 2012;482(7386):552-556.
43. Guo D, van Dorp EJ, Mulder-Krieger T, van Veldhoven JP, Brussee J, IJzerman AP, Heitman LH. Dual-point competition association assay: a fast and high-throughput kinetic screening method for assessing ligand-receptor binding kinetics. *J Biomol Screen* 2013;18(3):309-320.
44. Cheng Y, Prusoff WH. Relationship between the inhibition constant (K_I) and the concentration of inhibitor which causes 50 per cent inhibition (I_{50}) of an enzymatic reaction. *Biochem Pharmacol* 1973;22(23):3099-3108.

Chapter 5

Functional efficacy of adenosine A_{2A} receptor agonists is positively correlated to their receptor residence time

Guo D, Mulder-Krieger T, IJzerman AP, Heitman LH.
Adapted from: *Br J Pharmacol* 2012; 166(6): 1846-1859.

About this chapter

This chapter assesses the binding kinetics of $A_{2A}R$ agonists and explores a possible relationship with their functional efficacy. A kinetic radioligand binding assay (a so-called competition association assay) has been set up, validated and optimized at the $A_{2A}R$ to examine the binding kinetics of unlabeled ligands. Functional efficacies of $A_{2A}R$ agonists were determined in two different assays: a novel label-free impedance-based assay and a more traditional cAMP determination. A correlation was observed between the receptor residence time of $A_{2A}R$ agonists and their intrinsic efficacies in both functional assays. The affinity of $A_{2A}R$ agonists was not correlated to their functional efficacy. This study indicates that the molecular basis of different agonist efficacies at the $A_{2A}R$ lies within their different residence times at this receptor.

5.1 Introduction

Extracellular adenosine is a ubiquitous local hormone that has been reported to play an important physiological role in numerous tissues, for instance in the sleep/wake cycle and in inflammation. The nucleoside can bind and activate four subtypes of adenosine receptors.[1] These are the adenosine A_1, A_{2A}, A_{2B} and A_3 receptors, which belong to the superfamily of G protein-coupled receptors (GPCRs). The adenosine A_1 and A_3 receptors are mainly coupled to the enzyme adenylate cyclase in an inhibitory fashion via a G_i protein, whereas the A_{2A} and A_{2B} receptors stimulate this enzyme via a G_s protein.[2] In this study we focused on agonists for the human adenosine A_{2A} receptor ($hA_{2A}R$), which have clinical relevance in various pathological conditions such as respiratory disorders and inflammatory conditions.[3]

Traditionally, drug discovery campaigns of $A_{2A}R$ (and other GPCRs) agents usually include the identification of lead compounds in a dose-dependent assessment of activities (i.e., EC_{50} or K_i values) under equilibrium conditions. The binding kinetics of the drug-target interaction are usually not taken into account. However, awareness of the importance of binding kinetics has started to increase, since accumulating evidence suggests that the *in vivo* effectiveness of ligands may be attributed to the time ligands reside at their receptor.[4-7] The duration a drug stays in complex with the target is defined as 'drug-target residence time', which equals the reciprocal of the dissociation rate constant ($1 / k_{off}$).[8]

A recent study at the muscarinic M_3 receptor showed a tight correlation between receptor residence time and agonist efficacy.[9] This finding suggests that the molecular basis behind ligand efficacy may be inextricably linked to the ligand-receptor residence time. To verify this possible relationship, we determined the binding kinetics of ten $A_{2A}R$ agonists from different chemical classes (Figure 5.1) and extensively explored the putative relationship to their functional efficacies at the $hA_{2A}R$. The agonist binding kinetics were quantified using a competition association method,[10] which we adopted and further optimized into a fast, medium-throughput format. The $A_{2A}R$ agonist efficacies were measured, for the first time, in a novel label-free impedance-based assay and in a 'traditional' cAMP assay.

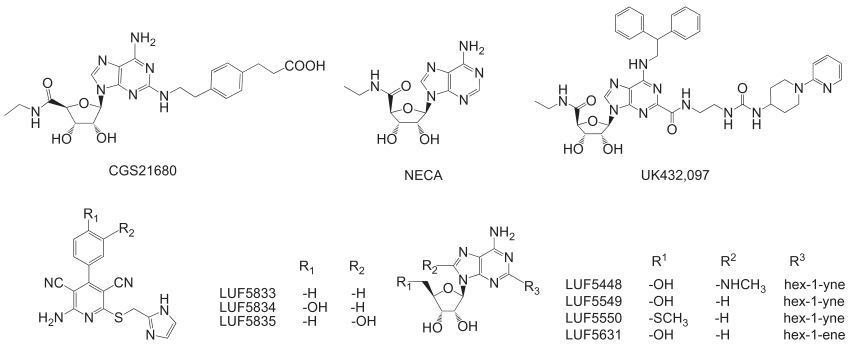


Figure 5.1 | Chemical structures of ten $A_{2A}R$ agonists used in this chapter.

5.2 Methods

Chemicals and reagents

[^{3}H]-ZM241385 (specific activity 28.4 Ci/mmol) was purchased from ARC Inc. (St. Louis, USA). Unlabeled ZM241385 was a gift from Dr. S. M. Poucher (Astra-Zeneca, Macclesfield, UK). CGS21680 was a gift from Dr. R. A. Lovell (Ciba-Geigy, Summit, NJ). NECA was purchased from Sigma-Aldrich (Steinheim, Germany), UK432,097 was purchased from Axon (Groningen, Netherlands). LUF5448 and LUF5631 were synthesized in our laboratory as described previously by van Tilburg *et al.*[11]; LUF5549 and LUF5550 were described by van Tilburg *et al.*[12]; LUF5833, LUF5834 and LUF5835 were described by Beukers *et al.*[13]. Guanosine triphosphate (GTP) was purchased from Acros Organics (Geel, Belgium). Adenosine deaminase (ADA) was purchased from Boehringer Mannheim (Mannheim, Germany). Bicinchoninic acid (BCA) and BCA protein assay reagent were obtained from Pierce Chemical Company (Rockford, IL, U.S.A.). Human embryonic kidney 293 cells stably expressing the $hA_{2A}R$ (HEK293$hA_{2A}R$) were kindly provided by Dr. J Wang (Biogen/IDEC, Cambridge, MA). All other chemicals were of analytical grade and obtained from standard commercial sources.

Cell culture

HEK293hA_{2A}R cells were grown in culture medium consisting of Dulbecco's Modified Eagle's Medium (DMEM) supplemented with 10% newborn calf serum (NCS), 50 μg/mL streptomycin, 50 IU/mL penicillin, and 500 μg/mL G418 at 37 ˚C and 7% CO_2. Cells were subcultured twice a week at a ratio of 1:8 on 10 cm ø plates.

Cell membrane preparation

HEK293hA_{2A}R cells were grown to 80%-90% confluency and detached from plates by scraping them into 5 mL PBS. Detached cells were collected and centrifuged at 700×g (3000 r.p.m.) for 5 min. Pellets derived from 30 plates (15 cm ø) were pooled and resuspended in 20 mL of ice-cold 25 mM Tris-HCl buffer, pH 7.4. An UltraThurrax was used to homogenize the cell suspension. Membranes and the cytosolic fraction were separated by centrifugation at 100,000×g (31,000 r.p.m.) in a Beckman Optima LE-80K ultracentrifuge at 4 ˚C for 20 min. The pellet was resuspended in 10 mL of Tris buffer and the homogenization and centrifugation step was repeated. Tris buffer (10 mL) was used to resuspend the pellet and ADA was added (0.8 IU/mL) to break down endogenous adenosine. Membranes were stored in 250 μL aliquots at -80 ˚C. Membrane protein concentrations were measured using the BCA (bicinchoninic acid) method.[14]

Radioligand saturation and displacement assays

Membrane aliquots containing 20 μg of protein were incubated in a total volume of 100 μl of assay buffer (25 mM Tris-HCl, pH 7.4, supplemented with 5 mM $MgCl_2$ and 0.1% (w/v) 3-[(3-cholamidopropyl) dimethylammonio]-1-propanesulfonate (CHAPS) at 5 ˚C for 2 hours to ensure the equilibrium was reached at all concentrations of radioligand. For saturation experiments,

a range of concentrations (~0.2-10 nM) of [^{3}H]-ZM241385 was used. Nonspecific binding was determined at three concentrations of radioligand in the presence of 100 μM CGS21680. Radioligand displacement experiments were performed using eleven concentrations of competing ligand in the presence of 5.5 nM [^{3}H]-ZM241385. In such experiments ZM241385 and NECA were tested in the absence or presence of 100 μM GTP. Nonspecific binding was determined in the presence of 100 μM CGS21680 and represented less than 10% of the total binding. [^{3}H]-ZM241385 did not bind specifically to membranes prepared from parental HEK293 cells. Incubations were terminated by rapid vacuum filtration to separate the bound and free radioligand through 96-well GF/B filter plates using a Perkin Elmer Filtermate-harvester (Perkin Elmer, Groningen, Netherlands) after the indicated incubation time. Filters were subsequently washed three times with ice-cold wash buffer (25 mM Tris HCl, pH 7.4, supplemented with 5 mM $MgCl_2$). The filter-bound radioactivity was determined by scintillation spectrometry using the P-E 1450 Microbeta Wallac Trilux scintillation counter (Perkin Elmer, Groningen, Netherlands).

Radioligand association and dissociation assays

Association experiments were performed by incubating membrane aliquots containing 20 μg of protein in a total volume of 100 μl of assay buffer (25 mM Tris-HCl, pH 7.4, supplemented with 5 mM $MgCl_2$ and 0.1% CHAPS) at 25 ˚C or 5 ˚C with 5.5 nM [^{3}H]-ZM241385. The amount of radioligand bound to the receptor was measured at different time intervals during incubation for 30 min at 25 ˚C or 2 hours at 5 ˚C. Dissociation experiments were performed by pre-incubating membrane aliquots containing 20 μg of protein in a total volume of 100 μl of assay buffer (25 mM Tris-HCl, pH 7.4, supplemented with 5 mM $MgCl_2$ and 0.1% CHAPS) either at 25 ˚C for 30 minutes or at 5 ˚C for 2 hours with 5.5 nM [^{3}H]-ZM241385. After the pre-incubation, the dissociation was initiated by addition of 1 μM of unlabeled ZM241385 in 5 μL. The amount of radioligand still bound to the receptor was measured at various time intervals for a total duration of 30 min at 25 ˚C or 4 hours at 5 ˚C to ensure that [^{3}H]-ZM241385 was fully dissociated from the $hA_{2A}R$. Incubations were terminated and samples were obtained as described under *Radioligand saturation and displacement assays.*

Radioligand competition association assay

The binding kinetics of unlabeled ligands were determined at 5 ˚C using the competition association assay as developed by Motulsky and Mahan.[10] In the standard assay, three different concentrations of unlabeled ZM241385 or NECA were tested, namely at 1-, 3- and 10-fold its K_i value. For NECA its kinetics were also determined in the presence of 100 μM GTP. We also assessed binding kinetics in a simplified one-concentration competition association assay, at only 10-fold of the respective K_i value of the unlabeled ligands. The experiment was initiated by adding membrane aliquots containing 20 μg of protein at different time points. Incubations were terminated and samples were obtained as described under *Radioligand saturation and displacement assays*.

Label-free whole cell analysis (xCELLigence RTCA system)

Whole cell assays were performed on the xCELLigence RTCA system.[15,16] Briefly, a monolayer of cells adheres to an arrayed microelectrode embedded at the bottom of each well of an E-plate 96 (Roche Applied Science, Germany), which is compatible with the xCELLigence RTCA system. Upon activation of GPCR-mediated signaling, cell morphology changes and thereby affects the local ionic environment at the cell-electrode interface. This leads to an increased electronic readout of cell-sensor impedance (Z), which is displayed in real-time as the Cell Index (CI). Specifically, the CI value at each time point is defined as $(Z_i\text{-}Z_0)$ Ω /15 Ω, where Z_i is the impedance at each individual time point, and Z_0 is the impedance derived from electrode/solution interface in the absence of cells prior to the start of the experiment. Thus, a loss of adhesion would generate a lower CI; an increase in cell adhesion, which is typical seen with GPCR-mediated activation, results in an overall increase in the CI.[17-19]

HEK293hA_{2A}R cells were cultured as a monolayer on 10 cm ø culture plates to 80%-90% confluency and subsequently harvested and centrifuged two times at 1000 r.p.m for 5 min. Initially, 45 μL of culture media was added to wells in E-Plates 96 to obtain background readings (Z_0) followed by the addition of 50 μL of cell suspension containing 20,000 cells / well.

The E-plate containing the cells was left at room temperature for 15 min before being placed on the recording device station in the incubator at 37 ˚C in 5% CO_2. Afterwards, cell attachment, spreading and proliferation were continuously monitored every 30 minutes. The cells were cultured until the end of log phase (~18-20 h) to obtain an optimal assay window. Prior to agonist application the interval between two measurements was adjusted to 1 min. Subsequently 5 µL compound solution (final concentration of 0.5 % DMSO) or vehicle control was added to each well, after which the CI was recorded for 30 minutes. For data analysis the individual CI traces were normalized by subtracting the baseline (vehicle control) to correct for any agonist-independent signals.

cAMP assay

HEK293hA_{2A}R cells were cultured as a monolayer on 10 cm ø culture plates to 80%-90% confluency. Cells were harvested and centrifuged two times at 1000 r.p.m for 5 min. The amount of cAMP produced was determined with the LANCE cAMP 384 kit (Perkin-Elmer, Groningen, Netherlands). In short, 2500 cells/well were pre-incubated for 45 min at 37 ˚C and subsequently at room temperature for three hours with a range of agonist concentrations. cAMP generation was performed in the medium containing cilostamide (50 µM), rolipram (50 µM), and adenosine deaminase (0.8 IU/mL). The incubation was stopped by adding detection mix and antibody solution, according to the instructions of the manufacturer. The generated fluorescence intensity was quantified on the EnVision® Multilabel Reader (PerkinElmer, Groningen, Netherlands). cAMP production by agonists tested at 100-fold their K_i value on the parental HEK293 cell line represented less than 5% of maximal stimulation of cAMP production by 10 µM CGS21680 at the cells expressing the adenosine A_{2A} receptor.

Data analysis

All experimental data was analyzed by using GraphPad Prism 5.0 (GraphPad Software Inc., San Diego, CA). K_D and B_{max} values of [^{3}H]-ZM241385 at

$hA_{2A}R$ membranes were obtained by computational analysis of saturation curves. IC_{50} values obtained from competition displacement binding data were converted into K_i values using the Cheng-Prusoff equation.[20]

Association data was fitted using *one phase exponential association*. Values for k_{on} were obtained by converting k_{obs} values using Equation 3 describe in Chapter 3. k_{off} values were assessed from independent dissociation experiments. Dissociation data was fitted using *one phase exponential decay*. The association and dissociation rates were used to calculate the 'kinetic K_D' using Equation 8 described in Chapter 3.

Association and dissociation rates for unlabeled ligands were calculated by fitting the data in the competition association model using '*kinetics of competitive binding*' describe in Chapter 3 (Equation 7).[10]

EC_{50} and E_{max} values in label-free whole cell assay were obtained by analyzing the normalized CI traces using RTCA Software 1.2 (Roche, Germany) to obtain peak responses within 30 min after compound addition. These peak values were exported to Prism 5.0, which yielded dose-response curves and were analyzed by nonlinear regression.

The relative efficacies (τ) of agonists in label-free whole cell experiment and cAMP assay were also evaluated. Data were fitted to the operational model of Black and Leff,[21] which correlates a biological effect E with agonist concentration [A] as a function of three parameters: E_m, K_A, and τ:

$$E = \frac{E_m \cdot \tau \cdot [A]}{K_A + (\tau + 1)[A]}$$

where E_m, the operational maximum, represents the maximum possible effect in the tissue. K_A is the dissociation constant of agonist and τ is the relative efficacy. The E_m value was generated by fitting the dose-response curve for the full agonist (i.e., UK432,097). Its best-fit values were recorded to fit dose-response curves of partial agonists and other full agonists by global fitting in the operational model in Prism 5.0 to generate their relative efficacies. All values obtained are means of at least three independent experiments performed in duplicate.

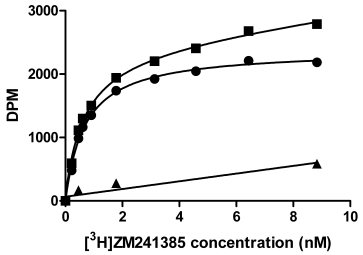


Figure 5.2 | Saturation experiment of [^{3}H]-ZM241385 (~0.2-10 nM, final concentration) binding to HEK293hA_{2A}R membranes at 5 °C, total binding (squares); non-specific binding (triangles); specific binding (spheres). Representative graph from one experiment performed in duplicate.

5.3 Results

Quantification of the K_D and B_{max} of [^{3}H]-ZM241385 in saturation experiments

Saturation binding experiments were performed with [^{3}H]-ZM241385 at 5 °C. The result of a representative saturation experiment is shown in Figure 5.2. [^{3}H]-ZM241385 bound to a single class of binding sites at HEK293hA_{2A}R membranes. The K_D value was determined as 0.60 ± 0.07 nM and B_{max} was 1.9 ± 0.04 pmol/mg protein. The K_D value for [^{3}H]-ZM241385 obtained with these experiments was used to derive K_i values from IC_{50} values for ten A_{2A}R agonists, as well as the unlabeled antagonist ZM241385 (see below).

Quantification of the affinity (K_i) of A_{2A}R ligands in displacement experiments

Displacement experiments with several A_{2A}R ligands were performed to determine their affinities to the hA_{2A}R. All compounds produced a concentration-dependent inhibition of specific [^{3}H]-ZM241385 binding

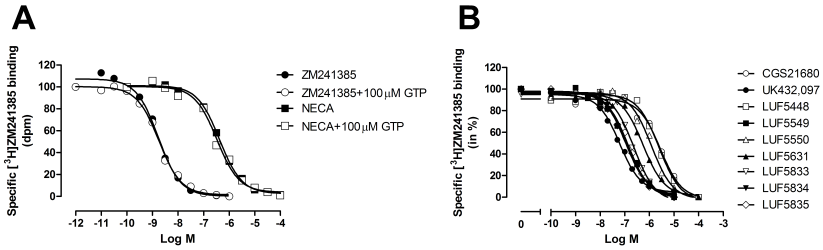


Figure 5.3 | Panel A: displacement of specific [^{3}H]-ZM241385 binding from the $hA_{2A}R$ by ZM241385 and NECA in the absence (closed symbols) or presence of 100 μM GTP (open symbols). Panel B: displacement of specific [^{3}H]-ZM241385 binding from the $hA_{2A}R$ by the other nine agonists. Representative graphs from one experiment performed in duplicate.

(Figure 5.3) and their affinities are detailed in Table 5.1 and Table 5.3. Amongst all tested ligands, ZM241385 showed the highest affinity for the $hA_{2A}R$ with a K_i value of 0.4 ± 0.03 nM (Table 5.1) in the absence of 100 μM GTP; its K_i value determined in the presence of 100 μM GTP was the same (0.4 ± 0.02 nM, Figure 5.3A). Similarly, there was no significant difference between the kinetic or K_i values of NECA tested in the absence or presence of 100 μM GTP (Tables 5.2 and 5.3, Figure 5.3A). Affinities of other $A_{2A}R$ agonists were determined and showed a range of K_i values in the lower to higher nanomolar range (Table 5.3). The agonist with the lowest affinity was CGS21680 (K_i = 376 ± 12 nM), while the agonist with the highest affinity was LUF5835 (K_i =15 ± 4 nM). In general, the affinities of the ribose-containing agonists (e.g., LUF5448) were lower than those of the non-ribose agonists (e.g., LUF5833), as shown in Table 5.3.

Quantification of the association [k_{on} (k_1)] and dissociation rates [k_{off} (k_2)] of [^{3}H]-ZM241385 at different temperatures

To optimize the experimental conditions of the kinetic binding assays, [^{3}H]-ZM241385 association and dissociation experiments were carried out at both 25 ˚C and 5 ˚C. At both temperatures, the association and dissociation curve of [^{3}H]-ZM241385 at the $hA_{2A}R$ were monophasic. At 25 ˚C (Figure

Table 5.1 | Comparison of the affinity, dissociation constants and kinetic rates of reference antagonist ZM241385 obtained in different radioligand binding assays.

Assay	K_D / K_i *(nM)*	k_{on} *(M^{-1}·min^{-1})*	k_{off} *(min^{-1})*
Saturation binding [a]	0.60 ± 0.07	*N.A*	*N.A*
Displacement [b]	0.40 ± 0.03	*N.A*	*N.A*
Association and dissociation [c]	0.70 ± 0.01	1.5 ± 0.06 × 10^7	0.011 ± 0.001
Standard competition association [d]	0.95 ± 0.2[f]	2.0 ± 0.2 × 10^7	0.019 ± 0.003
Simplified competition association [e]	0.89 ± 0.3[f]	2.8 ± 0.5 × 10^7	0.025 ± 0.006

Values are means ± s.e.m of three separate experiments each performed in duplicate. *N.A.*, not applicable. [a] [^{3}H]-ZM241385 (~0.2-10 nM) binding to HEK293hA_{2A} membranes at 5 ˚C. [b] Displacement of specific [^{3}H]-ZM241385 binding from the hA_{2A}R at 5 ˚C. [c] Association and dissociation of [^{3}H]-ZM241385 at the hA_{2A}R at 5 ˚C. [d] The binding kinetics of unlabeled ZM241385 were determined by adding a concentration equivalent to 1-, 3- and 10-fold the K_i value of unlabeled ZM241385 at 5 ˚C. [e] The binding kinetics of unlabeled ZM241385 were determined by adding a concentration equivalent to only 10-fold the K_i value of unlabeled ZM241385 at 5 ˚C. [f] 'kinetic K_D' = k_{off} / k_{on}.

5.4A), [^{3}H]-ZM241385 had a very fast association (k_{on} = 2.4 ± 0.05 × 10^8 M^{-1}·min^{-1}) and dissociation rate (k_{off} = 0.48 ± 0.03 min^{-1}). Decreasing the experimental temperature to 5 ˚C resulted in slower binding kinetics of [^{3}H]-ZM241385 with an association rate of 1.5 ± 0.06 × 10^7 M^{-1}·min^{-1} and a dissociation rate of 0.011 ± 0.001 min^{-1} (Figure 5.4B, Table 5.1). We also conducted experiments at 15 ˚C; the kinetic rates determined were also fast (data not shown). Based on these initial tests, we chose 5 ˚C as the standard experimental condition for this study, since it enabled better accuracy and reproducibility of kinetic data.

Validation and optimization of the competition association assay at the hA_{2A}R

With the pre-determined k_{on} (k_1) and k_{off} (k_2) values of [^{3}H]-ZM241385 from association and dissociation experiments, k_{on} (k_3) and k_{off} (k_4) values of unlabeled ligands could be determined by fitting the kinetic parameters into the model of '*kinetics of competitive binding*' described in *methods*. Firstly,

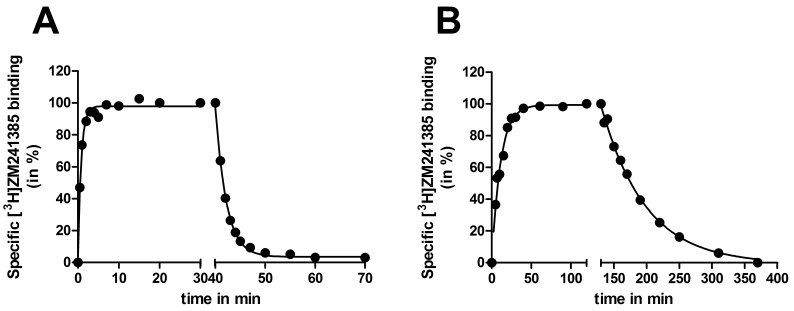


Figure 5.4 | Panel A: the association and dissociation of [^{3}H]-ZM241385 at the $hA_{2A}R$ at 25 ˚C; Panel B: the association and dissociation of [^{3}H]-ZM241385 at the $hA_{2A}R$ at 5 ˚C. Representative graphs from one experiment performed in duplicate.

we validated the competition association assay at the $hA_{2A}R$ using unlabeled ZM241385. Its k_{on} (k_3) and k_{off} (k_4) values determined in this assay were $2.0 \pm 0.2 \times 10^7$ $M^{-1}\cdot min^{-1}$ and 0.019 ± 0.003 min^{-1} respectively (Figure 5.5, Table 5.1), which corresponded rather well to the kinetic rates determined in 'traditional' association and dissociation experiments described in the previous paragraph ($k_{on} = 1.5 \pm 0.06 \times 10^7$ $M^{-1}\cdot min^{-1}$, $k_{off} = 0.011 \pm 0.001$ min^{-1}). Moreover, the 'kinetic K_D' (0.95 ± 0.2 nM) derived from the competition association assay for unlabeled ZM241385 was similar to the affinity constant ($K_i = 0.40 \pm 0.03$ nM) obtained from displacement experiments and the dissociation constant (K_D) derived from saturation experiments (0.60 ± 0.07 nM, Table 5.1). Taken together, this proved that the competition association assay can be applied to determine the binding kinetics of unlabeled ligands at the $hA_{2A}R$.

Secondly, we modified the assay and improved its throughput by reducing the three-concentration dependent method to a one-concentration based method. Instead of testing at concentrations equivalent to 1-, 3- and 10-fold the K_i value of unlabeled ZM241385, we only used 10-fold K_i. The latter yielded an assay window distinguishable from both the baseline and the control curve (Figure 5.5). Specifically, the data analyzed at 10-fold K_i alone of unlabeled ZM241385 showed a comparable result ($k_{on} = 2.8 \pm 0.5 \times 10^7$ $M^{-1}\cdot min^{-1}$, $k_{off} = 0.025 \pm 0.006$ min^{-1}) to that generated in a standard (three concentration) competition association experiment (Table 5.1).

Next to that, we also determined the effect of GTP (100 μM) on the

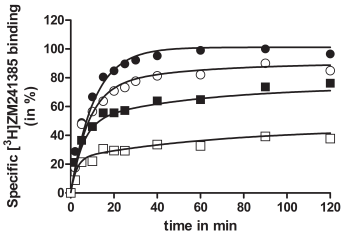


Figure 5.5 | Competition association experiment with [^{3}H]-ZM241385 in the absence of ligand (solid spheres) or in the presence of one-fold K_i value (empty spheres), three-fold K_i value (solid squares) or ten-fold K_i value (empty squares) of unlabeled ZM241385. Representative graphs from one experiment performed in duplicate (see Table 5.1 for kinetic values).

binding kinetics of an unlabeled agonist, NECA. Its k_{on} and k_{off} values determined in the standard three-concentration competition association assay in the absence of GTP were 8.1 ± 1.0 × 10^5 M^{-1}·min^{-1} and 0.038 ± 0.007 min^{-1} (Table 5.2, Figure 5.6A), which were similar to these values determined in the presence GTP (k_{on} = 9.8 ± 1.0 × 10^5 M^{-1}·min^{-1}, k_{off} = 0.036 ± 0.006 min^{-1}, Table 5.2, Figure 5.6B). Furthermore, k_{on} and k_{off} values of unlabeled NECA assessed by using a concentration of 10-fold its K_i only, either in the absence or presence of 100 μM GTP, showed comparable results to that determined by the standard assay mentioned above (Table 5.2). It is also noteworthy that the calculated kinetic K_D values from the one-concentration approach in the absence (K_D = 58 nM) or presence (K_D = 52 nM) of GTP are almost identical to the affinity determined in the displacement experiments (K_i = 64 ± 1 nM). Thus, the simplified one-concentration competition association assay in the absence of 100 μM GTP was used to determine the binding kinetics of other unlabeled agonists in the rest of this study.

Quantification of the binding kinetics of unlabeled ligands using the simplified competition association assay

By using the simplified competition association assay, the on- and off-rates of ten $A_{2A}R$ agonists were determined. Notably, a good correlation (Figure 5.7B, r^2 = 0.99, p < 0.0001) was observed between the affinities (K_i) determined

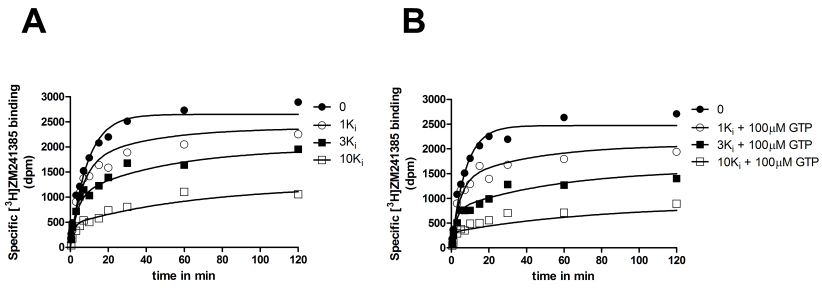


Figure 5.6 | [^{3}H]-ZM241385 competition association experiments in the absence (Panel A) or presence (Panel B) of 100 μM GTP with NECA concentrations of one, three or ten-fold its K_i value. Data were fitted to the equations described in *Methods* to calculate NECA's k_{on} and k_{off} values in the absence or presence of GTP. Representative graphs from one experiment performed in duplicate (see Table 5.2 for kinetic values).

Table 5.2 | The binding kinetics of reference agonist NECA in the absence or presence of 100 μM GTP.

Assay	***Control***		***+ 100 μM GTP***	
	k_{on} ($M^{-1}{\cdot}min^{-1}$)	k_{off} (min^{-1})	k_{on} ($M^{-1}{\cdot}min^{-1}$)	k_{off} (min^{-1})
Standard competition association [a]	8.1 ± 1.0 × 10^5	0.038 ± 0.007	9.8 ± 1.0 × 10^5	0.036 ± 0.006
Simplified competition association [b]	5.0 ± 0.6×10^5	0.029 ± 0.005	9.1 ± 2.0 × 10^5	0.047 ± 0.01

Values are means ± s.e.m of three separate experiments each performed in duplicate. [a] The binding kinetics of unlabeled NECA in the absence or presence of 100 μM GTP were determined by adding a concentration equivalent to 1-, 3- and 10-fold the K_i value of unlabeled NECA in the absence or presence of 100 μM GTP at 5 ˚C. [b] The binding kinetics of unlabeled NECA in the absence or presence of 100 μM GTP were determined by adding a concentration equivalent to only 10-fold the K_i value of unlabeled NECA in the absence or presence of 100 μM GTP at 5 ˚C.

in equilibrium binding studies and K_D values derived from the competition association assays (Table 5.3). This further proved that the simplified model is able to accurately quantify the association and dissociation rates of unlabeled ligands. Two distinct patterns of [^{3}H]-ZM241385 binding were found in the presence of the agonists, which are depicted in Figure 5.7A: 1) the specific binding of [^{3}H]-ZM241385 approached its equilibrium slowly and more gradually if [^{3}H]-ZM241385 dissociated slower than the competitor

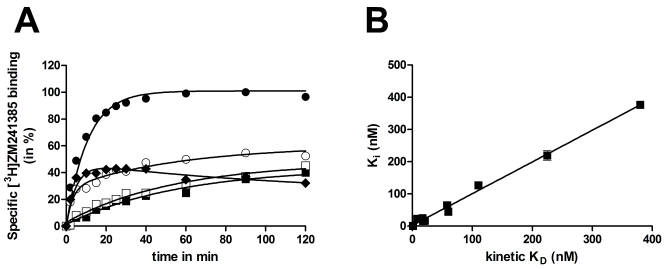


Figure 5.7 | Quantification of the binding kinetics of unlabeled ligands using the simplified competition association assay. Panel A, [^{3}H]-ZM241385 competition association binding in the absence of ligand (solid spheres) or in the presence of unlabeled CGS21680 (empty spheres), LUF5834 (solid squares), LUF5550 (empty squares) or UK432,097 (solid diamonds). Data were fitted to the equations described in *Methods* to calculate the k_{on} and k_{off} values of unlabeled ligands. Representative graphs from one experiment performed in duplicate (see Table 5.3 for kinetic values); Panel B, correlation between affinities (K_i) and 'kinetic K_D' values of all the tested compounds. K_i values were taken from the displacement experiments at equilibrium and K_D values were derived from the competition association experiments.

Table 5.3 | Binding parameters for agonists at HEK293hA_{2A}R derived from the simplified competition association assay and equilibrium radioligand displacement experiments.

Cmpd	*k_{on} (M^{-1}·min^{-1}) [a]*	*k_{off} (min^{-1}) [a]*	*RT (min) [b]*	*Kinetic K_D (nM) [c]*	*K_i (nM) [d]*
CGS21680	5.0 ± 1.0 × 10^4	0.019 ± 0.004	53 ± 6	380 ± 66	376 ± 12
NECA	5.0 ± 0.6 × 10^5	0.029 ± 0.005	35 ± 4	58 ± 7	64 ± 1
UK432,097	5.0 ± 0.8 × 10^5	0.004 ± 0.003	250 ± 115	8.0 ± 3.7	22 ± 5
LUF5448	2.8 ± 0.1 × 10^5	0.063 ± 0.020	16 ± 3	225 ± 39	219 ± 15
LUF5549	2.4 ± 0.5 × 10^6	0.041 ± 0.010	24 ± 3	17 ± 2	24 ± 7
LUF5550	8.0 ± 2.0 × 10^5	0.087 ± 0.020	12 ± 1	110 ± 19	126 ± 10
LUF5631	8.0 ± 2.0 × 10^5	0.048 ± 0.020	21 ± 5	60 ± 17	44 ± 9
LUF5833	8.5 ± 3.0 × 10^6	0.16 ± 0.08	6.3 ± 1.8	19 ± 7	17 ± 4
LUF5834	1.1 ± 0.4 × 10^7	0.23 ± 0.10	4.2 ± 1.0	21 ± 7	16 ± 5
LUF5835	1.6 ± 0.8 × 10^7	0.29 ± 0.10	3.4 ± 0.6	18 ± 6	15 ± 4

Data are shown as mean ± s.e.m of three separate experiments each performed in duplicate. [a] k_{on} and k_{off} of unlabeled A_{2A}R agonists were determined in one-concentration competition association assay. [b] RT (Residence Time) = 1 / k_{off}. [c] Kinetic K_D = k_{off} / k_{on}. [d] Displacement of specific [^{3}H]-ZM241385 binding from the hA_{2A}R at 5 °C.

($k_2 < k_4$, e.g., LUF5834); 2) the specific binding [^{3}H]-ZM241385 became biphasic with a typical 'overshoot' followed by a continuous decline towards equilibrium if [^{3}H]-ZM241385 dissociated faster than the competitor ($k_2 > k_4$, e.g., UK432,097). In accordance with these observations, UK432,097 had a much slower off-rate (k_{off} = 0.004 ± 0.003 min^{-1}) than [^{3}H]-ZM241385 (k_{off} = 0.011 ± 0.001 min^{-1}). LUF5834 (k_{off} = 0.23 ± 0.10 min^{-1}) or LUF5550 (k_{off} = 0.087 ± 0.020 min^{-1}) dissociated much faster from the receptor than [^{3}H]-ZM241385. Furthermore, it follows from Table 5.3 that the values for binding kinetics of ribose-containing agonists were significantly different from those of non-ribose agonists. For instance, LUF5631 was 10-fold slower in association and 3.3-fold slower in dissociation compared to LUF5833.

Quantification of functional efficacies of $A_{2A}R$ agonists in a label-free whole cell assay

Changes in cell morphology by the addition of CGS21680 and other $A_{2A}R$ agonists to HEK293h$A_{2A}R$ cells were assessed in real-time with the impedance-based assay system. Typically, upon agonist addition to HEK293h$A_{2A}R$ cells the impedance (displayed as cell index, CI) resulted in an immediate dose-dependent increase to a peak level. After that, the CI trace decreased and gradually reached a plateau without returning to the baseline when monitored over a period of 30 min. A representative measurement of CGS21680-induced impedance changes is plotted in Figure 5.8A. Concentration-effect curves were obtained from peak analysis of corresponding agonist-induced CI changes (Figure 5.8B). Agonist potencies, intrinsic efficacies and their relative efficacies (τ) analyzed in the operational model are detailed in Table 5.4. Specifically, amongst all tested agonists, UK432,097 had the highest efficacy, with a value of 114 ± 4% compared to the reference agonist CGS21680 (set at 100%). Efficacies of other ribose-containing agonists LUF5448, LUF5549, LUF5550 and LUF5631 were 83 ± 5%, 92 ± 4%, 63 ± 6% and 91 ± 8%, while the efficacies of the non-ribose agonists LUF5833, LUF5835 and LUF5834 were 54 ± 9%, 47 ± 6% and 54 ± 8%, respectively. In Figure 5.9A and 5.9B, correlations are shown between the agonist efficacy and either their affinities or receptor residence times, respectively. It follows from Figure 5.9A that there was very little correlation between the affinity of the agonists and their efficacy, if at all (r^2 = 0.13, p = 0.32). Interestingly, when the efficacy

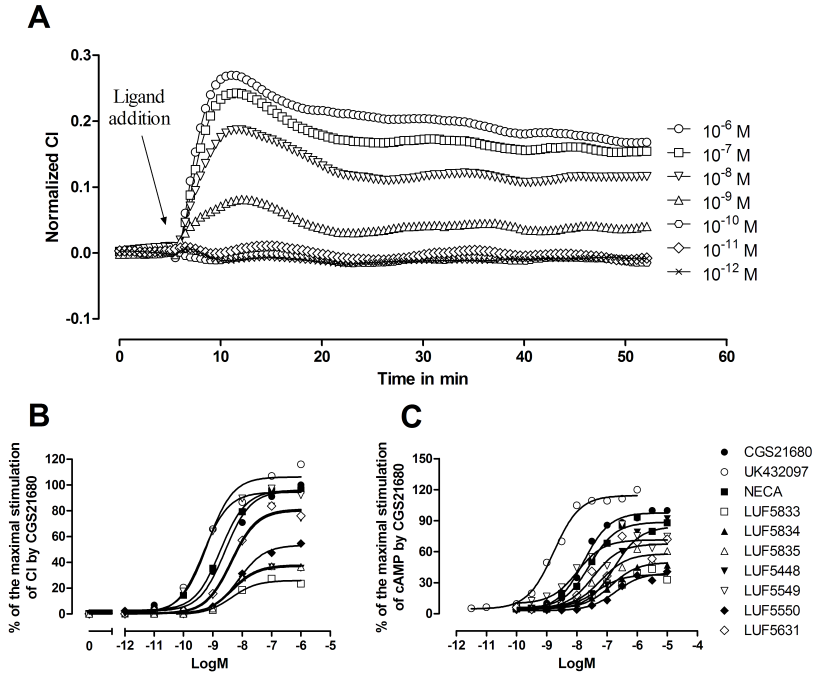


Figure 5.8 | Quantification of functional efficacies of $A_{2A}R$ agonists in a label-free whole cell assay. Panel A, representative graph of normalized cell-electrode impedance (expressed as CI) after the addition of different concentrations of CGS21680 in a label-free impedance-based assay: agonist stimulation of HEK293 $hA_{2A}R$ cells results in an increased CI. The change in CI was normalized over time against the vehicle control. Panel B, concentration-response curves for difference $A_{2A}R$ agonists at HEK293$hA_{2A}R$ derived from peak-analysis of CI changes in the xCELLigence RTCA system. The cellular response was normalized and shown as % of the maximal CI by 1 μM CGS21680; Panel C, concentration-response curves of cAMP stimulation by ten $A_{2A}R$ agonists in a cAMP assay. Data were normalized and shown as % of the maximal cAMP production by 10 μM CGS21680 in HEK293 $hA_{2A}R$ cells (= 100%). Representative graphs from one experiment performed in duplicate.

Table 5.4 | Agonist potency and efficacy derived from both cAMP and label-free whole cell assays.

Agonist	*Label-free whole cell assay* [a]			*cAMP assay*		
	EC_{50}, nM	E_{max}, %	τ [b]	EC_{50}, nM	E_{max}, %	τ [b]
CGS21680	3.8 ± 0.4	100 ± 1	13 ± 5	19 ± 0.6	100 ± 2	4 ± 0.4
NECA	2.5 ± 0.1	90 ± 4	4 ± 0.8	27 ± 0.9	88 ± 3	3 ± 0.3
UK432,097	0.47 ± 0.01	114 ± 4	51 ± 5	1.7 ± 0.1	115 ± 2	14 ± 5
LUF5448	2.4 ± 1	83 ± 5	2 ± 0.4	172 ± 15	84 ± 3	2 ± 0.4
LUF5549	1.0 ± 0.4	92 ± 4	6 ± 0.8	10 ± 3	71 ± 6	1 ± 0.2
LUF5550	5.8 ± 1	63 ± 6	0.7 ± 0.07	195 ± 12	39 ± 1	0.5 ± 0.04
LUF5631	4.3 ± 1	91 ± 8	2 ± 0.3	36 ± 23	67 ± 5	1 ± 0.2
LUF5833	3.9 ± 0.6	54 ± 9	1 ± 0.3	44 ± 2	38 ± 2	0.5 ± 0.04
LUF5834	3.6 ± 0.7	47 ± 6	0.8 ± 0.2	21 ± 1	50 ± 1	0.7 ± 0.06
LUF5835	5.7 ± 2	54 ± 8	0.8 ± 0.08	17 ± 1	58 ± 2	0.9 ± 0.09

Data are shown as mean ± s.e.m of three separate experiments each performed in duplicate. [a] agonist potency (EC_{50}) and efficacy (E_{max}) were calculated from concentration-response curves derived from peak-analysis of CI changes. [b] The relative efficacy (τ) was analyzed by the operational model of Black and Leff using global fitting.[21]

of each agonist was compared to the logarithm of its residence time (Figure 5.9B), a much better correlation was obtained (r^2 = 0.90, p <0.0001), where the highest efficacy ligand UK432,097 had the longest residence time of 250 ± 115 min. In addition, no correlation was observed between functional potency and the logarithm of its residence time (r^2 = 0.077, p = 0.44). The ranking of the relative efficacy, τ, is quite comparable to the intrinsic efficacy, where UK432,097 had the highest τ value of 51 ± 5; LUF5550 had the lowest value of 0.7 ± 0.07 (Table 5.4). Similarly, a positive link between receptor residence time and relative efficacy was observed (r^2 = 0.60, p < 0.01).

Quantification of functional efficacies of $A_{2A}R$ agonists in a cAMP assay

The functional efficacy of all $A_{2A}R$ agonists was tested in a classic cAMP assay as well. The cAMP production was stimulated by adding increasing concentrations of different agonists. The effects were normalized and are

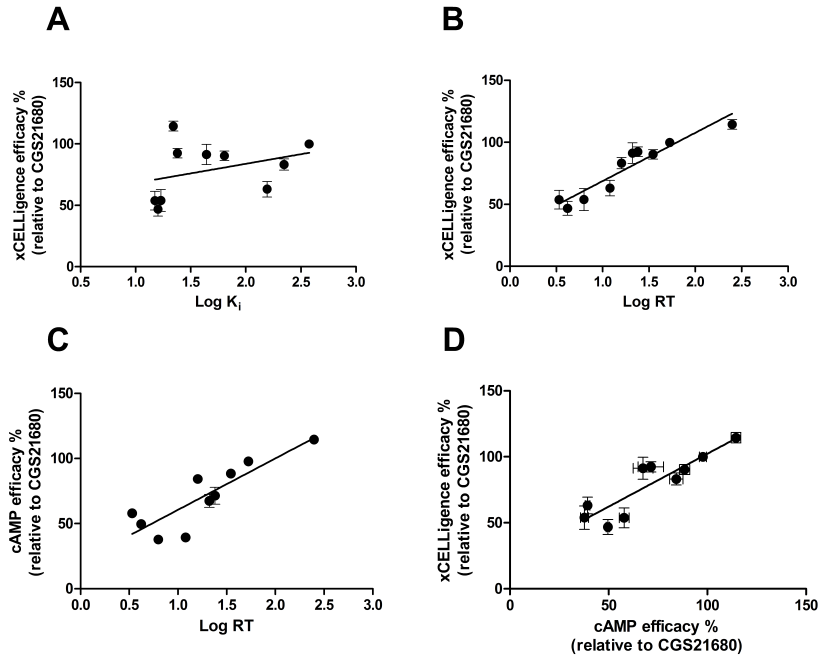


Figure 5.9 | Panel A, correlation of the functional efficacy (E_{max}) derived from label-free whole cell assay against Log K_i (r^2 = 0.13, p = 0.32); Panel B, correlation of the functional efficacy derived from label-free whole cell assay against Log RT (RT, residence time, r^2 = 0.90, $p < 0.0001$). Panel C, correlation of the functional efficacy derived from cAMP assay against Log RT (r^2 = 0.74, $p < 0.001$); Panel D, correlation of the functional efficacy derived from label-free whole cell assay against the functional efficacy derived from cAMP assay (r^2 = 0.79, $p < 0.001$). Data used in these plots are detailed in Table 5.3 and Table 5.4. Data are expressed as mean ± s.e.m. from at least three independent experiments.

shown as a percentage of maximal stimulation of cAMP production by 10 μM CGS21680 (= 100%). Amongst all tested agonists (Figure 5.8C, Table 5.4), UK432,097 had the highest efficacy of 115 ± 2% in this assay. Efficacies of ribose-containing agonists LUF5448, LUF5549, LUF5550 and LUF5631 were 84 ± 3%, 71 ± 6%, 39 ± 1% and 67 ± 5%, while the efficacies of the non-ribose agonists LUF5833, LUF5834 and LUF5835 were 38 ± 2%, 50 ± 1% and 58 ± 2%, respectively. Notably, the ranking of the agonists by their efficacy measured in the cAMP assay is quite comparable to the efficacy-ranking obtained with the impedance-based assay (Figure 5.9D, r^2 = 0.79, p < 0.001). Similarly, a positive link between the functional efficacy and the logarithm of a compound's residence time was observed in this assay as well (Figure 5.9C, r^2 = 0.74, p < 0.001), while no correlation was observed between functional efficacy and the logarithm of its K_i value (r^2 = 0.10, p = 0.40). The ranking of the relative efficacy, τ, in this assay is also quite comparable to that obtained from the whole cell impedance-based assay, where UK432,097 had the highest (τ = 14 ± 5) and LUF5550 had the lowest relative efficacy (τ = 0.5 ± 0.04; Table 5.4). These relative efficacies were again closely correlated to the receptor residence times of the agonists in the present chapter (r^2 = 0.80, p < 0.001).

5.4 Discussion

In this study, the binding kinetics of unlabeled $A_{2A}R$ ligands were determined for the first time using the competition association assay method at the $hA_{2A}R$. This approach has been shown to be highly accurate in determining the binding kinetics at the β-adrenergic receptor[22,23] and more recently at the muscarinic M_3 receptor.[9,24] However, the standard model is laborious and time consuming when the kinetics of multiple compounds need to be determined, since it implies the use of three concentrations of each unlabeled ligand. In this study, the tested agonists were considered competitive with the radioligand as they fully displaced [^{3}H]-ZM241385 from the receptor (Figure 5.3B). Therefore, we modified the three-concentration dependent assay into a one-concentration based method. From Table 5.1, it follows that this simplified method is sufficient in quantifying the binding kinetics, which eventually enables testing in a faster medium-throughput format, yet without loss of accuracy. Since we used an antagonistic radioligand, [^{3}H]-

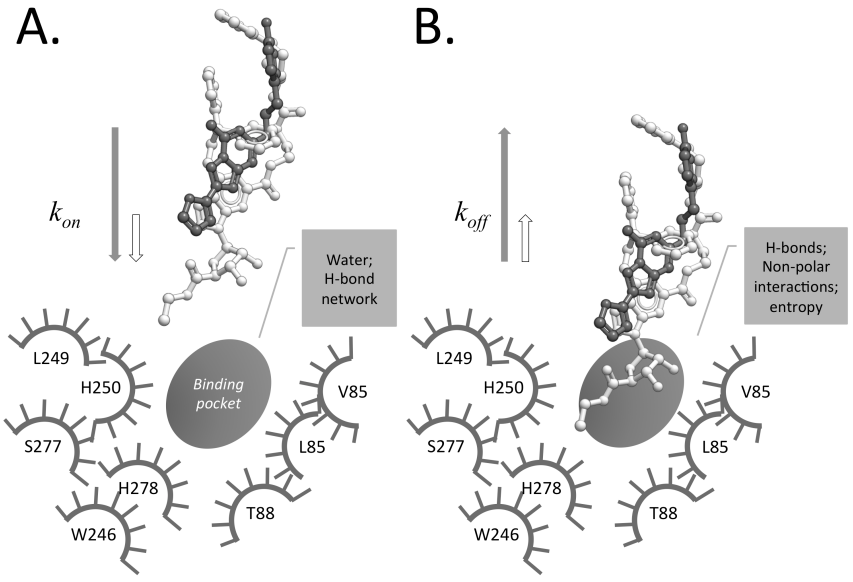


Figure 5.10 | Proposed schematic representation of (Panel A) obstacles at the bottom of the binding pocket and (Panel B) the stabilization effects of the ribose moiety after agonist binding to the receptor. Molecule in black is ZM241385; molecule in white is UK432,097. The length of arrows in black (ZM241385) and white (UK432,097) indicates the speed of ligand association and dissociation. The relative position of these two molecules is coordinated according to the surrounding amino acids based on the crystal structures reported by Jaakola *et al.* (PDB code: 3EML) and Xu *et al.* (PDB code: 3QAK).[29,31] In comparison to ZM241385 (non-ribose compound), UK432,097 (ribose containing compound), binds deeper in the main binding pocket, hence before receptor activation obstacles such as water molecules or structural H-bond networks slow down the association of UK432,097 (Panel A). After ligand binding to the receptor, the ribose part of UK432,097 is stabilized by H-bonds and non-polar interactions and stays in an entropy favorable state after the displacement of explicit water molecules (as present in the ZM241385 crystal structure). This would represent a molecular mechanism accounting for the slower dissociation of ribose containing agonists vs. antagonists (Panel B).

ZM241385, we checked the GTP effect on the equilibrium affinity and the binding kinetics of one representative $A_{2A}R$ agonist, namely NECA. In our system $hA_{2A}R$ was insensitive to GTP (Table 5.2) and only one single binding site was observed (Figure 5.3A). Hence we did not continue to apply GTP in our assays. Subsequent quantification of the binding kinetics of ten $A_{2A}R$ agonists in the simplified model generated comparable 'kinetic K_D' to their K_i values (Table 5.3). This excellent correlation (Figure 5.7B, $r^2 = 0.99$, $p < 0.0001$) proved the accuracy and efficiency of the one-concentration based competition association assay for the determination of a ligand's association and dissociation rates at the $hA_{2A}R$.

To guarantee an accurate kinetic determination, experiments were carried out at 5˚C. Firstly, increasing the experimental temperature resulted in very fast kinetics of the radioligand, which is less practical to quantify the ligand-receptor binding kinetics. Secondly, it is reasonable to speculate that differences in receptor residence times will be more pronounced at 5˚C than at higher temperatures, which would allow an easier identification of compounds with longer residence times in future screening campaigns. It might be argued that such a low temperature cannot be representative for residence times observed *in vivo*. However, it was reported in a guinea pig bronchoconstriction model that UK432,097 (the agonist with the longest residence time in our studies) had a duration of action that lasted over eight hours, whereas the effect of the reference agonist CGS21680 quickly returned to baseline within 60 min.[25,26] Admittedly, the long-lasting effect is likely to be influenced by a number of other factors such as dissolution rate, system pharmacokinetics or tissue residence/rebinding.[27,28] Even so, it is noteworthy that a kinetic difference determined by this protocol (i.e., at 5 ˚C) is still inextricably linked to the *in vivo* efficacy of a drug candidate.

In the present chapter, we observed a broad range of ligand-receptor residence times from 3.4 ± 0.6 min for LUF5835 to 250 ± 115 min for UK432,097. From Table 5.3, it follows that a non-ribose agonist (LUF5833, LUF5834 and LUF5835) associates to the receptor 10-100 fold faster, but remained at the receptor much shorter than a ribose-containing agonist (for structures see Figure 5.1). This observation supports the integral role of a ribose moiety in the binding kinetics upon agonist receptor activation. To activate the $A_{2A}R$, common requirements include the destabilization of H-bond networks at $W246^{6.48}$ and $H278^{7.43}$ (superscripts refer to Ballesteros-Weinstein numbering[46]) and, for example, the displacement of several structural water molecules.[29,30] One can imagine that such 'obstacles' in

the binding cavity will prevent the coordination of the ribose group and, as a result, slow down the agonist association process (Figure 5.10A). The lower on-rates of ribose-containing agonists that were observed compared to those of non-ribose agonists fit this hypothesis. It has been shown that upon receptor activation (Figure 5.10B), the ribose moiety inserts deeply into the binding cavity, as illustrated in the agonist-bound $A_{2A}R$ crystal structures,[31,32] and is stabilized by key residues like S277$^{7.42}$ and H278$^{7.43}$. These residues, together with V84$^{3.32}$, L249$^{6.51}$, are in close contact with the agonist ribose ring, and form essential H-bonds or non-polar interactions with the ribose moiety for agonist binding. Moreover, displacement of the structural water molecules from the hydrophobic pocket favors entropic energy,[33] which further stabilizes the molecule in its interactions and allows it to stay longer. For the co-crystallized UK432,097 in particular it was shown that it has an extensive ligand-receptor interaction network, which includes eleven hydrogen bonds, one aromatic stacking and a number of van der Waals interactions, in the $A_{2A}R$/UK432,097 complex.[31] This further corroborates our finding that UK432,097 has the longest residence-time in the $hA_{2A}R$.

In the present chapter the $A_{2A}R$-mediated activation was determined in two different functional assays, namely, in a novel label-free impedance-based assay (xCELLigence RTCA system), which was compared to a classic cAMP assay. Recently, label-free impedance-based technologies have been shown to have promising applications in assaying functional activity of GPCRs.[34,35] In particular, this assay does not require any labeling or recombinant expression of receptor or reporter proteins, since it is based on detection of cell morphological changes induced by an agonist. Using this impedance-based technology, we were able to discriminate full from partial agonists at the $hA_{2A}R$ (Figure 5.8B and Table 5.4). Their efficacies were similar to those obtained in a traditional cAMP assay (Figure 5.8C and Table 5.4), which indicates that the novel label-free technology is a useful tool to study $A_{2A}R$-mediated activation. Notably, we observed a similar correlation between the residence time of an agonist and its functional efficacy in both assays: rather than the equilibrium affinity, the receptor residence time of an $A_{2A}R$ agonist has a much better correlation to its intrinsic efficacy (Figure 5.9). This correlation was found in other studies as well. For instance, in the case of the α_2-adrenoceptor, the full agonist UK14,304 had a 12-fold longer residence time than the partial agonist clonidine.[36] In another study, Sykes *et al*. tested seven agonists with a broad range of efficacies at the muscarinic M_3 receptor.[9] Similarly, they found that a slowly dissociating M_3 agonist appeared to cause

a higher efficacy in functional assays. Taken together with these observations, our results suggest that receptor residence time and functional efficacies are positively correlated, which may lead us to further understand the molecular basis of agonist functional efficacy at the $hA_{2A}R$.

In the label-free impedance based assay, we observed that the potencies (EC_{50}) of the $A_{2A}R$ agonists were generally higher than the respective binding affinities (compare Table 5.4 to Table 5.3). A similar observation was reported in a study by Dionisotti *et al*. for the functional potency and binding affinity of NECA and CGS21680.[37] Firstly, this discrepancy could be related to the effect of receptor reserve. Occupation of a fraction of the receptor is sufficient to obtain maximal activation in the signal transduction cascade,[37] which is supported by the relative low values of the relative efficacies (Table 5.4). Secondly, we have used an antagonist radioligand ([^{3}H]-ZM241385) to determine agonist affinity, which generally yields lower affinity values than when an agonist radioligand is used.[38-40] It has been shown that the use of an agonistic radioligand, such as [^{3}H]-NECA or [^{3}H]-CGS21680 at the $A_{2A}R$, results in agonist affinities close to their functional potencies.[41,42] In the present chapter, we decided to use an antagonistic radioligand because it recognizes the whole receptor population (G protein-coupled and –uncoupled), which as a result provided a robust condition for kinetic measurements. Moreover, it should be mentioned that the results from the label-free impedance-based assay represent the integration of several signaling pathways, which might explain the difference in agonist potencies obtained in the impedance-based and the cAMP assay. To elaborate this phenomenon, several lines of research indeed indicate that the $A_{2A}R$ can interact with several 'less traditional' scaffold proteins, such as β-arrestin and α-actinin.[43-45] This may further engage cell morphological changes next to effects induced via the classical G_s pathway, and as a result cause an increased, or at least different, potency in a whole cell impedance-based assay. We also explored the relative efficacy, τ, of agonists in the operational model of Black and Leff.[21] Critically, we observed a correlation between the receptor residence time and the relative efficacy in the xCELLigence assay (r^2 = 0.60, p < 0.01) but it was less significant than the correlation found in the cAMP assay (r^2 = 0.80, p < 0.001). This might also be due to the fact that the label-free impedance-based assay combines cell morphological changes induced via several signaling pathways, as stated above.

In summary, we set up and validated a simplified competition association assay at the $hA_{2A}R$, which allowed an accurate and fast measurement of a

ligand's binding kinetics. Agonist efficacy at the $hA_{2A}R$ was determined in a cAMP assay and, for the first time, in a novel label-free impedance-based system. In both functional assays, our data provide evidence that the receptor residence time is correlated to the functional efficacy at the $hA_{2A}R$ rather than the 'traditional' equilibrium affinity of a compound. This finding may lead to a further understanding of the fundamental basis of agonist efficacy at the $hA_{2A}R$.

References:

1. Fredholm BB, IJzerman AP, Jacobson KA, Linden J, Müller CE. International Union of Basic and Clinical Pharmacology. LXXXI. Nomenclature and classification of adenosine receptors--an update. *Pharmacol Rev* 2011;63(1):1-34.
2. Gao ZG, Jacobson KA. Emerging adenosine receptor agonists. *Expert Opin Emerg Drugs* 2007;12(3):479-492.
3. Jacobson KA, Gao ZG. Adenosine receptors as therapeutic targets. *Nat Rev Drug Discov* 2006;5(3):247-264.
4. Copeland RA, Pompliano DL, Meek TD. Drug-target residence time and its implications for lead optimization. *Nat Rev Drug Discov* 2006;5(9):730-739.
5. Swinney DC. Can binding kinetics translate to a clinically differentiated drug? From theory to practice. *Lett Drug Des Discov* 2006;3(8):569-574.
6. Tummino PJ, Copeland RA. Residence time of receptor-ligand complexes and its effect on biological function. *Biochemistry* 2008;47(20):5481-5492.
7. Zhang R, Monsma F. Binding kinetics and mechanism of action: toward the discovery and development of better and best in class drugs. *Expert Opin Drug Discov* 2010;5(11):1023-1029.
8. Copeland RA. *Evaluation of enzyme inhibitors in drug discovery: A guide for medicinal chemists and pharmacologists.* New York: Wiley; 2005. 1-265 p.
9. Sykes DA, Dowling MR, Charlton SJ. Exploring the mechanism of agonist efficacy: a relationship between efficacy and agonist dissociation rate at the muscarinic M_3 receptor. *Mol Pharmacol* 2009;76(3):543-551.
10. Motulsky HJ, Mahan LC. The kinetics of competitive radioligand binding predicted by the law of mass action. *Mol Pharmacol* 1984;25(1):1-9.
11. Van Tilburg EW, Gremmen M, von Frijtag Drabbe Kunzel J, de Groote M, IJzerman AP. 2,8-Disubstituted adenosine derivatives as partial agonists for the adenosine A_{2A} receptor. *Bioorg Med Chem* 2003;11(10):2183-2192.
12. Van Tilburg EW, von Frijtag Drabbe Kunzel J, de Groote M, IJzerman AP. 2,5'-Disubstituted adenosine derivatives: evaluation of selectivity and efficacy for the adenosine A(1), A(2A), and A(3) receptor. *J Med Chem* 2002;45(2):420-429.
13. Beukers MW, Chang LC, von Frijtag Drabbe Kunzel JK, Mulder-Krieger T, Spanjersberg RF, Brussee J, IJzerman AP. New, non-adenosine, high-potency agonists for the human adenosine A_{2B} receptor with an improved selectivity profile compared to the reference agonist

N-ethylcarboxamidoadenosine. *J Med Chem* 2004;47(15):3707-3709.
14. Smith PK, Krohn RI, Hermanson GT, Mallia AK, Gartner FH, Provenzano MD, Fujimoto EK, Goeke NM, Olson BJ, Klenk DC. Measurement of protein using bicinchoninic acid. *Anal Biochem* 1985;150(1):76-85.
15. Xi B, Yu N, Wang X, Xu X, Abassi YA. The application of cell-based label-free technology in drug discovery. *Biotechnol J* 2008;3(4):484-495.
16. Yu N, Atienza JM, Bernard J, Blanc S, Zhu J, Wang X, Xu X, Abassi YA. Real-time monitoring of morphological changes in living cells by electronic cell sensor arrays: an approach to study G protein-coupled receptors. *Anal Chem* 2006;78(1):35-43.
17. Denelavas A, Weibel F, Prummer M, Imbach A, Clerc RG, Apfel CM, Hertel C. Real-time cellular impedance measurements detect $Ca^{(2+)}$ channel-dependent oscillations of morphology in human H295R adrenoma cells. *Biochim Biophys Acta* 2011;1813(5):754-762.
18. Flynn AN, Tillu DV, Asiedu MN, Hoffman J, Vagner J, Price TJ, Boitano S. The protease-activated receptor-2-specific agonists 2-aminothiazol-4-yl-LIGRL-NH2 and 6-aminonicotinyl-LIGRL-NH_2 stimulate multiple signaling pathways to induce physiological responses *in vitro* and *in vivo*. *J Biol Chem* 2011;286(21):19076-19088.
19. Scandroglio P, Brusa R, Lozza G, Mancini I, Petro R, Reggiani A, Beltramo M. Evaluation of cannabinoid receptor 2 and metabotropic glutamate receptor 1 functional responses using a cell impedance-based technology. *J Biomol Screen* 2010;15(10):1238-1247.
20. Cheng Y, Prusoff WH. Relationship between the inhibition constant (K_1) and the concentration of inhibitor which causes 50 per cent inhibition (I_{50}) of an enzymatic reaction. *Biochem Pharmacol* 1973;22(23):3099-3108.
21. Black JW, Leff P. Operational models of pharmacological agonism. *Proc R Soc Lond B Biol Sci* 1983;220(1219):141-162.
22. Affolter H, Hertel C, Jaeggi K, Portenier M, Staehelin M. (-)-S-[^{3}H]CGP-12177 and its use to determine the rate constants of unlabeled beta-adrenergic antagonists. *Proc Natl Acad Sci U S A* 1985;82(3):925-929.
23. Contreras ML, Wolfe BB, Molinoff PB. Kinetic analysis of the interactions of agonists and antagonists with beta adrenergic receptors. *J Pharmacol Exp Ther* 1986;239(1):136-143.
24. Dowling MR, Charlton SJ. Quantifying the association and dissociation rates of unlabeled antagonists at the muscarinic M_3 receptor. *Br J Pharmacol* 2006;148(7):927-937.
25. Mantell SJ, Stephenson PT, Monaghan SM, Maw GN, Trevethick MA, Yeadon M, Keir RF, Walker DK, Jones RM, Selby MD, Batchelor DV, Rozze S, Chavaroche H, Hobson TJ, Dodd PG, Lemaitre A, Wright KN, Stuart EF. Inhaled adenosine A(2A) receptor agonists for the treatment of chronic obstructive pulmonary disease. *Bioorg Med Chem Lett* 2008;18(4):1284-1287.
26. Mantell SJ, Stephenson PT, Monaghan SM, Maw GN, Trevethick MA, Yeadon M, Walker DK, Selby MD, Batchelor DV, Rozze S, Chavaroche H, Lemaitre A, Wright KN, Whitlock L, Stuart EF, Wright PA, Macintyre F. SAR of a series of inhaled A(2A) agonists and comparison of inhaled pharmacokinetics in a preclinical model with clinical pharmacokinetic data. *Bioorg Med Chem Lett* 2009;19(15):4471-4475.
27. Vauquelin G. Rebinding: or why drugs may act longer in vivo than expected from their in vitro target residence time. *Expert Opin Drug Discov* 2010;5(10):927-941.
28. Vauquelin G, Van Liefde I. Slow antagonist dissociation and long-lasting *in vivo* receptor protection. *Trends Pharmacol Sci* 2006;27(7):356-359.
29. Jaakola VP, Griffith MT, Hanson MA, Cherezov V, Chien EY, Lane JR, IJzerman AP, Stevens RC. The 2.6 angstrom crystal structure of a human A_{2A} adenosine receptor bound to an antagonist.

Science 2008;322(5905):1211-1217.
30. Kim SK, Gao ZG, Van Rompaey P, Gross AS, Chen A, Van Calenbergh S, Jacobson KA. Modeling the adenosine receptors: comparison of the binding domains of A_{2A} agonists and antagonists. *J Med Chem* 2003;46(23):4847-4859.
31. Xu F, Wu H, Katritch V, Han GW, Jacobson KA, Gao ZG, Cherezov V, Stevens RC. Structure of an agonist-bound human A_{2A} adenosine receptor. *Science* 2011;332(6027):322-327.
32. Lebon G, Warne T, Edwards PC, Bennett K, Langmead CJ, Leslie AG, Tate CG. Agonist-bound adenosine A_{2A} receptor structures reveal common features of GPCR activation. *Nature* 2011;474(7352):521-525.
33. Borea PA, Dalpiaz A, Varani K, Gessi S, Gilli G. Binding thermodynamics at A_1 and A_{2A} adenosine receptors. *Life Sci* 1996;59(17):1373-1388.
34. McGuinness R. Impedance-based cellular assay technologies: recent advances, future promise. *Curr Opin Pharmacol* 2007;7(5):535-540.
35. Peters MF, Scott CW. Evaluating cellular impedance assays for detection of GPCR pleiotropic signaling and functional selectivity. *J Biomol Screen* 2009;14(3):246-255.
36. Hoeren M, Brawek B, Mantovani M, Löffler M, Steffens M, Velthoven V, Feuerstein TJ. Partial agonism at the human α_{2A}-autoreceptor: role of binding duration. *Naunyn-Schmiedeberg's Arch Pharmacol* 2008;378(1):17-26.
37. Dionisotti S, Ongini E, Zocchi C, Kull B, Arslan G, Fredholm BB. Characterization of human A_{2A} adenosine receptors with the antagonist radioligand [^{3}H]-SCH 58261. *Br J Pharmacol* 1997;121(3):353-360.
38. Bruns RF, Fergus JH, Badger EW, Bristol JA, Santay LA, Hays SJ. PD 115,199: an antagonist ligand for adenosine A_2 receptors. *Naunyn-Schmiedeberg's Arch Pharmacol* 1987;335(1):64-69.
39. Nonaka H, Mori A, Ichimura M, Shindou T, Yanagawa K, Shimada J, Kase H. Binding of [^{3}H] KF17837S, a selective adenosine A_2 receptor antagonist, to rat brain membranes. *Mol pharmacol* 1994;46(5):817-822.
40. Zocchi C, Ongini E, Ferrara S, Baraldi PG, Dionisotti S. Binding of the radioligand [^{3}H]-SCH 58261, a new non-xanthine A_{2A} adenosine receptor antagonist, to rat striatal membranes. *Brit J Pharmacol* 1996;117(7):1381-1386.
41. Jarvis MF, Schulz R, Hutchison AJ, Do UH, Sills MA, Williams M. [^{3}H]CGS21680, a selective A_2 adenosine receptor agonist directly labels A_2 receptors in rat brain. *J Pharmacol Exp Ther* 1989;251(3):888-893.
42. Müller CE, Maurinsh J, Sauer R. Binding of [^{3}H]MSX-2 (3-(3-hydroxypropyl)-7-methyl-8-(m-methoxystyryl)-1-propargylxanthine) to rat striatal membranes--a new, selective antagonist radioligand for A_{2A} adenosine receptors. *Eur J Pharm Sci* 2000;10(4):259-265.
43. Verzijl D, IJzerman AP. Functional selectivity of adenosine receptor ligands. *Purinergic Signal* 2011;7(2):171-192.
44. Burgueno J, Blake DJ, Benson MA, Tinsley CL, Esapa CT, Canela EI, Penela P, Mallol J, Mayor F, Jr., Lluis C, Franco R, Ciruela F. The adenosine A_{2A} receptor interacts with the actin-binding protein alpha-actinin. *J Biol Chem* 2003;278(39):37545-37552.
45. Keuerleber S, Gsandtner I, Freissmuth M. From cradle to twilight: the carboxyl terminus directs the fate of the A(2A)-adenosine receptor. *Biochim Biophys Acta* 2011;1808(5):1350-1357.
46. Ballesteros JA, Weinstein H. Integrated methods for the construction of three dimensional models and computational probing of structure–function relations in G-protein coupled receptors. *Methods Neurosci* 1995;25:366–428.

Chapter 6

Molecular basis of allosteric modulation Insight from a binding kinetics study at the human adenosine A_1 receptor

Guo D, Venhorst SN, Massink A, Van Veldhoven JPD, Vauquelin G, IJzerman AP, Heitman LH.
Adapted from: *Br J Pharmacol.* submitted

About this chapter

Many G protein-coupled receptors (GPCRs) can be allosterically modulated by small molecule ligands. This modulation is best understood in terms of the kinetics of the ligand-receptor interaction. However, many current kinetic assays require at least the (radio-) labeling of the orthosteric ligand, which is impractical for studying a range of ligands. In this chapter we describe the application of a competition association assay at the adenosine A_1 receptor (A_1R) for this purpose. We used the competition association assay to examine the binding kinetics of several unlabeled A_1R orthosteric agonists in the absence or presence of two allosteric modulators. We also tested two bitopic ligands, in which an orthosteric and an allosteric pharmacophore were covalently linked with different spacer lengths in between. The relevance of the competition association assay for the bitopic ligands' binding kinetics was also explored by analyzing simulated data. The binding kinetics of an unlabeled 'cold' orthosteric ligand was influenced upon the addition of an allosteric modulator and such an effect was probe- and concentration-dependent. Covalently linking the orthosteric and allosteric pharmacophores into one bitopic molecule had a substantial effect on the overall on- or off-rate. The competition association assay is a useful tool for exploring the allosteric modulation of the human adenosine A_1 receptor. This assay may have general applicability to study allosteric modulation at other GPCRs as well.

6.1 Introduction

Adenosine receptors are a subfamily within the class A of G protein-coupled receptors (GPCRs), which includes four subtypes, A_1, A_{2A}, A_{2B} and A_3.[1] These receptors are ubiquitously expressed in many tissues and have been shown to play important roles in numerous physiological processes.[2] Adenosine receptors can be activated by their endogenous ligand adenosine or by a range of synthetic small molecule agonists that share the same binding site as the natural ligand, which is referred to as the orthosteric site.[3] Adenosine receptors also possess an allosteric site, which is a binding pocket topographically distinct from the orthosteric site.[4] Currently, many GPCRs, including the adenosine receptor subfamily, have been reported to have one or several allosteric binding sites that interact with an allosteric modulator.[5-10] Such a binding event is believed to result in receptor conformational changes, which in turn affect the binding of the orthosteric ligand, its potency and/or level of activation.[11,12] Moreover, the extent of allosteric modulation also depends on the nature of the orthosteric ligand, so-called probe-dependency.[8,13] These complexities add difficulties in understanding the concept and mechanism of allosteric modulation.

Recently, an increasing amount of evidence suggests that ligand-receptor binding kinetics is an overlooked key factor in the broader concept of a drug's mechanism of action (MOA).[14,15] Insight in the ligand-receptor binding kinetics may further our knowledge of the molecular mechanism of GPCR allosterism and improve our understanding of this concept.[16] However, current kinetic studies of GPCR allosterism mostly rely on the 'probe' dissociation experiment, i.e., determining the change in a radiolabeled orthosteric ligand's dissociation rate.[12,17,18] This radiolabeling process is both labor intensive and, importantly, only practical for high affinity ligands. As a consequence, the investigation of GPCR allosterism from a kinetic point of view has been limited. Therefore, it is highly desirable to measure the binding kinetics of label-free orthosteric ligands in the absence or presence of an allosteric modulator.

To determine the binding kinetics, we followed a recently validated competition association assay on the hA_1R in our lab,[19] based on the mathematical model described by Motulsky and Mahan.[20] In the current study we examined the association and dissociation rates of several A_1R agonists in the absence or presence of different allosteric modulators (Figure

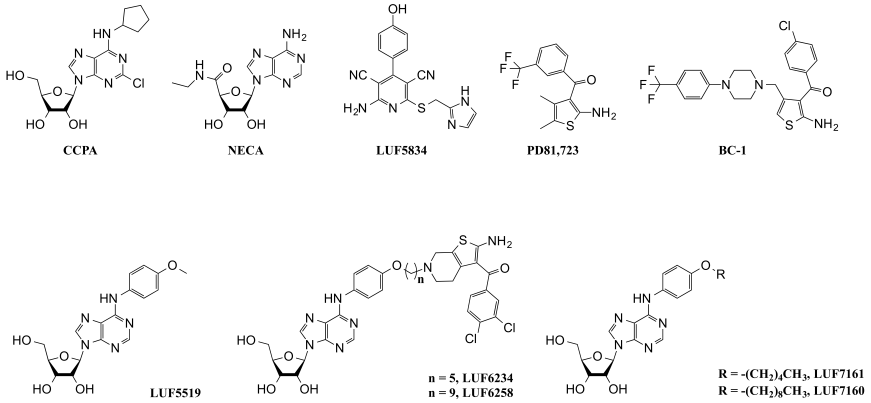


Figure 6.1 | Chemical structures of compounds used in this chapter. CCPA, NECA and LUF5519 are ribose-containing adenosine A_1 receptor agonists, while LUF5834 is a non-ribose agonist;[21-23] PD81,723 and BC-1 are allosteric enhancers for adenosine A_1 receptor agonists.[24] LUF6234 and LUF6258 are in-house synthesized bitopic ligands for the adenosine A_1 receptor with five-carbon linker and nine-carbon linker, respectively.[26] LUF7161 and LUF7160 are newly synthesized monovalent ligands with five-atom linker and nine-atom linker, respectively.

6.1). Amongst these compounds, CCPA (2-chloro-*N*^{6}-cyclopentyladenosine) and NECA (*N*-5'-ethylcarboxamidoadenosine) are ribose-containing A_1R receptor agonists,[21,22] while LUF5834 (2-amino-4-(4-hydroxyphenyl)-6-(1H-imidazol-2ylmethyl-sulfanyl)-pyridine-3,5-dicarbonitrile) is a A_1R agonist without the ribose moiety.[23] The allosteric modulators, PD81,723 (2-amino-4,5-dimethyl-3-thienyl)-[3-(trifluoromethyl)-phenyl]methanone) and BC-1 [i.e., compound 8j by Romagnoli *et al.*[24], 2-amino-4-((4-(4-(trifluoromethyl) phenyl)piperazin-1-yl)methyl)thiophen-3-yl)(4-chlorophenyl)methanone] are allosteric enhancers of the A_1R[24,25]. The binding kinetics of two in-house synthesized 'bitopic' ligands, namely LUF6234 and LUF6258 (Figure 6.1),[26] were also investigated, as they are useful tools for the exploration of A_1R allosteric modulation.[27] These bitopic ligands share the same orthosteric and allosteric pharmacophores, mimicking LUF5519 [A_1R agonist, *N*^{6}-(4-methoxyphenyl)adenosine] and PD81,723 respectively, which are covalently linked via a spacer with different lengths, i.e., five- and nine-carbon atoms, respectively.

6.2 Methods

Chemicals and reagents

[^{3}H]-1,3-dipropyl-8-cyclopentylxanthine ([^{3}H]-DPCPX, specific activity 103 Ci/mmol) was purchased from ARC, Inc. (St. Louis, MO, USA). Unlabeled DPCPX and CCPA were from Sigma (St. Louis, MO, USA). NECA was purchased from Sigma-Aldrich (Steinheim, Germany). N^6-cyclopentyladenosine (CPA) was obtained from Research Biochemicals Inc. (Natick, MA, U.S.A.). LUF5834, PD81,723 and BC-1 were prepared in-house following synthesis routes as reported previously.[23-25] LUF5519, LUF6234 and LUF6258 were also synthesized in-house as described by Narlawar *et al.*[26] The synthesis of LUF7160 [N^6-(4-nonyloxyphenyl) adenosine] and LUF7161 [N^6-(4-pentyloxyphenyl)adenosine] was performed following the same method in Narlawar *et al.*[26]. CHAPS [3-((3-cholamidopropyl)-dimethylammonio)-1-propanesulfonate)] was obtained from Carl Roth GmbH (Karlsruhe, Germany). Chinese hamster ovary (CHO) cells stably expressing the human A_1R (CHO-hA_1R) were obtained from Prof. Steve Hill (University of Nottingham, UK). All other chemicals were of analytical grade and obtained from standard commercial sources.

Cell culture and membrane preparation

Cell culture and membrane preparation were performed as reported previously.[19]

Radioligand displacement assays

Membrane aliquots containing 5 μg of protein were incubated in a total volume of 100 μL assay buffer (50 mM Tris-HCl [pH 7.4], supplemented with 5 mM $MgCl_2$ and 0.1% [w/v] CHAPS) at 25 ˚C for one hour. The

displacement experiments were performed using eleven concentrations of competing ligands with 2.6 nM [^{3}H]-DPCPX in the absence or presence of 10 μM of PD81,723 or BC-1. For the determination of the allosteric potency of PD81,723 and BC-1, 100 nM (IC_{80} value) CCPA was used in the presence of increasing concentrations of these two allosteric modulators to examine the potentiated [^{3}H]-DPCPX displacement. Nonspecific binding was determined in the presence of 100 μM CPA and represented less than 10% of the total binding. Incubations were terminated and samples were obtained as described previously.[19]

Radioligand association and dissociation assays

Association experiments were performed by incubating membrane aliquots containing 5 μg of protein in a total volume of 100 μL of assay buffer at 25 ˚C with 2.6 nM [^{3}H]-DPCPX. The amount of radioligand bound to the receptor was measured at different time intervals during a total incubation of 45 min in the absence or presence of 10 μM PD81,723. For the dissociation assay, membrane aliquots containing 5 μg of protein were allowed to reach equilibrium for one hour with the same amount of radioligand. After the pre-incubation, radioligand dissociation was started by adding 10 μM of DPCPX at different time points in the absence or presence of 10 μM PD81,723. The amount of radioligand still bound to the receptor was measured at various time intervals for a total of one hour. Incubations were terminated and samples were obtained as described previously.[19]

Radioligand competition association assay

The binding kinetics of unlabeled ligands was quantified at 25 ˚C using the competition association assay based on the theoretical framework by Motulsky and Mahan.[20] This method has been recently adopted and validated on the adenosine A_1R in our lab,[19] which enables accurate determination of unlabeled ligands' binding kinetics. In the present chapter we followed the same method. In brief, we used a concentration of approximately 3- to 10-fold K_i of the unlabeled ligand with or without the co-incubation of 1,

10 or 33 μM PD81,723 or BC-1. The experiment was initiated by adding membrane aliquots containing 5 μg of protein in a total volume of 100 μl assay buffer at different time points for a total incubation of one hour, except for LUF6234 and LUF6258, which were incubated for 2 hours given their slow kinetic profiles. Incubations were terminated and samples were obtained as described previously.[19]

Data analysis

All experimental data was analyzed by using GraphPad Prism 5.0 (GraphPad Software Inc., San Diego, CA). Radioligand displacement curves were fitted to one and two state/site binding models. k_{obs} and k_{off} values of [^{3}H]-DPCPX in the absence or presence of PD81,723 were obtained from the association and dissociation curves. Values for k_{on} were obtained by converting k_{obs} values using the following equation:

$$k_{on} = \frac{k_{obs} - k_{off}}{[radioligand]} \tag{1}$$

Association and dissociation rates for unlabeled ligands were calculated by fitting the data in the competition association model using 'kinetics of competitive binding':[20]

$$K_A = k_1 \cdot [L] \cdot 10^{-9} + k_2$$
$$K_B = k_3 \cdot [I] \cdot 10^{-9} + k_4$$
$$S = \sqrt{(K_A - K_B)^2 + 4 \cdot k_1 \cdot k_3 \cdot L \cdot I \cdot 10^{-18}}$$
$$K_F = 0.5 \cdot (K_A + K_B + S)$$
$$K_S = 0.5 \cdot (K_A + K_B - S)$$
$$Q = \frac{B_{max} \cdot k_1 \cdot L \cdot 10^{-9}}{K_F - K_S}$$
$$Y = Q \cdot \left(\frac{k_4 \cdot (K_F - K_S)}{K_F \cdot K_S} + \frac{k_4 - K_F}{K_F}(-K_F \cdot X) - \frac{k_4 - K_S}{K_S} e^{(-K_S \cdot X)}\right) \tag{2}$$

Where X is the time, Y is the specific [^{3}H]-DPCPX binding (DPM), k_1 and k_2 are the k_{on} ($M^{-1} \cdot min^{-1}$) and k_{off} (min^{-1}) of [^{3}H]-DPCPX pre-determined

in radioligand association and dissociation assay respectively, L the concentration of [^{3}H]-DPCPX used (nM), B_{max} the total binding (DPM) and I the concentration unlabeled ligand (nM). Fixing these parameters allows the following parameters to be calculated: k_3, which is the k_{on} value ($M^{-1}\cdot min^{-1}$) of the unlabeled ligand and k_4, which is the k_{off} value (min^{-1}) of the unlabeled ligand. Ligand-receptor residence times (RT) were calculated using the following equation:[28]

$$RT = 1 / k_{off} \tag{3}$$

The derived association and dissociation rates of the unlabeled ligand were used to calculate the 'kinetic K_D' using the following equation:

$$K_D = \frac{k_{off}}{k_{on}} \tag{4}$$

Data simulations

Differential equations (see below, Equations 5-11) were used to follow the time (*t*)-wise changes in target 'AB' occupancy by a bitopic ligand, 'ab', or a monovalent ligand, 'c', based on the thermodynamic model in Figure 6.2.[29] The abbreviation notions for different molecular complexes are in parentheses in Figure 6.2.

$$\frac{d[AB]}{d(t)} = k_{-a}\cdot[aAB] - k_{+a}\cdot[AB]\cdot[ab] + k_{-b}\cdot[ABb] - k_{+b}\cdot[AB]\cdot[ab] + k_{+c}\cdot[cAB] - k_{+c}\cdot[AB]\cdot[c] \tag{5}$$

$$\frac{d[aAB]}{d(t)} = k_{+a}\cdot[AB]\cdot[ab] - k_{-a}\cdot[aAB] + k_{-b}\cdot[aABb] - k_{+b}\cdot[aAB]\cdot[L] \tag{6}$$

$$\frac{d[ABb]}{d(t)} = k_{+b}\cdot[AB]\cdot[ab] - k_{-b}\cdot[ABb] + \frac{k_{-a}\cdot[aABb]}{\alpha'_{ab}} - \alpha_{ab}\cdot k_{+a}\cdot[aABb]\cdot[L] + k_{-c}\cdot[cABb] - k_{+c}[ABb]\cdot[c] \tag{7}$$

$$\frac{d[aABb]}{d(t)} = k_{+a}\cdot[ABb]\cdot[L] - k_{-a}\cdot[aABb] + k_{+b}\cdot[aAB]\cdot[L] - k_{-b}\cdot[aABb] \tag{8}$$

$$\frac{d[cAB]}{d(t)} = k_{+c}\cdot[AB]\cdot[c] - k_{-c}\cdot[cAB] + k_{-b}\cdot[cABb] - k_{+b}\cdot[cAB]\cdot[ab] \tag{9}$$

$$\frac{d[cABb]}{d(t)} = k_{+b}\cdot[cAB]\cdot[ab] - k_{-c}\cdot[cABb] + k_{+c}\cdot[ABb]\cdot[c] - k_{-c}\cdot[cABb] \tag{10}$$

$$[AB]_{occ} = 100\cdot\frac{[aAB]+[aABb]+[ABb]+[cABb]}{[AB]+[aAB]+[aABb]+[ABb]+[cABb]+[cAB]} \tag{11}$$

Where k_{+a} and k_{+b} ($M^{-1}\cdot min^{-1}$) are the microscopic association rate constants of the bitopic ligand, ab, for a-A and b-B binding, k_{-a} and k_{-b} (min^{-1}) are the dissociation rate constants of the bitopic ligand, ab, for a-A and b-B unbinding, L the total concentration of the bitopic ligand (M), c the concentration of the monovalent ligand (M), k_{+c} and k_{-c} are the association rate and dissociation rate for c-A binding/unbinding. α_{ab} and α'_{ab} are the penalty factors to correct the kinetics of binding/unbinding of the second pharmacophore of a bitopic ligand. The macroscopic k_{on} and k_{off} value of a bitopic ligand can be theoretically calculated using the following equations:[29]

$$k_{on} = k_{+a} + k_{+b} \tag{12}$$

$$k_{off} = k_{-a} \cdot \frac{k_{-b}}{[L] \cdot k_{+a}} + k_{-b} \cdot \frac{k_{-a}}{[L] \cdot k_{+b}} \tag{13}$$

Data simulations were performed to mimic the binding of a radioligand (represented by the target occupancy of 'c') by solving Equations 5-11 during a period of 5 min, either alone or in the presence of increasing concentrations of 'ab' with different combinations of microscopic kinetics defined as follows:

1) $k_{+a} = 1 \times 10^5\ M^{-1}\cdot min^{-1}$, $k_{-a} = 1\ min^{-1}$, $k_{+b} = 1 \times 10^5\ M^{-1}\cdot min^{-1}$, $k_{-b} = 1\ min^{-1}$;
2) $k_{+a} = 1 \times 10^5\ M^{-1}\cdot min^{-1}$, $k_{-a} = 1\ min^{-1}$, $k_{+b} = 1 \times 10^6\ M^{-1}\cdot min^{-1}$, $k_{-b} = 1\ min^{-1}$;
3) $k_{+a} = 1 \times 10^6\ M^{-1}\cdot min^{-1}$, $k_{-a} = 1\ min^{-1}$, $k_{+b} = 1 \times 10^5\ M^{-1}\cdot min^{-1}$, $k_{-b} = 1\ min^{-1}$.

The binding kinetics of the monovalent ligand 'c' was defined as $k_{+c} = 1 \times 10^7\ M^{-1}\cdot min^{-1}$, $k_{-c} = 0.3\ min^{-1}$ and [c] = 100 nM. The simulated data were collected at 0.5 min intervals for a total of 5 min and subsequently subjected to the competition association model using '*kinetics of competitive binding*'.[20] The kinetics data obtained thereof were compared to the theoretically calculated values (by subjecting the defined microscopic rate constants mentioned above into Equation 12 and 13) to explore the relevance of using competition association assay for bitopic ligands' binding kinetics.

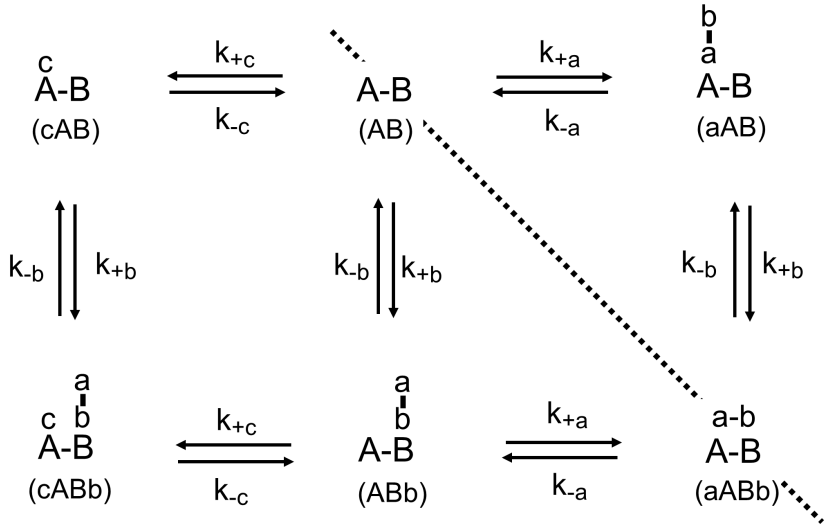


Figure 6.2 | Schematic representation of the monovalent, 'c', and bitopic, 'ab', ligand-target site interactions. The bitopic ligand bears two distinct pharmacophores: 'a' and 'b'. 'AB' is the target with distinct binding sites 'A' and 'B'. 'a' and 'c' only bind to 'A' in a competitive manner and 'b' only binds to 'B'. The abbreviated notation for the free target and target complexes is in parentheses. Formation of a trimeric species in which two bitopic ligands are bound to a single target (i.e. one via 'a' and the other via 'b') is not included in the model because, with the present microscopic rate constants, this species only marginally contributes to the total binding (data not shown). k_{+a}, k_{+b} and k_{+c} (in $M^{-1}\cdot min^{-1}$) are the microscopic association rate constants and k_{-a}, k_{-b} and k_{-c} (in min^{-1}) are the microscopic dissociation rate constants for a-A, b-B and c-A binding, respectively. The broken line divides the thermodynamic cycle model of bivalent ligand binding into two pathways/lanes that 'ab' can adopt to form the fully bound aABb state as outlined elsewhere.[29]

6.3 Results

Quantification of the affinity (K_i) of A_1R ligands in the absence or presence of PD81,723 or BC-1 in displacement experiments

To determine the affinities of several agonists at the A_1R in the absence or presence of allosteric modulators, radioligand displacement experiments were performed. All compounds tested produced concentration-dependent inhibition of specific [^{3}H]-DPCPX binding (Figure 6.3) and their affinities are detailed in Table 6.1. Among the agonists tested, the binding of CCPA and NECA were preferably fitted by a two-site/state competition model, whereas the non-ribose agonist LUF5834 was best described by a one-site/state competition model. In the presence of 10 μM PD81,723, CCPA demonstrated a significant increase of both its high and low affinity (K_H = 2 ± 1 nM, K_L = 77 ± 5 nM). This effect was even more pronounced upon the addition of BC-1. Notably, the two-site binding curve of CCPA was shifted to a one-site binding curve (K_i = 4.5 ± 0.3 nM) in the presence of this allosteric modulator. Similarly to CCPA, NECA had 3.7-fold and 21-fold increased affinities (110 ± 50 nM and 20 ± 2 nM) in the presence of PD81,723 or BC-1, respectively. Both were mainly from a gain in affinity at the low-affinity binding site. In contrast to the ribose-containing agonists, i.e., CCPA and NECA, the binding affinity of LUF5834 to the A_1R was not significantly altered by the presence of either allosteric modulator.

Quantification of the potency of two allosteric modulators

The potencies of PD81,723 and BC-1 were investigated by examining the enhanced [^{3}H]-DPCPX displacement from the A_1R by 100 nM CCPA (IC_{80}) in the presence of increasing concentrations of these two allosteric modulators. It follows from Figure 6.3D that BC-1 had a 13-fold higher potency (EC_{50} = 1.5 ± 0.2 μM) than PD81,723 (EC_{50} = 19 ± 2 μM) for modulating CCPA binding to the A_1R.

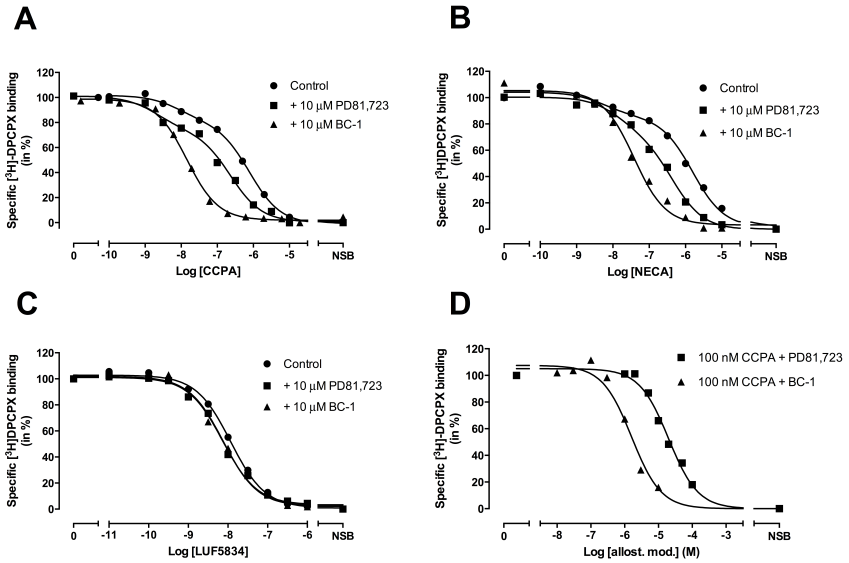


Figure 6.3 | Displacement of specific [^{3}H]-DPCPX binding from the adenosine A_1 receptor at 25 °C by CCPA (Panel A), NECA (Panel B) or LUF5834 (Panel C) in the absence or presence of 10 µM PD81,723 or BC-1 or by 100 nM CCPA (normalized as 100%) in the presence of increased concentrations of PD81,723 or BC-1 (Panel D). Representative graphs from one experiment performed in duplicate.

Quantification of the association (k_{on} (k_1)) and dissociation rates (k_{off} (k_2)) of [^{3}H]-DPCPX in the absence or presence of PD81,723

Since knowledge of the association [k_{on} (k_1)] and dissociation rates [k_{off}(k_2)] of [^{3}H]-DPCPX was necessary for subsequent competition association assays in the presence of an allosteric modulator, we performed a direct [^{3}H]-DPCPX association and dissociation assay to determine DPCPX's binding kinetics in the absence or presence of 10 µM PD81,723. As detailed in Table 6.2, [^{3}H]-DPCPX displayed a fast association ($1.7 \pm 0.3 \times 10^8$ $M^{-1}\cdot min^{-1}$) and dissociation rate (0.23 ± 0.02 min^{-1}) in the absence of PD81,723, which values were not significantly affected by the presence of PD81,723 (k_{on} =

Table 6.1 | [^{3}H]-DPCPX displacement experiments by CCPA, NECA and LUF5834 on CHO-hA_1R membranes in the absence or presence of 10 μM PD81,723 or BC-1

Cmpd	*CCPA*				*NECA*				*LUF5834*
	K_H (nM)	K_L (nM)	R_H (%)	K_i (nM)	K_H (nM)	K_L (nM)	R_H (%)	K_i (nM)	K_i (nM)
Control	16±1	338±27	20±4	184±18	4±1	731±94	18±3	411±52	7.8±1.5
+ 10 μM PD81,723	2±1	77±5	27±7	43±8	6±4	200±78	26±9	110±50	9.6±2.6
+ 10 μM BC-1	n.a.	n.a.	n.a	4.5±0.3	8±2	128±27	10±3	20±2	6.7±1.5

Data are shown as mean ± s.e.m of three separate experiments each performed in duplicate. K_H and K_L, K_i values for the high and low-affinity state, respectively and are shown for data that could be fitted to a two-state model; a one-state K_i analysis was also performed to effectively compare all affinities. R_H, the fraction of receptors in the high affinity state and is shown in %. n.a., not available.

$1.8 \pm 0.1 \times 10^8$ $M^{-1}\cdot min^{-1}$; k_{off} = 0.22 ± 0.01 min^{-1}). Similarly, BC-1, sharing the same chemical scaffold as PD81,723 (Figure 6.1), was reported to have a negligible effect on the binding of [^{3}H]-DPCPX.[24] Hence, it allowed us to further explore the binding kinetics of unlabeled agonists in the absence or presence of an allosteric modulator using the rate constants (k_1 = 1.7 ± 0.3 × 10^8 $M^{-1}\cdot min^{-1}$ and k_2 = 0.22 ± 0.01 min^{-1}) of the antagonist [^{3}H]-DPCPX.

Quantification of the binding kinetics of unlabeled agonists on the A_1R in the absence or presence of an allosteric modulator by using the competition association assay

In our previous work at the adenosine A_1R, we have validated the competition association assay to test a ligand's binding kinetics.[19] Here we adopted the method to examine the binding kinetics of three A_1R agonists (CCPA, NECA, and LUF5834) in the absence or presence of two allosteric modulators (PD81,723 and BC-1). Several observations were made. Firstly, both allosteric modulators affected the orthosteric ligand's affinity by influencing their binding kinetics (Table 6.3, Figure 6.4). Taking CCPA as an example, its dissociation rate decreased almost four-fold in the presence of 10 μM PD81,723 (k_{off} = 0.29 ± 0.02 min^{-1}), while its association rate increased 2.5-fold. As a result, the affinity (K_D = 131 ± 21 nM) of CCPA was increased

Table 6.2 | The association and dissociation rates of [^{3}H]-DPCPX binding to CHO-hA$_1$R membranes in the absence or presence of 10 μM PD81,723.

Cmpd	k_{on} ($M^{-1}.min^{-1}$)[a]	k^{off} (min^{-1})[b]	K_D (nM)[c]
DPCPX	1.7 ± 0.3 x 10^8	0.23 ± 0.02	1.5 ± 0.3
+ PD81,723	1.8 ± 0.1 x 10^8	0.22 ± 0.01	1.2 ± 0.1

Values are means ± s.e.m of three separate experiments each performed in duplicate. [a] Association [k_{on} (k_1)] of [^{3}H]-DPCPX to CHO-hA$_1$R membrane at 25°C; k_{on} = (k_{obs} – k_{off}) / [radioligand]. [b] Dissociation [k_{off} (k_2)] of [^{3}H]-DPCPX from CHO-hA$_1$R membrane at 25°C. [c]'kinetic K_D' = k_{off} / k_{on}.

over 10-fold in the presence of PD81,723 (11 ± 1 nM). In comparison, 10 μM BC-1 lowered CCPA's off-rate by ten-fold (k_{off} = 0.11 ± 0.02 min^{-1}) and raised its on-rate by three-fold (k_{on} = 2.7 ± 0.4 × 10^7 M^{-1}·min^{-1}). Overall, this resulted in an increased A$_1$R affinity of 4.1 ± 0.6 nM. This finding correlated to our aforementioned statement that BC-1 is a more potent A$_1$R allosteric modulator than PD81,723, yet with more detailed kinetic information. Secondly, the allosteric effect was concentration-dependent. It follows from Table 6.3 and Figure 6.4B that BC-1 slowed the dissociation rate of CCPA by eight- to ten-fold at low concentrations (i.e., 1 μM or 10 μM), while at a relatively high concentration (i.e., 33 μM), it further decreased CCPA's off-rate by another three-fold. A similar trend was observed for PD81,723, though the effect was smaller in comparison to that of BC-1 (Figure 6.4A). Thirdly, A$_1$R allosteric modulation was 'probe-dependent', i.e., the on- and off-rates of different orthosteric ligands were influenced to varying degrees in the presence of the same allosteric modulator. For instance, in the presence of 10 μM PD81,723, the dissociation rates of ribose-containing agonists (CCPA and NECA) were decreased by approximately two- to five-fold, while the dissociation rate of the non-ribose agonist (LUF5834) was not significantly affected (0.92 ± 0.09 min^{-1} versus 0.78 ± 0.08 min^{-1}, P = 0.31). Similarly, in the presence of the more potent allosteric modulator BC-1, all three orthosteric ligands underwent varying changes in their dissociation rates. A significant difference was observed for the residence times of LUF5834 and CCPA, i.e., three- or ten-fold increased to 3.1 ± 0.2 min^{-1} and 9.1 ± 0.9 min^{-1}, respectively. Furthermore, it is interesting to note that an opposite effect on the non-ribose agonist's (LUF5834) association process was observed, compared to the ribose-containing ligands in the presence of 10 μM BC-1. CCPA and NECA had an almost three-fold increase in their on-rates, while for LUF5834 a slightly decreased k_{on} value was observed (1.1 ± 0.1 ×

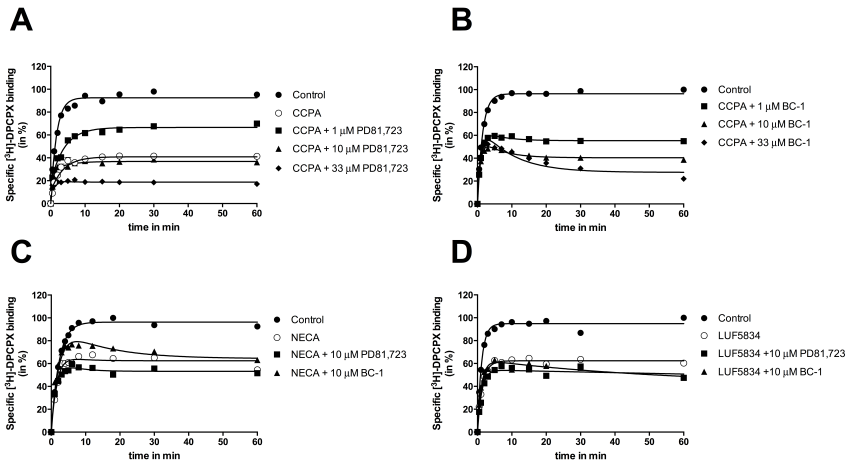


Figure 6.4 | Panel A, [^{3}H]-DPCPX competition association assay in the absence or presence of unlabeled CCPA with or without different concentrations of PD81,723. Panel B, [^{3}H]-DPCPX competition association assay in the absence or presence of unlabeled CCPA with different concentrations of BC-1. Panel C, [^{3}H]-DPCPX competition association assay in the absence or presence of unlabeled NECA with or without 10 μM PD81,723 or BC-1. Panel D, [^{3}H]-DPCPX competition association assay in the absence or presence of unlabeled LUF5834 with or without 10 μM PD81,723 or BC-1. Concentrations of 3- to 10-fold K_i of the unlabeled orthosteric ligands were used to obtain the binding data, which were fitted to Equation 2 described in the methods to calculate the k_{on} and k_{off} values of unlabeled ligands. Representative graphs from one experiment performed in duplicate. (See Table 6.3 for kinetic values).

10^8 $M^{-1}{\cdot}min^{-1}$). Lastly, a good correlation (r^2 = 0.90, p < 0.0001) between the pK_i (K_i values from one-state K_i analysis) obtained from equilibrium displacement assays and the kinetically derived pK_D values was found for all tested ligands. This proved the accuracy of the competition association assay for determination of an orthosteric agonist's binding kinetics in the absence or presence of an allosteric modulator.

Table 6.3 | Binding kinetic 'inventory' (association rate, dissociation rate, residence time and kinetic K_D) for CCPA, NECA and LUF5834 in the absence or presence of an allosteric modulator (PD81,723 or BC-1) at CHO-hA_1R derived from competition association assays.

Cmpd	k_{on} ($M^{-1}.min^{-1}$)[a]	k_{off} (min^{-1})[a]	*RT (min)*[b]	K_D (nM)[c]
CCPA	9.6 ± 1.8 x 10^6	1.17 ± 0.24	0.86 ± 0.17	131 ± 21
+1 μM PD81,723	1.9 ± 0.5 x 10^7	0.77 ± 0.03	1.3 ± 0.1	43 ± 7
+10 μM PD81,723	2.4 ± 0.5 x 10^7	0.29 ± 0.02	3.4 ± 0.2	11 ± 1
+33 μM PD81,723	3.4 ± 0.8 x 10^7	0.20 ± 0.02	5.0 ± 0.4	5.9 ± 1.9
+1 μM BC-1	3.5 ± 0.4 x 10^7	0.15 ± 0.01	6.6 ± 0.4	4.4 ± 0.3
+10 μM BC-1	2.7 ± 0.4 x 10^7	0.11 ± 0.02	9.1 ± 0.9	4.1 ± 0.6
+33 μM BC-1	3.2 ± 0.3 x 10^7	0.038 ± 0.004	26 ± 3	1.2 ± 0.1
NECA	0.9 ± 0.4 x 10^6	0.47 ± 0.19	2.1 ± 0.5	482 ± 167
+10 μM PD81,723	3.0 ± 0.3 x 10^6	0.21 ± 0.02	4.8 ± 0.3	70 ± 6
+10 μM BC-1	3.2 ± 0.5 x 10^6	0.09 ± 0.03	11 ± 2	28 ± 6
LUF5834	2.0 ± 0.2 x 10^8	0.92 ± 0.09	1.1 ± 0.1	4.6 ± 0.4
+10 μM PD81,723	2.6 ± 0.2 x 10^8	0.78 ± 0.08	1.3 ± 0.1	3.0 ± 0.2
+10 μM BC-1	1.1 ± 0.1 x 10^8	0.32 ± 0.02	3.1 ± 0.2	2.9 ± 0.2

Data are shown as mean ± s.e.m of three separate experiments each performed in duplicate. [a] k_{on} (k_3) and k_{off} (k_4) of unlabeled A_1R agonists in the absence or presence of an allosteric modulator (PD81,723 or BC-1) were determined in [^{3}H]-DPCPX (2.6 nM) competition association assays. [b] RT (Residence Time) = 1 / k_{off}. [c] Kinetic K_D = k_{off} / k_{on}; k_{on} (k_3) and k_{off} (k_4) values of unlabeled antagonists were generated from [^{3}H]-DPCPX (2.6 nM) competition association assay association assays at 25 ˚C.

Quantification of the binding kinetics of bitopic ligands for the A_1R in the absence or presence of an allosteric modulator by using the competition association assay

The binding kinetics of two in-house synthesized A_1R bitopic ligands were investigated in the competition association assay. These two ligands, i.e., LUF6234 with five-carbon spacer length and LUF6258 with nine-carbon spacer length (Figure 6.1), were previously designed and synthesized as tools for understanding A_1 receptor allosterism.[26] Here we further examined

Table 6.4 | Binding parameters for bitopic ligands and their constituent parts in the absence or presence of PD81,723 at CHOhA$_1$R derived from competition association assays.

Cmpd	k_{on} ($M^{-1}.min^{-1}$)[a]	k^{off} (min^{-1})[a]	*RT (min)*[b]	K_D (nM)[c]
LUF5519	2.0 ± 0.4 x 10^6	1.19 ± 0.19	0.8 ± 0.1	595 ± 92
+ 10 μM PD81,723	2.4 ± 1.4 x 10^6	0.38 ± 0.05	2.6 ± 0.4	158 ± 41
LUF6234 (linker n=5)	5.3 ± 0.7 x 10^4	0.052 ± 0.007	19 ± 3	981 ± 65
+ 10 μM PD81,723	3.1 ± 0.1 x 10^6	0.40 ± 0.05	2.5 ± 0.3	129 ± 13
LUF6258 (linker n=9)	0.8 ± 0.3 x 10^4	0.021 ± 0.008	48 ± 11	2625 ± 810
+ 10 μM PD81,723	3.0 ± 1.4 x 10^4	0.021 ± 0.011	48 ± 15	700 ± 284
+ 33 μM PD81,723	5.8 ± 3.4 x 10^4	0.023 ± 0.014	43 ± 15	397 ± 194
LUF7161	2.7 ± 0.7 x 10^5	1.21 ± 0.32	0.8 ± 0.2	4481 ± 985
+ 10 μM PD81,723	3.8 ± 0.9 x 10^6	0.87 ± 0.21	1.1 ± 0.1	229 ± 45

Data are shown as mean ± s.e.m of three separate experiments each performed in duplicate. [a] k_{on} (k_3) and k_{off} (k_4) of unlabeled A_1R agonists in the absence or presence of an allosteric modulator (PD81,723 or BC-1) were determined in [^{3}H]-DPCPX (2.6 nM) competition association assays. [b] RT (Residence Time) = 1 / k_{off}. [c] Kinetic K_D = k_{off} / k_{on}; k_{on} (k_3) and k_{off} (k_4) values of unlabeled antagonists were generated from [^{3}H]-DPCPX (2.6 nM) competition association assay association assays at 25°C.

the binding kinetics of both compounds and compared their values to the orthosteric ligand LUF5519 in combination with PD81,723 (each representing the orthosteric and allosteric pharmacophore of LUF6234 and LUF6258, respectively; see Figure 6.1 for chemical structures). In the absence of an allosteric modulator, LUF5519 displayed an on-rate of 2.0 ± 0.4 × 10^6 M^{-1}·min^{-1} and off-rate of 1.19 ± 0.19 min^{-1}, which led to an affinity of 595 ± 92 nM (Figure 6.5, Table 6.4). Upon the addition of 10 μM PD81,723, the association rate of LUF5519 (k_{on} = 2.4 ± 1.4 × 10^6 M^{-1}·min^{-1}) did not significantly change while the dissociation rate decreased by approximately three-fold from 1.19 ± 0.19 min^{-1} to 0.38 ± 0.05 min^{-1} (Figure 6.5A and Table 6.4). However, after covalently linking the allosteric and orthosteric pharmacophores, both bitopic ligands demonstrated a significantly decreased association rate in comparison to LUF5519 (LUF6234, 5.3 ± 0.7 × 10^4 M^{-1}·min^{-1} and LUF6258, 0.8 ± 0.3 × 10^4 M^{-1}·min^{-1}), indicative of an extra hurdle for the receptor to accommodate large flexible molecules. With respect to their off-rates, both compounds displayed significantly longer receptor residence times (LUF6234, RT = 19 ± 3 min and LUF6258, RT = 48 ±

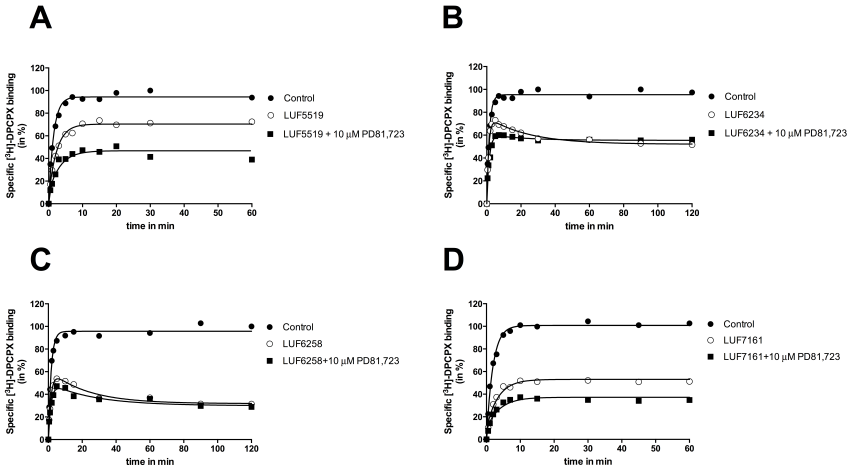


Figure 6.5 | Panel A, [^{3}H]-DPCPX competition association assay in the absence or presence of unlabeled LUF5519 with or without 10 µM PD81,723. Panel B, [^{3}H]-DPCPX competition association assay in the absence or presence of unlabeled LUF6234 with or without 10 µM PD81,723. Panel C, [^{3}H]-DPCPX competition association assay in the absence or presence of unlabeled LUF6258 with or without 10 µM PD81,723. Panel D, [^{3}H]-DPCPX competition association assay in the absence or presence of unlabeled LUF7161 with or without 10 µM PD81,723. Concentrations of 3- to 10-fold K_i of the unlabeled orthosteric ligands were used to obtain the binding data, which were fitted to the equations described in the methods to calculate the k_{on} and k_{off} values of unlabeled ligands. Representative graphs from one experiment performed in duplicate. (See Table 6.4 for kinetic values).

11 min) than LUF5519 (RT = 0.8 ± 0.1 min). Interestingly, the presence of 'external' PD81,723 significantly increased the association rates of both bitopic ligands (LUF6234, k_{on} = 3.1 ± 0.1 × 10^6 M^{-1}·min^{-1}; LUF6258, k_{on} = 3.0 ± 1.4 × 10^4 M^{-1}·min^{-1}), though LUF6258 was less affected than its five-carbon linker analogue. As for the dissociation rate, both bitopic ligands demonstrated different profiles upon the addition of PD81,723: LUF6234's residence time was significantly reduced to 2.5 ± 0.3 min, while LUF6258's residence time was not affected (48 ± 15 min), even after further raising the concentration of PD81,723 to 33 µM (Table 6.4). In addition, we examined the binding kinetics of a newly synthesized monovalent ligand LUF7161 (Figure 6.1), which served as a control, since it contains the orthosteric part and the five-atom linker. It follows from Table 6.4 that LUF7161 had a similar dissociation rate (k_{off} = 1.21 ± 0.32 min^{-1}) as LUF5519, yet its association rate

Table 6.5 | Binding of the monovalent ligand 'c' (k_{+c} = 1 × 10^7 M^{-1}·min^{-1}, k_{-c} = 0.3 min^{-1} and [c] = 100 nM) was simulated during a time lapse of 5 min in the absence or presence of different concentrations of three bitopic ligands 'ab' (their 'microscopic' association and dissociation kinetic constants of both pharmacophores were defined as Examples 1 to 3, input parameters). The 'macroscopic' kinetic binding parameters of the bitopic ligands were calculated by using Equation 12 and 13 or by subjecting the simulated data into the competition association assay.[20]

Example	***Input parameters***[a]				***Calculated parameters***[b]		***Collected parameters***[c]	
	k_{+a} (M^{-1}.min^{-1})	k_{-a} (min^{-1})	k_{+b} (M^{-1}.min^{-1})	k_{-b} (min^{-1})	k_{on} (M^{-1}.min^{-1})	k_{off} (min^{-1})	k_{on} (M^{-1}.min^{-1})	k_{off} (min^{-1})
1	1 x 10^5	1	1 x 10^5	1	2.0 x 10^5	0.069	1.90 x 10^5	0.11
2	1 x 10^5	1	1 x 10^6	1	1.1 x 10^6	0.035	1.04 x 10^6	0.083
3	1 x 10^6	1	1 x 10^5	1	1.1 x 10^6	0.035	1.07 x 10^6	0.036

[a] k_{+a} and k_{+b} are the microscopic association rate constants and k_{-a} and k_{-b} are the microscopic dissociation rate constants of the bitopic ligand, 'ab', for a-A, and b-B binding to the target, 'AB', respectively. [b] The 'macroscopic' kinetic binding parameters of the bitopic ligands were calculated by using Equation 12 and 13. [c] k_{on} and k_{off} values were determined by analyzing the simulated data in the competition association model '*kinetics of competitive binding*'.[20]

to the A_1R was approximately ten-fold lower (k_{on} = 2.7 ± 0.7 × 10^5 M^{-1}·min^{-1}) than LUF5519. Upon the addition of 10 μM PD81,723, the association rate of LUF7161 was 14-fold higher, while its dissociation rate was less affected in comparison to its kinetics in the absence of the allosteric modulator. The other monovalent ligand, i.e., with nine-atom linker (LUF7160), did not display significant radioligand displacement up to concentrations of 33 μM (data not shown), thus its binding kinetics were not determined.

Data simulations and assay validation for determining the bitopic ligands' binding kinetics in the competition association assay

Simulated data were collected by consecutively solving the differential equations in *Methods* (Equations 5-11), which mimic the binding of a radioligand in the absence or presence of a bitopic ligand. Next, the

binding kinetics of the bitopic ligand were analyzed using two methods: 1) by subjecting the defined microscopic kinetic constants (Table 6.5, 'input parameters') into Equation 12 and 13 to obtain the theoretical macroscopic binding parameters (Table 6.5, 'calculated parameters'); 2) by subjecting the simulated data into the model of competition association assay to obtain the 'collected parameters' in Table 6.5. In general, the binding kinetics analyzed by using both methods correlate well with each other. The association rates of the bitopic ligands from the competition association assay are similar to the theoretical values in all three examples. For instance, the collected k_{on} value in Example 1 is 1.90×10^5 $M^{-1}.min^{-1}$, which correlates to its corresponding theoretical k_{on} value of 2.0×10^5 $M^{-1}.min^{-1}$. Likewise, the dissociation rate can be reliably determined by using the competition association assay, although Example 2 demonstrates an approximately two-fold difference between the theoretically calculated k_{off} (0.035 min^{-1}) and the corresponding value from the competition association assay (0.085 min^{-1}), which is robust enough for practical applications. Thus, the competition association assay enables the determination of a bitopic ligand's binding kinetics.

6.4 Discussion

In the present chapter we examined the allosteric modulation of the adenosine A_1 receptor from a kinetic perspective. We used a competition association assay to determine the binding kinetics of several unlabeled orthosteric agonists upon the addition of two allosteric modulators, i.e., PD81,723 and BC-1. The competition association assay offers several, not yet 'tapped' advantages for the investigation of allosteric modulation. Firstly, it enables the measurement of the kinetic characteristics of a probe in an unlabeled form, expanding the availability of orthosteric ligands for probe-dependent investigations. Secondly, the method allows the determination of a complete 'inventory' of binding kinetics. This includes a ligand's association rate, dissociation rate, residence time and the 'kinetic K_D'. These abundant details are very useful to interpret the dynamic interactions between the ligand and receptor, especially given that many allosteric modulators have the propensity to alter the orthosteric ligand's dissociation rates. For instance, upon the addition of PD81,723 or BC-1 the receptor-residence times of CCPA or NECA were prolonged. Such a change can be immediately captured in

the competition association assay from the typical 'overshoot' pattern as in Figure 6.4B or 6.4C, indicating a compound's slower dissociation process than the radioligand.[20] PD81,723 and other GPCR allosteric modulators are known to influence a probe's affinity by changing its dissociation rate.[25,30-33] Their effect on the orthosteric ligand's association rate, however, has been less investigated. Here, by using the competition association assay we found that an allosteric modulator could also change an orthosteric ligands' affinity by influencing its association rate. For instance, CCPA's association rate increased 2.5-fold upon the addition of 10 μM PD81,723, which, together with the four-fold decrease in the dissociation rate, resulted in the overall ten-fold change in CCPA's affinity. We also reaffirmed that the allosteric effect of both A_1R modulators was concentration-dependent, evidenced by the concentration-dependent increase in CCPA's RT (Table 6.3). Moreover, the kinetics of different orthosteric ligands were not equally altered, which reflects the specific feature of GPCR allosteric modulation, the so-called 'probe-dependency'.[13] Such a phenomenon is not only limited to an orthosteric ligand's affinity or potency, the parameters often investigated for GPCR allosterism, but is also reflected in the less examined orthosteric ligand's dissociation and association rate. As evidence, CCPA and NECA's association and dissociation rates were significantly changed upon the addition of 10 μM PD81,723, while not for LUF5834 (Table 6.3). Apparently, all these details of ligand-receptor interaction can be simultaneously obtained by using the competition association approach.

In the present chapter, we furthermore performed a competition association assay with bitopic ligands to study their kinetic behavior. A bitopic ligand is a useful tool to study the molecular mechanism of allosteric modulation.[27] However, interpretation of its binding can be very complex. Different bitopic ligands may display three divergent binding modes: the ligand can be bound to the allosteric site only, to the orthosteric site only, or to both sites simultaneously if the length of the linker is optimal. Moreover, one receptor can be occupied by two bitopic ligands, i.e., one to the allosteric site and the other to the orthosteric site.[26,27,34] A kinetics investigation of the bitopic ligand could add information to an affinity- or potency-based evaluation. Therefore, we selected two previously reported bitopic ligands,[26] namely LUF6234 and LUF6258, and examined their binding kinetics in the present chapter. We found that the theoretically calculated macroscopic kinetics correlated well with the values that were determined by analyzing the simulated data in the competition association assay (Table 6.5). Thus,

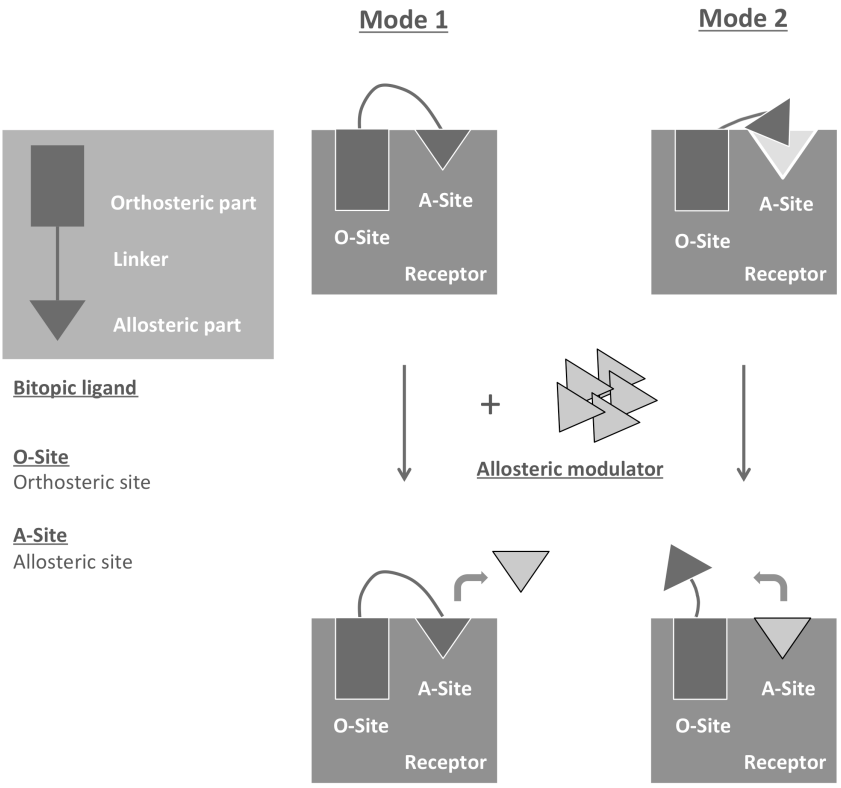


Figure 6.6 | Proposed diagram of two distinct binding modes for the bitopic ligands in the absence or presence of further added allosteric modulator. Mode 1: the linker length of a bitopic is optimal to occupy both orthosteric and allosteric sites of the receptor. Mode 2: the linker length of a bitopic is sufficient to occupy both sites on the receptor, yet in a non-optimal manner. Upon the addition of excess allosteric modulator, the monovalent ligand can occupy the allosteric site on the receptor and prevent the rebinding of the freshly dissociated allosteric pharmacophore in Mode 2 due to the bitopic ligand's less optimal binding pose. In contrast, the binding of the bitopic ligand with optimal linker length (Mode 1) is less affected in the presence of the monovalent ligand.

the competition association assay enables sufficient quantification of the net changes of the bitopic ligands' macroscopic binding kinetics. Next, we observed that due to covalently linking the orthosteric and allosteric pharmacophores the dissociation rates of both compounds were much slower than their orthosteric constituent, LUF5519, in the presence of PD81,723 (Table 6.4). Such phenomenon can be explained by the fact that a freshly dissociated pharmacophore is obliged to remain in 'forced proximity' to its cognate binding site as long as the tethered, companion pharmacophore is still bound. This favors its rebinding to that site, thereby significantly slowing down the net dissociation process.[29,35] To our knowledge, our present observation of the gained target-residence time of the bitopic ligand provides the first experimental evidence for such rebinding mechanism of low molecular weight ligands.

To further understand the two bitopic ligands' mode of binding to the A_1R, we examined the effect of the addition of 'external' PD81,723 in studies with the bitopic ligand. In this way the monovalent modulator should be able to occupy the allosteric site on the receptor and thus prevent the rebinding of the freshly dissociated allosteric pharmacophore. Interestingly, both association and dissociation of LUF6234 became faster compared to its kinetics in the absence of PD81,723, indicative of competition between the allosteric part of LUF6234 and the 'free' allosteric modulator at the A_1R allosteric binding site. In contrast, the dissociation rate of LUF6258 was unaffected upon the addition of 10 μM PD81,723, which was also the case when we raised the concentration of PD81,723 to 33 μM. Further increasing the concentration of the allosteric modulator may allow it to displace the allosteric pharmacophore of LUF6258 from the A_1R allosteric site.[35] However, we did not attempt to do so, given that PD81,723 also significantly displaces the binding of an orthosteric ligand at concentrations of 100 μM and higher,[36] while solubility is an issue too. Apparently, the monovalent ligand PD81,723 is less efficient in preventing the rebinding of the nine-linker compound than its five-linker analogue at the same concentration. Such a discrepancy is most likely due to the flexibility of their linkers, where the nine-carbon linker has more freedom of rotation and thus increased the likelihood that both pharmacophores can tightly interact with the receptor (Figure 6.6, Mode 1). In contrast, the shorter five-carbon linker might be able to bridge both allosteric and orthosteric sites simultaneously, yet in a non-optimal manner due to its short length and thus higher energy constraint (Figure 6.6, Mode 2).

Notably, our proposed binding modes of the two bitopic ligands expand on the conclusions previously drawn by Narlawar *et al.*[26] where the authors suggested that the bitopic ligand with linker length of five (LUF6234) failed to completely occupy both allosteric site and orthosteric site while the one with linker length of nine (LUF6258) was able to occupy both sites. This conclusion was based on the hypothesis that if the linker is of sufficient length to allow simultaneous occupancy of the allosteric and orthosteric binding sites, the addition of further PD81,723 will have a minimal effect on the potency of the bitopic ligand, while for the bitopic ligand with insufficient linker length affinity will be significantly increased.[26] Following this hypothesis, we would have reached the same conclusion if merely affinity was taken into consideration, since we also observed that LUF6234 displayed a strongly increased affinity upon the addition of PD81,723, while less so for LUF6258. However, it is also noteworthy from our study that both LUF6234 and LUF6258 displayed significantly increased receptor residence times compared to that of the monovalent ligand in the presence of PD81,723 (Table 6.4). Such a result strongly indicates that both allosteric and orthosteric sites on the A_1R were simultaneously occupied for both compounds, which appeared to induce a synergistic effect—greater than simply combining two monovalent ligands—on the global receptor conformation. If LUF6234's linker length had been insufficient to occupy both sites, it should have had a residence time comparable to the monovalent LUF7161, which in fact is not the case for this bitopic ligand. Apparently, investigation of binding kinetics adds significantly to understanding the molecular mechanism of the binding of a bitopic ligand.

In summary, we validated and showed the use of a competition association assay at the hA_1R to determine the allosteric modulation of the binding kinetics of different A_1R agonists. Our data suggests that the influence of an A_1R allosteric enhancer (positive allosteric modulator) on the binding kinetics of the orthosteric agonist is dependent on the concentration of the allosteric modulator and the nature of the orthosteric ligand and that both the association and dissociation rates can be affected. Furthermore, we examined the binding kinetics of two bitopic ligands and investigated their binding mode. The relevance of the competition association assay for bitopic ligands' binding kinetics was also explored by analyzing a series of simulations and comparing the result to the theoretically determined kinetics. Taken together, the competition association assay enables accurate determination of the binding kinetics of an orthosteric ligand, whether radiolabeled or no, in the

absence or presence of an allosteric modulator. We believe that this approach will have general applicability for the study of allosteric modulation at other GPCRs as well.

References:

1. Fredholm BB, IJzerman AP, Jacobson KA, Linden J, Müller CE. International Union of Basic and Clinical Pharmacology. LXXXI. Nomenclature and classification of adenosine receptors--an update. *Pharmacol Rev* 2011;63(1):1-34.
2. Gao ZG, Jacobson KA. Emerging adenosine receptor agonists. *Expert Opin Emerg Drugs* 2007;12(3):479-492.
3. Gao ZG, Kim SK, IJzerman AP, Jacobson KA. Allosteric modulation of the adenosine family of receptors. *Mini Rev Med Chem* 2005;5(6):545-553.
4. Göblyös A, IJzerman AP. Allosteric modulation of adenosine receptors. *Biochim Biophys Acta* 2011;1808(5):1309-1318.
5. Müller CE, Schiedel AC, Baqi Y. Allosteric modulators of rhodopsin-like G protein-coupled receptors: opportunities in drug development. *Pharmacol Ther* 2012;135(3):292-315.
6. Gregory KJ, Sexton PM, Christopoulos A. Allosteric modulation of muscarinic acetylcholine receptors. *Curr Neuropharmacol* 2007;5(3):157-167.
7. Davie BJ, Christopoulos A, Scammells PJ. Development of M_1 mAChR Allosteric and Bitopic Ligands: Prospective Therapeutics for the Treatment of Cognitive Deficits. *ACS Chem Neurosci* 2013;4(7):1026-1048.
8. Keov P, Sexton PM, Christopoulos A. Allosteric modulation of G protein-coupled receptors: a pharmacological perspective. *Neuropharmacology* 2011;60(1):24-35.
9. Wang CI, Lewis RJ. Emerging opportunities for allosteric modulation of G-protein coupled receptors. *Biochem Pharmacol* 2013;85(2):153-162.
10. Gao ZG, Jacobson KA. Allosteric modulation and functional selectivity of G protein-coupled receptors. *Drug Discov Today Technol* 2013;10(2):e237-e243.
11. Melancon BJ, Hopkins CR, Wood MR, Emmitte KA, Niswender CM, Christopoulos A, Conn PJ, Lindsley CW. Allosteric modulation of seven transmembrane spanning receptors: theory, practice, and opportunities for central nervous system drug discovery. *J Med Chem* 2012;55(4):1445-1464.
12. Christopoulos A, Kenakin T. G protein-coupled receptor allosterism and complexing. *Pharmacol Rev* 2002;54(2):323-374.
13. Christopoulos A. Allosteric binding sites on cell-surface receptors: novel targets for drug discovery. *Nat Rev Drug Discov* 2002;1(3):198-210.
14. Zhang R, Monsma F. Binding kinetics and mechanism of action: toward the discovery and development of better and best in class drugs. Expert Opin Drug Discov 2010;5(11):1023-1029.
15. Copeland RA, Pompliano DL, Meek TD. Drug-target residence time and its implications for lead optimization. *Nat Rev Drug Discov* 2006;5(9):730-739.
16. May LT, Self TJ, Briddon SJ, Hill SJ. The effect of allosteric modulators on the kinetics of agonist-G protein-coupled receptor interactions in single living cells. *Mol Pharmacol* 2010;78(3):511-523.
17. Kostenis E, Mohr K. Two-point kinetic experiments to quantify allosteric effects on radioligand

dissociation. *Trends Pharmacol Sci* 1996;17(8):280-283.
18. De Amici M, Dallanoce C, Holzgrabe U, Trankle C, Mohr K. Allosteric ligands for G protein-coupled receptors: a novel strategy with attractive therapeutic opportunities. *Med Res Rev* 2010;30(3):463-549.
19. Guo D, van Dorp EJ, Mulder-Krieger T, van Veldhoven JP, Brussee J, IJzerman AP, Heitman LH. Dual-point competition association assay: a fast and high-throughput kinetic screening method for assessing ligand-receptor binding kinetics. *J Biomol Screen* 2013;18(3):309-320.
20. Motulsky HJ, Mahan LC. The kinetics of competitive radioligand binding predicted by the law of mass action. *Mol Pharmacol* 1984;25(1):1-9.
21. Lohse MJ, Klotz KN, Schwabe U, Cristalli G, Vittori S, Grifantini M. 2-Chloro-*N*-6-cyclopentyladenosine - a highly selective agonist at A_1 adenosine receptors. *Naunyn-Schmiedeberg's Arch Pharmacol* 1988;337(6):687-689.
22. Müller CE. A1 adenosine receptors and their ligands: overview and recent developments. *Farmaco* 2001;56(1-2):77-80.
23. Beukers MW, Chang LC, von Frijtag Drabbe Kunzel JK, Mulder-Krieger T, Spanjersberg RF, Brussee J, IJzerman AP. New, non-adenosine, high-potency agonists for the human adenosine A_{2B} receptor with an improved selectivity profile compared to the reference agonist *N*-ethylcarboxamidoadenosine. *J Med Chem* 2004;47(15):3707-3709.
24. Romagnoli R, Baraldi PG, Carrion MD, Cara CL, Cruz-Lopez O, Iaconinoto MA, Preti D, Shryock JC, Moorman AR, Vincenzi F, Varani K, Andrea Borea P. Synthesis and biological evaluation of 2-amino-3-(4-chlorobenzoyl)-4-[*N*-(substituted) piperazin-1-yl]thiophenes as potent allosteric enhancers of the A_1 adenosine receptor. *J Med Chem* 2008;51(18):5875-5879.
25. Bruns RF, Fergus JH. Allosteric enhancement of adenosine A_1 receptor binding and function by 2-amino-3-benzoylthiophenes. *Mol Pharmacol* 1990;38(6):939-949.
26. Narlawar R, Lane JR, Doddareddy M, Lin J, Brussee J, IJzerman AP. Hybrid ortho/allosteric ligands for the adenosine A_1 receptor. *J Med Chem* 2010;53(8):3028-3037.
27. Lane JR, Sexton PM, Christopoulos A. Bridging the gap: bitopic ligands of G-protein-coupled receptors. *Trends Pharmacol Sci* 2013;34(1):59-66.
28. Copeland RA. *Evaluation of enzyme inhibitors in drug discovery: A guide for medicinal chemists and pharmacologists*. New York: Wiley; 2005. 1-265 p.
29. Vauquelin G. Simplified models for heterobivalent ligand binding: when are they applicable and which are the factors that affect their target residence time. *Naunyn-Schmiedeberg's Arch Pharmacol* 2013:1-14.
30. Bhattacharya S, Linden J. The allosteric enhancer, PD 81,723, stabilizes human A1 adenosine receptor coupling to G proteins. Biochim Biophys Acta 1995;1265(1):15-21.
31. Gao ZG, Van Muijlwijk-Koezen JE, Chen A, Muller CE, IJzerman AP, Jacobson KA. Allosteric modulation of A_3 adenosine receptors by a series of 3-(2-pyridinyl)isoquinoline derivatives. *Mol Pharmacol* 2001;60(5):1057-1063.
32. Lazareno S, Birdsall NJ. Detection, quantitation, and verification of allosteric interactions of agents with labeled and unlabeled ligands at G protein-coupled receptors: interactions of strychnine and acetylcholine at muscarinic receptors. *Mol Pharmacol* 1995;48(2):362-378.
33. Bauer M, Chicca A, Tamborrini M, Eisen D, Lerner R, Lutz B, Poetz O, Pluschke G, Gertsch J. Identification and quantification of a new family of peptide endocannabinoids (Pepcans) showing negative allosteric modulation at CB_1 receptors. *J Biol Chem* 2012;287(44):36944-36967.
34. Steinfeld T, Mammen M, Smith JAM, Wilson RD, Jasper JR. A novel multivalent ligand that bridges the allosteric and orthosteric binding sites of the M_2 muscarinic receptor. *Mol Pharmacol*

2007;72(2):291-302.
35. Vauquelin G, Charlton SJ. Exploring avidity: understanding the potential gains in functional affinity and target residence time of bivalent and heterobivalent ligands. *Br J Pharmacol* 2013;168(8):1771-1785.
36. Van der Klein PA, Kourounakis AP, IJzerman AP. Allosteric modulation of the adenosine A_1 receptor. Synthesis and biological evaluation of novel 2-amino-3-benzoylthiophenes as allosteric enhancers of agonist binding. *J Med Chem* 1999;42(18):3629-3635.

Chapter 7

Conclusions and perspectives

About this chapter

This thesis focuses on an emerging trend in medicinal chemistry, i.e. drug-target residence time. In this concluding chapter, new insights gained from case studies at the adenosine A_1 and A_{2A} receptors are elaborated on, and suggestions for future investigations in this field are presented.

7.1 Conclusions from this thesis

In the present thesis we have characterized the binding kinetics of several series of compounds on the adenosine A_1 and A_{2A} receptors. The spectrum of their residence times varies significantly, ranging from a few seconds to several minutes or hours. For instance, the residence times of 35 A_1R antagonists lasted from 20 sec to 48 min at room temperature (Chapter 3). Likewise, the series of ZM241385 derivatives displayed divergent residence times at the $A_{2A}R$, from 2 min to more than 5 h at 4 °C (chapter 4). Such values, in general, agree well with similar ranges of other ligand-GPCR residence times, which have been summarized in Chapter 2. One example is aprepitant, an NK_1 receptor antagonist for chemotherapy-induced emesis. It has a target-residence time of 222 min at 25 °C.[1] Of note is that the ligands having receptor residence times longer than one or two hours are scarce for the adenosine receptors. So far we have not identified a residence time lasting as long as tiotropium (>24 h at the M_3 receptor, 37 °C) or PF-4850890 (6.79 h at the CRF_1 receptor, 25 °C).[2,3] It is worth mentioning that ZM241385 displayed a target-residence time of 2.1 min at 25 °C, which was nearly 30-fold shorter than its value (72 min) at 5 °C (Chapter 5). We speculate that the observed relatively short RT of adenosine receptor ligands may be derived from the nature of the ligands' binding modes. Both tiotropium and PF-4850890 bind deeply into their respective receptors[4,5] and the binding cavities are covered by relatively large extracellular loops. In contrast, many adenosine receptor ligands, e.g., ZM241385 or UK432,097, are bound closer to the extracellular domain of the receptor, which, in addition, consists of relatively short and flexible extracellular loops.[6,7]

The association rates of the adenosine receptor ligands also vary substantially. Their values are across several orders-of-magnitude. Such information greatly updates our current knowledge, which has taken the on-rate to be diffusion-limited.[8] We have found that this general assumption is not necessarily valid. For instance, the $A_{2A}R$ antagonists' on-rates varied significantly from 0.10 $nM^{-1}\cdot min^{-1}$ to 0.0057 $nM^{-1}\cdot min^{-1}$ (Chapter 4)—more than two orders-of-magnitude from the diffusion-limited value (approximately $10^{10}\,M^{-1}\cdot min^{-1}$).[9] The latter only describes the transport rate of one binding partner (e.g. a ligand) through the reaction solution toward the other (e.g. a receptor), which is quite different from the association rate (k_{on})

of the binding process (formation of the ligand-receptor binary complex). The former depends on the viscosity of the medium, while the latter depends on the reaction mechanism.[10] For the association rate of agonists, their values ranged from 5.0×10^4 $M^{-1}\cdot min^{-1}$ to 1.6×10^7 $M^{-1}\cdot min^{-1}$ at the adenosine A_{2A} receptor (chapter 5), which are far from the diffusion-limited rate as well. Additionally, a ligand for a membrane-bound receptor could also partition into the membrane and then diffuse laterally to the binding site, a proposed mechanism for lipophilic compounds associating with the corticotropin-releasing factor receptor 1.[5] Apparently, an association rate can be far from the diffusion-limited rate. It is therefore necessary to examine both the on- and off-rate of a ligand for an optimized receptor interaction.

It is also of great interest to compare our results at the adenosine receptors with kinases or other enzymes. Of particular note is the induced, significant target isomerization upon ligand binding that is often encountered for enzyme-inhibitor interactions, a state also known as the transition-state. Such alternation of target conformations could yield a tightly bound binary complex, and thus "lock" the ligand for a long duration to exert its inhibitory effect. One example is GW572016 (Lapatinib), a tyrosine kinase inhibitor targeting epidermal growth factor receptor (EGFR) for cancer treatment.[11] It has a very slow off-rate from the purified intracellular domains of EGFR (0.0023 min^{-1}, equivalent to a half-life of 5 h) compared with OSI-774 and another EGFR selective inhibitor, ZD-1839 (Iressa). The latter two have a rapid off-rate, which translates to a half-life of less than 10 min. The difference in their binding kinetics was reflected in the distinct enzyme-inhibitor crystal structures, where GW572016 was in an inactive-like conformation while OSI-774 and ZD-1839 were not. Ligands binding to the adenosine receptors may also select a certain conformation, which comes to mind when considering the fast exchange of receptor states between the G protein-coupled and uncoupled forms. However, it is important to point out that such state transformations of GPCRs are much faster than the 'induced-fit' mechanism observed in the enzyme-inhibitor interactions. As evidence, a plot of k_{obs} values of [^{3}H]-NECA vs [^{3}H]-NECA concentrations displayed a significant linear correlation ($r^2 = 0.96$, $p < 0.0001$) at the adenosine A_{2A} receptor, indicative of a one-step association and dissociation process, quite distinct from the 'induced-fit' mechanism (which would yield a hyperbolic relationship).[8]

Several binding kinetics assays have been used in the present thesis. One of the more traditional assays is the direct kinetic radioligand binding assay. It

is a straightforward method enabling robust and quantitative measurements of ligand-receptor binding kinetics. However, this assay's low-throughput format and the technical difficulty of radiolabeling limit its application in kinetic profiling. The competition association assay based on the model of Motulsky and Mahan is a good alternative for the quantitative measurement of unlabeled ligands' binding kinetics.[12] It has been extensively applied in this thesis from Chapter 3 to Chapter 6 to examine the on- and off-rates of ligands of interest. We have also adopted the competition association assay and modified it into a fast, high-throughput screening assay, requiring only two assay points per compound (Chapter 3). This assay can be of general application for kinetics studies at other drug targets as well.

Kinetic profiling of a ligand-receptor interaction is an important addition to the classic equilibrium-based pharmacological evaluations. Combining both kinetics and equilibrium-based metrics can provide extra information for our understanding of complex pharmacological concepts, such as efficacy/intrinsic activity and allosteric modulation. An attempt to explain different agonists' functional efficacy was presented in Chapter 5, where we found that a sustained target-residence time was important for a higher level of cell signaling, at least for the adenosine A_{2A} receptor. Likewise, we gained more molecular understanding of the phenomenon of allosteric modulation at the A_1R. We learned that an allosteric modulator could alter an orthosteric ligand's affinity not only via influencing its dissociation rate but also via changing its association rate. Additionally, linking an allosteric modulator with an orthosteric ligand into one molecule (a so-called bitopic ligand) displayed a synergistic effect on residence time, which was much longer than the combination of two monovalent ligands. Apparently, the analysis of ligand-receptor binding kinetics can add a wealth of knowledge to current pharmacological receptor concepts.

7.2 Future perspectives

The studies outlined in this thesis aimed to explore ligand-receptor binding kinetics at G protein-coupled receptors, by a careful examination of the adenosine A_1 and A_{2A} receptors. In the (near) future, more knowledge can be obtained by further investigating the molecular basis of receptor kinetics, facilitated by the development of new technologies for rapid, online assessment

of kinetic profiles of new compounds. Furthermore, translating the *in vitro* binding kinetics to *in vivo* effects of future drug candidates targeting the adenosine receptors (ARs) could potentially decrease drug attrition rates and eventually lead to the discovery of more efficacious and safer medicines.

Molecular understanding

a) Physiochemical and hydration properties of dynamic ligand-receptor interactions

For future investigations the combination of binding kinetics, structural biology and molecular dynamics may greatly advance our understanding of the dynamic process of ligand-receptor interactions. For instance, we could compute physicochemical properties and hydration properties of the protein target, especially to map the binding sites that trap water molecules in hydrophobic surroundings. Displacing such less stable, 'unhappy', water molecules could elicit a favorable binding state of the receptor, compared to its (unliganded) apo states, hence influencing a ligand's residence time.[13] It is thus of great interest to take the explicit water molecules into consideration for future molecular understanding of the dynamic process of ligand-receptor interactions. The important role of water molecules was also addressed in recent molecular dynamics simulations at the β_2 receptor and the muscarinic M_3 receptor.[4,14,15] It was revealed that during the binding and unbinding process tremendous hydration and dehydration of both the ligand and the receptor was involved, which appears to be a critical process of great generality for a ligand's association to and egress from its receptor. Structure-based drug discovery aimed for kinetically optimized compounds (e.g. compounds displacing 'unhappy' water molecules) can now be performed at the $A_{2A}R$ given the availability of a high-resolution crystal structure (PDB: 4EIY) and the more than 60 water molecules contained in the transmembrane domains.[6] Moreover, the recent boom of adenosine A_{2A} receptor crystal structures[6,7,16,17] may greatly facilitate the molecular dynamic simulations of the ligand-receptor interactions. It was suggested that for the M_3R and the β-adrenergic receptors their ligands traversed a dominant two-step pathway

as they bind to or unbind from the receptor, initially making contact with a vestibule on the receptors' extracellular surface.[4,14] Such observations could be common for other GPCRs as well. It will be of great interest to perform similar molecular dynamic simulations at the adenosine receptors for an atomic-level description of its kinetic process.

b) New pharmacological models to understand the nature of functional efficacy

In chapter 5, we have illustrated that the intrinsic efficacy of an A_{2A} receptor agonist is inextricably linked to its receptor residence time. This gained knowledge aids us to further understand cell signaling upon ligand stimulation. Interestingly, one of the first attempts to define drug action from a kinetic perspective dates back to the early 1960s, when Paton proposed the 'rate theory' for a mechanistic explanation of efficacy.[18] However, only few studies continued on the track of kinetics since then,[19-21] which was later prevailed by other models that describes efficacy in terms of the ability to stabilize an active receptor conformation[10,11] or a more recently proposed 'stochastic switch' of ligand binding between functionally distinct orientiations.[22] Of note is that the kinetics of agonist binding and the subsequent conformational change of its receptor can influence each other. The binding of an agonist can induce receptor conformational changes and these changes potentially influence the ligand's residence time, for instance, via the receptor isomerizing into a high-affinity state and thus effectively locking the agonist.[23,24] In our view both conformation-stabilization models and kinetic models are complementary to each other rather than contrasting. Thus, an integration of both elements may better explain the nature of functional efficacy.

Furthermore, still little is known about the pharmacological consequences of cell/tissue/body exposure to agonists with a spectrum of receptor residence times. Will long receptor-residence time ligands cause higher levels of receptor desensitization or internalization? What is the connection between agonist-receptor binding kinetics and the downstream signaling kinetics (i.e. link to biased signaling)? These are important questions for future mechanistic investigations. The results thereof will most likely affect the medicinal chemistry strategy aiming for long or short receptor residence time in the future.

c) Mathematical models for theoretical investigations of ligand-receptor binding kinetics

To further increase current molecular understanding of ligand-receptor binding kinetics, new theoretical models are also needed. A mathematical model and simulation have been presented in Chapter 6 for validation of the competition association assay. We used it to determine a bitopic ligand's binding kinetics, for which it provided a powerful theoretical support. The strength of mathematical simulations is not restricted to validating experimental data. It also facilitates our understanding of complicated ligand-receptor interactions especially for those experimental observations otherwise difficult to interpret. For instance, Vauquelin and colleagues reported several case studies where mathematical simulations were extensively used to examine the binding kinetics of a bitopic/bivalent ligand.[25-27] Another example was reported by Charlton and colleagues in which they simulated the different onset of action of two M_3R antagonists that bear distinct kinetic profiles.[28] More theoretical investigations of ligand-receptor binding kinetics should be performed in the future.

New technologies for assessing binding kinetics

An overview of current technologies for accessing ligand-receptor binding kinetics was described in Chapter 2. In general, most of kinetic profiling techniques rely heavily on radioligand binding or functional reversibility assays; the latter in a qualitative manner. New tools are welcome to satisfy the emerging requests in optimizing binding kinetics. Currently, there are several technologies that could be evaluated for future binding kinetics investigations. For instance, several groups recently reported the use of fluorescently labeled ligands in combination with confocal microscopy equipped with high flow perfusion to study ligand-receptor binding kinetics at the level of single living cells.[29,30] Such tools enable the visualization and quantification of time-dependent receptor occupancy at the cellular level. Other assay technologies can also be used for further development including fourier transform infrared spectroscopy (FTIR). This technology simultaneously collects spectral data in a wide spectral range, which can be translated into dynamic conformational

changes upon ligand-receptor or protein-protein interactions at an atomic level.[31] One application of the FTIR technology in the field of GPCRs was reported by Elgeti *et al*. to study the conformational diversity of rhodopsin in a membrane environment—a study that extended the static picture provided by the available crystal structures.[32] Cell-based label-free technologies, such as xCELLigence described in Chapter 5, enable real-time, online signal readout upon ligand addition—a feature that might be used in binding kinetics characterizations, as well. Additionally, surface plasmon resonance (SPR) is also a good tool to measure ligand-receptor binding kinetics, which has been well reviewed by Nunez *et al*.[33] This assay is complementary to classical radioligand binding assays when a radioligand is not available. Of note is the current difficulty in the purification of target proteins from a membrane environment for the assay set-up—a technical bottleneck that needs to be overcome for its general application. It is also worth mentioning that applications of the above-mentioned new technologies might be limited to low throughput assay formats due to inherent technical difficulties. For a high-throughput format testing, one could consider scintillation proximity assay (SPA) or the recently developed Tag-lite® platform, avoiding a wash or filtration step as in traditional radioligand binding studies. Both assays allow continuous, multiple reads from one sample. The application of these two technologies has been exemplified at the GnRH receptor (SPA) and at the dopamine D_2 receptor (Tag-lite® platform), respectively.[34,35]

Translation of *in vitro* binding kinetics to *in vivo* evaluation

Translating *in vitro* binding kinetics into an *in vivo* setting is essential for the prediction of drug efficacy and safety. Such a progress, needless to say, is quite difficult and complex. Two major issues need to be taken into account, which are addressed as follows.

1) There are mismatches in binding kinetics between human and laboratory animal species. An expected margin of safety in one species could possibly disappear in human if on- /off-rates at the target vary in different species. On the other hand, a compound discarded due to a poor margin of safety or selectivity in animal models could be adequately selective for the desired over the unwanted effects in human. Such variation in ligand-receptor binding kinetics would be particularly important when efficacy and safety

studies are conducted in different species. Thus, we suggest including the investigation of ligand-receptor binding kinetics—at least for those candidate compounds progressing into (pre-) clinical phases—in those species that are anticipated in later proof-of-concept testing.

2) The *in vivo* duration of drug action is not only dependent on macroscopic pharmacokinetic properties and long-lasting target binding but is also influenced by target rebinding. The local environment of many effect compartments may largely prevent the diffusion of free drug molecules moving away from their target. This could result in consecutive (re-)binding to the same target and/or targets nearby even when the drug's concentration in the bulk phase has already dropped to near-zero levels.[36,37] In light of this, one could consider examining ligand-receptor binding kinetics in more physiological relevant conditions, for instance, by using intact (primary) cells and assay conditions reflecting those *in vivo* (e.g. buffer, temperature, pH).[28,38] Data obtained under such circumstances could establish a bridge between the *in vitro* and *in vivo* setting and thus help their translation.

It is worth mentioning that there is not always a direct link between slow dissociation and long-lasting *in vivo* target engagement, as the rate of free drug elimination from the effect compartment is also a key influencing factor—a finding commented on by several groups.[10,36,39,40] A collection of data sets from isolated cells, tissues, and animal models will provide more information.

7.3 Final note

Ligand-receptor binding kinetics is increasingly recognized to play a pivotal role in the early phase of drug design and discovery. In this thesis, we extensively investigated the ligand-receptor binding kinetics, particularly residence time, at the adenosine A_1 and A_{2A} receptors. Our case studies at these two prototypical GPCRs demonstrate that binding kinetics as an emerging paradigm can provide additional information of drug-target interactions at the molecular level.

We propose that a better molecular understanding of binding kinetics is needed to aid the development of drug candidates with optimized kinetics. We also anticipate the ensuing emergence of new technologies enabling rapid assessment of a compound's binding kinetics in the future. Linking

these findings in *in vitro* settings to an existing data set of *ex vivo* / *in vivo* experiments may provide an evaluation scheme that is more predictive for drug efficacy and safety. Hopefully, this thesis will be an impetus for further binding kinetics-directed research in the (near) future.

References:

1. Hale JJ, Mills SG, MacCoss M, Finke PE, Cascieri MA, Sadowski S, Ber E, Chicchi GG, Kurtz M, Metzger J, Eiermann G, Tsou NN, Tattersall FD, Rupniak NM, Williams AR, Rycroft W, Hargreaves R, MacIntyre DE. Structural optimization affording 2-(*R*)-(1-(*R*)-3,5-bis(trifluoromethyl) phenylethoxy)-3-(*S*)-(4-fluoro)phenyl-4- (3-oxo-1,2,4-triazol-5-yl)methylmorpholine, a potent, orally active, long-acting morpholine acetal human NK-1 receptor antagonist. *J Med Chem* 1998;41(23):4607-4614.
2. Ramsey SJ, Attkins NJ, Fish R, van der Graaf PH. Quantitative pharmacological analysis of antagonist binding kinetics at CRF_1 receptors *in vitro* and *in vivo*. *Br J Pharmacol* 2011;164(3):992-1007.
3. Casarosa P, Bouyssou T, Germeyer S, Schnapp A, Gantner F, Pieper M. Preclinical evaluation of long-acting muscarinic antagonists: comparison of tiotropium and investigational drugs. *J Pharmacol Exp Ther* 2009;330(2):660-668.
4. Kruse AC, Hu J, Pan AC, Arlow DH, Rosenbaum DM, Rosemond E, Green HF, Liu T, Chae PS, Dror RO, Shaw DE, Weis WI, Wess J, Kobilka BK. Structure and dynamics of the M_3 muscarinic acetylcholine receptor. *Nature* 2012;482(7386):552-556.
5. Hollenstein K, Kean J, Bortolato A, Cheng RK, Dore AS, Jazayeri A, Cooke RM, Weir M, Marshall FH. Structure of class B GPCR corticotropin-releasing factor receptor 1. *Nature* 2013;499(7459):438-443.
6. Liu W, Chun E, Thompson AA, Chubukov P, Xu F, Katritch V, Han GW, Roth CB, Heitman LH, IJzerman AP, Cherezov V, Stevens RC. Structural basis for allosteric regulation of GPCRs by sodium ions. *Science* 2012;337(6091):232-236.
7. Xu F, Wu H, Katritch V, Han GW, Jacobson KA, Gao ZG, Cherezov V, Stevens RC. Structure of an agonist-bound human A_{2A} adenosine receptor. *Science* 2011;332(6027):322-327.
8. Tummino PJ, Copeland RA. Residence time of receptor-ligand complexes and its effect on biological function. *Biochemistry* 2008;47(20):5481-5492.
9. Jorg M, Agostino M, Yuriev E, Mak FS, Miller ND, White JM, Scammells PJ, Capuano B. Synthesis, molecular structure, NMR spectroscopic and computational analysis of a selective adenosine A(2A) antagonist, ZM 241385. *Struct Chem* 2013;24(4):1241-1251.
10. Vauquelin G, Packeu A. Ligands, their receptors and ... plasma membranes. *Mol Cell Endocrinol* 2009;311(1-2):1-10.
11. Wood ER, Truesdale AT, McDonald OB, Yuan D, Hassell A, Dickerson SH, Ellis B, Pennisi C, Horne E, Lackey K, Alligood KJ, Rusnak DW, Gilmer TM, Shewchuk L. A unique structure for epidermal growth factor receptor bound to GW572016 (Lapatinib): relationships among protein conformation, inhibitor off-rate, and receptor activity in tumor cells. *Cancer Res*

2004;64(18):6652-6659.
12. Motulsky HJ, Mahan LC. The kinetics of competitive radioligand binding predicted by the law of mass action. *Mol Pharmacol* 1984;25(1):1-9.
13. Mason JS, Bortolato A, Congreve M, Marshall FH. New insights from structural biology into the druggability of G protein-coupled receptors. *Trends Pharmacol Sci* 2012;33(5):249-260.
14. Dror RO, Pan AC, Arlow DH, Borhani DW, Maragakis P, Shan Y, Xu H, Shaw DE. Pathway and mechanism of drug binding to G-protein-coupled receptors. *Proc Natl Acad Sci U S A* 2011;108(32):13118-13123.
15. Pan AC, Borhani DW, Dror RO, Shaw DE. Molecular determinants of drug-receptor binding kinetics. *Drug Discov Today* 2013;18(13-14):667-673.
16. Jaakola VP, Griffith MT, Hanson MA, Cherezov V, Chien EY, Lane JR, IJzerman AP, Stevens RC. The 2.6 angstrom crystal structure of a human A_{2A} adenosine receptor bound to an antagonist. *Science* 2008;322(5905):1211-1217.
17. Lebon G, Warne T, Edwards PC, Bennett K, Langmead CJ, Leslie AG, Tate CG. Agonist-bound adenosine A_{2A} receptor structures reveal common features of GPCR activation. *Nature* 2011;474(7352):521-525.
18. Paton WD. A Theory of Drug Action Based on Rate of Drug-Receptor Combination. *Proc R Soc Ser B-Bio* 1961;154(954):21-+.
19. Leff P. The two-state model of receptor activation. *Trends Pharmacol Sci* 1995;16(3):89-97.
20. Samama P, Cotecchia S, Costa T, Lefkowitz RJ. A mutation-induced activated state of the beta 2-adrenergic receptor. Extending the ternary complex model. *J Biol Chem* 1993;268(7):4625-4636.
21. Weiss JM, Morgan PH, Lutz MW, Kenakin TP. The cubic ternary complex receptor-occupancy model. III. resurrecting efficacy. J *Theor Biol* 1996;181(4):381-397.
22. Bock A, Chirinda B, Krebs F, Messerer R, Batz J, Muth M, Dallanoce C, Klingenthal D, Trankle C, Hoffmann C, De Amici M, Holzgrabe U, Kostenis E, Mohr K. Dynamic ligand binding dictates partial agonism at a G protein-coupled receptor. *Nat Chem Biol* 2014;10(1):18-20.
23. Sykes DA, Dowling MR, Charlton SJ. Exploring the mechanism of agonist efficacy: a relationship between efficacy and agonist dissociation rate at the muscarinic M_3 receptor. Mol Pharmacol 2009;76(3):543-551.
24. Copeland RA. Conformational adaptation in drug-target interactions and residence time. *Future Med Chem* 2011;3(12):1491-1501.
25. Vauquelin G, Charlton SJ. Exploring avidity: understanding the potential gains in functional affinity and target residence time of bivalent and heterobivalent ligands. *Br J Pharmacol* 2013;168(8):1771-1785.
26. Vauquelin G. Simplified models for heterobivalent ligand binding: when are they applicable and which are the factors that affect their target residence time. *Naunyn-Schmiedeberg's Arch Pharmacol* 2013.
27. Vauquelin G, Bricca G, Van Liefde I. Avidity and positive allosteric modulation/cooperativity act hand in hand to increase the residence time of bivalent receptor ligands. Fundam Clin Pharm 2013. Doi: 10.1111/fcp.12052.
28. Sykes DA, Dowling MR, Leighton-Davies J, Kent TC, Renard E, Trifilieff A, Charlton SJ. The influence of receptor kinetics on the onset and duration of action, and the therapeutic index of NVA237 and tiotropium. *J Pharmacol Exp Ther* 2012; 343(2):520-8
29. Hoffmann C, Gaietta G, Bunemann M, Adams SR, Oberdorff-Maass S, Behr B, Vilardaga JP, Tsien RY, Ellisman MH, Lohse MJ. A FlAsH-based FRET approach to determine G protein-

coupled receptor activation in living cells. *Nat Methods* 2005;2(3):171-176.
30. May LT, Bridge LJ, Stoddart LA, Briddon SJ, Hill SJ. Allosteric interactions across native adenosine-A(3) receptor homodimers: quantification using single-cell ligand-binding kinetics. *Faseb J* 2011;25(10):3465-3476.
31. Chakrabarti PP, Daumke O, Suveyzdis Y, Kotting C, Gerwert K, Wittinghofer A. Insight into catalysis of a unique GTPase reaction by a combined biochemical and FTIR approach. *J Mol Biol* 2007;367(4):983-995.
32. Elgeti M, Rose AS, Bartl FJ, Hildebrand PW, Hofmann KP, Heck M. Precision vs flexibility in GPCR signaling. *J Am Chem Soc* 2013;135(33):12305-12312.
33. Nunez S, Venhorst J, Kruse CG. Target-drug interactions: first principles and their application to drug discovery. *Drug Discov Today* 2012;17(1-2):10-22.
34. Heise CE, Sullivan SK, Crowe PD. Scintillation proximity assay as a high-throughput method to identify slowly dissociating nonpeptide ligand binding to the GnRH receptor. *J Biomol Screen* 2007;12(2):235-239.
35. Pierre N. Determination of Association (k_{on}) and Dissociation (k_{off}) Rates of Spiperone on the Dopamine D_2 Receptor Using a Platform for GPCR Applications. Volume 2013. Bedford: American Laboratory; 2011.
36. Vauquelin G, Charlton SJ. Long-lasting target binding and rebinding as mechanisms to prolong *in vivo* drug action. *Br J Pharmacol* 2010;161(3):488-508.
37. Vauquelin G, Van Liefde I. Slow antagonist dissociation and long-lasting *in vivo* receptor protection. *Trends Pharmacol Sci* 2006;27(7):356-359.
38. Vauquelin G. Rebinding: or why drugs may act longer *in vivo* than expected from their *in vitro* target residence time. *Expert Opin Drug Discov* 2010;5(10):927-941.
39. Dahl G, Akerud T. Pharmacokinetics and the drug-target residence time concept. *Drug Discov Today* 2013;18(15-16):697-707.
40. Lindstrom E, von Mentzer B, Pahlman I, Ahlstedt I, Uvebrant A, Kristensson E, Martinsson R, Noven A, de Verdier J, Vauquelin G. Neurokinin 1 receptor antagonists: correlation between *in vitro* receptor interaction and *in vivo* efficacy. *J Pharmacol Exp Ther* 2007;322(3):1286-1293.

Summary

The present thesis starts with a general description of the current drug research pipeline and the high attrition rate therein (Chapter 1). Lack of clinical efficacy was reported as the main cause for drug failure. The concept drug-target residence time was then introduced, which is a paradigm suggested to be a better predictor for drug efficacy than the equilibrium–based metrics (i.e., K_i or IC_{50}). The adenosine A_1 and A_{2A} receptors were chosen as two prototypical GPCRs for this thesis, since many ligands have been developed for these receptors after decades of medicinal chemistry efforts. Those compounds were good starting points for investigating ligand-receptor binding kinetics.

In Chapter 2, a series of prototypic GPCR ligands that have known kinetic information is reviewed. This is followed by an extensive discussion of the kinetic behaviour of GPCR ligands at four representatives GPCRs, which are the muscarinic M_3, tachykinin NK_1, dopamine D_2 and corticotropin-releasing CRF_1 receptors. It was found that there is much less kinetic data for GPCR ligands than equilibrium-based data determined in the early phases of drug discovery; almost no detailed structure-kinetics relationship (SKR) studies have been reported previously, if any.

Chapter 3 contains the set-up, validation and optimization of a novel kinetic screening method, the so-called dual-point competition association assay. This method enables fast and high-throughput screening, since it only requires a measurement of radioligand binding at two different time points. Such a dual-point measurement yields the kinetic rate index (KRI), a parameter coined for quickly assessing kinetic parameters. In this chapter, a screen with 35 high affinity A_1R antagonists was described. Seven compounds were identified with a KRI-value above 1.2, indicating a relatively slow dissociation from the target. All other compounds had a KRI-value below or equal to 1.0, predicting a relatively fast dissociation rate. Several of these compounds were selected for follow-up kinetic quantification and were shown to have off-rates that corresponded to their KRI-values. Thus, the KRI and the dual-point assay can robustly predict a competitor's dissociation rate. This assay can be applied to a wide range of drug targets as well.

In Chapter 4, we performed an extensive SKR study on the $A_{2A}R$ in addition to a traditional SAR analysis—a combination strategy proposed in Chapter 2. The ensemble of 24 $A_{2A}R$ antagonists, all ZM241385 derivatives, displayed only minor or insignificant changes in affinity, while they varied substantially in their dissociation rates from the receptor. We believe such a combination of SKR and SAR analysis as on the $A_{2A}R$ will have general importance for other drug targets as well, since it can serve as a new strategy to tailor the interaction between a ligand and its receptor.

An exploration of the molecular basis behind ligand (*in vitro*) efficacy is described in Chapter 5. In this chapter the binding kinetics of ten $A_{2A}R$ agonists from different chemical classes were determined and the putative relationship to their functional efficacies at the $hA_{2A}R$ was extensively examined in Chapter 5. Agonist binding kinetics were determined using the competition association method. The $A_{2A}R$ agonist funtional efficacies were measured in a label-free impedance-based assay and in a cAMP assay. It was found that the ligands' efficacy at the adenosine A_{2A} receptor is correlated with their divergent target-residences times.

Likewise, the investigation of A_1R allosterism from a binding kinetics perspective helped us in further understanding the molecular basis of receptor allosterism (Chapter 6). We showed that an allosteric modulator can alter the orthosteric ligand's dissociation rate as well as the association rate; the latter less investigated before in literature. Such influence was probe- and concentration-dependent. This chapter also contains an examination of the binding kinetics of two bitopic ligands, LUF6234 and LUF6258, which consist of an allosteric and an orthosteric pharmacophore connected via a linker. Covalently linking both parts into one molecule had a substantial effect on the overall on- and off-rate. These (mathematical) analyses in terms of binding kinetics can add a wealth of knowledge to current pharmacological receptor concepts.

Finally, general conclusions from the research described in this thesis are given and future perspectives in this field are presented (Chapter 7). In short, this thesis provides insights in drug-target binding kinetics. We hope this thesis will bring more awareness of the importance of ligand-receptor binding kinetics and thus result in more kinetics-based studies in future early phases of drug design and discovery, eventually leading to different or even better-in-class drug candidates for future clinical applications.

Samenvatting

Dit proefschrift begint met een beschrijving van het huidige proces van geneesmiddelontwikkeling en het hoge percentage van kandidaat geneesmiddelen dat voor lancering op de markt faalt (hoofdstuk 1). Gebrek aan klinische werkzaamheid is gerapporteerd als de belangrijkste oorzaak voor het falen van geneesmiddelontwikkeling. Al eerder is aangetoond, dat met behulp van de bindingskinetiek beter voorspeld kan worden welke kandidaat geneesmiddelen een goede werking zullen hebben dan met bestaande parameters, welke onder evenwichtscondities bepaald worden (K_i of IC_{50}). De adenosine A_1 en A_{2A} receptoren werden gekozen als twee prototypische receptoren (G protein-coupled receptors of afgekort GPCRs) voor dit proefschrift, omdat door decennia van farmacochemische inspanningen al veel liganden voor deze receptoren ontwikkeld zijn. Deze chemische verbindingen waren goede aanknopingspunten voor het onderzoeken van de kinetiek van ligand-receptor binding.

In hoofdstuk 2 wordt een reeks prototypische GPCR liganden beschreven waarvan kinetische informatie beschikbaar is in de literatuur. Hierna volgt een uitvoerige beschrijving van het kinetische gedrag van GPCR liganden op vier representatieve GPCRs; de muscarine M_3, de tachykinine NK_1, de dopamine D_2 en corticotropine releasing CRF_1 receptoren. Het blijkt dat tijdens de vroege fasen van geneesmiddelontwikkeling veel minder kinetische gegevens beschikbaar zijn in vergelijking tot data bepaald onder evenwichtscondities. Daarom zijn er nog bijna geen gedetailleerde structuur-kinetiek relaties (SKR) gerapporteerd, terwijl al decennia lang structuur-affiniteit relaties (SAR) bepaald worden.

Hoofdstuk 3 omvat de opzet, validatie en optimalisatie van een nieuwe kinetische methode voor ligand screening, de zogenaamde twee-punts competitie associatie test. Deze methode zorgt voor een snelle en high-throughput screening, omdat het slechts een meting van radioligand binding op twee verschillende tijdstippen vereist. Zo bepaalt een dual-point meting de kinetic rate index (KRI), een parameter die door ons werd ontwikkeld voor het snel beoordelen van ligand-receptor bindingskinetiek.

In dit hoofdstuk wordt een selectie van 35 A_1 receptor antagonisten met hoge affiniteit beschreven. Zeven verbindingen werden geïdentificeerd met een KRI-waarde boven de 1.2, wat wijst op een relatief langzame dissociatie van de receptor. Alle andere verbindingen hadden een KRI-waarde lager of gelijk aan 1.0, wat een relatief snelle dissociatiesnelheid voorspelt. Verscheidene van deze verbindingen werden geselecteerd voor vervolgstudies waarin dissociatiesnelheden met behulp van kinetische bindingsexperimenten werden bepaald. Het bleek dat deze dissociatiesnelheden overeenkomen met de eerder bepaalde KRI waarden. De KRI en de dual-point meting zijn dus in staat een robuuste voorspelling van de dissociatiesnelheid van het onderzochte ongelabelde ligand te geven. Deze test kan, naast adenosine receptoren, ook op andere GPCRs en aangrijpingspunten voor geneesmiddelen worden toegepast.

In hoofdstuk 4 wordt een uitgebreide SKR studie van de A_{2A} receptor beschreven naast een traditionele SAR studie – een combinatiestrategie zoals beschreven in hoofdstuk 2. De groep van 24 A_{2A} receptor antagonisten, alle ZM241385 derivaten, vertoont geen, of slechts kleine, verschillen in de affiniteit, terwijl aanzienlijke variatie in dissociatiesnelheden werd gevonden. Wij denken dat een dergelijke combinatie van SKR en SAR analyse op de A_{2A} receptor ook van groot belang kan zijn voor andere GPCRs en aangrijpingspunten voor geneesmiddelen. Dan kan het dienen als een nieuwe strategie voor het op maat maken van de interactie tussen een ligand en zijn receptor.

Een verkenning van de moleculaire grondslag van de werkzaamheid van liganden (*in vitro*) wordt beschreven in hoofdstuk 5. In dit hoofdstuk werd de bindingskinetiek van tien A_{2A} receptor agonisten uit verschillende chemische klassen bepaald en werd de relatie met hun functionele effectiviteit onderzocht. De bindingskinetiek van de agonisten werd bepaald met behulp van de competitie associatie test. De functionele werkzaamheid werd gemeten met een label-vrije - op electrische weerstand gebaseerde - methode en in een cAMP test. Er werd een correlatie gevonden tussen de effectiviteit van de liganden in de functionele experimenten en hun bindingskinetiek.

Door het concept van allostere modulatie van de A_1 receptor te benaderen vanuit het perspectief van bindingskinetiek waren we in staat om de moleculaire basis van allostere modulatie beter te begrijpen (hoofdstuk 6). We toonden aan dat een allostere modulator zowel de associatie- als de dissociatiesnelheid van het orthostere ligand kan veranderen. Het effect op de associatiesnelheid is in de literatuur nog zeer weinig beschreven. Dit effect bleek zowel structuur- als de concentratieafhankelijk.

Dit hoofdstuk bevat ook een onderzoek naar de bindingskinetiek van twee

bitopische liganden, LUF6234 en LUF6258, welke bestaan uit een allostere en een orthostere farmacofoor verbonden via een linker. Het covalent koppelen van beide delen van een molecuul had een aanzienlijk effect op de totale associatie- en dissociatiesnelheden. Door een wiskundig model te gebruiken om de bindingskinetiek te analyseren waren we in staat een schat aan kennis toe te voegen aan de huidige farmacologische receptorconcepten.

Tot slot wordt een overzicht gegeven van de conclusies die zijn verkregen uit het in dit proefschrift beschreven onderzoek (hoofdstuk 7). Daarnaast worden toekomstperspectieven besproken. Kort samengevat geeft dit proefschrift inzichten in de bindingskinetiek van geneesmiddelen op hun aangrijpingspunt. We hopen dat dit proefschrift meer aandacht vestigt op het belang van het evalueren van bindingskinetiek voor de ontwikkeling van nieuwe geneesmiddelen. Dit zal hopelijk leiden tot andere en mogelijk betere kandidaat geneesmiddelen voor toekomstige klinische toepassingen.

Curriculum Vitae

Dong Guo was born on May 8th, 1984 in Xuzhou, China. In 2003, he started his university education at the Western China School of Pharmacy, Sichuan University (China), majoring in biopharmaceutical science. After obtaining his Bachelor degree in 2007, Dong joined a cooperation project between Sichuan University and Leiden University (Netherlands), which allowed him to study Biopharmaceutical Sciences at the then Leiden/Amsterdam Center for Drug Research (Now Leiden Academic Centre for Drug Research, LACDR). During this stage he performed two master projects in Prof. Ad IJzerman's group at the Division of Medicinal Chemistry. Later in his master study (2008), Dong did a third internship at the University of Copenhagen (Denmark) under the guidance of Prof. Mette Rosenkilde and Prof. Thue Schwartz.

After obtaining his master in Biopharmaceutical Sciences in 2009, Dong moved back to Leiden and started his doctorate project on "Drug-target residence time—a case for the adenosine A_1 and A_{2A} receptors" under the supervision of Prof. Ad IJzerman and Dr. Laura Heitman at the Division of Medicinal Chemistry (Jan, 2010 – Jan, 2014). His areas of interest included the set-up of kinetic assays and investigation of ligand-receptor binding kinetics at the adenosine A_1 and A_{2A} receptors. During this stage, Dong presented his research at several (inter)national symposia and congresses. In 2012 he received the first prize at the LACDR Spring Symposium for his oral communication entitled: "Attrition? Residence time! An overlooked parameter in drug design and discovery". Accordingly, he was elected as the representative of Leiden University for the national PhD competition held during the FIGON Dutch Medicines Days. Later that year, Dong was elected as 'the most promising young professional' from the CALN (Chinese Association of Life-Science in the Netherlands) at the CALN pharmaceutical science seminar 2012. Additionally, Dong was awarded three best poster prizes for his posters "Affinity? Residence time! The relationship between residence time and functional efficacy of adenosine A_{2A} receptor agonists" and one best poster prize for his poster "Drug-target residence time-A case

for the adenosine A_{2A} receptor" at several (inter)national conferences from 2010 to 2014.

Following this doctorate study, Dong joined the K4DD consortium, which is financially supported by Europe's Innovative Medicines Initiative (IMI) program and major Pharma companies, as a postdoctoral scientist at the same division (Jan, 2014). His current research area involves the application of mathematical modeling for molecular understanding of ligand-receptor binding kinetics.

list of publications

Guo D, Mocking T, Dror R, Pan A, Shaw DE, Heitman LH, IJzerman AP. Molecular basis of ligand dissociation from the adenosine A_{2A} receptor. In preparation.

Guo D, IJzerman AP, Heitman LH. "Importance of Drug-Target Residence Time at G protein-Coupled Receptors - A Case for the Adenosine Receptors," in *Kinetics and Thermodynamics of Drug Binding*, G. Keseru, D. Swinney, Eds. Wiley-VCH. Submitted.

Guo D, Venhorst SN, Massink A, Van Veldhoven JPD, Vauquelin G, IJzerman AP, Heitman LH. *Br J Pharmacol*. Submitted.

Louvel J, **Guo D**, Agliardi M, Mocking T, Kars R, Pham TP, Xia L, De Vries H, Brussee J, Heitman LH; IJzerman AP. Agonists for the Adenosine A_1 Receptor with tunable residence time. A case for non-ribose 4-amino-6-aryl-5-cyano-2-thiopyrimidines. *J Med Chem*. 2014; 57(8): 3213-3222.

Guo D, Xia L, Van Veldhoven JPD, Hazeu M, Mocking T, Brussee J, IJzerman AP, Heitman LH. Binding Kinetics of ZM241385 Derivatives at the Human Adenosine A_{2A} Receptor, *ChemMedChem*. 2014; 9(4): 752-761.

Guo D, Hillger JM., IJzerman AP, Heitman LH. Drug-Target Residence Time - A Case for G Protein-Coupled Receptors, *Med Res Rev*. DOI: 10.1002/med.21307.

Steen A, Sparre-Ulrich AH, Thiele S, **Guo D**, Frimurer TM, Rosenkilde MM. Gating Function of Isoleucine-116 in TM3 (position III:16/3.40) for the activity state of the CC-chemokine receptor 5 (CCR5), *Br J Pharmacol*. 2014; 171(6): 1566-1579.

Steen A, Thiele S, **Guo D**, Hansen LS, Frimurer TM, Rosenkilde MM. Biased and constitutive signaling in the CC-chemokine receptor CCR5 by manipulating the interface between transmembrane helices 6 and 7, *J Biol Chem*. 2013; 288(18): 12511-12521.

Guo D, Van Dorp EJH., Mulder-Krieger T, Van Veldhoven JPD, Brussee J, IJzerman AP, Heitman LH. Dual-Point Competition Association Assay: A Fast and High-Throughput Kinetic Screening Method for Assessing Ligand-Receptor Binding Kinetics, *J Biomol Screen*. 2013; 18(3): 309-320.

Guo D, Mulder-Krieger T, IJzerman AP, Heitman LH. Functional efficacy of adenosine A_{2A} receptor agonists is positively correlated to their receptor residence time, *Br J Pharmacol*. 2012; 166(6): 1846-1859.

Peeters MC, Van Westen GJP, **Guo D**, Wisse LE, Müller CE, Beukers MW, IJzerman AP. GPCR Structure and Activation: An Essential Role for the First Extracellular Loop in Activating the Adenosine A_{2B} Receptor, *FASEB J*. 2011; 25(2): 632-643.

Shagufta S, **Guo D**, Klaasse E, De Vries H, Brussee J, Nalos L, Rook M, Vos M, Van der Heyden MAG, IJzerman AP. Exploring Chemical Substructures Essential for hERG K^+ Channel Blockade by Synthesis and Biological Evaluation of Dofetilide Analogues, *ChemMedChem*. 2009; 4(10): 1722-1732.

Acknowledgements

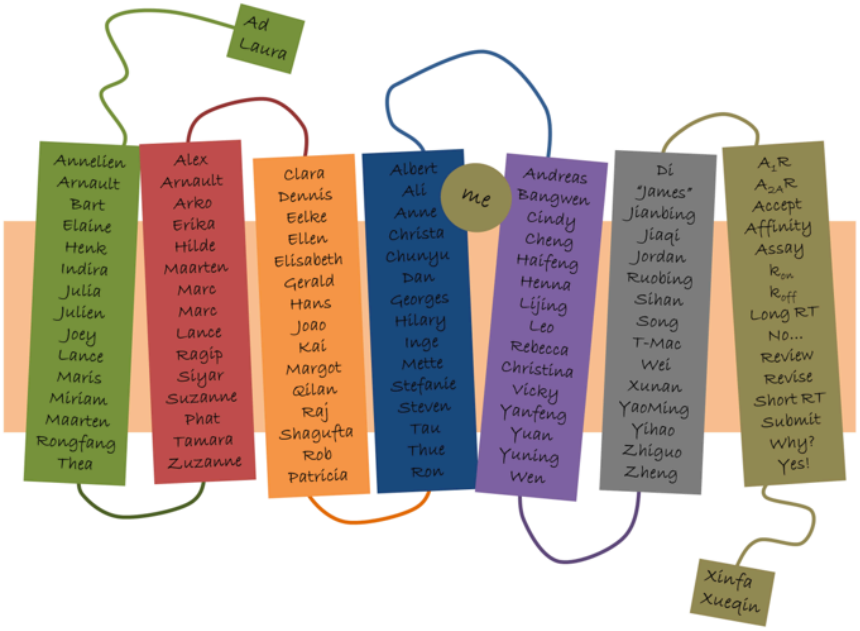


Figure 1. | Dong's GPCR world: those I owe sincere gratitude and indebtedness to during my four-year "residence time" in Leiden. N terminal: Supervisors, Ad and Laura, who have guided me on the track towards a proper scientist; TM 1: Colleagues, who have kept inspiring me during group meetings and journal clubs; TM 2: Former students, together with whom I have gained knowledge in every project; TM 3: Former colleagues, who gave me tips and advice in the early years of my doctorate study; TM 4: Collaborators, who have broadened my vision and greatly facilitated my research projects; TM 5: Friends, who have accompanied me during seasonal changes in Leiden; TM 6: Basketball superstars, who have kept refilling my energy and motivation every week. TM 7: Keywords from my doctorate project, which made the past four years joyful, colorful and beautiful. C terminal: Parents, who have always been there for me, and whom I should definitely spend more time with.